STUDIES OF SELF-ASSEMBLED SUBSTITUTED POLY(ACRYLATE) NETWORKS AS POTENTIAL SUSTAINED DRUG DELIVERY SYSTEMS AND OF FLUORESCENT CONJUGATED POLYMER NANOPARTICLES IN CELL IMAGING

Liang Yan

(严良)

Thesis submitted for the degree of

Doctor of Philosophy

in

Department of Chemistry

The Univeristy of Adelaide

November, 2016

TABLE OF CONTENTS

ABSTRACT

Polymer networks are promising biomaterials for drug delivery as they have porous structures and are often biocompatible. The general aspects of the host-guest complexation capability of polymer networks containing cyclodextrins as well as their application in drug delivery are considered in Chapter 1. The introduction of cyclodextrins into polymer networks has the potential to improve drug loading capacity and modulate subsequent drug release behavior due to the host-guest complexation by cyclodextrins of drug molecules. Thus, Chapter 2 and Chapter 3 are concerned with new research on water soluble β-cyclodextrin, adamantyl and octadecyl substituted poly(acrylate) networks, respectively, as potential sustained drug delivery systems.

In Chapter 2, research into self-assembled poly(acrylate) networks cross-linked through host-guest complexation between β-cyclodextrin, β-CD, substituents and adamantyl, AD, substituents as potential sustained drug delivery systems is described. A poly(acrylate) (PAA) 8.8% randomly substituted with β-CD through an ethyl tether, PAAβ-CDen, is synthesized as a host poly(acrylate). Poly(acrylate)s 3.3%, 3.0% and 2.9% randomly substituted with AD substituents, respectively, through ethyl, hexyl and dodecyl tethers in the PAAADen, PAAADhn and PAAADddn are synthesized as guest polymers. The host-guest complexation of PAAADen, PAAADhn, and PAAADddn by PAAβ-CDen in aqueous solution produce three self-assembled poly(acrylate) networks. These complexations are characterized by isothermal titration calorimetry, ITC, 2D NOESY ^{1}H NMR spectroscopy, and rheology. It is found that the length of the tether between the AD group and the poly(acrylate) backbone has a substantial influence on the complexation constants, K_{ITC}, as well as the associated enthalpy change, ΔH, and entropy change, ΔS. The smallest and largest K_{ITC} occur for PAAADen with the shortest tether and PAAADddn with the longest tether, which coincides with the lowest

and highest viscosities occurring for the aqueous PAAβ-CDen/PAAADen and PAAβ-CDen/PAAADddn networks. The complexation of three different dye molecules, acting as drug models, by the β-CD substituents in these networks is characterized by UV-Vis spectroscopy and 2D NOESY ^{1}H NMR studies. The results suggest that dye complexation by the β-CD substituents in the three poly(acrylate) networks is weaker by comparison with the complexation by native β-CD and PAAβ-CDen, as indicated by decreased complexation constants. The poly(acrylate) networks exhibit complexation-controlled dye release behavior, and thereby sustained dye release profiles. Thus, the three poly(acrylate) networks studied, which form hydrogels at higher concentrations, have substantial potential as sustained drug delivery systems.

In Chapter 3, the complexation and release behavior of six dyes in a β-CD- and octadecyl-substituted poly(acrylate) network is explored to further extend the understanding of the host-guest complexation between β-CD substituents and guest molecules within a fourth polymer network system and its influence on the release of guest molecules from the polymer network. Thus, β-CD substituents are 9.3% randomly substituted onto poly(acrylate) through an ethyl tether to give PAAβ-CDen and octadecyl, C18, substituents are 3.5% randomly substituted onto poly(acrylate) to give PAAC18. The network forms through the host-guest complexation between the β-CD substituents and C18 substituents, and is characterized by a complexation constant of $K = 1.13 \times 10^{4}$ dm^{3} mol^{-1}, associated with ΔH = −21.55 kJ mol^{-1} and $T\Delta S$ = 1.59 kJ mol^{-1}. The complexation of the dyes by the β-CD substituents in the PAAβ-CDen/PAAC18 network is characterized by UV-Vis absorption and fluorescence spectroscopy and 2D NOESY ^{1}H NMR studies. The results suggest that the complexation of dyes by the β-CD substituents in the PAAβ-CDen/PAAC18 network is weaker by comparison with the complexation by native β-CD and PAAβ-CDen, as indicated

by decreased complexation constants. The PAAβ-CDen/PAAC18 network exhibits complexation-controlled dye release behavior and thereby sustained dye release profiles. Thus, the PAAβ-CDen/PAAC18 network, or hydrogel at higher concentration, is a potential sustained drug delivery system.

Conjugated polymer nanoparticles are promising fluorescent probes as a consequence of their high brightness and photostability. Chapter 1 introduces the general methods of preparing conjugated polymer nanoparticles and their wide ranges of biological applications. However, conjugated polymer nanoparticles exhibit large-scale aggregation and precipitation at the high ionic strengths encountered under physiological conditions, which presents an impediment to their biological applications. In seeking to address this issue, the research described in Chapter 4 and Chapter 5 addresses stabilization of conjugated polymer nanoparticles using hydrophobic linear alkyl group substituted poly(acrylate)s and bovine serum albumin and explores their deployment in cell imaging applications.

In Chapter 4, the synthesis of hydrophobic linear alkyl group substituted poly(acrylate)s, PAAC*n*, is described as is their employment as conjugated polymer nanoparticle stabilizers. (When n = 18, 16 and 10 the alkyl groups are octadecyl, hexadecyl and decyl, respectively.) The carboxylate groups of PAAC*n* increase the surface charge of the conjugated polymer nanoparticles and thereby stabilize them in phosphate buffered saline, PBS. Nanoparticles of the green-yellow emitting conjugated polymer, F8BT, stabilized with PAAC*n*, F8BT-PAAC*n*, are prepared using a nano-precipitation method. In contrast to the significant aggregation with a negligible yield (~ 0%) of bare F8BT nanoparticles in PBS, high yields approaching 90% are observed for F8BT nanoparticles stabilized with PAAC18 at 1%, PAAC16 at 3%, and PAAC10 at 10% substitution. The F8BT-PAAC*n* nanoparticles have small sizes ranging from 50 to 70 nm in diameter, highly negative surface charge and high colloidal stability over 4 weeks in PBS. These properties pave the way for the deployment of F8BT-PAAC*n*

nanoparticles in biological applications. Spectroscopic results indicate the PAAC*n* has no adverse effect on the UV-Vis absorptivity and fluorescence brightness of F8BT-PAAC*n* nanoparticles relative to bare F8BT nanoparticles. In addition, F8BT-PAAC*n* nanoparticles are internalized by HEK 293 cells and exhibit negligible cytotoxicity. Thus, PAAC*n* are versatile and robust stabilizing materials that facilitate the application of F8BT-PAAC*n* nanoparticles as fluorescent probes in cell imaging.

The research described in Chapter 5 shows that bovine serum albumin, BSA, stabilizes conjugated polymer nanoparticles in phosphate buffered saline, PBS, evidently due to the combined effects of the negatively charged surfaces arising from the BSA carboxylate groups and the steric effect of the bulk 3D structure of BSA. Three multicolored conjugate polymers, PDOF, F8BT, and MEHPPV, are employed to prepare their corresponding nanoparticles using a nano-precipitation method. In contrast to the significant aggregation with negligible yields (~ 0%) of bare conjugated polymer nanoparticles occurring in PBS, high yields approaching 100% are observed for conjugated polymer nanoparticles stabilized with BSA, CP-BSA nanoparticles, in PBS. These CP-BSA nanoparticles have small sizes ranging from 20 to 60 nm, negative surface charges and high colloidal stability. Spectroscopic results indicate the BSA has no adverse effect on the UV-Vis absorptivity and fluorescence brightness of the CP-BSA nanoparticles relative to bare conjugated polymer nanoparticles. These properties potentially pave the way for the deployment of these CP-BSA nanoparticles in biological applications.

DECLARATION

This is to declare that the work presented within this thesis is original and was carried out at the University of Adelaide during the period of 2011-2016. This work contains no material which has been accepted for the award of any other degree or diploma in any university or other tertiary institution and, to the best of my knowledge and belief, contains no material previously published or written by another person, except where due reference is given.

I give consent to this copy of my thesis, when deposited in the University of Adelaide Library, being made available for loan and photocopying, subject to the provisions of Copyright Act 1968.

I also give permission for the digital version of my thesis to be made available on the web, via the University's digital research repository, the Library catalogue, the Australasian Digital Theses program (ADT) and also through web search engines, unless permission has been granted by the University to restrict access for a period of time.

Liang Yan (严良)

01/11/2016

ACKNOWLEDGEMENTS

Doing a PhD research is a meaningful and rewarding experience, which I will cherish in my entire life. It would have never been possible for me to finish this thesis without the guidance of my supervisors, the help and support from my collaborators, colleagues and my family.

I would like to sincerely thank my supervisor Professor Stephen F. Lincoln. I benefitted greatly not only from his immerse knowledge, but also his moral support. Thanks to his guidance and encouragement, I overcame crucial barriers to the completion of my PhD. In addition, I would like to express my gratitude to Professor Stephen F. Lincoln for his understanding when I needed to take several long absences to look after my ill father-in-law. My heartfelt gratitude also goes to my co-supervisor Associate Professor Tak W. Kee. His passion for exploring, discovering and researching has motivated me to seek for the answers persistently. I am also very grateful for his helpful comments on my academic writings.

I would like to express my gratitude to Professor Xuhong Guo and Dr. Jie Wang in East China University of Science and Technology for their help with rheological measurements. I would also like to thank Associate Professor Sheng Dai and Xiaolin Cui at the School of Chemical Engineering in the University of Adelaide for their help with cytotoxicity and fluorescence imaging characterization. My special thanks go to Phil Clements for his assistance with NMR characterization, Gino Farese for his advice on experimental setup and Matthew Bull for his offer of several chemicals at the Department of Chemistry in the University of Adelaide.

I would like to thank Lincoln and Kee group members, Dr. Duc-Truc Pham, Hamish McTernan, Dr. JianJia Liu, Noby Leong, Dr. Takaaki Harada and Dr. Hanh-Trang Nguyen for their help, encouragement, friendship and patience. Dr. Duc-Truc Pham has helped me a lot, from experimental design to result analysis. Dr. JianJia Liu is a good friend and colleague. Our

conversations involve a wide range of topics, including food, travel and research. My special thanks go to Hamish and Noby. I will never forget how you helped me to figure out resolutions for experimental difficulties, to prepare my PhD final talk and conference talk and to revise my thesis draft. Thank you all very much!

Finally, I would like to thank my family, my parents, my parents-in-law, my wife and my son. Without their understanding and support, I would have never been able to finish this PhD thesis.

ABBREVIATIONS

General

ΔH	enthalpy change
ΔS	entropy change
ITC	isothermal titration calorimetry
UV-Vis	ultraviolet/visible
A	observed absorbance
ε	molar absorbance (mol^{-1} dm^3 cm^{-1})
F	observed fluorescence
f	molar fluorescence
et al.	et alia
Hz	Hertz
I	ionic strength (mol dm^{-3})
K	complexation constants (dm^3 mol^{-1})
NMR	nuclear magnetic resonance
δ	chemical shift (ppm)
NOESY	nuclear overhauser enhancement spectroscopy
ROESY	rotating frame overhauser enhancement spectroscopy
pH	$-\log[H^+]$
ppm	parts per million
T	temperature
wt	weight
Φ	fluorescence quantum yield
η	refractive index

Chemicals

α-, β-, γ-CD	α-, β-, γ-cyclodextrin
AD	adamantyl
en	ethyl

hn	hexyl
ddn	dodecyl
β-CDen	6^A-(2-aminoethyl)amino-6^A-deoxy-6^A-β-CD
ADen	1-(2-aminoethyl)amidoadamantyl
ADhn	1-(6-aminohexyl)amidoadamantyl
ADddn	1-(12-aminododecyl)amidoadamantyl
PAAβ-CDen	β-CDen randomly substituted poly(acrylate)
PAAADen	ADen randomly substituted poly(acrylate)
PAAADhn	ADhn randomly substituted poly(acrylate)
PAAADddn	ADddn randomly substituted poly(acrylate)
MR	sodium salt of methyl red
MO	sodium salt of methyl orange
EO	sodium salt of ethyl orange
C18	octadecyl
PAAC18	octadecyl randomly substituted poly(acrylate)
ANS	sodium 8-anilinonaphthalene-1-sulfonate
TNS	sodium 6-(*p*-toluidino)naphthalene-2-sulfonate
BNS	sodium 6-(*p*-*t*-butylphenylamino)naphthalene-2-sulfonate
C6	hexyl
C10	decyl
C12	dodecyl
C14	tetradecyl
C16	hexadecyl
PAAC6	hexyl randomly substituted poly(acrylate)
PAAC10	decyl randomly substituted poly(acrylate)
PAAC12	dodecyl randomly substituted poly(acrylate)
PAAC14	tetradecyl randomly substituted poly(acrylate)
PAAC16	hexadecyl randomly substituted poly(acrylate)
F8BT	poly[(9,9-dioctylfluorenyl-2,7-diyl)-alt-co-(1,4-benzo-[2,1,3]-thiadiazole)]
PDOF	poly(9,9-dioctylfluorenyl-2,7-diyl)-End capped with DMP
MEHPPV	poly[2-methoxy-5-(2-ethylhexyloxy)-1-4-phenylenevinylene]-End capped with DMP

BSA	bovine serum albumin

This page is intentionally left blank.

CHAPTER 1

INTRODUCTION

1.1. Cyclodextrins

1.1.1 General introduction to cyclodextrins

As defined by 1987 Nobel Prize Laureate Lehn, supramolecular chemistry is chemistry beyond the molecule.[1] Unlike traditional chemistry which is dominantly dependent on covalent bonding, supramolecular chemistry is dependent on inter-molecular non-covalent interactions through which one species acting as a receptor or host species partially or totally envelopes a second species, or guest, to form a host-guest complex in which the ratio of host to guest species varies from 1:1 through a range of ratios.[1,2] The thermodynamic stability of these host-guest complexes varies substantially as a consequence of stereoselective, polarity and hydrophobic and hydrophilic characteristics often collectively termed "molecular recognition".[2]

Among supramolecular macrocyclic host molecules, cyclodextrins are particularly versatile building blocks for the fabrication of sophisticated supramolecular architectures exemplified by a molecular machine harnessing the energy of molecular recognition to do work,[3] to a light-responsive nanotube-nanoparticle system,[4] and further to a supramolecular hydrogel exhibiting self-healing, redox-responsive expansion-contraction, and shape-memory features.[5] Cyclodextrins (CDs) are cyclic oligosaccharides, the products of starch degradation by the enzyme CD glucosyltransferase. The discovery of CDs by Antoine Villiers, a French pharmacist and chemist, dates back to 1891. When Villiers investigated enzymatic degradation and reduction of potato starch, some unknown crystals, most likely α-CD and β-CD, were found. It was not until 20 years later that Schardinger successfully isolated the microorganism able to produce CD glucosyltransferase, *Bacillus macerans*.[6] The most commonly encountered CDs are α-CD, β-CD, and γ-CD which comprise 6, 7 and 8 α-1,4-linked D-glucopyranose

units, respectively. Larger CDs comprising 9, 10, 14, and 26 α-1,4-linked D-glucopyranose units have been successfully crystallized and their structures have been elucidated in detail.[7-9] However, there has been no report of CDs comprising less than 6 α-1,4-linked D-glucopyranose units presumably as a consequence of ring strain preventing the formation of a macrocycle consisting of 5 and fewer α-1,4-linked D-glucopyranose units.

The cyclodextrins α-CD, β-CD, and γ-CD are composed of α-1,4-linked D-glucopyranose units in the $^4C_1$ chair conformation. They exhibit the overall shape of a hollow truncated cone, as shown in Figure 1.1. All secondary hydroxy groups, O(2)H and O(3)H, are located on the wide rim of the cone, while the primary hydroxy groups, O(6)H, are on the narrow rim. These hydroxy groups endow CDs with hydrophilic rims which render them water soluble. The interior cavity, or annulus, is lined with H(3), H(5), and H(6) hydrogen atoms and glycosidic O(4) oxygen atoms which produces a hydrophobic interior. The unique truncated cone shape of CDs with outer hydrophilic rims and interior hydrophobic cavity are stabilized by intra-molecular hydrogen bonding between secondary hydroxy groups of adjacent glucopyranose units. The annular depth of α-CD, β-CD, and γ-CD is 0.79 nm (Figure 1.1), while annular diameters measured from the C(3) hydrogens increase from α-CD (0.57 nm) and β-CD (0.78 nm), to γ-CD (0.95 nm), as the number of glucopyranose units increases.[10] (The conical truncated exterior and annular outlines are both shown in Figure 1.1, but only the annular outline is shown to avoid unnecessary complexity in the majority of figures involving CDs in this thesis.)

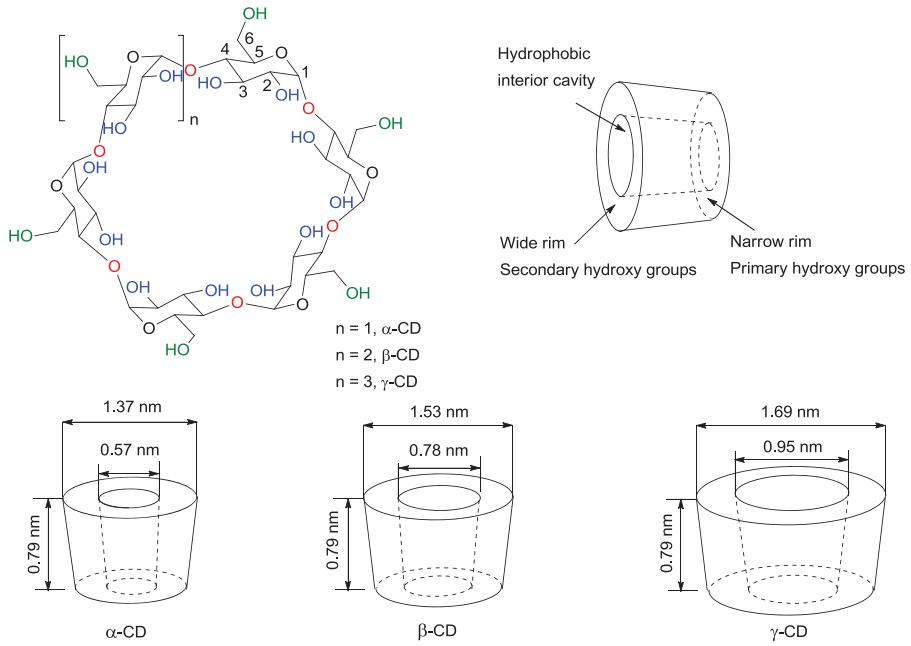

Figure 1.1. Schematic illustration of structures of α-CD, β-CD, and γ-CD and their dimensions.[10]

In aqueous solution, CDs provide a micro hydrophobic environment as a consequence of the hydrophobic interior cavity which facilitates the encapsulation of size-matched guests into the inner cavities to form host-guest complexes (Figure 1.2). Variation of the annular diameters and volumes from α-CD to γ-CD provide opportunities for complexation, or encapsulation, of a wide range of guests, including small organic molecules,[11-19] inorganic anions and cations,[20,21] and polymers.[22-24] The ability to form a host-guest complex is the most attractive feature of CDs and has inspired wide usage in food,[25] pharmaceutics,[26-28] catalysis,[29] and enzyme technologies.[30]

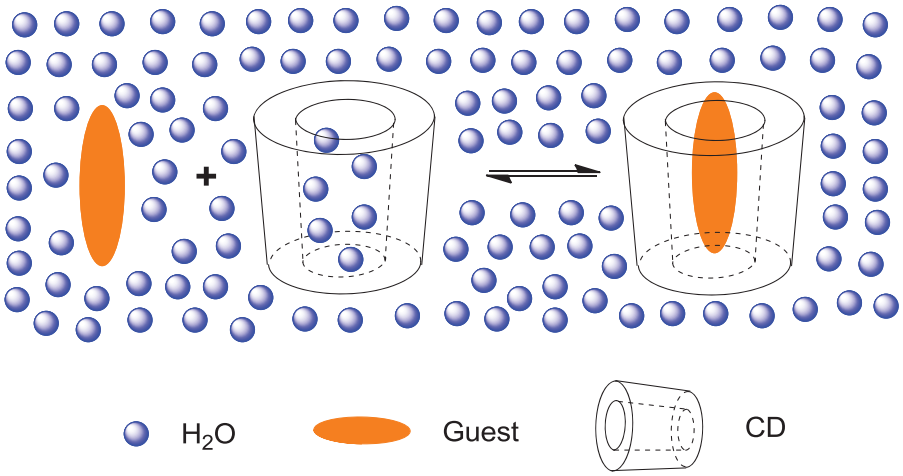

Figure 1.2. Schematic illustration of the formation of CD host-guest complex in an aqueous solution.

1.1.2. Cyclodextrin host-guest complexation process

Host-guest complexes between CDs and guests dominantly rely on non-covalent interactions, yet they can be highly stable as determined by the nature of the CD and guest. The most likely complexation mode involves encapsulation of the less polar part of a guest molecule inside the hydrophobic annulus of a CD. The complexation of guests by CDs is hypothesized to be driven primarily by van der Waals and hydrophobic interactions.[10,31] Most such complexes have been studied in aqueous solution wherein it is widely accepted that the release of "high energy" water from CD annulus plays a major role in host-guest complexation.[10] Water molecules inside CD annulus are unable to form as complete a hydrogen bonding array as do those in bulk water, and are therefore considered to be of "high energy". The expulsion of these "high energy" water molecules by an entering guest is thought to stabilize the host-guest complex partially as a consequence of the decrease in entropy occurring through the combination of the host and guest into the single host-guest complex being offset by the release of the water occupying the CD annulus.[10] Moreover, it has been

reported that the release of CD conformational strain[32,33] and hydrogen bonding between the guest and the CD[34] also contribute to driving the formation of host-guest complexes. It is expected that substantial variations in these individual contributions occur.

The CD host-guest complexation is a dynamic and reversible process whereby an equilibrium is established between the associated CD host-guest complexes and the dissociated free CD and free guest. Common stiochiometries of the CD host-guest complexes include 1:1 CD:guest, 1:2 CD:guest, 2:1 CD:guest, 2:2 CD:guest and 1:1:1 CD:guest1:guest2.[10,31,35] The equilibrium for a 1:1 CD host-guest complexation is shown in Equation 1.1. Equation 1.2 shows the complexation constant, *K*, characterizing the 1:1 CD-guest complexation equilibrium.

$$\text{CD} + \text{guest} \underset{}{\overset{K}{\rightleftharpoons}} \text{CD.guest} \qquad (\mathbf{1.1})$$

$$K = [\text{CD.guest}]/([\text{CD}][\text{guest}]) \qquad (\mathbf{1.2})$$

The magnitude of the complexation constant, *K*, for an equilibrium for CD-guest complexation is a direct indication of the strength of interaction between the CD and the guest and of the stability of the CD.guest complex. There are a variety of experimental techniques used to determine the complexation constant. Widely used experimental methods include isothermal titration calorimetry (ITC),[36-38] UV-Vis,[39,40] fluorescence,[41,42] nuclear magnetic resonance (NMR),[11,15] and circular dichroism (CD).[43,44] Using these experimental techniques, a titration approach is commonly employed to determine the complexation constant. In general, a CD solution is titrated into a guest solution or vice-versa. The formation of CD-guest complex causes variation in a physical property, such as fluorescence intensity or NMR chemical shift, and an algorithm for a particular CD host-guest stoichiometry is fitted to the experimental variation of the physical property to yield the complexation constant.[45] The choice of experimental technique depends on the physical properties of the guest or CD.

In addition to the complexation constant, the enthalpy change, ΔH, and entropy change,

ΔS, for CD host-guest complexation are fundamental thermodynamic parameters. In terms of experimental technique, isothermal titration calorimetry, ITC, is the only experimental technique by which complexation enthalpy change may be directly determined. For other techniques, complexation constants at different temperatures are analyzed using the van't Hoff equation to determine the corresponding enthalpy and entropy change. According to published collections of thermodynamic parameters, negative enthalpy change, as well as negative entropy change, is usually observed in CD host-guest complexation. Consequently, CD host-guest complexation is said to be enthalpy driven.[10] Negative enthalpy changes are generally a result of van der Waals interactions between the CD and guest, while negative entropy changes usually arise from reduced translational and conformational freedoms of the CD and guest upon complexation. However, in some cases, negative enthalpy change is concurrent with positive entropy change, usually due to extensive desolvation of the CD and guest or release of water molecules from the CD annulus.[31,46-48]

The variation of ΔH and ΔS as the composition of the CD host-guest complex varies provides insight into the thermodynamics of complexation and, while this is affected by the structure of the complexes formed, it does not provide direct structural information. To this end, 2D ^{1}H Rotating frame Overhauser Enhancement Spectroscopy, ROESY, and Nuclear Overhauser Enhancement Spectroscopy, NOESY, are powerful tools for elucidation of the structures of the CD-guest complexes in solution. Dipolar through space inter-proton interactions produce cross-peaks in both 2D ^{1}H ROESY and NOESY NMR spectra (provided that they are within 0.4 nm of each other using the 600 MHz spectrometer of this study). Consequently, if a guest, or a part of a guest, is encapsulated into a CD annulus, cross-peaks arising from the guest protons and the CD annular H3, 5, 6 protons are observed. These cross-peaks provide not only direct evidence of CD-guest complex formation, but also information on complexation mode.[49] In addition, crystallographic X-ray technique is used to

obtain particularly precise information about the structures of CD host-guest complexes in solid state.[50]

1.1.3. Modification of cyclodextrins

Chemical modification of CDs has been extensively explored.[10] The introduction of additional functional groups changes the properties of native CDs, such as solubility and complexation capability, and thereby offers new host CD species to meet requirements in demanding applications. In addition, CDs with reactive groups can be specifically integrated into versatile functional systems, such as hydrogel networks and functional nanoparticles, to broaden their application horizons.

Cyclodextrins can be chemically modified through their hydroxy groups, namely O(2)H, O(3)H and O(6)H. The primary O(6)H groups are the most basic and nucleophilic, while the secondary O(2)H groups are the most acidic and O(3)H groups are least accessible. In addition, the intra-molecular hydrogen bonding between secondary O(2)H and O(3)H groups makes them less reactive. Consequently, these differences allow for selective modification at the 6-position of CDs.[51] Modification at the C6-position commonly involves an electrophilic substitution of O(6)H groups under weak base conditions in which the deprotonation of O(2)H groups, the most acidic groups, is unfavourable. Due to identical reactivity of all O(6)H groups, electrophiles indiscriminately attack O(6)H groups yielding a mixture of mono-, di-, or tri-substituted products. Chromatographic purification is often needed to separate out mono-substituted CDs. The most popular mono-modification at the C6-position of CDs is to use mono-6-tosyl-CD as a precursor followed by nucleophilic displacement of the tosyl group by a nucleophile containing the desired group, as shown in Figure 1.3. Mono-6-tosyl-CD can be synthesized through a well-known reaction of CD with tosyl chloride in alkaline aqueous solution or in pyridine.[52] As tosyl substituent is a good leaving

group, the subsequent nucleophilic substitution by an appropriate nucleophile produces azido-,[53,54] alkylamino-,[55] or thio-CDs.[56] In addition, Yoon *et al.* reported the synthesis of cyclodextrinyl aldehyde through DMSO oxidation of mono-6-tosyl-CD. The obtained cyclodextrinyl aldehyde may then be converted to cyclodextrinyl carboxylic acid.[57]

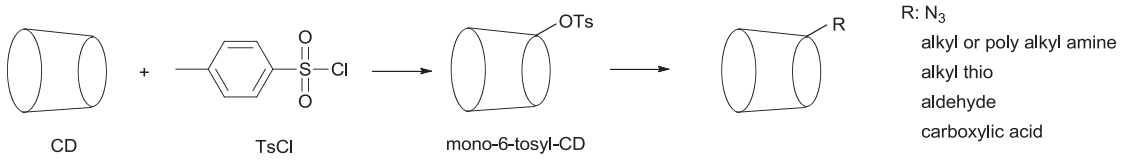

Figure 1.3. General scheme for mono-modification of O(6)H groups of CDs.

Mono-tosylation at the C2-position of CDs is difficult, due to the competing reaction of the more reactive O(6)H groups yielding the byproduct, 6-tosyl-CD. Nevertheless, a tosyl transfer strategy has been reported for the preparation of mono-2-tosyl-CD through the reaction of *m*-nitrophenyl tosylate with CD. In this reaction, *m*-nitrophenyl tosylate is encapsulated into the CD inner cavity to form complexes which direct the tosyl groups to the C2-position to yield mono-2-tosyl-CD.[58] In addition, as the O(2)H groups are the most acidic they are first to become deprotonated under strong base conditions. Thus, sodium hydride maybe used to deprotonate the O(2)H groups and the obtained oxyanion shows more nucleophilicity than non-deprotonated O(6)H groups, which facilitates tosylation at the C2-position to exclusively yield mono-2-tosyl-CD.[59] A method of protection-deprotection at the C6-position of CDs has also been used to produce 2-tosylated-CD.[60] Modification at the C3-position of CDs is the most difficult, as the O(3)H groups are least accessible. A common method is to use *mano*-mono-2,3-epoxyCD obtained from 2-tosyl-CD as a precursor followed by nucleophilic attack to yield the corresponding modified CD at the C3-position.[51]

1.1.4. Cyclodextrins in pharmaceutics

Cyclodextrins have been intensively investigated as components of pharmaceutical formulations to improve therapeutic efficacy, because of their biocompatibility[61,62] and powerful complexation capability that potentially alters physical, chemical and biological properties of drugs through the formation of CD.drug complexes.[26,63] The first patent for CDs in pharmaceutical formulations, filed by Karl Freudenberg, Friedrich Cramer, and Hans Plieninger, dates back to 1953.[6] This patent concerned the protection of drugs from air oxidation and their solubility enhancement in water upon formation of CD.drug complexes. Presently, native CDs and modified CDs are widely found in commercially available pharmaceutical products, some of which are shown in Table 1.1.[63]

Table 1.1. Marketed pharmaceutical products containing native CDs or modified CDs.[63]

CD	Drug	Therapeutic usage	Formulation	Trade name
α-CD	Alprostadil	Treatment of erectile dysfunction	Intracavernous solution	Caverject Dual
β-CD	Cetirzine	Antibacterial agent	Chewing tablets	Certrizin
	Dexamethasone	Anti-inflammatory steroid	Ointment, tablets	Glymesason
	Nicotine	Nicotine replacement product	Sublingual tablets	Nicorette
	Nimesulide	Non-steroidal anti-inflammatory drug	Tablets	Nimedex
	Piroxicam	Non-steroidal anti-inflammatory drug	Tablets, suppository	Brexin
HPβ-CD[a]	Indomethacin	Non-steroidal anti-inflammatory drug	Eye drop solution	Indocid
	Itraconazole	Antifungal agent	Oral and IV solution	Sporanox
	Mitomycin	Antifungal agent	IV infusion	MitoExtra
SBEβ-CD[b]	Aripiprazole	Antipsychotic drug	IM solution	Abilify
	Maropitant	Anti-emetic drug (motion sickness in dogs)	Parenteral solution	Cerenia
	Voriconazole	Antifungal agent	IV solution	Vfend
	Ziprasidone mesylate	Antipsychotic drug	IM solution	Geodon
HPγ-CD[c]	Diclofenac sodium salt	Non-steroidal anti-inflammatory drug	Eye drop solution	Voltaren Ophtha
	Tc-99 Teoboroxime	Diagnostic aid, Cardiac imaging	IV solution	CardioTec

[a]2-hydroxypropyl-β-cyclodextrin (HPβ-CD)

[b]Sulfobutylether β-cyclodextrin sodium salt (SBEβ-CD)

[c]2-hydroxypropyl-γ-cyclodextrin (HPγ-CD)

The most common pharmaceutical application of CDs is for the enhancement of drug solubility in aqueous solutions through the formation of CD.drug complexes. Thus, Straubinger *et al.* reported that the aqueous solubility of paclitaxel, an anti-cancer drug, in the presence of β-CD (1.5% w/v) and γ-CD (15% w/v) was 12.5 and 50 times greater, respectively, than the aqueous solubility of paclitaxel alone.[64] However, the relatively low solubility of native CDs in water (14.5 g 100 mL^{-1} for α-CD, 1.85 g 100 mL^{-1} for β-CD and 23.2 g 100 mL^{-1} for γ-CD at 298.2 K)[10] presents an impediment to further enhancement of

drug solubility. Thus, various modified CDs with improved solubility and complexation capacity have been used in pharmaceutical formulations. By comparison with the moderate 12.5-fold enhancement of the aqueous solubility of paclitaxel in the presence of β-CD, in the presence of dimethyl-β-CD (50% w/v) and hydroxypropyl-β-CD paclitaxel solubility increased by 99000 and 2140 times, respectively.[64] The solubilization effect of modified CDs is markedly influenced by the degree of substitution. Thus, randomly methylated β-CD with an average substitution degree of 4.2 showed greater solubilization of hydrocortisone than that with an average substitution degree of 12.6.[65] Müller and Brauns observed that the decrease in average substitution degree of 2-hydroxyethyl-β-CD from 11 to 3 was concomitant with enhanced solubility of digitoxin from 1.7 to 9.5 mg/mL.[66] In cases where CDs are modified with charged groups, the length of tether between the CD and charged groups also affects complexation capability of modified CDs. It appears that the longer the tether, the stronger the complexation. For example, the complexation of chlorpromazine by β-CD sulfate, characterized by a complexation constant of 1640 dm^3 mol^{-1}, was much weaker than complexation by sulfobutyl-β-CD, characterized by a complexation constant of 16100 dm^3 mol^{-1}.[26] Thus, in contrast to β-CD sulfate exhibiting very weak complexation of acidic and neutral drugs, such as flufenamic acid, flurbiprofen, diazepam and steroids, sulfobutyl-β-CD was reported to be an excellent solubilizer for various poorly water-soluble drugs such as steroids, indomethacin, naproxen and cinnarizine.[26,67]

Another important pharmaceutical application of CDs is to enhance drug stability. Upon the formation of CD.drug complexes, drug molecules are encapsulated into the inner cavities of CDs, which separates labile drug molecules from environmental reactive species and stabilizes the drugs. Thus, doxorubicin, an anti-cancer drug, is unstable in aqueous solution and subject to degradation through acid-catalyzed glycosidic bond hydrolysis. In the presence of 5% w/v γ-CD, the observed rate constant for first-order degradation of doxorubicin

decreased by 59% at pH 1.01 and 42% at pH 5.90 at 75°C, respectively.[68] In another study, aspirin was effectively stabilized by 2-hydroxypropyl-β-CD and 2-hydroxypropyl-γ-CD, as reflected by the observed first-order rate constant for degradation decreasing by 75% and 60%, respectively.[69] In the presence of CDs, the observed drug degradation is the weighted average of free drug degradation and CD.drug complex degradation. Thus, for a given drug, complexation capability and concentration of CDs affect the proportion of free drug, and therefore influence the stabilizing effect of the CD used.

In addition to solubilization and stabilization, CDs have also been used to enhance adsorption of poorly soluble and highly permeable drugs by lipophilic biological membranes, such as skin and gastrointestinal mucosa. These lipophilic membranes normally have an aqueous exterior which limits availability of poorly soluble drugs on the membrane surface and further limits drug permeation through the membrane. However, CDs are able to solubilize and stabilize drugs of low solubility through the formation of CD.drug complexes, thereby transferring drugs to the biological membrane surface and enhancing drug permeation. It has been reported that only the free drug is able to penetrate lipophilic membranes, while CDs and CD.drug complexes are unable to penetrate lipophilic membranes.[70] Thus, usage of CDs generally needs to be optimized given that an excess amount of CDs results in a high proportion of CD.drug complexes and an insufficient amount of CDs reduces available drug at the membrane surface. Nevertheless, CD- or modified CD-based formulations of carbamazepine,[71] digoxin[72] and miconazole[73] have been reported to greatly increase oral bioavailability and adsorption.

1.1.5. Cyclodextrin-based drug delivery systems

Inspired by availability on an industrial scale, benefits in pharmaceutical applications and ease of functionalization, CDs have been extensively employed to fabricate various drug

delivery systems ranging from microscopic molecular delivery vehicles and nano-carriers to macroscopic polymer networks. In early studies, native and modified CDs were used as drug delivery vehicles,[26,27,67,70] some of which have been marketed as shown in Table 1.1. On account of comprising two CD cavities in close vicinity, linked-CD dimers exhibit enhanced complexation capability through cooperative binding.[74] Thus, Kee *et al.* used succinamide and urea linked γ-CD dimers, 66γ-CD_2su and 66γ-CD_2ur, as molecular-scale delivery vehicles for the medicinal pigment curcumin.[75] UV-Vis spectroscopic titration studies demonstrated strong 1:1 complexations between both 66γ-CD_2su and 66γ-CD_2ur and curcumin (Figure 1.4), characterized by high complexation constants of 8.7×10^6 dm^3 mol^{-1} and 2.0×10^6 dm^3 mol^{-1}, respectively. Consequently, 66γ-CD_2su and 66γ-CD_2ur remarkably stabilized curcumin in aqueous phosphate buffer solution at pH 7.4, as reflected by significantly increased half-life from less than 30 min for curcumin alone to approximately 16 h and 71 h for curcumin in the presence of 66γ-CD_2su and 66γ-CD_2ur, respectively. By comparison with 66γ-CD_2su, 66γ-CD_2ur provided better stabilization of curcumin, which was attributed to a shorter and less flexible urea linker resulting in a narrower gap between the two γ-CD units, thus further limiting the access of water to the curcumin keto-enol group. Furthermore, 66γ-CD_2su nor 66γ-CD_2ur had any detectable cytotoxicity against PC-3 cells and were efficient intracellular delivery vehicles.[76]

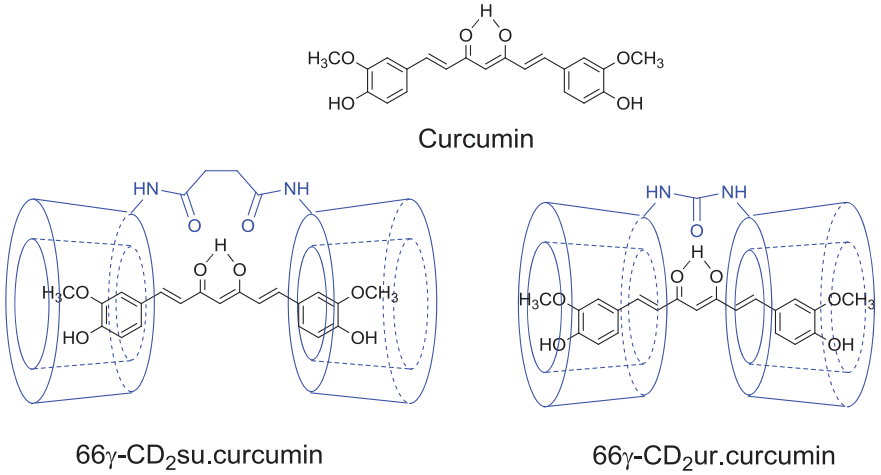

Figure 1.4. Structures of curcumin and its complexes with 66γ-CD_2su and 66γ-CD_2ur.[75]

Another type of CD-based drug delivery system is the CD-based polymeric drug. In contrast to covalent attachment of drug molecules to polymer backbones, the host-guest complexation between CD groups and drug moieties also attaches drug molecules to polymer backbones. Ritter *et al.* synthesized an adamantane-bearing analogue of 5-fluorocytosine (Figure 1.5) with the prodrug being metabolized by bacterial and fungal cytosine deaminase to a commonly used chemotherapeutic agent, 5-fluorouracil.[77] A polymer containing β-CD pendant groups was prepared through radical copolymerization of mono-methacrylate β-CD and *N*-isopropylacrylamide (Figure 1.5). Through the strong complexation of adamantyl moieties by β-CD groups, the active drug species were successfully attached to copolymer backbones to fabricate a polymeric anti-tumor agent. The drug was released through enzymatic hydrolysis of β-CD groups by α-amylase.

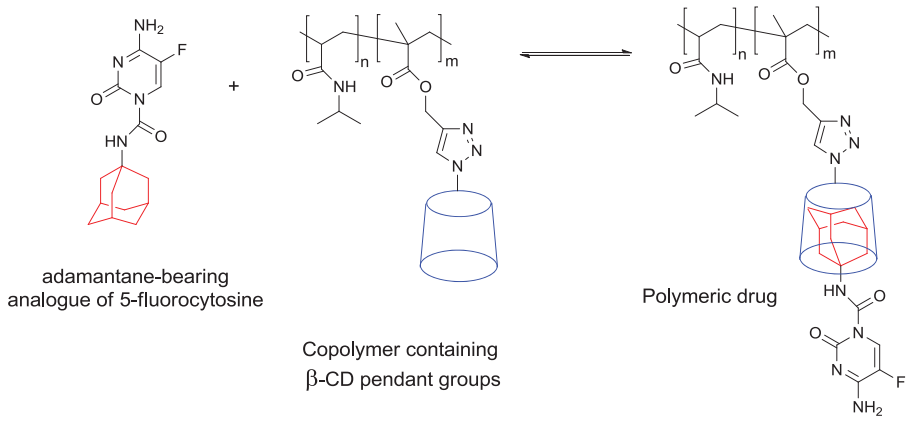

Figure 1.5. Structures of a polymeric drug with the drug molecules attached to a copolymer backbone through the host-guest complexation of adamantyl moieties by β-CD groups.[77]

Cyclodextrins complex polymers to form polyrotaxanes in which multiple CDs thread onto a polymer chain which may be end-capped with bulky groups as stoppers.[23] The plentiful hydroxy groups of the CDs in the polyrotaxanes allow the attachment of various drug molecules to form drug-polyrotaxane conjugates (Figure 1.6).[78-81] The drug may then be released from drug-polyrotaxane conjugates by either cutting off the stoppers causing disassembly of polyrotaxane[78] or cleavage of the linkage between the drug and polyrotaxane,[81] as shown in Figure 1.6. In addition to the drugs, a cell-penetrating peptide may also be incorporated into drug-polyrotaxane conjugates which greatly improved cellular internalization of drug-polyrotaxane conjugates by cancer cells and, thus, chemotherapy efficacy.[82]

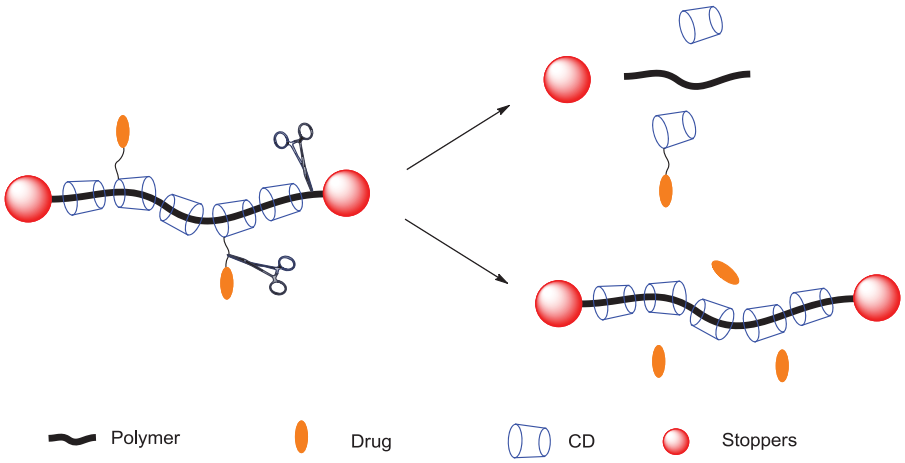

Figure 1.6. Schematic illustration of the structure of drug-polyrotaxane conjugates and drug release.

Nanomaterials, especially those of sub-100 nm size, are appealing drug delivery vehicles in cancer therapy on account of their enhanced permeation and retention, EPR effect for passive tumor targeting.[83] Thus, CDs have been employed to construct supramolecular assemblies or aggregates at the nano-scale to formulate drug species. Ravoo *et al.* have developed CD bilayer vesicles with an average diameter of 100-150 nm on the basis of amphiphilic CDs which contain hydrophilic oligo(ethylene glycol) substituents on the secondary face and hydrophobic linear alkyl substituents on the primary face.[84] In an aqueous mixture of α-CD bilayer vesicles, azobenzene-carbohydrate cross-linkers and lectins, the host-guest complexation between α-CD on the surface of the bilayer vesicles and the azobenzene moiety of azobenzene-carbohydrate cross-linkers and lectin-carbohydrate interactions facilitated formation of ternary complexes (Figure 1.7) in which lectins were buried between α-CD vesicles.[85] Upon UV irradiation at 350 nm, the azobenzene moiety photoisomerized from *trans* to *cis*, which resulted in detachment of the azobenzene-carbohydrate cross-linkers from the α-CD vesicles and further dissociation of ternary complexes. The association and dissociation of the ternary complexes were fully reversible, which held great promise for on-demand release of lectins. A similar design of

ternary complexes has also been used to delivery single-stranded DNA.[86]

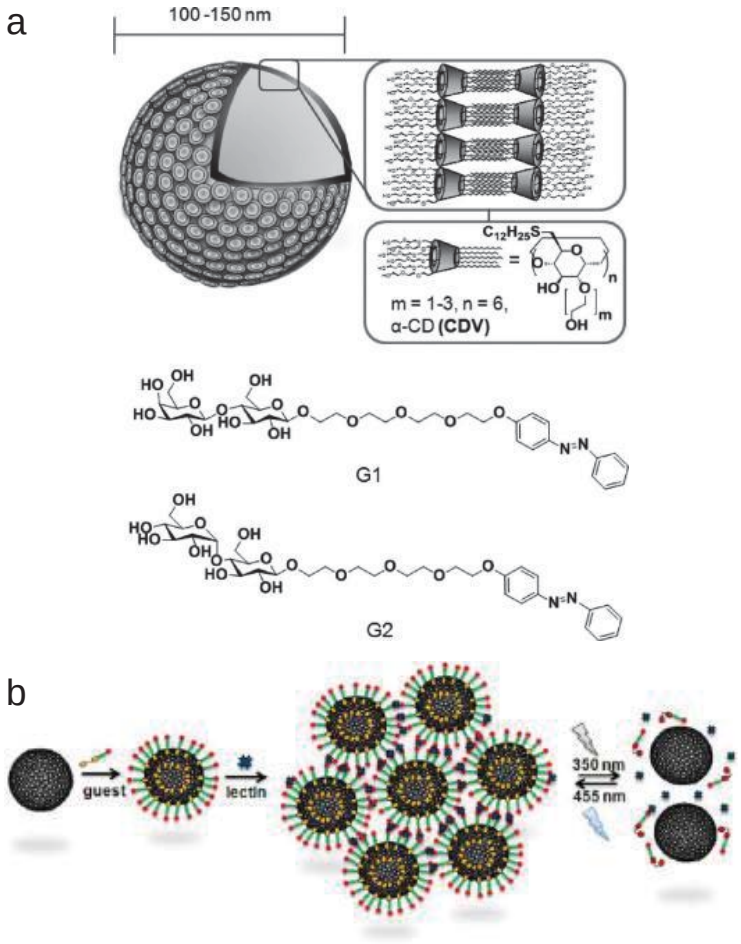

Figure 1.7. (a) Schematic illustration of α-CD bilayer vesicles and molecular structures of amphiphilic α-CD and azobenzene-carbohydrate cross-linkers. (b) Light-responsive association and dissociation of a ternary complex of α-CD bilayer vesicles, azobenzene-carbohydrate cross-linkers and lectins.[85]

In addition to amphiphilic CDs, CD-based polypseudorotaxanes have also been used to construct nanosystems for drug delivery.[87-90] For instance, Ji *et al.* reported a robust and versatile strategy to prepare stable polypseudorotaxane prodrug micelles.[90] In their design, an anti-cancer drug, doxorubicin, DOX, was first grafted onto α-CD through the reaction of α-CD-hydrazide and DOX.HCl in DMSO. When the obtained α-CD-hydrazide-DOX.HCl was mixed with a double-hydrophilic block copolymer, poly(ethylene

glycol)-*b*-poly(2-methacryl-oyloxyethyl phosphorylcholine), PEG-*b*-PMPC, in aqueous solution, stable polypseudorotaxane prodrug micelles were formed through the threading of α-CD-hydrazide-DOX.HCl onto PEG segments of copolymers (Figure 1.8). Fluorescence microscope images clearly showed internalization of the obtained polypseudorotaxane prodrug micelles by human hepatocellular carcinoma cells, HepG2 cells. After cellular uptake, DOX was released at endosomal/lysosomal pH through cleavage of the acid-labile hydrazone bond linker and successfully inhibited growth of cancer cells.

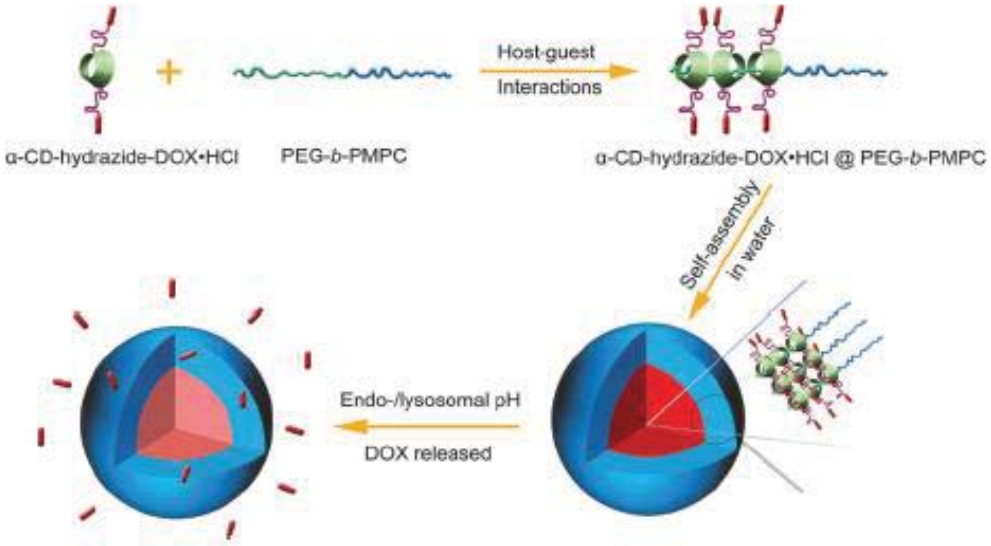

Figure 1.8. Schematic illustration of pseudopolyrotaxane prodrug micelle formation and subsequent release of DOX under endosomal/lyosomal pH.[90]

Apart from nanocarriers based on CD-polypseudorotaxane, host-guest complexation-induced nanosystems have also been intensively explored as drug delivery systems.[91-97] Tseng *et al*. developed a facile way to construct size-tunable supramolecular nanoparticles.[92] Driven by the strong host-guest complexation between β-CD and adamantyl, AD, moieties, three molecular building blocks, adamantyl-substituted polyamidoamine dendrimer, AD-PAMAM, β-CD-substituted branched polyethylenimine, CD-PEI, and adamantyl-substituted poly(ethylene glycol), AD-PEG, self-assembled into supramolecular

nanoparticles (Figure 1.9). Through tuning the mixing ratios of these three different building blocks, the size of obtained supramolecular nanoparticles could be easily controlled, ranging from 30 to 450 nm in diameter. When camptothecin substituted poly(L-glutamic acid), CPT-PGA, was mixed with the previously mentioned three building blocks in aqueous solution, the anticancer drug camptothecin, CPT, was loaded into supramolecular nanoparticles through coulombic interactions between the negatively charged PGA and the positively charged supramolecular nanoparticle.[94] By tuning the mixing ratios of these building blocks, two supramolecular nanopaticles loaded with CPT of 37 and 104 nm in diameter, respectively, were obtained. Positron emission tomography, PET, imaging-based biodistribution studies showed that the 37 nm nanoparticles accumulated in the tumor 100% to a greater extent than the 104 nm nanoparticles.

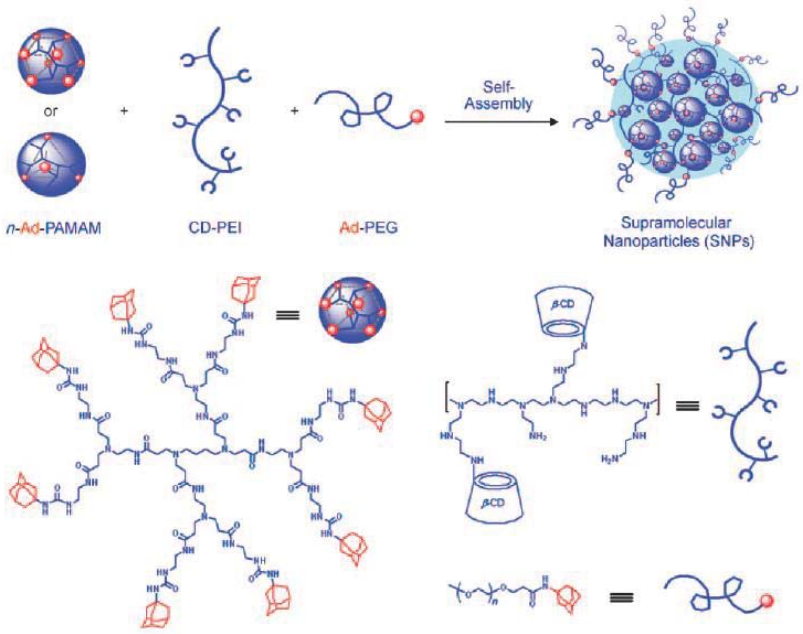

Figure 1.9. Schematic illustration of self-assembly of AD-PAMAM, CD-PEI and AD-PEG into supramolecular nanoparticles and molecular structures of AD-PAMAM, CD-PEI and AD-PEG.[92] (NB. In this Figure taken from the original literature, Ad is used to indicate the adamantyl group, whereas AD is used throughout this thesis.)

In addition to the delivery vehicles of molecular scale, exemplified by the CD dimer and

CD-polymer, and nano-scale delivery systems, exemplified by the amphiphilic CD nano-aggregates and CD-guest complexation-induced nanoparticles, hydrogels containing CD moieties at macroscopic scale have also attracted significant attention in drug delivery applications as is considered in the following section.

1.2. Cyclodextrin-based hydrogels in drug delivery

Hydrogels are three-dimensional cross-linked polymer networks which entrap a great amount of water. Due to high water content and biocompatibility, tunable porous structures and controllable viscoelastic properties, hydrogels are promising drug delivery systems.[98-101] Depending on the nature of their polymer inter-strand cross-links, CD-based hydrogels can be classified into two categories: covalently and non-covalently cross-linked CD-based hydrogels.

1.2.1. Covalently cross-linked cyclodextrin-based hydrogels in drug delivery

1.2.1.1. Covalently cross-linked cyclodextrin networks as drug delivery systems

Cyclodextrins have multiple hydroxy groups, which can react with bi- or multi-functional molecules as cross-linking agents to create cross-linked CD networks (Figure 1.10). Cyclodextrin moieties in the formed CD networks retain host-guest complexation capability which may improve drug loading capacity and control subsequent drug release behaviour. Bi-functional cross-linking agents are exemplified by epichlorohydrin,[102-107] diisocyanates,[108,109] ethyleneglycol diglycidylether[110] and anhydrides.[111] Epichlorohydrin, EPI, is the most commonly used cross-linking agent. It has two reactive groups which can react with hydroxy groups of CDs or other EPI molecules in alkaline media leading to formation of cross-linked CD, CD-EPI, networks. The CD content in the CD-EPI network is influenced by

the molar EPI to CD reaction ratio, reaction temperature, reaction time and concentration of NaOH.[103] The CD moieties in the CD-EPI network preserve their complexation capability and can complex a wide range of hydrophobic drugs.[102] Thus, in the presence of 50 mmol L^{-1} β-CD-EPI network, the aqueous solubility of a nonsteroidal anti-inflammatory drug, naproxen, increased by some 120 times.[104] Cross-linked networks of α-CD/β-CD and β-CD/γ-CD have also been prepared using EPI as a cross-linking agent.[107] Loading of naproxen into these networks was found to be determined mainly by the strength of complexation between the CD component and the drug. The observed sustained release of naproxen from these CD networks was attributable to the complexation of naproxen by the CD moieties.

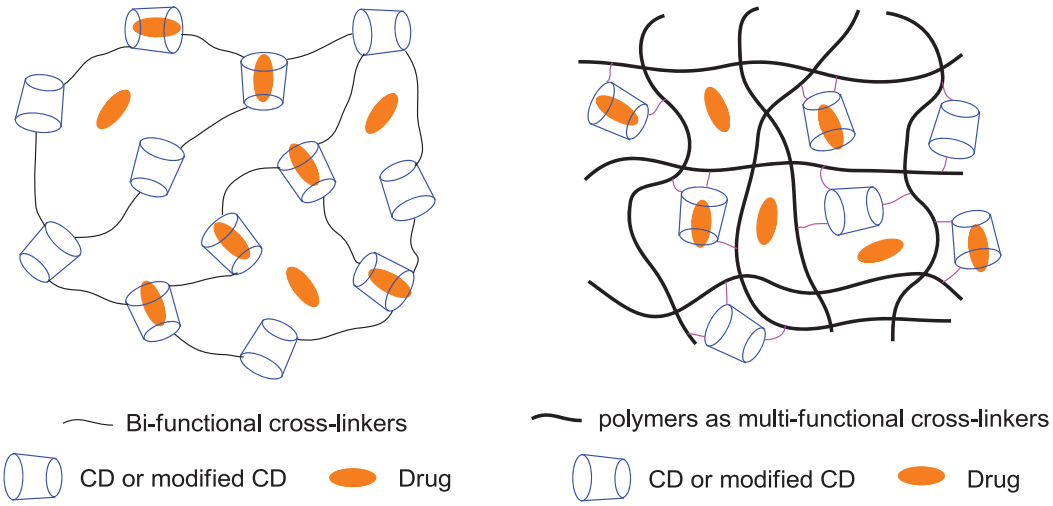

Figure 1.10. Schematic illustration of covalently cross-linked CD networks.

Pre-existing polymers can be used as multi-functional cross-linking agents to prepare CD/polymer or modified CD/polymer networks.[112-117] Ross *et al.* developed cross-linked networks by coupling either β-CD or hydroxypropyl β-CD (HPβ-CD) and poly(acrylic acid), PAA, through esterification of the hydroxy groups of β-CD or HPβ-CD with the carboxylic acid groups of PAA.[115] They characterized the complexation between β-CD moieties in the

β-CD/PAA and HPβ-CD/PAA networks and two drugs, diflunisal and fluconazole, by complexation constants determined using ^{19}F NMR spectroscopy. Release of the two drugs from β-CD/PAA and HPβ-CD/PAA networks were found to be regulated by drug complexation by the β-CD moieties in these two networks. Li *et al.* prepared β-CD/gelatin cross-linked networks and found that the loading level of an anti-cancer drug, methotrexate, MTX, increased with increase in β-CD content in the β-CD/gelatin network due to complexation of MTX by the network β-CD moieties which resulted in a sustained MTX release profile.[116]

1.2.1.2. Covalently cross-linked polymer networks containing cyclodextrin pendant groups as drug delivery systems

In contrast to CDs being involved in cross-links, CDs can also be grafted into polymer networks as pendant groups, as shown in Figure 1.11. This type of polymer network is commonly synthesized by copolymerization of a vinyl modified CD monomer with other vinyl monomers.[110,118-120] Liu and Fan prepared cross-linked poly(2-hydroxyethyl acrylate), PHEA, networks containing β-CD pendant groups through copolymerization of glycidyl methacrylate modified β-CD and 2-hydroxyethyl acrylate initiated with an ammonium persulfate/sodium bisulfite redox system.[119] Incorporation of β-CD into PHEA networks exhibited a negative role in hydrogel swelling, because of the rigidity and large volume of β-CD reducing network flexibility. By comparison with its rapid release from the β-CD-free PHEA network, sustained release of the drug, *N*-acety-5-methoxytryptamine, occurred from the PHEA network containing β-CD pendant groups which was ascribed to complexation of drug molecules by these β-CD pendant groups in the network. Siemoneit *et al.* reported the preparation of acrylic acid/γ-CD hydrogels through free radical polymerization of sodium

acrylate, acrylamidomethyl-γ-CD and *N,N'*-methylene-(bisacrylamide).[120] A hydrophobic drug, triamcinolone acetonide, TA, was selected to evaluate drug loading capacity and drug release behaviour of this hydrogel. A 55-fold enhancement of TA loading and 3-fold retardation of TA release were observed for these acrylic acid/γ-CD hydrogels as a consequence of the complexation of TA by γ-CD, by comparison with γ-CD-free acrylic acid hydrogels.

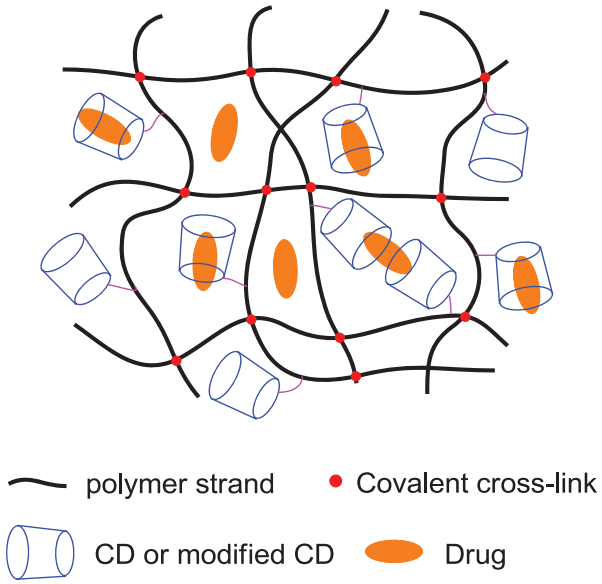

Figure 1.11. Schematic illustration of covalently cross-linked polymer networks containing CD pendant groups.

1.2.2. Physically cross-linked cyclodextrin-based hydrogels in drug delivery

Covalently cross-linked hydrogels generally have significant mechanical strength due to covalent bonds acting as cross-links. Thus, they are promising materials for implantable devices. However, there are several intrinsic disadvantages limiting their application range in drug delivery. Firstly, the cross-linking reaction may involve toxic cross-linkers. Secondly, the loading of drug by sorption is often time-consuming. Additionally, the covalently cross-linked hydrogels may also be non-biodegradable and of ill-defined composition.

Therefore, physically cross-linked hydrogels have attracted much attention as drug delivery systems, not only because they achieve gelation and drug loading simultaneously, but also due to potential stimuli-responsiveness to facilitate controlled drug delivery.[121,122] Physically cross-linked CD-based hydrogels can be broadly divided into two categories: polypseudorotaxane hydrogels and hydrogels cross-linked by CD-guest complexation.

1.2.2.1. Polypseudorotaxane hydrogels as drug delivery systems

A vast majority of polypseudorotaxane hydrogels are formed between α-CD and poly(ethylene glycol) (PEG), with a few exceptions such as β-CD/poly(propylene glycol)[123] or γ-CD/PEG.[124,125] In aqueous media, multiple α-CDs thread onto a single PEG chain to form polypseudorotaxanes and subsequent entanglement or aggregation of α-CD/PEG polypseudorotaxane segments driven by hydrogen bonding and crystallite formation leads to formation of α-CD/PEG hydrogels (Figure 1.12).[126] As α-CD and PEG are biocompatible, α-CD/PEG hydrogel systems have attracted extensive attention as drug delivery systems. In addition, the viscosity of α-CD/PEG hydrogels significantly decreases under shear stress and regain their original viscosity after shear stress removal.[121] This thixotropic property makes α-CD/PEG hydrogels excellent candidates for injectable drug delivery systems.

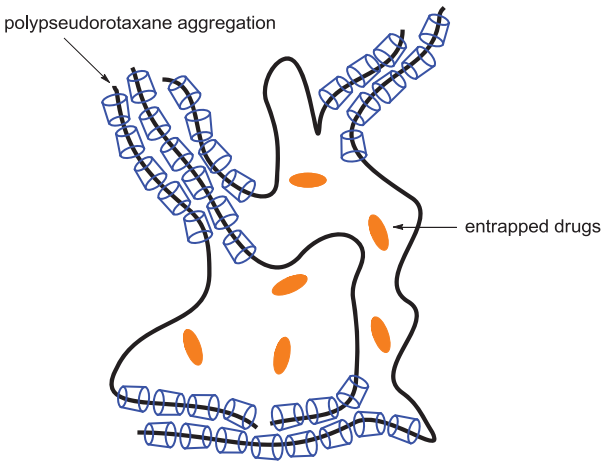

Figure 1.12. Schematic illustration of polypseudorotaxane hydrogels with entrapped drugs.

Harada *et al.* first reported the formation of α-CD/PEG hydrogels in 1994.[127] These researchers found that α-CD/PEG hydrogels formed only if molecular weight of PEG was higher than 2000 g mol^{-1}. Otherwise, the PEG chain was fully encapsulated by α-CD which resulted in precipitation. In another study, fluorescein isothiocyanate-labeled dextran, dextran-FITC, was selected as a drug model to evaluate the drug delivery properties of α-CD/PEG hydrogels.[128] Through mixing α-CD, PEG and dextran-FITC in aqueous media, dextran-FITC loaded α-CD/PEG hydrogels were formed *in situ* at room temperature. The molecular weight of PEG substantially affected stability of the formed hydrogel, thereby also affecting the release rate of dextran-FITC. The release rate decreased rapidly as the molecular weight of PEG increased up to 35,000 g mol^{-1}. This was attributable to changes in the chain entanglement effect and different complex stability within α-CD/PEG. It was found that in order to prolong drug release, it is critical to use high molecular weight PEG (> 10,000 g mol^{-1}).

The requirement of high molecular weight PEG (> 10,000 g mol^{-1}) is problematic because PEG is not biodegradable and is difficult to be eliminated from the human body as its molecular weight increases. Thus, in order to reinforce hydrogel mechanical properties and stability, additional cross-linking interactions have been incorporated (Figure 1.13), such as hydrophobic interaction[129] and hydrogen bonding.[130] This strategy avoids the usage of high molecular weight PEG to obtain stronger mechanical properties. Li *et al.* reported hydrogel formation between α-CD and an amphiphilic triblock copolymer, poly(ethylene glycol)-poly[(*R*)-3-hydroxybutyrate]-poly(ethylene glycol), PEG-PHB-PEG, in which the PEG block is around 5000 g mol^{-1} in molecular weight and the PHB block is biodegradable.[129] The aggregation of polypseudorotaxane α-CD/PEG segments and hydrophobic interactions between PHB blocks resulted in a strong cross-linked polymer

network. In contrast to a α-CD/PEG (PEG of molecular weight 35,000 g mol^{-1}) hydrogel sustaining dextran-FITC release for 5 days, the α-CD/PEG-PHB-PEG hydrogel sustained dextran-FITC release for around 30 days. Alternatively, Dong *et al.* incorporated hydrogen bonding to strengthen the polymer network.[130] They designed a di-block copolymer, poly(L-glutamic acid)-*block*-poly(ethylene glycol), PLG-PEG, with a PEG block of around 5000 g mol^{-1}. Upon addition of α-CD, hydrogen bonding interactions among PLG segments and the aggregation of polypseudorotaxane α-CD/PEG segments induced formation of a polymer network. These α-CD/PLG-PEG hydrogels exhibited high loading content of 10% of the anti-cancer drug, doxorubicin hydrochloride, DOX, and sustained DOX release for 45 days.

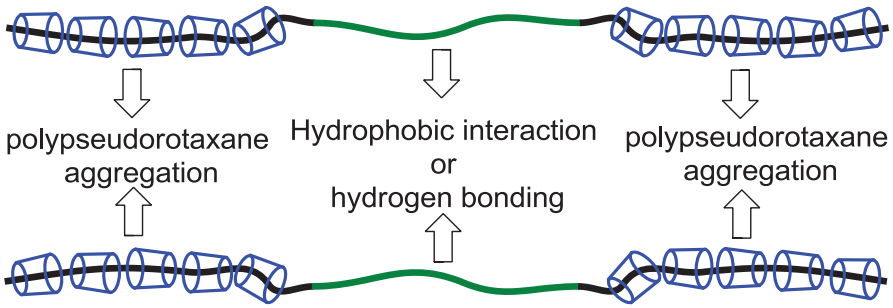

Figure 1.13. Schematic illustration of polypseudorotaxane hydrogels formed by α-CD and a triblock copolymer, PEG-polymer-PEG.[129,130]

Aggregation of the α-CD/PEG polypseudorotaxane is also used to cross-link some biodegradable hydrophilic polymer networks, such as dextran[131] and chitosan.[132] Poly(ethylene glycol) of molecular weight 2000 g mol^{-1}, although unable to form a hydrogel with α-CD, was grafted onto dextran or chitosan as side groups. Upon addition of α-CD, the α-CD/PEG polypseudorotaxane formed and aggregated leading to either cross-linked dextran or chitosan networks.[131,132] Several hybrid hydrogels containing PEG grafted nanomaterials,

such as gold[133] and silica[134] nanoparticles, have also been reported. Inspired by the dynamic nature of the cross-link, Jiang *et al.* reported a light responsive α-CD/PEG hydrogel.[135] When α-CD and PEG of molecular weight 10,000 g mol^{-1} were mixed in aqueous media, multiple α-CDs threaded onto a single PEG chain to form polypseudorotaxanes. Subsequently, α-CD/PEG polypseudorotaxane segments entangled or aggregated to form a α-CD/PEG hydrogel. After the addition of a modified azobenzene, 1-[p-(phenyl-azo)benzyl]pyridinium bromide, Azo-C1-N^+, the competitive host-guest complexation between α-CD and *trans*-azobenzene moieties of Azo-C1-N^+ resulted in the de-threading of α-CD from PEG chains and thus the dissociation of the α-CD/PEG hydrogel. However, after UV irradiation, the azobenzene moieties of Azo-C1-N^+ photoisomerized from *trans* to *cis*, which escaped from α-CD inner cavities. Therefore, α-CD complexed PEG chains again leading to the regeneration of α-CD/PEG hydrogel. The light-responsive sol-gel and gel-sol transitions could be repeated for cycles.

1.2.2.2. Hydrogels cross-linked by host-guest complexation as drug delivery systems

Hydrogel networks may also be cross-linked by host-guest complexation between a CD and a guest. Thus, when CDs are covalently substituted onto a polymer strand to form the host polymer and an appropriate guest is substituted onto a second polymer strand to form the guest polymer, host-guest complexation forms cross-links between the polymer strands to give a hydrogel network in aqueous solution as shown in Figure 1.14. (The backbones of the polymer strands in the host and guest polymers can be the same or different.) Due to strong complexation characterized by a high complexation constant of 10^4 dm^3 mol^{-1} magnitude,[136] β-CD/adamantane (β-CD/AD) complexation has been widely used to cross-link poly(acrylate),[137-140] chitosan[141] and hyaluronic acid[142] networks by this method. For instance,

Lincoln *et al.* used poly(acrylate) substituted with β-CD as the host polymer and poly(acrylate) substituted with AD as the guest polymer to prepare cross-linked poly(acrylate) networks. The length of the tether grafting either β-CD or AD groups onto poly(acrylate) backbones were found to substantially affect β-CD/AD complexation and the respective extent of intra- and inter-molecular interactions.[137-140] Additionally, stimuli responsive association and dissociation of the α-CD/azobenzene,[143,144] β-CD/azobenzene[145] and β-CD/ferrocene[146-148] complexes have been used to create stimuli responsive hydrogels, exhibiting stimuli responsive sol-gel transition, which potentially allowed for release of drugs in a controlled manner.

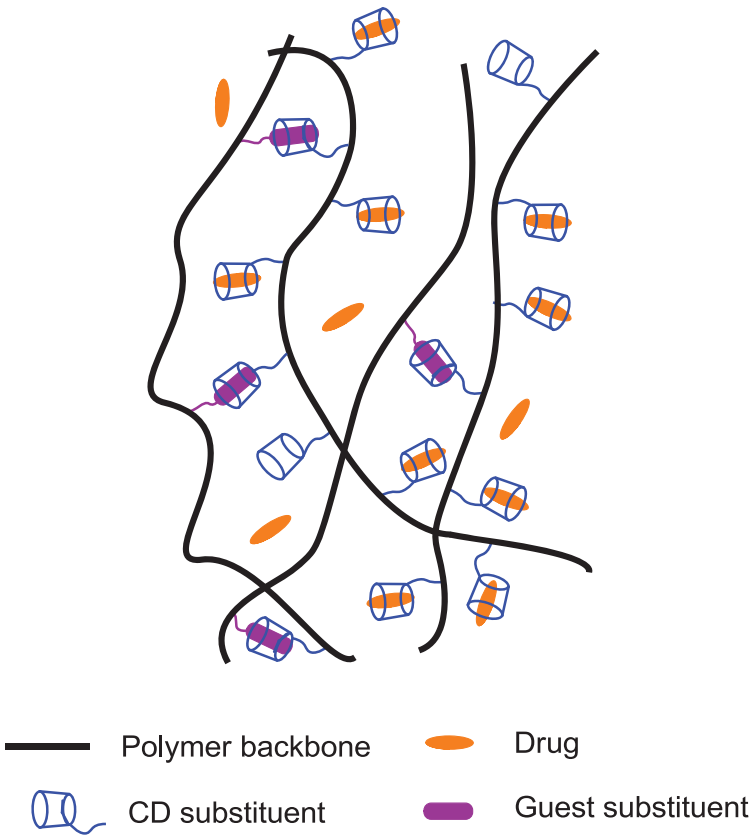

Figure 1.14. Representation of polymer networks cross-linked by CD-guest complexation and entrapped drugs either in free state or complexed by CD substituents.

In polymer networks cross-linked by CD-guest complexation, CD substituents may also be able to complex hydrophobic drug species, as shown in Figure 1.14. Complexation of drug

species by CD substituents may improve drug loading capacity and sustain subsequent drug release to some extent, depending on complexation strength. Thus, polymer networks cross-linked by CD-guest complexation have been utilized in drug delivery.[145,149-151] Amiel *et al.* examined the performance of an associative network based on β-CD/AD complexation for drug delivery and selected poly[(methyl vinyl ether)-*alt*-(maleic acid)] substituted with β-CD groups, P(MVE-MA)-*g*-β-CD, as the host polymer and dextran substituted with adamantyl, AD, groups, dext-AD, as the guest polymer.[150] In their study, a polymer network formed through complexation of AD substituents by β-CD substituents, and was characterized by a high complexation constant of 2×10^4 dm^3 mol^{-1} as determined by isothermal titration calorimetry, ITC. The loading capacity for a hydrophobic drug, benzophenone, Bz, was found to increase as the number of β-CD substituents increased. This was consistent with the complexation of Bz by β-CD substituents enhancing loading capacity of the polymer network. A sustained release of Bz over a period of 11 days was observed, mainly due to the complexation of Bz by β-CD substituents retarding Bz release from the network. Kros *et al.* created a light responsive β-CD- and azobenzene- substituted dextran hydrogel system as a controlled protein delivery system as shown for the green fluorescent protein, GFP.[145] The network was formed through complexation of *trans*-azobenzene substituents by β-CD substituents. Upon UV light irradiation, *trans*-azobenzene photoisomerized to *cis*-azobenzene, resulting in dissociation of the network and the release of GFP. Thus, in contrast to 10% of GFP being released after 60 minutes without UV light irradiation, a significantly faster release was observed under UV light irradiation and 40% of GFP was released within 60 minutes. Thus, this light responsive hydrogel system is a possible basis for the design of controlled protein or drug delivery systems where UV light is applicable.

1.3. Conjugated polymer nanoparticles in biological applications

Conjugated polymer nanoparticles, CPNPs, are promising fluorescent probes due to their outstanding photoluminescence properties. Frequently used conjugated polymers are exemplified by polyfluorene, PDOF and PDHF, fluorine-based copolymers, PFBT and PFPV, poly(phenylene ethynylene), PPE and poly(phenylene vinylene). MEHPPV, whose molecular structures are shown in Figure 1.15. Conjugated polymer nanoparticles made from these polymers generally show wide UV-Vis absorption wavelength ranges. At specific wavelengths, they exhibit high light-harvesting capacity characterized by a high absorption cross section. The peak absorption cross section of single particle of approximately 15 nm diameter, made from either PDOF, PPE, PFPV, PFBT or MEHPPV, was reported to be of a magnitude around 10^{-13} cm^2, 10 to 100 times larger than that of CdSe quantum dots and 1000 times larger than typical organic dyes.[152] Conjugated polymer nanoparticles have been developed with emissions ranging from the visible to near-infrared (NIR) regions, exhibiting fluorescence quantum yields from 1% to 60% depending on the identity of the polymer.[152-159] Fluorescence brightness can be evaluated using the product of peak absorption cross section and fluorescence quantum yield. In terms of this parameter, PFBT NPs of ~ 10 nm diameter have been found to be around 30 times brighter than two commonly used fluorescent probes, IgG-Alexa 488 and Qdot 565, at an excitation wavelength of 488 nm.[160] In addition to high fluorescent brightness, CPNPs also show a fast fluorescence emission rate, paving the way for high speed applications, such as flow cytometry. The photostability of a fluorescent probe is another salient consideration and can be evaluated from its photobleaching quantum yield. By comparison with photobleaching quantum yields of typical organic dyes ranging from 10^{-4} to 10^{-6},[161] photobleaching quantum yields of CPNPs, made from either PDOF, PPE, PFPV, PFBT or MEHPPV, of ~ 15 nm diameter are 10^{-8} to 10^{-10}.[152] This indicates that CPNPs have

much higher photostability than conventional fluorescent dyes. In summary, CPNPs exhibit a large absorption cross section, high fluorescence brightness and photostability, all of which make them excellent fluorescent probe candidates.

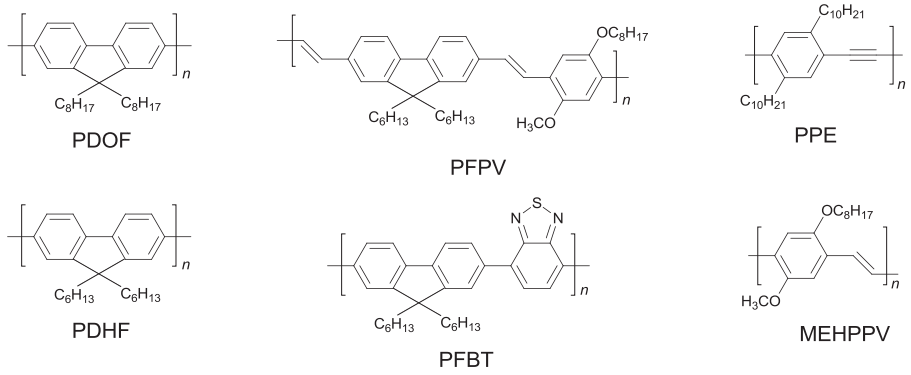

Figure 1.15. Molecular structures of frequently used conjugated polymers.

1.3.1. Preparation methods for conjugated polymer nanoparticles

Typical methods for the preparation of CPNPs include mini-emulsion and nano-precipitation techniques.[162] In the mini-emulsion method, conjugated polymers are first dissolved in a water-immiscible organic solvent, such as chloroform and dichloromethane. The resulting conjugated polymer solution is then added to a surfactant solution, such as sodium dodecyl sulphate, SDS, under ultrasonication, and the CPNPs are formed in the emulsified droplet solution. After removal of the organic solvent and excessive surfactants, a stable dispersion of CPNPs is obtained. Landfester *et al.* have used the mini-emulsion process to prepare several CPNPs of spherical morphologies and sizes between 75 and 150 nm.[163] The size of CPNPs is determined by the concentration of conjugated polymers in the chloroform and of SDS in the aqueous solution. Generally, a lower concentration of conjugated polymers in chloroform and higher concentration of SDS in aqueous solution yielded smaller particle sizes.

In a typical nano-precipitation process, conjugated polymers are first dissolved in a water-miscible organic solvent, such as tetrahydrofuran, THF. After mixing the conjugated polymer solution and water, a decrease in conjugated polymer solubility and hydrophobic interactions within and between conjugated polymer chains cause aggregation of conjugated polymer chains and the formation of CPNPs.[162] After evaporation of the organic solvent, a stable aqueous dispersion of CPNPs is obtained. Particle size can be easily tuned by controlling the concentration of conjugated polymers in the precursor solution. Conjugated polymer nanoparticles prepared by the nano-precipitation method normally have small sizes between 5 to 60 nm and spherical morphologies.[152,162,164] Aqueous dispersions of CPNPs are stable for months. Kee *et al.* ascribed this to surface chemical defects as a consequence of oxidation of the conjugated polymer in the formation of CPNPs, leading to negatively charged surfaces.[165] In order to provide surface reactive sites for incorporation of functional biomolecules, Chiu *et al.* developed a modified nano-precipitation method.[160,166] Thus, amphiphilic polymers with functional groups were mixed with conjugated polymers in a THF solution, which was then rapidly injected into deionized water. In the resultant CPNPs, the hydrophobic segments of the amphiphilic polymers are most likely inserted into the hydrophobic conjugated polymer core while the hydrophilic segments bearing functional groups are located on the surface and supply reactive sites for further bioconjugation.

In addition to the two popular methods discussed above, Park *et al.* introduced the preparation of CPNPs from phase-separated films of phospholipids and conjugated polymers.[167] These researchers first made a phased-separated thin film of poly[2,6-(4,4-bis-(2-ethylhexyl)-4H-cyclopenta[2,1-b; 3,4-b']-dithiophene)-alt-4,7-(2,1,3-benzothiadiazole)], PCPDTBT, and a phospholipid. The formation of phase-separated morphology occurred due to immiscibility between the hydrophobic PCPDTBT and charged heads of the phospholipid. In the presence of water, the thin film was broken by the

penetration of water molecules because of the existence of these phospholipid charged heads. Thus, aqueous dispersions of PCPDTBT/phospholipid nanoparticles of ~60 nm diameter was obtained.

1.3.2. Conjugated polymer nanoparticles in biological applications

High photoluminescence and small size are properties that drive the exploration of CPNPs in biological applications. However, toxicity of CPNPs is an important issue in terms of biological applications. Dailey *et al.* examined the toxicity of F8BT NPs (F8BT, poly[(9,9-di-noctylfluorenyl-2,7-diyl)-alt-(benzo [2,1,3] thiadiazol-4,8-diyl)]) against J774A.1 cells using MTT assay.[168] The F8BT NPs were found to exhibit negligible toxicity towards J774A.1 cells after 24 h incubation. Negligible toxicity of F8BT NPs towards J774A.1 cells was also reported by Christensen *et al.*[169] In addition, the toxicity of PPE NPs (PPE, poly(*p*-phenylene ethynylene)) to BHK cells was evaluated by Moon *et al.* using the CellTiter-Glo assay kit showing that PPE NPs exhibit minimal viability inhibition towards BHK cells after incubation of 7 days.[170] Thus, high biocompatibility of CPNPs paves the way for biological applications.

As CPNPs exhibit high fluorescent brightness and photostability, they have been used as fluorescent probes in cell imaging application. McNeill *et al.* examined the feasibility of multicolour CPNPs in intracellular imaging and found that CPNPs were successfully internalized by J774.A1 macrophages.[152] Thus, these CPNPs showed great potential for use as bright fluid phase markers of pinocytosis. Further studies on cellular uptake mechanisms revealed that PFBT NPs were internalized by J774.A1 cells through constitutive macropinocytosis rather than clathrin-dependent or caveolin-dependent mechanisms.[169] As the cellular uptake of CPNPs is a non-specific process, intracellular imaging lacks specificity. In order to address this issue, Chiu *et al.* prepared PFBT NPs with surface carboxylic acid

groups, which were further functionalized by streptavidin.[160] (Streptavidin is a common reagent used to specifically label a cellular target due to its strong binding with biotin.) Then MCF-7 cells with an epithelial cell adhesion molecule (EpCAM) on their surfaces were incubated with PFBT NPs functionalized with streptavidin, the primary anti-EpCAM antibody and biotinylated goat anti-mouse IgG secondary antibody. Fluorescence images (Figure 1.16a) clearly showed that PFBT NPs functionalized with streptavidin could specifically label EpCAM on the surface of MCF-7 cells, but only in the presence of biotinylated goat anti-mouse IgG secondary antibody. These results highlighted the ability of PFBT NPs functionalized with streptavidin to specifically label a cellular target. Additionally, CPNPs with near-infrared, NIR, emission have also been developed for cell imaging applications. Based on the donor-acceptor concept, Chan *et al.* synthesized conjugated polymers with NIR emission through polymerization of fluorene (electron-donating units) with a series of quinoxaline-based monomers (electron-accepting units) as NIR emitters.[159] The corresponding CPNPs were also functionalized with streptavidin and could specifically label the surface target of HeLa cells.

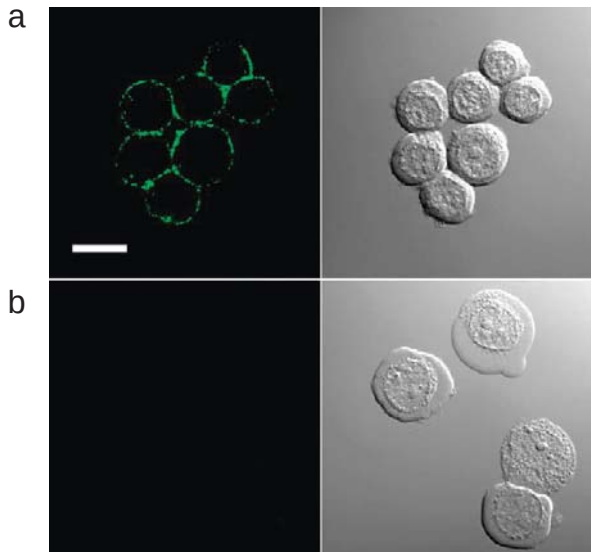

Figure 1.16. The fluorescence (Left) and differential interference contrast (Right) image of MCF-7 cells incubated with streptavidin-modified PFBT NPs and the primary anti-EpCAM antibody, in the presence (a) and absence (b) of biotinylated goat anti-mouse IgG secondary antibody.[160]

Along with cell imaging applications, CPNPs are also widely used to construct biological sensors. The common working mechanism is based on Förster resonance energy transfer, FRET. Appropriate functional modalities with emissions sensitive to either analyte level or environmental change are integrated into CPNPs through doping, surface conjugation or covalent attachment to conjugated polymer backbones. Efficient FRET from conjugated polymers results in highly bright emissions of functional modalities, responsive to analyte level or environmental change. CPNPs have been used to construct ratiomeric pH,[171,172] temperature,[173] oxygen,[174,175] fluoride[176] and mercury[177] sensors. McNeil *et al.* developed PDHF NPs (PDHF, poly(9,9-dihexylfluorene)) doped with platinum octaethylporphine (PtOEP) as an oxygen sensor (Figure 1.17a), in which PtOEP served as oxygen-sensitive modalities.[174] Upon excitation with 350 nm wavelength of light where PtOEP had negligible absorption, FRET occurred efficiently from PDHF to PtOEP leading to bright phosphorescence highly sensitive to dissolved oxygen level. As shown in Figure 1.17b,

nitrogen-saturated aqueous dispersion of PDHF NPs doped with PtOEP showed an intense red emission. In contrast, aqueous dispersion of PDHF NPs doped with PtOEP saturated with air or oxygen exhibited very weak emission, as a consequence of oxygen quenching phosphorescence of PtOEP. In addition to the doping strategy, Chiu *et al.* covalently conjugated a pH-sensitive dye, fluorescein, to the surface of PPE NPs (PPE, poly(2,5-di(3',7'-dimethyloctyl)phenylene-1,4-ethynylene)).[171] Efficient FRET from PPE to fluorescein resulted in pH-sensitive bright fluorescein emission. As fluorescein emission of PPE remained constant under pH ranges from 5.0 to 8.0, the ratio of fluorescein emission intensity to PPE emission intensity exhibited linear variation with pH change from 5.0 to 8.0. Thus, PPE NPs with surface conjugation of fluorescein served as a ratiometric pH sensor. Very recently, Dmitriev *et al.* used a polyfluorene copolymer containing metalloporphyrin moieties in the copolymer backbones to prepare nanoparticles.[175] In the resultant copolymer NPs of 30-100 nm diameter, polyfluorene served as a FRET antenna and phosphorescent metalloporphyrin moieties served as oxygen sensing modalities. Under both one- and two-photon excitation modes, efficient FRET from the antenna resulted in high brightness and oxygen-sensitive phosphorescence of metalloporphyrin moieties, making copolymer NPs promising cellular oxygen sensors.

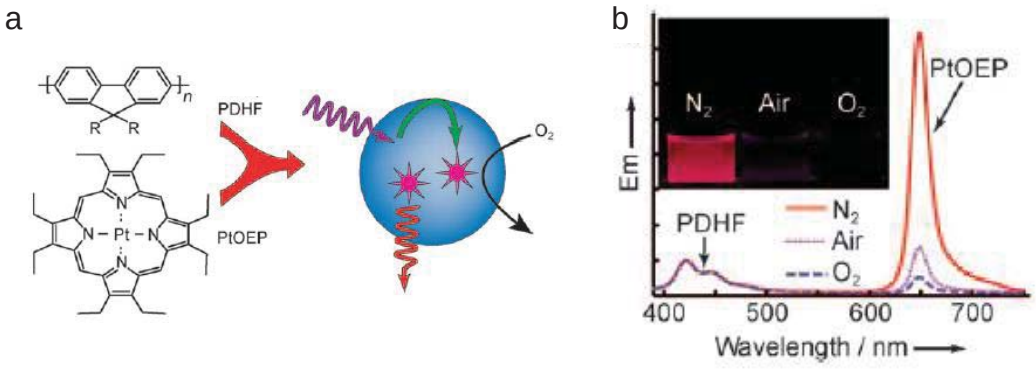

Figure 1.17. (a) Schematic illustration of PDHF NPs doped with PtOEP for oxygen sensing. (b) Oxygen-dependent emission spectra of PDHF NPs doped with PtOEP (excitation wavelength = 350 nm). The inset shows photographs of aqueous dispersions of PDHF NPs doped with PtOEP saturated with nitrogen, air and oxygen, respectively, under a UV lamp.[174]

Conjugated polymer nanoparticles have also been used to construct therapeutic platforms, serving as drug delivery vehicles,[178] photothermal[179] and photodynamic[180] therapy agents. For instance, Wang *et al.* prepared CPNPs for delivery of the anti-cancer drug, doxorubicin.[178] The formation of CPNPs was due to the electrostatic interactions between cationic poly(fluorene), PFO, and anionic poly(L-glutamic acid) substituted with doxorubicin, PG-Dox. When PFO/PG-Dox NPs were exposed to carboxypeptidase or internalized by cancer cells, hydrolysis of poly(L-glutamic acid) caused the release of doxorubicin. As a consequence, doxorubicin quenched the fluorescence of PFO, the release of doxorubicin could be monitored by the fluorescence "turn-on" signals of PFO. The use of CPNPs in photothermal tumor therapy was exemplified by Liu *et al,*[179] who used a conjugated polymer, poly[9,9-bis(4-(2-ethylhexyl)phenyl)fluorene-alt-co-6,7-bis(4-(hexyloxy)phenyl)-4,9-di(thiophen-2-yl)-thiadiazoloquinoxaline, PFTTQ, with strong near-infrared, NIR, absorption and high heat conversion efficiency and 1,2-distearoyl-*sn*-glycero-3-phosphoethanolamine-*N*-[methoxy(polyethylene glycol)-2000], DSPE-PEG_{2000}, as a coating material for nanoparticle preparation. The obtained PFTTQ NPs coated with DSPE-PEG_{2000} exhibited a large NIR absorption coefficient of 3.6 L g^{-1} cm^{-1}. Consequently, the temperature of aqueous dispersions of PFTTQ NPs coated with DSPE-PEG_{2000} (0.5 mg/mL) increased from 22 °C to 52 °C within 10 minutes under 808 nm laser irradiation (0.75 W/cm^2). In contrast, under the same conditions the temperature of pure water only increased from 22 °C to 31 °C. These PFTTQ NPs coated with DSPE-PEG_{2000} showed negligible toxicity to both MDA-MB-231 and HeLa cells. However, upon laser irradiation for 10 minutes, over 80% of these cells were killed. This indicated efficient photothermal tumor therapy of the PFTTQ NPs coated with DSPE-PEG_{2000}. Xu *et al.* demonstrated use of CPNPs doped with photosensitizer for photodynamic therapy in cancer cells.[180] Efficient FRET from the conjugated polymer to the photosensitizer remarkably enhanced the efficiency of singlet oxygen generation by

two-photon excitation and, thereby, two-photon photodynamic tumor therapy activity.

1.4. Research aims

Polymer networks are appealing biomaterials for drug delivery due to their biocompatibility and porous structures. The introduction of cyclodextrins into polymer networks offers potential for improvement in drug loading capacity and the benefit of modulating subsequent drug release behaviour due to host-guest complexation of drug molecules by cyclodextrins.

Chapter 2 explores the properties of self-assembled poly(acrylate) networks cross-linked by host-guest complexation between β-CD substituents and adamantyl (AD) substituents as sustained drug delivery systems in terms of dye complexation and release behavior. Poly(acrylate)s substituted with β-CD is used as the host polymer and poly(acrylate)s substituted with AD groups through three tethers with varied length are used as the guest polymers. The host-guest complexation of AD substituents by β-CD substituents are studied by isothermal titration calorimetry, ITC, and 2D NOESY ^{1}H NMR. The thermodynamic parameters and possible complexation modes are used to evaluate the effect of tether length on the complexation of AD substituents by β-CD substituents. The complexation of three dyes, as drug models, by β-CD substituents in the self-assembled poly(acrylate) networks is studied by UV-Vis spectroscopic titrations and 2D NOESY ^{1}H NMR. The effects of the substitution of β-CD onto the poly(acrylate) backbone and the subsequent networks on dye complexation are compared with dye complexation by native β-CD. The macroscopic viscosities of aqueous poly(acrylate) networks in the absence and presence of three dyes is determined by rheological measurements. The dye release profiles from aqueous poly(acrylate) networks and related systems are studied to clarify the effect of dye

complexation by β-CD substituents.

Chapter 3 describes the aqueous β-CD- and octadecyl (C18)-substituted poly(acrylate) network in sustained drug delivery. The host-guest complexation of C18 substituents by β-CD substituents is studied by isothermal titration calorimetry, ITC, and 2D NOESY ^{1}H NMR. Six dyes are used as drug models to explore the complexation capability of β-CD substituents in the poly(acrylate) network. The complexation of dyes by β-CD substituents in the formed poly(acrylate) network is studied by UV-Vis and fluorescence spectroscopic titrations and 2D NOESY ^{1}H NMR. The viscosities of aqueous β-CD- and C18-substituted poly(acrylate) network with and without dyes are determined by rheological measurements. The release behaviours of dyes from the network and related systems are characterized.

Conjugated polymer nanoparticles have emerged as promising fluorescent probes due to their outstanding characteristics, such as high brightness and photostability. However, these nanoparticles exhibit large-scale aggregation and precipitation at the high ionic strengths encountered under physiological conditions, which presents an impediment to their biological applications.

Chapter 4 demonstrates the preparation of highly stable and fluorescent conjugated polymer nanoparicles stabilized with hydrophobic linear alkyl substituted poly(acrylate)s (PAAC*n*) and their uses in cell imaging. A green-yellow emitting conjugated polymer, poly[9,9-dioctylfluorenyl-2,7-diyl-alt-co-(1,4-benzo-[2,1,3]-thiadiazole)], F8BT, is used to examine the effectiveness of the stabilizing material, PAAC*n*. A nano-precipitation method is used to prepare F8BT nanoparticles stabilized with PAAC*n*, F8BT-PAAC*n* nanoparticles. The length and substitution percentage of the alkyl substituents and the usage of PAAC*n* is optimized according to the preparation yield of F8BT-PAAC*n* nanoparticles. The hydrodynamic diameters, particle morphologies, zeta potential and long-term colloidal stability of F8BT-PAAC*n* nanoparticles are measured. Optical properties, including

absorption and fluorescence spectra and fluorescence quantum yields, of the F8BT-PAAC*n* nanoparticles are investigated. The toxicity of F8BT-PAAC*n* nanoparticles is characterized using the MTT assay and the internalization of F8BT-PAAC*n* nanoparticles by cells is evaluated by fluorescence confocal microscopy techniques.

Chapter 5 describes the use of bovine serum albumin, BSA, as stabilizers for multicolour conjugated polymer nanoparticles, CP-BSA nanoparticles. Three conjugated polymers, poly(9,9-dioctylfluorenyl-2,7-diyl), PDOF, poly[(9,9-dioctylfluorenyl-2,7-diyl)-alt-co-(1,4-benzo-[2,1,3]-thiadiazole)], F8BT, and poly[2-methoxy-5-(2-ethylhexyloxy)-1-4-phenylenevinylene], MEHPPV, are used. These CP-BSA nanoparticles are prepared using a nano-precipitation method. The physical properties, such as the size, zeta potential and colloidal stability, and the optical properties including the absorption and fluorescence spectra and fluorescence quantum yields of these CP-BSA nanoparticles are reported.

1.5. References

(1) Lehn, J.-M. Supramolecular chemistry — Scope and perspectives molecules, supermolecules, and molecular devices (Nobel Lecture). *Angew. Chem. Int. Ed.* **1988,** *27*, 89-112.

(2) Lehn, J.-M. Perspectives in supramolecular chemistry — From molecular recognition towards molecular information processing and self-organization. *Angew. Chem. Int. Ed.* **1990,** *29*, 1304-1319.

(3) Coulston, R. J.; Onagi, H.; Lincoln, S. F.; Easton, C. J. Harnessing the energy of molecular recognition in a nanomachine having a photochemical on/off switch. *J. Am. Chem. Soc.* **2006,** *128*, 14750-14751.

(4) Sun, H.-L.; Chen, Y.; Zhao, J.; Liu, Y. Photocontrolled reversible conversion of nanotube and nanoparticle mediated by β-cyclodextrin dimers. *Angew. Chem. Int. Ed.* **2015,** *54*, 9376-9380.

(5) Miyamae, K.; Nakahata, M.; Takashima, Y.; Harada, A. Self-healing, expansion-contraction, and shape-memory properties of a preorganized supramolecular hydrogel through host-guest interactions. *Angew. Chem. Int. Ed.* **2015,** *54*, 8984-8987.

(6) Crini, G. Review: A history of cyclodextrins. *Chem. Rev.* **2014,** *114*, 10940-10975.

(7) Fujiwara, T.; Tanaka, N.; Kobayashi, S. Structure of δ-cyclodextrin $13.75H_2O$. *Chem. Lett.* **1990,** *19*, 739-742.

(8) Jacob, J.; Geßler, K.; Hoffmann, D.; Sanbe, H.; Koizumi, K.; Smith, S. M.; Takaha, T.; Saenger, W. Strain-induced "band flips" in cyclodecaamylose and higher homologues. *Angew. Chem. Int. Ed.* **1998,** *37*, 605-609.

(9) Gessler, K.; Usón, I.; Takaha, T.; Krauss, N.; Smith, S. M.; Okada, S.; Sheldrick, G. M.; Saenger, W. V-amylose at atomic resolution: X-ray structure of a cycloamylose with 26 glucose residues (cyclomaltohexaicosaose). *Proc. Natl. Acad. Sci.* **1999,** *96*, 4246-4251.

(10) Easton, C.; Lincoln, S. *Modified cyclodextrins: Scaffolds and templates for supramolecular chemistry*; Imperial College Press: London, 1999.

(11) Brereton, I. M.; Spotswood, T. M.; Lincoln, S. F.; Williams, E. H. Fluorine-19 nuclear magnetic resonance study of the inclusion of fluoro- and difluoro-trans-cinnamates by α-cyclodextrin. *J. Chem. Soc., Faraday Trans. 1* **1984,** *80*, 3147-3156.

(12) Pisaniello, D. L.; Lincoln, S. F.; Coates, J. H. The inclusion of haloperidol and trifluperidol by α- and γ-cyclodextrins. A ^{19}F nuclear magnetic resonance study. *J. Chem. Soc.,*

Faraday Trans. 1 **1985,** *81*, 1247-1253.

(13) Lincoln, S. F.; Hounslow, A. M.; Coates, J. H.; Doddridge, B. G. The inclusion of diflunisal by α- and β-cyclodextrins. A ^{19}F Nuclear magnetic resonance and spectrophotometric study. *J. Chem. Soc., Faraday Trans. 1* **1987,** *83*, 2697-2703.

(14) Smith, N. J.; Spotswood, T. M.; Lincoln, S. F. The inclusion of the enantiomers of N-trifluoroacetyl-4-fluorophenylalanine and N-trifluoroacetylphenylalanine by cyclomaltohexaose: A ^{2}H- and ^{19}F-N.M.R. study. *Carbohydr. Res.* **1989,** *192*, 9-15.

(15) Brown, S. E.; Coates, J. H.; Lincoln, S. F.; Coghlan, D. R.; Easton, C. J. Chiral molecular recognition: a ^{19}F nuclear magnetic resonance study of the diastereoisomer inclusion complexes formed between fluorinated amino acid derivatives and α-cyclodextrin in aqueous solution. *J. Chem. Soc., Faraday Trans.* **1991,** *87*, 2699-2703.

(16) Brown, S. E.; Haskard, C. A.; Easton, C. J.; Lincoln, S. F. Complexation of phenylalanine and histidine by β-cyclodextrin, 6-(3-aminopropylamino)-6-deoxy-β-cyclodextrin and its metallocyclodextrins in aqueous solution. *J. Chem. Soc., Faraday Trans.* **1995,** *91*, 1013-1018.

(17) Hendrickson, K.; Easton, C. J.; Lincoln, S. F. Cyclodextrin and termethylated cyclodextrin complexation of aromatic carboxylic acids and their conjugate bases in aqueous solution: the effect of size, hydrophobicity and charge. *Aust. J. Chem.* **1995,** *48*, 1125-1132.

(18) Dhillon, R.; Easton, C. J.; Lincoln, S. F.; Papageorgiou, J. Complexation of benzoic, 4-methylbenzoic, and (R)- and (S)-2-phenylpropanoic acids and their conjugate bases by 3^{A}-Amino-3^{A}-deoxy-(2^{A}S,3^{A}S)-β-cyclodextrin in aqueous solution. *Aust. J. Chem.* **1995,** *48*, 1117-1124.

(19) Brown, S. E.; Coates, J. H.; Easton, C. J.; van Eyk, S. J.; Lincoln, S. F.; May, B. L.; Stile, M. A.; Whalland, C. B.; Williams, M. L. Tryptophan anion complexes of β-cyclodextrin (cyclomaltaheptaose), an aminopropylamino-β-cyclodextrin and its enantioselective nickel(II) complex. *J. Chem. Soc., Chem. Commun.* **1994**, 47-47.

(20) Rohrbach, R. P.; Rodriguez, L. J.; Eyring, E. M.; Wojcik, J. F. An equilibrium and kinetic investigation of salt-cycloamylose complexes. *J. Phys. Chem.* **1977,** *81*, 944-948.

(21) Bates, P. S.; Kataky, R.; Parker, D. Selective binding and detection of onium ions by lipophilic neutral cyclodextrins. *J. Chem. Soc., Chem. Commun.* **1993**, 691-693.

(22) Nepogodiev, S. A.; Stoddart, J. F. Cyclodextrin-based catenanes and rotaxanes. *Chem. Rev.* **1998,** *98*, 1959-1976.

(23) Wenz, G.; Han, B.-H.; Müller, A. Cyclodextrin rotaxanes and polyrotaxanes. *Chem.*

Rev. **2006,** *106*, 782-817.

(24) Araki, J.; Ito, K. Recent advances in the preparation of cyclodextrin-based polyrotaxanes and their applications to soft materials. *Soft Matter* **2007,** *3*, 1456-1473.

(25) Astray, G.; Gonzalez-Barreiro, C.; Mejuto, J. C.; Rial-Otero, R.; Simal-Gándara, J. A review on the use of cyclodextrins in foods. *Food Hydrocoll.* **2009,** *23*, 1631-1640.

(26) Uekama, K.; Hirayama, F.; Irie, T. Cyclodextrin drug carrier systems. *Chem. Rev.* **1998,** *98*, 2045-2076.

(27) Davis, M. E.; Brewster, M. E. Cyclodextrin-based pharmaceutics: past, present and future. *Nat. Rev. Drug Discov.* **2004,** *3*, 1023-1035.

(28) Simoes, S. M. N.; Rey-Rico, A.; Concheiro, A.; Alvarez-Lorenzo, C. Supramolecular cyclodextrin-based drug nanocarriers. *Chem. Commun.* **2015,** *51*, 6275-6289.

(29) Hapiot, F.; Bricout, H.; Tilloy, S.; Monflier, E. Functionalized cyclodextrins as first and second coordination sphere ligands for aqueous organometallic catalysis. *Eur. J. Inorg. Chem.* **2012,** *2012*, 1571-1578.

(30) Villalonga, R.; Cao, R.; Fragoso, A. Supramolecular chemistry of cyclodextrins in enzyme technology. *Chem. Rev.* **2007,** *107*, 3088-3116.

(31) Rekharsky, M. V.; Inoue, Y. Complexation thermodynamics of cyclodextrins. *Chem. Rev.* **1998,** *98*, 1875-1918.

(32) Saenger, W. Cyclodextrin inclusion compounds in research and industry. *Angew. Chem. Int. Ed.* **1980,** *19*, 344-362.

(33) Saenger, W.; Noltemeyer, M.; Manor, P. C.; Hingerty, B.; Klar, B. “Induced-fit”-type complex formation of the model enzyme α-cyclodextrin. *Bioorg. Chem.* **1976,** *5*, 187-195.

(34) Ross, P. D.; Rekharsky, M. V. Thermodynamics of hydrogen bond and hydrophobic interactions in cyclodextrin complexes. *Biophys. J.* **1996,** *71*, 2144-2154.

(35) Schuette, J. M.; Ndou, T. T.; Munoz de la Pena, A.; Mukundan, S.; Warner, I. M. Influence of alcohols on the β-cyclodextrin/acridine complex. *J. Am. Chem. Soc.* **1993,** *115*, 292-298.

(36) Zhang, B.; Breslow, R. Enthalpic domination of the chelate effect in cyclodextrin dimers. *J. Am. Chem. Soc.* **1993,** *115*, 9353-9354.

(37) Nguyen, H.-T.; Pham, D.-T.; Lincoln, S. F.; Wang, J.; Guo, X.; Easton, C. J.; Prud'homme, R. K. Host-guest chemistry of linked β-cyclodextrin trimers and adamantyl substituted poly(acrylate)s in aqueous solution. *Polym. Chem.* **2013,** *4*, 820-829.

(38) Weickenmeier, M.; Wenz, G. Cyclodextrin sidechain polyesters — synthesis and

inclusion of adamantan derivatives. *Macromol. Rapid Commun.* **1996,** *17*, 731-736.

(39) Pham, D.-T.; Clements, P.; Easton, C. J.; Papageorgiou, J.; May, B. L.; Lincoln, S. F. Complexation of 6-(4′-(toluidinyl) naphthalene-2-sulfonate by β-cyclodextrin and linked β-cyclodextrin dimers. *New J. Chem.* **2008,** *32*, 712-718.

(40) Pham, D.-T.; Clements, P.; Easton, C. J.; Papageorgiou, J.; May, B. L.; Lincoln, S. F. Dimerisation and complexation of 6-(4′-t-butylphenylamino)naphthalene-2-sulphonate by β-cyclodextrin and linked β-cyclodextrin dimers. *Supramol. Chem.* **2009,** *21*, 510-519.

(41) Wang, J.; Pham, D.-T.; Kee, T. W.; Clafton, S. N.; Guo, X.; Clements, P.; Lincoln, S. F.; Prud'homme, R. K.; Easton, C. J. Aggregation and host-guest interactions in dansyl-substituted poly(acrylate)s in the presence of β-cyclodextrin and a β-cyclodextrin dimer in aqueous solution: A UV–Vis, fluorescence, ^{1}H NMR, and rheological study. *Macromolecules* **2011,** *44*, 9782-9791.

(42) Liu, Y.; Chen, Y.; Li; Zhang, H.-Y.; Liu, S.-X.; Guan, X.-D. Bridged bis(β-cyclodextrin)s possessing coordinated metal center(s) and their inclusion complexation behavior with model substrates: Enhanced molecular binding ability by multiple recognition. *J. Org. Chem.* **2001,** *66*, 8518-8527.

(43) Kano, K.; Yoshiyasu, K.; Yasuoka, H.; Hata, S.; Hashimoto, S. Chiral recognition by cyclic oligosaccharides. Enantioselective complexation of bilirubin with β-cyclodextrin through hydrogen bonding in water. *J. Chem. Soc., Perkin Trans. 2* **1992**, 1265-1269.

(44) Ueno, A.; Chen, Q.; Suzuki, I.; Osa, T. Detection of organic compounds by guest-responsive circular dichroism variations of ferrocene-appended cyclodextrins. *Anal. Chem.* **1992,** *64*, 1650-1655.

(45) Thordarson, P. Determining association constants from titration experiments in supramolecular chemistry. *Chem. Soc. Rev.* **2011,** *40*, 1305-1323.

(46) Rekharsky, M. V.; Inoue, Y. Complexation and chiral recognition thermodynamics of 6-Amino-6-deoxy-β-cyclodextrin with anionic, cationic, and neutral chiral guests: Counterbalance between van der Waals and coulombic interactions. *J. Am. Chem. Soc.* **2002,** *124*, 813-826.

(47) Rekharsky, M.; Inoue, Y. Chiral recognition thermodynamics of β-Cyclodextrin: The thermodynamic origin of enantioselectivity and the enthalpy-entropy compensation effect. *J. Am. Chem. Soc.* **2000,** *122*, 4418-4435.

(48) Rekharsky, M.; Inoue, Y. 1:1 and 1:2 Complexation thermodynamics of γ-cyclodextrin with N-carbobenzyloxy aromatic amino acids and ω-phenylalkanoic acids. *J.*

Am. Chem. Soc. **2000,** *122*, 10949-10955.

(49) Schneider, H.-J.; Hacket, F.; Rüdiger, V.; Ikeda, H. NMR Studies of cyclodextrins and cyclodextrin complexes. *Chem. Rev.* **1998,** *98*, 1755-1786.

(50) Saenger, W.; Jacob, J.; Gessler, K.; Steiner, T.; Hoffmann, D.; Sanbe, H.; Koizumi, K.; Smith, S. M.; Takaha, T. Structures of the common cyclodextrins and their Larger analogues beyond the doughnut. *Chem. Rev.* **1998,** *98*, 1787-1802.

(51) Khan, A. R.; Forgo, P.; Stine, K. J.; D'Souza, V. T. Methods for selective modifications of cyclodextrins. *Chem. Rev.* **1998,** *98*, 1977-1996.

(52) Takahashi, K.; Hattori, K.; Toda, F. Monotosylated α- and β-cyclodextrins prepared in an alkaline aqueous solution. *Tetrahedron Lett.* **1984,** *25*, 3331-3334.

(53) Melton, L. D.; Slessor, K. N. Synthesis of monosubstituted cyclohexaamyloses. *Carbohydr. Res.* **1971,** *18*, 29-37.

(54) Tsujihara, K.; Kurita, H.; Kawazu, M. The Highly selective sulfonylation of cycloheptaamylose and syntheses of its pure amino derivatives. *Bull. Chem. Soc. Jpn.* **1977,** *50*, 1567-1571.

(55) Petter, R. C.; Salek, J. S.; Sikorski, C. T.; Kumaravel, G.; Lin, F. T. Cooperative binding by aggregated mono-6-(alkylamino)-β-cyclodextrins. *J. Am. Chem. Soc.* **1990,** *112*, 3860-3868.

(56) Siegel, B. Preparation and redox properties of a cyclodextrin based ferredoxin model. *J. Inorg. Nucl. Chem.* **1979,** *41*, 609-610.

(57) Yoon, J.; Hong, S.; Martin, K. A.; Czarnik, A. W. A general method for the synthesis of cyclodextrinyl aldehydes and carboxylic acids. *J. Org. Chem.* **1995,** *60*, 2792-2795.

(58) Ueno, A.; Breslow, R. Selective sulfonation of a secondary hydroxyl group of β-cyclodextrin. *Tetrahedron Lett.* **1982,** *23*, 3451-3454.

(59) Rong, D.; D'Souza, V. T. A convenient method for functionalization of the 2-position of cyclodextrins. *Tetrahedron Lett.* **1990,** *31*, 4275-4278.

(60) van Dienst, E. v.; Snellink, B. H. M.; von Piekartz, I.; Gansey, M. H. B. G.; Venema, F.; Feiters, M. C.; Nolte, R. J. M.; Engbersen, J. F. J.; Reinhoudt, D. N. Selective functionalization and flexible coupling of cyclodextrins at the secondary hydroxyl face. *J. Org. Chem.* **1995,** *60*, 6537-6545.

(61) Irie, T.; Uekama, K. Pharmaceutical applications of cyclodextrins. III. Toxicological issues and safety evaluation. *J. Pharm. Sci.* **1997,** *86*, 147-162.

(62) Arima, H.; Motoyama, K.; Irie, T. Recent findings on safety profiles of cyclodextrins,

cyclodextrin conjugates, and polypseudorotaxanes. In *Cyclodextrins in Pharmaceutics, Cosmetics, and Biomedicine*; John Wiley & Sons, Inc., 2011, pp 91-122.

(63) Kurkov, S. V.; Loftsson, T. Cyclodextrins. *Int. J. Pharm.* **2013,** *453*, 167-180.

(64) Sharma, U. S.; Balasubramanian, S. V.; Straubinger, R. M. Pharmaceutical and physical properties of paclitaxel (taxol) complexes with cyclodextrins. *J. Pharm. Sci.* **1995,** *84*, 1223-1230.

(65) Sigurðoardóttir, A. M.; Loftsson, T. The effect of polyvinylpyrrolidone on cyclodextrin complexation of hydrocortisone and its diffusion through hairless mouse skin. *Int. J. Pharm.* **1995,** *126*, 73-78.

(66) Müller, B. W.; Brauns, U. Solubilization of drugs by modified β-cyclodextrins. *Int. J. Pharm.* **1985,** *26*, 77-88.

(67) Loftsson, T.; Brewster, M. E. Pharmaceutical applications of cyclodextrins. 1. Drug solubilization and stabilization. *J. Pharm. Sci.* **1996,** *85*, 1017-1025.

(68) Brewster, M. E.; Loftsson, T.; Estes, K. S.; Lin, J.-L.; Fridriksdóttir, H.; Bodor, N. Effect of various cyclodextrins on solution stability and dissolution rate of doxorubicin hydrochloride. *Int. J. Pharm.* **1992,** *79*, 289-299.

(69) Loftsson, T.; Ólafsdóttir, B. J.; Friðriksdóttir, H.; Jónsdóttir, S. Cyclodextrin complexation of NSAIDSs: physicochemical characteristics. *Eur. J. Pharm. Sci.* **1993,** *1*, 95-101.

(70) Loftsson, T.; Jarho, P.; Másson, M.; Järvinen, T. Cyclodextrins in drug delivery. *Expert Opin. Drug Deliv.* **2005,** *2*, 335-351.

(71) Brewster, M. E.; Anderson, W. R.; Meinsma, D.; Moreno, D.; Webb, A. I.; Pablo, L.; Estes, K. S.; Derendorf, H.; Bodor, N.; Sawchuk, R.; Cheung, B.; Pop, E. Intravenous and oral pharmacokinetic evaluation of a 2-hydroxypropyl-β-cyclodextrin-based formulation of carbamazepine in the dog: Comparison with commercially available tablets and suspensions. *J. Pharm. Sci.* **1997,** *86*, 335-339.

(72) Uekama, K.; Fujinaga, T.; Hirayama, F.; Otagiri, M.; Yamasaki, M.; Seo, H.; Hashimoto, T.; Tsuruoka, M. Improvement of the oral bioavailability of digitalis glycosides by cyclodextrin complexation. *J. Pharm. Sci.* **1983,** *72*, 1338-1341.

(73) Tenjarla, S.; Puranajoti, P.; Kasina, R.; Mandal, T. Preparation, characterization, and evaluation of miconazole-cyclodextrin complexes for improved oral and topical delivery. *J. Pharm. Sci.* **1998,** *87*, 425-429.

(74) Liu, Y.; Chen, Y. Cooperative binding and multiple recognition by bridged

bis(β-cyclodextrin)s with functional linkers. *Acc. Chem. Res.* **2006,** *39*, 681-691.

(75) Harada, T.; Pham, D.-T.; Leung, M. H. M.; Ngo, H. T.; Lincoln, S. F.; Easton, C. J.; Kee, T. W. Cooperative binding and stabilization of the medicinal pigment curcumin by diamide linked γ-cyclodextrin dimers: A spectroscopic characterization. *J. Phys. Chem. B* **2011,** *115*, 1268-1274.

(76) Harada, T.; Giorgio, L.; Harris, T. J.; Pham, D.-T.; Ngo, H. T.; Need, E. F.; Coventry, B. J.; Lincoln, S. F.; Easton, C. J.; Buchanan, G.; Kee, T. W. Diamide linked γ-cyclodextrin dimers as molecular-scale delivery systems for the medicinal pigment curcumin to prostate cancer cells. *Mol. Pharmaceutics* **2013,** *10*, 4481-4490.

(77) Maciollek, A.; Munteanu, M.; Ritter, H. New generation of polymeric drugs: Copolymer from NIPAAM and cyclodextrin methacrylate containing supramolecular-attached antitumor derivative. *Macromol. Chem. Phys.* **2010,** *211*, 245-249.

(78) Ooya, T.; Yui, N. Synthesis of theophylline–polyrotaxane conjugates and their drug release via supramolecular dissociation. *J. Control. Release* **1999,** *58*, 251-269.

(79) Moon, C.; Kwon, Y. M.; Lee, W. K.; Park, Y. J.; Chang, L.-C.; Yang, V. C. A novel polyrotaxane-based intracellular delivery system for camptothecin: In vitro feasibility evaluation. *J. Biomed. Mater. Res. Part A* **2008,** *84A*, 238-246.

(80) Li, J.; Yang, C.; Li, H.; Wang, X.; Goh, S. H.; Ding, J. L.; Wang, D. Y.; Leong, K. W. Cationic supramolecules composed of multiple oligoethylenimine-grafted β-cyclodextrins threaded on a polymer chain for efficient gene delivery. *Adv. Mater.* **2006,** *18*, 2969-2974.

(81) Yu, S.; Zhang, Y.; Wang, X.; Zhen, X.; Zhang, Z.; Wu, W.; Jiang, X. Synthesis of paclitaxel-conjugated β-cyclodextrin polyrotaxane and its antitumor activity. *Angew. Chem. Int. Ed.* **2013**.

(82) Moon, C.; Kwon, Y. M.; Lee, W. K.; Park, Y. J.; Yang, V. C. In vitro assessment of a novel polyrotaxane-based drug delivery system integrated with a cell-penetrating peptide. *J. Control. Release* **2007,** *124*, 43-50.

(83) Davis, M. E.; Chen, Z.; Shin, D. M. Nanoparticle therapeutics: an emerging treatment modality for cancer. *Nat. Rev. Drug Discov.* **2008,** *7*, 771-782.

(84) Ravoo, B. J.; Darcy, R. Cyclodextrin bilayer vesicles. *Angew. Chem. Int. Ed.* **2000,** *39*, 4324-4326.

(85) Samanta, A.; Stuart, M. C. A.; Ravoo, B. J. Photoresponsive capture and release of lectins in multilamellar complexes. *J. Am. Chem. Soc.* **2012,** *134*, 19909-19914.

(86) Nalluri, S. K. M.; Voskuhl, J.; Bultema, J. B.; Boekema, E. J.; Ravoo, B. J.

Light-responsive capture and release of DNA in a ternary supramolecular complex. *Angew. Chem. Int. Ed.* **2011,** *50*, 9747-9751.

(87) Adeli, M.; Hakimpoor, F.; Parsamanesh, M.; Kalantari, M.; Sobhani, Z.; Attyabi, F. Quantum dot-pseudopolyrotaxane supramolecules as anticancer drug delivery systems. *Polymer* **2011,** *52*, 2401-2413.

(88) Adeli, M.; Sarabi, R. S.; Yadollahi Farsi, R.; Mahmoudi, M.; Kalantari, M. Polyrotaxane/gold nanoparticle hybrid nanomaterials as anticancer drug delivery systems. *J. Mater. Chem.* **2011,** *21*, 18686-18695.

(89) Chang, J.; Li, Y.; Wang, G.; He, B.; Gu, Z. Fabrication of novel coumarin derivative functionalized polypseudorotaxane micelles for drug delivery. *Nanoscale* **2013,** *5*, 813-820.

(90) Wang, Y.; Wang, H.; Chen, Y.; Liu, X.; Jin, Q.; Ji, J. Biomimetic pseudopolyrotaxane prodrug micelles with high drug content for intracellular drug delivery. *Chem. Commun.* **2013,** *49*, 7123-7125.

(91) Zhang, J.; Ma, P. X. Polymeric core-shell assemblies mediated by host-guest interactions: Versatile nanocarriers for drug delivery. *Angew. Chem. Int. Ed.* **2009,** *48*, 964-968.

(92) Wang, H.; Wang, S.; Su, H.; Chen, K.-J.; Armijo, A. L.; Lin, W.-Y.; Wang, Y.; Sun, J.; Kamei, K.-i.; Czernin, J.; Radu, C. G.; Tseng, H.-R. A supramolecular approach for preparation of size-controlled nanoparticles. *Angew. Chem. Int. Ed.* **2009,** *48*, 4344-4348.

(93) Zhang, J.; Ellsworth, K.; Ma, P. X. Hydrophobic pharmaceuticals mediated self-assembly of β-cyclodextrin containing hydrophilic copolymers: Novel chemical responsive nano-vehicles for drug delivery. *J. Control. Release* **2010,** *145*, 116-123.

(94) Chen, K.-J.; Tang, L.; Garcia, M. A.; Wang, H.; Lu, H.; Lin, W.-Y.; Hou, S.; Yin, Q.; Shen, C. K. F.; Cheng, J.; Tseng, H.-R. The therapeutic efficacy of camptothecin-encapsulated supramolecular nanoparticles. *Biomaterials* **2012,** *33*, 1162-1169.

(95) Lee, J.-H.; Chen, K.-J.; Noh, S.-H.; Garcia, M. A.; Wang, H.; Lin, W.-Y.; Jeong, H.; Kong, B. J.; Stout, D. B.; Cheon, J.; Tseng, H.-R. On-demand drug release system for *in vivo* cancer treatment through self-assembled magnetic nanoparticles. *Angew. Chem. Int. Ed.* **2013,** *52*, 4384-4388.

(96) Yang, Y.; Zhang, Y.-M.; Chen, Y.; Chen, J.-T.; Liu, Y. Targeted polysaccharide nanoparticle for adamplatin prodrug delivery. *J. Med. Chem.* **2013,** *56*, 9725-9736.

(97) Ang, C. Y.; Tan, S. Y.; Wang, X.; Zhang, Q.; Khan, M.; Bai, L.; Tamil Selvan, S.; Ma, X.; Zhu, L.; Nguyen, K. T.; Tan, N. S.; Zhao, Y. Supramolecular nanoparticle carriers self-assembled from cyclodextrin- and adamantane-functionalized polyacrylates for

tumor-targeted drug delivery. *J. Mater. Chem. B* **2014,** *2*, 1879-1890.

(98) Peppas, N. A.; Hilt, J. Z.; Khademhosseini, A.; Langer, R. Hydrogels in biology and medicine: From molecular principles to bionanotechnology. *Adv. Mater.* **2006,** *18*, 1345-1360.

(99) Kopeček, J. Hydrogel biomaterials: A smart future? *Biomaterials* **2007,** *28*, 5185-5192.

(100) Hoare, T. R.; Kohane, D. S. Hydrogels in drug delivery: Progress and challenges. *Polymer* **2008,** *49*, 1993-2007.

(101) Qiu, Y.; Park, K. Environment-sensitive hydrogels for drug delivery. *Adv. Drug Deliv. Rev.* **2012,** *64, Supplement*, 49-60.

(102) Szeman, J.; Fenyvesi, E.; Szejtli, J.; Ueda, H.; Machida, Y.; Nagai, T. Water soluble cyclodextrin polymers: Their interaction with drugs. *J. incl. phenom.* **1987,** *5*, 427-431.

(103) Renard, E.; Deratani, A.; Volet, G.; Sebille, B. Preparation and characterization of water soluble high molecular weight β-cyclodextrin-epichlorohydrin polymers. *Eur. Polym. J.* **1997,** *33*, 49-57.

(104) Mura, P.; Faucci, M. T.; Maestrelli, F.; Furlanetto, S.; Pinzauti, S. Characterization of physicochemical properties of naproxen systems with amorphous β-cyclodextrin-epichlorohydrin polymers. *J. Pharm. Biomed. Anal.* **2002,** *29*, 1015-1024.

(105) Vélaz, I.; Isasi, J. R.; Sánchez, M.; Uzqueda, M.; Ponchel, G. Structural characteristics of some soluble and insoluble β-cyclodextrin polymers. *J. Incl. Phenom. Macro.* **2007,** *57*, 65-68.

(106) Machín, R.; Isasi, J. R.; Vélaz, I. β-Cyclodextrin hydrogels as potential drug delivery systems. *Carbohydr. Polym.* **2012,** *87*, 2024-2030.

(107) Machín, R.; Isasi, J. R.; Vélaz, I. Hydrogel matrices containing single and mixed natural cyclodextrins. Mechanisms of drug release. *Eur. Polym. J.* **2013,** *49*, 3912-3920.

(108) Ma, M.; Li, D. New organic nanoporous polymers and their inclusion complexes. *Chem. Mater.* **1999,** *11*, 872-874.

(109) Binello, A.; Robaldo, B.; Barge, A.; Cavalli, R.; Cravotto, G. Synthesis of cyclodextrin-based polymers and their use as debittering agents. *J. Appl. Polym. Sci.* **2008,** *107*, 2549-2557.

(110) Moya-Ortega, M. D.; Alvarez-Lorenzo, C.; Sigurdsson, H. H.; Concheiro, A.; Loftsson, T. γ-Cyclodextrin hydrogels and semi-interpenetrating networks for sustained delivery of dexamethasone. *Carbohydr. Polym.* **2010,** *80*, 900-907.

(111) Girek, T.; Kozlowski, C. A.; Koziol, J. J.; Walkowiak, W.; Korus, I. Polymerisation of

β-cyclodextrin with succinic anhydride. Synthesis, characterisation, and ion flotation of transition metals. *Carbohydr. Polym.* **2005,** *59*, 211-215.

(112) Cesteros, L. C.; Ramírez, C. A.; Peciña, A.; Katime, I. Poly(ethylene glycol-β-cyclodextrin) gels: Synthesis and properties. *J. Appl. Polym. Sci.* **2006,** *102*, 1162-1166.

(113) Peng, K.; Tomatsu, I.; Korobko, A. V.; Kros, A. Cyclodextrin-dextran based in situ hydrogel formation: a carrier for hydrophobic drugs. *Soft Matter* **2010,** *6*, 85-87.

(114) Peng, K.; Cui, C.; Tomatsu, I.; Porta, F.; Meijer, A. H.; Spaink, H. P.; Kros, A. Cyclodextrin/dextran based drug carriers for a controlled release of hydrophobic drugs in zebrafish embryos. *Soft Matter* **2010,** *6*, 3778-3783.

(115) Kutyła, M. J.; Lambert, L. K.; Davies, N. M.; McGeary, R. P.; Shaw, P. N.; Ross, B. P. Cyclodextrin-crosslinked poly (acrylic acid): synthesis, physicochemical characterization and controlled release of diflunisal and fluconazole from hydrogels. *Int. J. Pharm.* **2013,** *444*, 175-184.

(116) Liu, C.; Zhang, Z.; Liu, X.; Ni, X.; Li, J. Gelatin-based hydrogels with β-cyclodextrin as a dual functional component for enhanced drug loading and controlled release. *RSC Adv.* **2013,** *3*, 25041-25049.

(117) Izawa, H.; Kawakami, K.; Sumita, M.; Tateyama, Y.; Hill, J. P.; Ariga, K. β-Cyclodextrin-crosslinked alginate gel for patient-controlled drug delivery systems: regulation of host-guest interactions with mechanical stimuli. *J. Mater. Chem. B* **2013,** *1*, 2155-2161.

(118) Liu, Y.-Y.; Fan, X.-D. Synthesis and characterization of pH- and temperature-sensitive hydrogel of *N*-isopropylacrylamide/cyclodextrin based copolymer. *Polymer* **2002,** *43*, 4997-5003.

(119) Liu, Y.-Y.; Fan, X.-D. Synthesis, properties and controlled release behaviors of hydrogel networks using cyclodextrin as pendant groups. *Biomaterials* **2005,** *26*, 6367-6374.

(120) Siemoneit, U.; Schmitt, C.; Alvarez-Lorenzo, C.; Luzardo, A.; Otero-Espinar, F.; Concheiro, A.; Blanco-Méndez, J. Acrylic/cyclodextrin hydrogels with enhanced drug loading and sustained release capability. *Int. J. Pharm.* **2006,** *312*, 66-74.

(121) Li, J.; Loh, X. J. Cyclodextrin-based supramolecular architectures: Syntheses, structures, and applications for drug and gene delivery. *Adv. Drug Deliv. Rev.* **2008,** *60*, 1000-1017.

(122) Li, J. Self-assembled supramolecular hydrogels based on polymer-cyclodextrin

inclusion complexes for drug delivery. *NPG Asia Mater.* **2010,** *2*, 112-118.

(123)Choi, H. S.; Kontani, K.; Huh, K. M.; Sasaki, S.; Ooya, T.; Lee, W. K.; Yui, N. Rapid induction of thermoreversible hydrogel formation based on poly(propylene glycol)-grafted dextran inclusion complexes. *Macromol. Biosci.* **2002,** *2*, 298-303.

(124)Abu Hashim, I. I.; Higashi, T.; Anno, T.; Motoyama, K.; Abd-ElGawad, A.-E. H.; El-Shabouri, M. H.; Borg, T. M.; Arima, H. Potential use of γ-cyclodextrin polypseudorotaxane hydrogels as an injectable sustained release system for insulin. *Int. J. Pharm.* **2010,** *392*, 83-91.

(125)Higashi, T.; Tajima, A.; Motoyama, K.; Arima, H. Cyclodextrin/poly(ethylene glycol) polypseudorotaxane hydrogels as a promising sustained-release system for lysozyme. *J. Pharm. Sci.* **2012,** *101*, 2891-2899.

(126)Liu, K. L.; Zhang, Z.; Li, J. Supramolecular hydrogels based on cyclodextrin-polymer polypseudorotaxanes: materials design and hydrogel properties. *Soft Matter* **2011,** *7*, 11290-11297.

(127)Li, J.; Harada, A.; Kamachi, M. Sol-gel transition during inclusion complex formation between α-cyclodextrin and high molecular weight poly (ethylene glycol) s in aqueous solution. *Polym. J.* **1994,** *26*, 1019-1026.

(128)Li, J.; Ni, X.; Leong, K. W. Injectable drug-delivery systems based on supramolecular hydrogels formed by poly (ethylene oxide) s and α-cyclodextrin. *J. Biomed. Mater. Res. Part A* **2003,** *65*, 196-202.

(129)Li, J.; Li, X.; Ni, X.; Wang, X.; Li, H.; Leong, K. W. Self-assembled supramolecular hydrogels formed by biodegradable PEO–PHB–PEO triblock copolymers and α-cyclodextrin for controlled drug delivery. *Biomaterials* **2006,** *27*, 4132-4140.

(130)Chen, Y.; Pang, X.-H.; Dong, C.-M. Dual Stimuli-responsive supramolecular polypeptide-based hydrogel and reverse micellar hydrogel mediated by host-guest chemistry. *Adv. Funct. Mater.* **2010,** *20*, 579-586.

(131)Huh, K. M.; Ooya, T.; Lee, W. K.; Sasaki, S.; Kwon, I. C.; Jeong, S. Y.; Yui, N. Supramolecular-structured hydrogels showing a reversible phase transition by inclusion complexation between poly(ethylene glycol) grafted dextran and α-cyclodextrin. *Macromolecules* **2001,** *34*, 8657-8662.

(132)Huh, K. M.; Cho, Y. W.; Chung, H.; Kwon, I. C.; Jeong, S. Y.; Ooya, T.; Lee, W. K.; Sasaki, S.; Yui, N. Supramolecular hydrogel formation based on inclusion complexation between poly(ethylene glycol)-modified chitosan and α-Cyclodextrin. *Macromol. Biosci.* **2004,**

4, 92-99.

(133)Yu, J.; Ha, W.; Sun, J.-n.; Shi, Y.-p. Supramolecular hybrid hydrogel based on host-guest interaction and its application in drug delivery. *ACS Appl. Mater. Interfaces* **2014,** *6*, 19544-19551.

(134)Guo, M.; Jiang, M.; Pispas, S.; Yu, W.; Zhou, C. Supramolecular hydrogels made of end-functionalized low-molecular-weight PEG and α-cyclodextrin and their hybridization with SiO_2 nanoparticles through host-guest interaction. *Macromolecules* **2008,** *41*, 9744-9749.

(135)Liao, X.; Chen, G.; Liu, X.; Chen, W.; Chen, F.; Jiang, M. Photoresponsive pseudopolyrotaxane hydrogels based on competition of host-guest interactions. *Angew. Chem. Int. Ed.* **2010,** *49*, 4409-4413.

(136)Eftink, M. R.; Andy, M. L.; Bystrom, K.; Perlmutter, H. D.; Kristol, D. S. Cyclodextrin inclusion complexes: studies of the variation in the size of alicyclic guests. *J. Am. Chem. Soc.* **1989,** *111*, 6765-6772.

(137)Li, L.; Guo, X.; Wang, J.; Liu, P.; Prud'homme, R. K.; May, B. L.; Lincoln, S. F. Polymer networks assembled by host-guest inclusion between adamantyl and β-cyclodextrin substituents on poly (acrylic acid) in aqueous solution. *Macromolecules* **2008,** *41*, 8677-8681.

(138)Guo, X.; Wang, J.; Li, L.; Pham, D.-T.; Clements, P.; Lincoln, S. F.; May, B. L.; Chen, Q.; Zheng, L.; Prud'homme, R. K. Tailoring polymeric hydrogels through cyclodextrin host-guest complexation. *Macromol. Rapid Commun.* **2010,** *31*, 300-304.

(139)Guo, X.; Wang, J.; Li, L.; Pham, D.-T.; Clements, P.; Lincoln, S. F.; May, B. L.; Chen, Q.; Zheng, L.; Prud'homme, R. K. Steric effects and competitive intra- and inter-molecular host-guest complexation between β-cyclodextrin and adamantyl substituted poly(acrylate)s in water: A ^{1}H NMR, rheological and preparative study. *J. Polym. Sci., Part B: Polym. Phys.* **2010,** *48*, 1818-1825.

(140)Wang, J.; Pham, D.-T.; Guo, X.; Li, L.; Lincoln, S. F.; Luo, Z.; Ke, H.; Zheng, L.; Prud'homme, R. K. Polymeric networks assembled by adamantyl and β-cyclodextrin substituted poly(acrylate)s: host-guest interactions, and the effects of ionic strength and extent of substitution. *Ind. Eng. Chem. Res.* **2010,** *49*, 609-612.

(141)Auzély-Velty, R.; Rinaudo, M. New supramolecular assemblies of a cyclodextrin-grafted chitosan through specific complexation. *Macromolecules* **2002,** *35*, 7955-7962.

(142)Charlot, A.; Auzély-Velty, R. Novel Hyaluronic acid based supramolecular assemblies stabilized by multivalent specific interactions: Rheological behavior in aqueous solution.

Macromolecules **2007,** *40*, 9555-9563.

(143)Tamesue, S.; Takashima, Y.; Yamaguchi, H.; Shinkai, S.; Harada, A. Photoswitchable supramolecular hydrogels formed by cyclodextrins and azobenzene polymers. *Angew. Chem. Int. Ed.* **2010,** *49*, 7461-7464.

(144)Yamaguchi, H.; Kobayashi, Y.; Kobayashi, R.; Takashima, Y.; Hashidzume, A.; Harada, A. Photoswitchable gel assembly based on molecular recognition. *Nat. Commun.* **2012,** *3*, 603.

(145)Peng, K.; Tomatsu, I.; Kros, A. Light controlled protein release from a supramolecular hydrogel. *Chem. Commun.* **2010,** *46*, 4094-4096.

(146)Nakahata, M.; Takashima, Y.; Yamaguchi, H.; Harada, A. Redox-responsive self-healing materials formed from host-guest polymers. *Nat. Commun.* **2011,** *2*, 511.

(147)Tan, L.; Liu, Y.; Ha, W.; Ding, L.-S.; Peng, S.-L.; Zhang, S.; Li, B.-J. Stimuli-induced gel-sol transition of multi-sensitive supramolecular β-cyclodextrin grafted alginate/ferrocene modified pluronic hydrogel. *Soft Matter* **2012,** *8*, 5746-5749.

(148)Peng, L.; Zhang, H.; Feng, A.; Huo, M.; Wang, Z.; Hu, J.; Gao, W.; Yuan, J. Electrochemical redox responsive supramolecular self-healing hydrogels based on host-guest interaction. *Polym. Chem.* **2015,** *6*, 3652-3659.

(149)Daoud-Mahammed, S.; Grossiord, J.; Bergua, T.; Amiel, C.; Couvreur, P.; Gref, R. Self-assembling cyclodextrin based hydrogels for the sustained delivery of hydrophobic drugs. *J. Biomed. Mater. Res. Part A* **2008,** *86*, 736-748.

(150)Layre, A.-M.; Volet, G. l.; Wintgens, V. r.; Amiel, C. Associative network based on cyclodextrin polymer: a model system for drug delivery. *Biomacromolecules* **2009,** *10*, 3283-3289.

(151)Li, J.; Li, H.; Yang, X.; Luo, P.; Wu, Z.; Zhang, X. The supramolecular hydrogel based on hyperbranched polyglycerol and dextran as a scaffold for living cells and drug delivery. *RSC Adv.* **2015,** *5*, 86730-86739.

(152)Wu, C.; Bull, B.; Szymanski, C.; Christensen, K.; McNeill, J. Multicolor conjugated polymer dots for biological fluorescence imaging. *ACS Nano* **2008,** *2*, 2415-2423.

(153)Wu, C.; Szymanski, C.; McNeill, J. Preparation and encapsulation of highly fluorescent conjugated polymer nanoparticles. *Langmuir* **2006,** *22*, 2956-2960.

(154)Wu, C.; Szymanski, C.; Cain, Z.; McNeill, J. Conjugated polymer dots for multiphoton fluorescence imaging. *J. Am. Chem. Soc.* **2007,** *129*, 12904-12905.

(155)Jin, Y.; Ye, F.; Zeigler, M.; Wu, C.; Chiu, D. T. Near-infrared fluorescent dye-doped

semiconducting polymer dots. *ACS Nano* **2011,** *5*, 1468-1475.

(156)Chan, Y.-H.; Ye, F.; Gallina, M. E.; Zhang, X.; Jin, Y.; Wu, I. C.; Chiu, D. T. Hybrid semiconducting polymer dot-quantum dot with narrow-band emission, near-infrared fluorescence, and high brightness. *J. Am. Chem. Soc.* **2012,** *134*, 7309-7312.

(157)Ye, F.; Wu, C.; Jin, Y.; Wang, M.; Chan, Y.-H.; Yu, J.; Sun, W.; Hayden, S.; Chiu, D. T. A compact and highly fluorescent orange-emitting polymer dot for specific subcellular imaging. *Chem. Commun.* **2012,** *48*, 1778-1780.

(158)Chen, C.-P.; Huang, Y.-C.; Liou, S.-Y.; Wu, P.-J.; Kuo, S.-Y.; Chan, Y.-H. Near-infrared fluorescent semiconducting polymer dots with high brightness and pronounced effect of positioning alkyl chains on the comonomers. *ACS Appl. Mater. Interfaces* **2014,** *6*, 21585-21595.

(159)Liu, H.-Y.; Wu, P.-J.; Kuo, S.-Y.; Chen, C.-P.; Chang, E.-H.; Wu, C.-Y.; Chan, Y.-H. Quinoxaline-based polymer dots with ultrabright red to near-infrared fluorescence for in vivo biological imaging. *J. Am. Chem. Soc.* **2015,** *137*, 10420-10429.

(160)Wu, C.; Schneider, T.; Zeigler, M.; Yu, J.; Schiro, P. G.; Burnham, D. R.; McNeill, J. D.; Chiu, D. T. Bioconjugation of ultrabright semiconducting polymer dots for specific cellular targeting. *J. Am. Chem. Soc.* **2010,** *132*, 15410-15417.

(161)Eggeling, C.; Widengren, J.; Rigler, R.; Seidel, C. A. M. Photobleaching of fluorescent dyes under conditions used for single-molecule detection: Evidence of two-step photolysis. *Anal. Chem.* **1998,** *70*, 2651-2659.

(162)Wu, C.; Chiu, D. T. Highly fluorescent semiconducting polymer dots for biology and medicine. *Angew. Chem. Int. Ed.* **2013,** *52*, 3086-3109.

(163)Landfester, K.; Montenegro, R.; Scherf, U.; Güntner, R.; Asawapirom, U.; Patil, S.; Neher, D.; Kietzke, T. Semiconducting polymer nanospheres in aqueous dispersion prepared by a miniemulsion process. *Adv. Mater.* **2002,** *14*, 651-655.

(164)Sun, K.; Chen, H.; Wang, L.; Yin, S.; Wang, H.; Xu, G.; Chen, D.; Zhang, X.; Wu, C.; Qin, W. Size-dependent property and cell labeling of semiconducting polymer dots. *ACS Appl. Mater. Interfaces* **2014,** *6*, 10802-10812.

(165)Clafton, S. N.; Beattie, D. A.; Mierczynska-Vasilev, A.; Acres, R. G.; Morgan, A. C.; Kee, T. W. Chemical defects in the highly fluorescent conjugated polymer dots. *Langmuir* **2010,** *26*, 17785-17789.

(166)Wu, C.; Jin, Y.; Schneider, T.; Burnham, D. R.; Smith, P. B.; Chiu, D. T. Ultrabright and bioorthogonal labeling of cellular targets using semiconducting polymer dots and click chemistry. *Angew. Chem. Int. Ed.* **2010,** *49*, 9436-9440.

(167) Yoon, J.; Kwag, J.; Shin, T. J.; Park, J.; Lee, Y. M.; Lee, Y.; Park, J.; Heo, J.; Joo, C.; Park, T. J.; Yoo, P. J.; Kim, S.; Park, J. Nanoparticles of conjugated polymers prepared from phase-separated films of phospholipids and polymers for biomedical applications. *Adv. Mater.* **2014,** *26*, 4559-4564.

(168) Ahmad Khanbeigi, R.; Abelha, T. F.; Woods, A.; Rastoin, O.; Harvey, R. D.; Jones, M.-C.; Forbes, B.; Green, M. A.; Collins, H.; Dailey, L. A. Surface chemistry of photoluminescent F8BT conjugated polymer nanoparticles determines protein corona formation and internalization by phagocytic cells. *Biomacromolecules* **2015,** *16*, 733-742.

(169) Fernando, L. P.; Kandel, P. K.; Yu, J.; McNeill, J.; Ackroyd, P. C.; Christensen, K. A. Mechanism of cellular uptake of highly fluorescent conjugated polymer nanoparticles. *Biomacromolecules* **2010,** *11*, 2675-2682.

(170) Moon, J. H.; McDaniel, W.; MacLean, P.; Hancock, L. F. Live-cell-permeable poly(p-phenylene ethynylene). *Angew. Chem. Int. Ed.* **2007,** *46*, 8223-8225.

(171) Chan, Y.-H.; Wu, C.; Ye, F.; Jin, Y.; Smith, P. B.; Chiu, D. T. Development of ultrabright semiconducting polymer dots for ratiometric pH sensing. *Anal. Chem.* **2011,** *83*, 1448-1455.

(172) Czaplyski, W. L.; Purnell, G. E.; Roberts, C. A.; Allred, R. M.; Harbron, E. J. Substituent effects on the turn-on kinetics of rhodamine-based fluorescent pH probes. *Org. Biomol. Chem.* **2014,** *12*, 526-533.

(173) Ye, F.; Wu, C.; Jin, Y.; Chan, Y.-H.; Zhang, X.; Chiu, D. T. Ratiometric temperature sensing with semiconducting polymer dots. *J. Am. Chem. Soc.* **2011,** *133*, 8146-8149.

(174) Wu, C.; Bull, B.; Christensen, K.; McNeill, J. Ratiometric single-nanoparticle oxygen sensors for biological imaging. *Angew. Chem. Int. Ed.* **2009,** *48*, 2741-2745.

(175) Dmitriev, R. I.; Borisov, S. M.; Düssmann, H.; Sun, S.; Müller, B. J.; Prehn, J.; Baklaushev, V. P.; Klimant, I.; Papkovsky, D. B. Versatile conjugated polymer nanoparticles for high-resolution O_2 imaging in cells and 3D tissue models. *ACS Nano* **2015,** *9*, 5275-5288.

(176) Huang, Y.-C.; Chen, C.-P.; Wu, P.-J.; Kuo, S.-Y.; Chan, Y.-H. Coumarin dye-embedded semiconducting polymer dots for ratiometric sensing of fluoride ions in aqueous solution and bio-imaging in cells. *J. Mater. Chem. B* **2014,** *2*, 6188-6191.

(177) Childress, E. S.; Roberts, C. A.; Sherwood, D. Y.; LeGuyader, C. L. M.; Harbron, E. J. Ratiometric fluorescence detection of mercury ions in water by conjugated polymer nanoparticles. *Anal. Chem.* **2012,** *84*, 1235-1239.

(178) Feng, X.; Lv, F.; Liu, L.; Tang, H.; Xing, C.; Yang, Q.; Wang, S. Conjugated polymer nanoparticles for drug delivery and imaging. *ACS Appl. Mater. Interfaces* **2010,** *2*, 2429-2435.

(179) Geng, J.; Sun, C.; Liu, J.; Liao, L.-D.; Yuan, Y.; Thakor, N.; Wang, J.; Liu, B. Biocompatible conjugated polymer nanoparticles for efficient photothermal tumor therapy. *Small* **2015,** *11*, 1603-1610.

(180) Shen, X.; Li, L.; Wu, H.; Yao, S. Q.; Xu, Q.-H. Photosensitizer-doped conjugated polymer nanoparticles for simultaneous two-photon imaging and two-photon photodynamic therapy in living cells. *Nanoscale* **2011,** *3*, 5140-5146.

This page is intentionally left blank.

CHAPTER 2

DYE COMPLEXATION AND RELEASE IN β-CYCLODEXTRIN- AND ADAMANTYL-SUBSTITUTED POLY(ACRYLATE) AQUEOUS NETWORKS

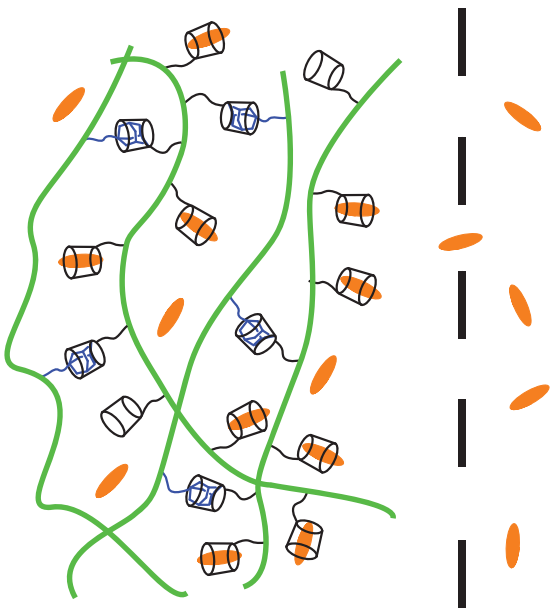

2.1. Introduction

Self-assembling hydrophilic polymer networks in which cross-links between polymer strands form through a variety of interactions exemplified by hydrogen bonding,[1] metal-ligand interactions,[2] and host-guest complexation,[3] have found a wide range of biomedical applications, exemplified by tissue engineering,[4-6] wound healing,[7-9] and drug delivery.[10-15] The host-guest complexation capacity of cyclodextrins[16-19] is prominent within this arena, and is central to the present study which characterizes the formation of networks through complexation by a β-cyclodextrin-substituted poly(acrylate) of adamantyl-substituted poly(acrylate)s and the complexation of dyes within these networks and the release therefrom in aqueous solution. Apart from their intrinsic interest, such systems are potentially models for controlled drug delivery systems.[20-30]

β-Cyclodextrin, β-CD, is the most common of the naturally occurring cyclic oligosaccharides, collectively called cyclodextrins, and is composed of seven α-1,4-linked D-glucopyranose units (Figure 2.1). As a consequence of the α-1,4-linked D-glucopyranose units adopting a $^4C_1$ chair conformation, β-CD has a toroidal shape where the wide and narrow hydrophilic faces are delineated by the C2 and C3 hydroxy groups and by the C6 hydroxy groups, respectively, and a hydrophobic annular interior. In aqueous solution, either β-CD alone or in the form of a polymer substituent complexes within its hydrophobic annulus a wide range of hydrophobic species to form host-guest complexes which exhibit a wide range of stabilities.[16] This characteristic is retained when β-CD is attached to poly(acrylate) (average M_W = 250,000 g mol^{-1}) through a -(2-aminoethyl)amino- tether to give the 8.8% 6^A-(2-aminoethyl)amino-6^A-deoxy-6^A-β-CD, β-CDen, randomly substituted poly(acrylate), PAAβ-CDen, which acts as the host polymer in this study (Figure 2.1). The 3.3%

1-(2-aminoethyl)amidoadamantyl, ADen, 3.0% 1-(6-aminohexyl)amidoadamantyl, ADhn, and 2.9% 1-(12-aminododecyl)amidoadamantyl, ADddn, randomly substituted poly(acrylate)s, PAAADen, PAAADhn and PAAADddn, were chosen as guest polymers in which the length of the tether between the adamantyl group, AD, and the poly(acrylate) backbone progressively increases (Figure 2.1). The AD group was selected as a guest as its particularly strong complexation by β-CD[31] and β-CD oligomers[32,33] and β-CD polymer substituents[34-36] drives the self-assembly of chitosan,[37] hyaluronic acid[38] and poly(acrylate) networks.[39-42]

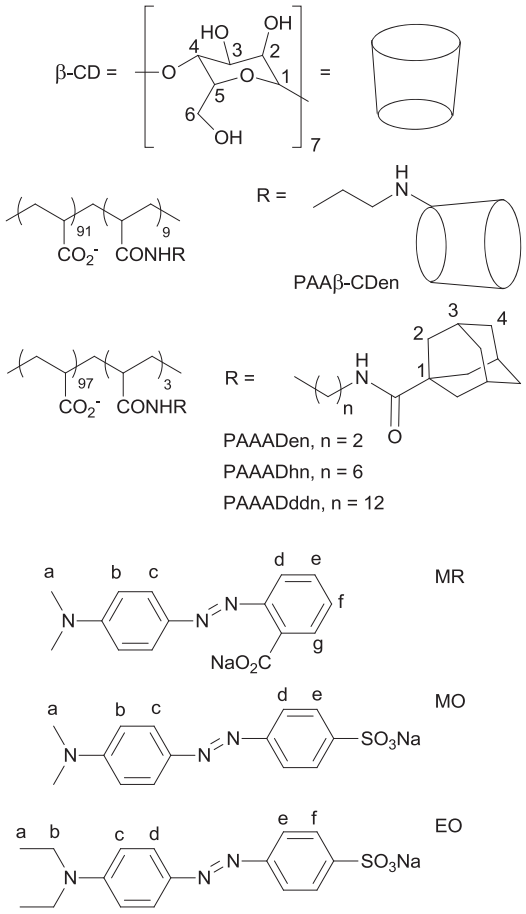

Figure 2.1. β-Cyclodextrin, substituted poly(acrylate)s PAAβ-CDen, PAAADen, PAAADhn, and PAAADddn, and the sodium salts of the dyes ethyl orange, EO, methyl orange, MO, and methyl red, MR.

In aqueous mixtures of PAAβ-CDen and either PAAADen, PAAADhn, or PAAADddn, the

concentration ratio of β-CDen substituents to either ADen, ADhn, or ADddn substituents is designed to be ~9:3 such that self-assembly of the substituted poly(acrylate) network leaves a surplus of β-CD substituents available to complex other guest species. The dyes, methyl red, MR, methyl orange, MO, and ethyl orange, EO, (Figure 2.1) are selected as the small molecule guest species complexed by the surplus β-CDen substituents of PAAβ-CDen as their environment sensitive-UV-Vis absorption spectra facilitates quantification of their complexation and because they are of similar structure and dimension to a variety of drugs.

Network formation by PAAβ-CDen and either PAAADen, PAAADhn, or PAAADddn was characterized by isothermal titration calorimetry, 2D NOESY ^{1}H NMR spectroscopy and rheology. Complexation of MR, MO and EO by β-CD, PAAβ-CDen and the three networks was characterized by UV-Vis and 2D ROESY and NOESY ^{1}H NMR spectroscopy; and release of the dyes from the networks and their components was characterized by UV-Vis spectroscopy.

2.2. Experimental section

2.2.1. Materials

The sodium salts of methyl red (BDH), methyl orange (BDH), and ethyl orange (Sigma-Aldrich) were used as received. Randomly 8.8 ± 0.2 % β-CD substituted PAAβ-CDen[43] and randomly, 3.3 ± 0.1%, 3.0 ± 0.1% and 2.9 ± 0.1%, adamantyl substituted poly(acrylate)s, PAAADen, PAAADhn and PAAADddn, respectively, were prepared according to reported methods.[39-41]

2.2.2. Characterization

1D ^{1}H NMR spectra were run on a Varian Inova 600 spectrometer at an operating frequency of 599.96 MHz. 2D NOESY and ROESY ^{1}H NMR spectra were run on the same spectrometer using standard pulse sequences with a mixing time of 0.3 s. All sample solutions were prepared in D_2O Na_2HPO_4/KH_2PO_4 buffer solutions at pD = 7.0 and I = 0.10 mol dm^{-3} and were equilibrated at the thermostated probe temperature of 298.2 ± 0.1 K for 30 min in 5 mm tubes prior to their spectra being recorded. Chemical shifts (δ, ppm) were internally referenced to residual HOD at δ= 4.79 ppm. The substitution percentage of the β-CDen substituents on the PAAβ-CDen backbones was determined from a comparison of the resonance area of the β-CD H1 protons with that of the poly(acrylate) protons. The substitution percentage of the ADen substituents on the PAAADen, ADhn substituents on the PAAADhn and ADddn substituents on the PAAADddn backbones were determined through a comparison of the resonance area of the methylene protons of both -$NHCH_2$ tether groups with that of the superimposed resonance areas of the poly(acrylate), adamantyl H2-4 and other tether methylene protons. The composition of sample solutions are detailed in the corresponding figure captions.

Rheological measurements were carried out with a Physica MCR 501 (Anton Parr GmbH) stress-controlled rheometer with a 25 mm cone and plate geometry. Temperature was controlled at 298.2 K by a Peltier plate. All solutions were prepared in aqueous Na_2HPO_4/KH_2PO_4 buffer solutions at pH = 7.0 and I = 0.10 mol dm^{-3}. The composition of sample solutions are detailed in the corresponding figure captions. The rheological measurements were performed by Dr. Jie Wang in Professor Xuhong Guo's research group in East China University of Science and Technology.

2.2.3. Isothermal titration calorimetric studies

Isothermal titration calorimetric, ITC, measurements were made using a MicroCal VP isothermal titration calorimeter. In each titration, 10 mm^3 aliquots of a 0.62 wt% PAAβ-CDen solution ([β-CDen substituents] = 2.84×10^{-3} mol dm^{-3}) were titrated into 1.46 cm^3 of a either 0.062 wt% PAAADen ([ADen substituents] = 2.06×10^{-4} mol dm^{-3}), 0.064 wt% PAAADhn ([ADhn substituents] = 1.91×10^{-4} mol dm^{-3}), or 0.072 wt% PAAADddn ([ADddn substituents] = 2.03×10^{-4} mol dm^{-3}) solution at 298.2 K using a computer-controlled micro-syringe at intervals of 210 s. All solutions were prepared in aqueous Na_2HPO_4/KH_2PO_4 buffer solutions at pH = 7.0 and I = 0.10 mol dm^{-3}.

In aqueous solution, the β-CDen substituents of PAAβ-CDen complex the ADen substituents of PAAADen, ADhn substituents of PAAADhn and ADddn substituents of PAAADddn to form self-assembled poly(acrylate) networks as exemplified by the host-guest complexation between the β-CDen substituents of PAAβ-CDen and the ADen substituents of PAAADen according to Equation 2.1.

$$\text{PAAβ-CDen} + \text{PAAADen} \underset{}{\overset{K_{ITC}}{\rightleftharpoons}} \text{PAAβ-CDen.PAAADen} \qquad (\mathbf{2.1})$$

The complexation constant, K_{ITC}, for the host-guest complexation for this equilibrium is given by Equation 2.2,

$$K_{ITC} = [\text{PAAβ-CDen.PAAADen}]/([\text{PAAβ-CDen}][\text{PAAADen}]) \qquad (\mathbf{2.2})$$

where [PAAβ-CDen], [PAAADen] and [PAAβ-CDen.PAAADen] represent the concentration of the β-CDen substituents of PAAβ-CDen, the ADen substituents of PAAADen and their complex at equilibrium, respectively, and,

$$N = [\text{β-CDen substituents complexed}]/[\text{ADen substituents complexed}] \qquad (\mathbf{2.3})$$

in the poly(acrylate) network. In case of 1:1 complexation it is expected that N = 1, while in polymer network systems N may be less than unity, as exemplified by N = 0.78 and 0.87 for

the PAAβ-CDen/PAAADen and PAAβ-CDen/PAAADhn systems, respectively, (Section 2.4) as a consequence of steric hindrance precluding all β-CDen substituents being available for complexation as has been reported for several other networks.[37,38,44,45] Nevertheless, the complexes formed are stoichiometrically 1:1 β-CDen.ADen substituent complexes. If one β-CD substituent complexes AD and a second β-CD substituent complexes its tether, two distinct titration curves will be observed if the thermodynamics of the complexations are sufficiently different. However, if the thermodynamics of the complexations are similar, their two titration curves may superimpose to give a single titration curve characterized by $N > 1$ as exemplified by $N = 1.45$ for the PAAβ-CDen/PAAADddn system (Section 2.4). The $N = 1.45$ infers that of the complexes formed 55% have a 1:1 β-CDen.ADddn substituent stoichiometry and 45% have a 2:1 $(\beta\text{-CDen})_2$.ADddn substituent stiochiometry as is discussed in more detail in Section 2.4.

The heats of dilution were determined by titrating aqueous Na_2HPO_4/KH_2PO_4 buffer (pH = 7.0 and $I = 0.10$ mol dm^{-3}) into similarly buffered PAAADen, PAAADhn or PAAADddn solutions, and by titrating similarly buffered PAAβ-CDen solution into the same buffer. These heats of dilution were subtracted from the total heats evolved to give the heats of host-guest complexation, from which the thermodynamic parameters of the host-guest complexation were calculated. The Origin 7.0 MicroCal protocol[46] was used to derive K_{ITC}, ΔH, $T\Delta S$, and N, based on a one-site complexation model.

2.2.4. UV-Vis spectroscopic titration studies

The UV-Vis absorbance spectra were recorded on a Cary-Varian 5000 UV-Vis spectrophotometer using 1 cm path length matched quartz cells. All the UV-Vis titration studies were performed in aqueous Na_2HPO_4/KH_2PO_4 buffer at pH = 7.0 and $I = 0.10$ mol dm^{-3} at

298.2 K. For the β-CD/dye titration studies, 50 mm^3 aliquots of a β-CD solution were sequentially titrated into 1.5 cm^3 of each dye solution and 1.5 cm^3 of each reference solution. The UV-Vis absorbance spectra were recorded prior to and after each of 20 sequential additions of β-CD solution. For the PAAβ-CDen/dye titration studies, 50 mm^3 aliquots of a PAAβ-CDen solution were sequentially titrated into 1.5 cm^3 of each dye solution and 1.5 cm^3 of each reference solution. The UV-Vis absorbance spectra were recorded prior to and after each of 20 sequential additions of PAAβ-CDen solution. For the PAAβ-CDen/AD substituted poly(acrylate)/dye titration studies, 25 mm^3 aliquots of a PAAβ-CDen solution followed by 25 mm^3 aliquots of either a PAAADen, PAAADhn, or PAAADddn solution were sequentially titrated into 1.5 cm^3 of each dye solution and 1.5 cm^3 of each reference solution. The UV-Vis absorbance spectra were recorded prior to and after each of 20 sequential additions of PAAβ-CDen and either PAAADen, PAAADhn, or PAAADddn solutions. The concentrations of all the solutions used in the UV-Vis titration studies are detailed in the corresponding titration figure captions.

In aqueous solutions, β-CD complexes dye molecules according to Equation 2.4.

$$\text{β-CD} + \text{dye} \underset{}{\overset{K}{\rightleftharpoons}} \text{β-CD.dye} \qquad (\mathbf{2.4})$$

The complexation constant, *K*, for the host-guest complexation between native β-CD and dye molecules at equilibrium is defined by Equation 2.5,

$$K = [\text{β-CD.dye}]/([\text{β-CD}][\text{dye}]) \qquad (\mathbf{2.5})$$

where [β-CD], [dye] and [β-CD.dye] represent the concentration of the native β-CD, the dye and their complex at equilibrium, respectively. Given that $[\text{β-CD}]_{total}$ and $[\text{dye}]_{total}$ are the initial concentrations of the two complexation partners, mass balances are given by Equations 2.6 and 2.7.

$$[\text{β-CD}]_{total} = [\text{β-CD}] + [\text{β-CD.dye}] \qquad (\mathbf{2.6})$$

$$[\text{dye}]_{\text{total}} = [\text{dye}] + [\beta\text{-CD.dye}] \quad (\mathbf{2.7})$$

The UV-Vis absorbance at a particular wavelength is given by Equation 2.8,

$$A = \varepsilon_{\text{dye}}[\text{dye}] + \varepsilon_{\beta\text{-CD.dye}}[\beta\text{-CD.dye}] \quad (\mathbf{2.8})$$

where A, ε_{dye} and $\varepsilon_{\beta\text{-CD.dye}}$ represent the observed absorbance and the molar absorbance of the dye and the host-gues complex, respectively. The value of ε_{dye} measured from the corresponding dye solution was used as an input into the calculation. The complexation constants, K, were derived by solving Equations 2.5-2.8 which were best-fitted to the data using a nonlinear least-squares program, *HypSpec*.[47,48]

The β-CDen substituents of PAAβ-CDen complex dye molecules in aqueous solutions, according to Equation 2.9.

$$\text{PAA}\beta\text{-CDen} + \text{dye} \overset{K}{\rightleftharpoons} \text{PAA}\beta\text{-CDen.dye} \quad (\mathbf{2.9})$$

The complexation constant, K, for the host-guest complexation between the β-CDen substituents of PAAβ-CDen and dye molecules at equilibrium is defined by Equation 2.10,

$$K = [\text{PAA}\beta\text{-CDen.dye}]/([\text{PAA}\beta\text{-CDen}][\text{dye}]) \quad (\mathbf{2.10})$$

where [PAAβ-CDen], [dye] and [PAAβ-CDen.dye] represent the concentration of the β-CDen substituents of PAAβ-CDen, the dye, and their complex at equilibrium, respectively. Given that $[\text{PAA}\beta\text{-CDen}]_{\text{total}}$ and $[\text{dye}]_{\text{total}}$ are the initial concentrations of the two complexation partners, mass balances are given by Equations 2.11 and 2.12.

$$[\text{PAA}\beta\text{-CDen}]_{\text{total}} = [\text{PAA}\beta\text{-CDen}] + [\text{PAA}\beta\text{-CDen.dye}] \quad (\mathbf{2.11})$$

$$[\text{dye}]_{\text{total}} = [\text{dye}] + [\text{PAA}\beta\text{-CDen.dye}] \quad (\mathbf{2.12})$$

The UV-Vis absorbance at a particular wavelength is given by Equation 2.13,

$$A = \varepsilon_{\text{dye}}[\text{dye}] + \varepsilon_{\text{PAA}\beta\text{-CDen.dye}}[\text{PAA}\beta\text{-CDen.dye}] \quad (\mathbf{2.13})$$

where A, ε_{dye} and $\varepsilon_{\text{PAA}\beta\text{-CDen.dye}}$ represent the observed absorbance and molar absorbance of the dye and the host-guest complex, respectively. The ε_{dye} measured from the corresponding

dye solution was used as an input into the calculation. The complexation constants, *K*, were derived by solving Equations 2.10-2.13 which were also best-fitted to the data using a nonlinear least-squares program, *HypSpec*.[47,48]

In the ternary mixtures of PAAβ-CDen and either PAAADen, PAAADhn, or PAAADddn, and a dye in aqueous solution, the β-CDen substituents of PAAβ-CDen complex both ADen, ADhn, or ADddn substituents and dye molecules. Thus, the equilibria for the self-assembled PAAβ-CDen/PAAADen network and for dye complexation by the β-CDen substituents within the network shown in Equations 2.1 and 2.14, respectively, together control the extent of dye complexation.

$$\text{PAAβ-CDen} + \text{PAAADen} \overset{K_{ITC}}{\rightleftharpoons} \text{PAAβ-CDen.PAAADen} \qquad (\mathbf{2.1})$$

$$\text{PAAβ-CDen} + \text{dye} \overset{K}{\rightleftharpoons} \text{PAAβ-CDen.dye} \qquad (\mathbf{2.14})$$

The complexation constant, K_{ITC} (Equation 2.2), for the host-guest complexation between the β-CDen substituents and ADen substituents has been determined in ITC titration studies.

$$K_{ITC} = [\text{PAAβ-CDen.PAAADen}]/([\text{PAAβ-CDen}][\text{PAAADen}]) \qquad (\mathbf{2.2})$$

The complexation constant, *K*, for the host-guest complexation between the β-CDen substituents in the self-assembled PAAβ-CDen/PAAADen network and dye molecules at equilibrium is defined by Equation 2.15,

$$K = [\text{PAAβ-CDen.dye}]/([\text{PAAβ-CDen}][\text{dye}]) \qquad (\mathbf{2.15})$$

where [PAAβ-CDen], [dye] and [PAAβ-CDen.dye] represent the concentration of the β-CDen substituents in the self-assembled PAAβ-CDen/PAAADen network, the dye, and their complex at equilibrium, respectively. Given that $[\text{PAAβ-CDen}]_{total}$, $[\text{dye}]_{total}$ and $[\text{PAAADen}]_{total}$ are the initial concentrations, mass balances are given by Equations 2.16 - 2.18.

$$[\text{PAA}\beta\text{-CDen}]_{total} = [\text{PAA}\beta\text{-CDen}] + [\text{PAA}\beta\text{-CDen.PAAADen}] + [\text{PAA}\beta\text{-CDen.dye}] \quad (\mathbf{2.16})$$

$$[\text{dye}]_{total} = [\text{dye}] + [\text{PAA}\beta\text{-CDen.dye}] \quad (\mathbf{2.17})$$

$$[\text{PAAADen}]_{total} = [\text{PAA}\beta\text{-CDen.PAAADen}] + [\text{PAAADen}] \quad (\mathbf{2.18})$$

The UV-Vis absorbance at a particular wavelength is given by

$$A = \varepsilon_{dye}[\text{dye}] + \varepsilon_{\text{PAA}\beta\text{-CDen.dye}}[\text{PAA}\beta\text{-CDen.dye}] \quad (\mathbf{2.19})$$

where A, ε_{dye} and $\varepsilon_{\text{PAA}\beta\text{-CDen.dye}}$ represent the observed absorbance and molar absorbance of the dye and the host-guest complex, respectively.

In the event that the concentrations of the β-CDen and ADen substituents and the dye were of similar concentrations in the UV-Vis absorbance titration studies of dye complexation, N = 0.78, 0.87 and 1.45 for the PAAβ-CDen/PAAADen, PAAβ-CDen/PAAADhn and PAAβ-CDen/PAAADddn systems, respectively, would have to be taken into account in deriving K from the UV-Vis absorbance titration data. However, typically the initial [dye] = 2.00×10^{-5} mol dm^{-3} and [β-CDen substituents]$_{total}$ = 1.46×10^{-4} mol dm^{-3} and [ADen substituents]$_{total}$ = 4.98×10^{-5} mol dm^{-3} after the first substituent titres are added and increase with the addition of subsequent titres such that both [β-CDen substituents]$_{total}$ and [ADen substituents]$_{total}$ are in substantial excess of the [dye]. Thus, N does not have to be included in the derivation of K for dye complexation. Similar considerations apply for the PAAβ-CDen/PAAADhn and PAAβ-CDen/PAAADddn systems.

The value of ε_{dye} measured from the corresponding dye solution and K_{ITC} measured from ITC titration studies were used as input into the calculation. The complexation constants, K, were derived by solving Equations 2.2 and 2.15-2.19 which were also best-fitted to the data using a nonlinear least-squares program, *HypSpec*.[47,48]

2.2.5. Dye release studies

Dye release studies were performed using a membrane diffusion system (Figure 2.20 in Section 2.10 Appendix) in which a 3500 g mol^{-1} molecular weight cut-off dialysis membrane (Spectr/Por 3) of surface area 7.0 cm^2 separated 5.0 cm^3 of the dye containing solution (made up in Na_2HPO_4/KH_2PO_4 buffer at pH = 7.0 and I = 0.10 mol dm^{-3} with MR, MO and EO concentrations = 2.00×10^{-3} mol dm^{-3}) from 200 cm^3 of aqueous Na_2HPO_4/KH_2PO_4 buffer at pH = 7.0 and I = 0.10 mol dm^{-3} which acted as the receiving solution. During the release experiments, the receiving solution was stirred at 298.2 K. At appropriate time intervals, a 2 cm^3 sample of the receptor solution was withdrawn, its UV-Vis spectrum was measured and the sample was then returned to the receiving solution. The dye concentration in the receiving solution was calculated by reference to its molar absorbance spectrum determined under the same conditions. Each dye solution composition is given in Table 2.4 in Section 2.10 Appendix. All solutions were stirred and equilibrated for 16 h at 298.2 K before use.

2.3. Synthesis of β-cyclodextrin and adamantyl substituted poly(acrylate)s

The substituted poly(acrylate)s (Figure 2.1): PAAβ-CDen,[43] PAAADen,[39] PAAADhn,[40,41] and PAAADddn[40,41] were synthesized according to reported procedures, and the degree of random substitution of the β-CDen substituents, ADen substituents, ADhn substituents, and ADddn substituents per mole of acrylate unit were determined from their ^{1}H NMR spectra to be 8.8, 3.3, 3.0 and 2.9%, respectively. The substituted poly(acrylate) network formation by PAAβ-CDen and either PAAADen, PAAADhn, or PAAADddn arising from host-guest complexation between their β-CDen and ADen, ADhn or ADddn substituents is central to this study and has been characterized by isothermal titration calorimetry, ITC, 2D NOESY ^{1}H NMR spectroscopy and rheology. Complexation of the dyes MR, MO and EO by the β-CD,

PAAβ-CDen and the three poly(acrylate) networks was characterized by UV-Vis and 2D NOESY and ROESY ^{1}H NMR spectroscopy.

The general picture which emerges for dye complexation in the PAAβ-CDen/PAAADen and PAAβ-CDen/PAAADhn networks is broadly shown in Figure 2.2. In the case of the PAAβ-CDen/PAAADddn network, the long dodecyl tether of the ADddn substituent appears to compete with the dyes for complexation in the β-CD annulus. Subsequently, the release of the dyes from the networks and their components through a dialysis membrane was characterized by UV-Vis spectroscopy.

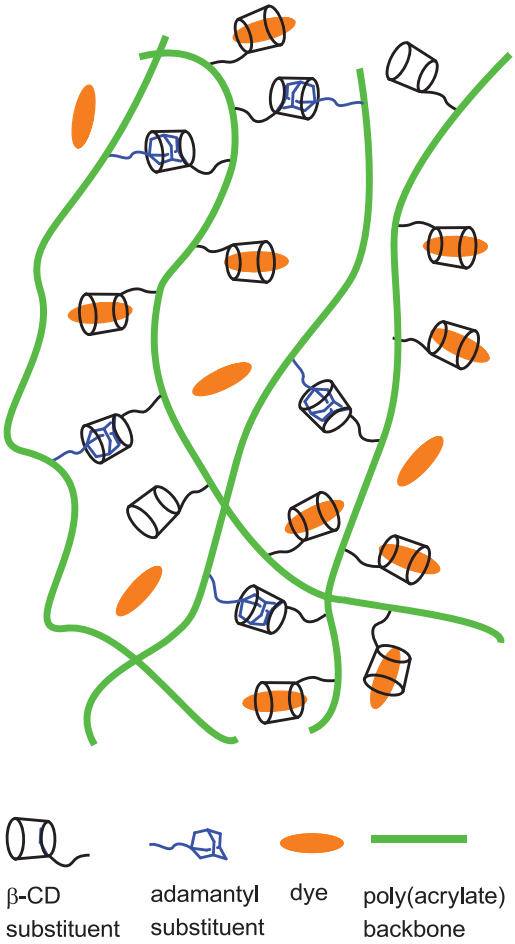

Figure 2.2. Representation of complexation of dye species in the PAAβ-CDen/PAAADen and PAAβ-CDen/PAAADhn networks.

2.4. ITC and NOESY ^{1}H NMR characterization of poly(acrylate) network formation

Isothermal titration calorimetry, ITC, was used to determine the complexation constant, K_{ITC}, and ΔH and $T\Delta S$ characterizing the host-guest complexes formed by the β-CDen and ADen, ADhn, or ADddn substituents of the substituted poly(acrylate)s. The ITC data also yields the ratio of the number of β-CDen to ADen, ADhn, or ADddn substituents in the complex formed, N, which is equal to the ratio corresponding to the inflexion point in the titration curve for the titration of a PAAβ-CDen solution into a solution of either PAAADen, PAAADhn or PAAADddn. The experimental data for the titration of a PAAβ-CDen solution into a PAAADen solution together with the best-fit of an algorithm for a single complexation (Equation 2.1) to these data are shown in Figure 2.3. The derived K_{ITC}, ΔH, $T\Delta S$ and N appear in Table 2.1. The observed $N = 0.78$ is less than $N = 1$ anticipated for each β-CDen substituent complexing an ADen substituent, which is attributable to either steric hindrance by the poly(acrylate) backbone, or hydrophobic association of the ADen substituents, or both, hindering complexation as has also been observed in other studies.[37,38,44,45]

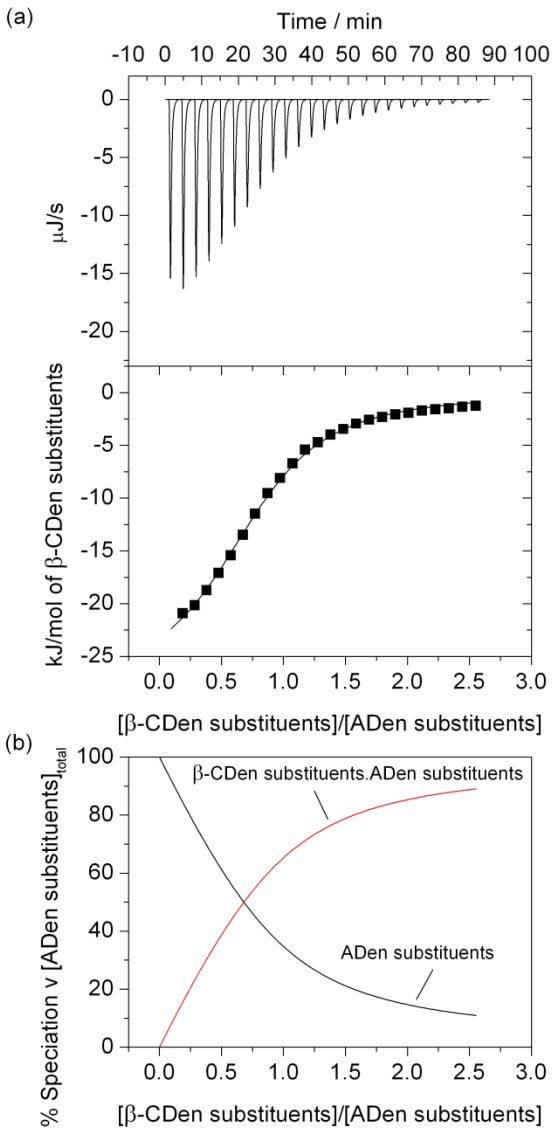

Figure 2.3. (a) (Top) ITC data for the titration of 10 mm^3 aliquots of a 0.62 wt% PAAβ-CDen solution ([β-CDen substituents] = 2.84 × 10^{-3} mol dm^{-3}) into 1.46 cm^3 of a 0.062 wt% PAAADen ([ADen substituents] = 2.06 × 10^{-4} mol dm^{-3}) solution at 298.2 K. Both solutions were prepared in aqueous Na_2HPO_4/KH_2PO_4 buffer solutions at pH = 7.0 and I = 0.10 mol dm^{-3}. (Bottom) The solid curve shows the best-fit of an algorithm for host-guest complexation between the β-CDen and ADen substituents to the experimental data points. (b) Speciation plot with $[ADen\ substituents]_{total}$ = 100%.

Table 2.1. Parameters determined for host-guest complexation between PAAβ-CDen and either PAAADen, PAAADhn, or PAAADddn in aqueous Na_2HPO_4/KH_2PO_4 buffer at pH 7.0 and I = 0.10 mol dm^{-3}.

Host	PAAβ-CDen[a]		
Guest	PAAADen	PAAADhn	PAAADddn
$10^{-3}K_{ITC}$ / dm^3 mol^{-1}	28.2 ± 0.15	28.4 ± 0.15	39.5 ± 0.08
ΔH / kJ mol^{-1}	-27.81 ± 0.55	-25.74 ± 0.48	-22.36 ± 0.09
$T\Delta S$ / kJ mol^{-1}	-2.42 ± 0.05	-0.35 ± 0.01	3.85 ± 0.08
N	0.78 ± 0.01	0.87 ± 0.01	1.45 ± 0.01
Host	β-CD[b]		
Guest	PAAADen	PAAADhn	PAAADddn
$10^{-3}K_{ITC}$ / dm^3 mol^{-1}	8.77 ± 0.24	14.4 ± 0.06	5.77 ± 0.18
ΔH / kJ mol^{-1}	-20.81 ± 0.12	-15.45 ± 0.09	-16.58 ± 0.17
$T\Delta S$ / kJ mol^{-1}	1.72 ± 0.18	8.29 ± 0.18	4.89 ± 0.24
N	0.86 ± 0.24	0.85 ± 0.06	0.83 ± 0.05

[a]This study. [b]Data from Reference 32 obtained under identical conditions to those of this study. The errors shown are the data fitting errors, and the experimental error is ≤ 5% in both studies.

Further insight into the complexation process is gained from the 2D NOESY ^{1}H NMR spectrum of a D_2O solution of PAAβ-CDen and PAAADen in which the β-CDen and ADen substituents are equimolar (Figure 2.4). Substitution of β-CD at C6^A, as in PAAβ-CDen, renders all of the D-glucopyranose subunits inequivalent. As a consequence, small differences in the chemical shifts of the resonances of each D-glucopyranose subunit result in a loss of definition in the β-CD group spectrum such that the H2-6 resonances cannot be separately identified as seen in Figure 2.4. Thus, the cross-peaks in box A cannot be unequivocally assigned to the anticipated dominant dipolar interactions between the β-CD annular H3,5,6 protons and the H2-4 AD protons. Nevertheless, there is a significant dipolar interaction between the β-CD and AD protons consistent with complexation of the AD group in the β-CD annulus as shown in Figure 2.5 a). (The 2D NOESY ^{1}H NMR spectrum of PAAβ-CDen alone

(Figure 2.21 in Section 2.10 Appendix) shows no cross-peaks in the region where those assigned to β-CD/AD group dipolar interactions in Figure 2.4 arise indicating that β-CD group proton dipolar interactions with PAAβ-CDen backbone protons are insignificant.) The ITC experimental data (Figure 2.22 in Section 2.10 Appendix) and the derived parameters (Table 2.1) for the PAAβ-CDen/PAAADhn system are similar to those for the PAAβ-CDen/PAAADen system as is the corresponding 2D NOESY ^{1}H NMR spectrum (Figure 2.23 in Section 2.10 Appendix).

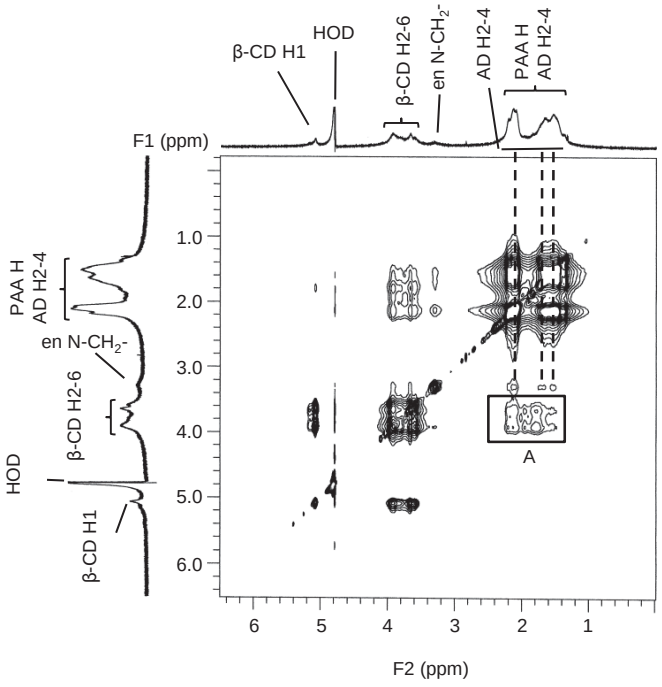

Figure 2.4. 2D NOESY ^{1}H NMR spectrum of 0.44 wt% PAAβ-CDen ([β-CDen substituents] = 2.0×10^{-3} mol dm^{-3}) and 0.60 wt% PAAADen ([ADen substituents] = 2.0×10^{-3} mol dm^{-3}) in D_2O Na_2HPO_4/KH_2PO_4 buffer solution at pD = 7.0 and I = 0.10 mol dm^{-3} at 298.2 K. Cross-peaks in box A arise from dipolar interactions between the annular H3,5,6 protons of the β-CD groups and the H2-4 protons of the AD groups.

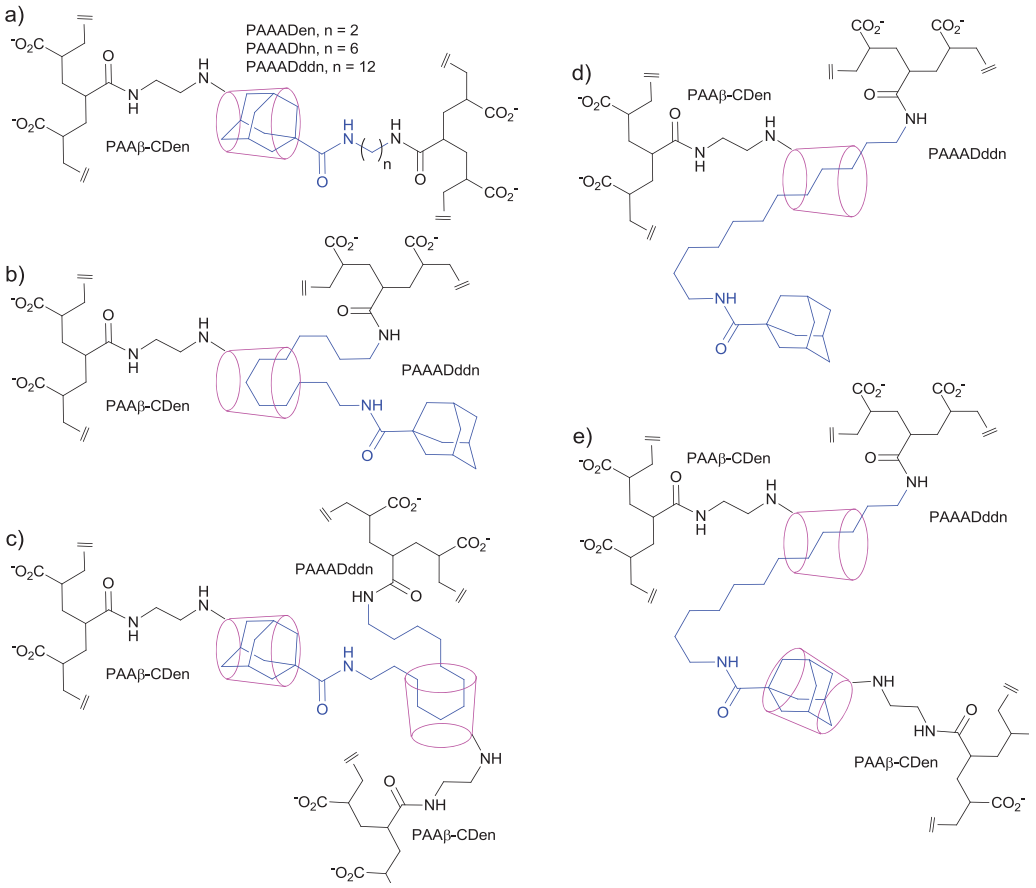

Figure 2.5. Modes of complexation between the β-CDen substituents of PAAβ-CDen and the ADen substituents of PAAADen, ADhn substituents of PAAADhn, and ADddn substituents of PAAADddn. a) Complexation of the AD group in the β-CD annulus. b) Complexation of the dodecyl tether of PAAADddn in the β-CD annulus. c) As for b) with complexation of the AD group in a second β-CD annulus. d) Complexation of the dodecyl tether of PAAADddn in the β-CD annulus after passage of the AD group through the annulus. e) As for d) with complexation of the AD group in a second β-CD annulus.

An algorithm for a single complexation analogous to that shown in Equation 2.1 fitted well to the ITC experimental data for the PAAβ-CDen/PAAADddn system (Figure 2.6). However, the ITC experimental data curve and derived parameters for the PAAβ-CDen/PAAADddn system differ markedly from the first two systems as seen from Figure 2.6 and Table 2.1. The N = 1.45 value is consistent with a single β-CDen substituent of PAAβ-CDen complexing a

single ADddn substituent of PAAADddn (Figure 2.5 a), b) and d)) and two β-CD substituents complexing a single ADddn substituent (Figure 2.5 c) and e)) in proportions which average to N = 1.45 as a result of the greater flexibility arising from the dodecyl tether although the individual contributions of these two complexations are not separately identifiable in the ITC data. It seems unlikely that the tether complexation shown in Figure 2.5 b) would compete effectively with AD group complexation and accordingly it seems likely that the tether complexation occurs after the complexation of the AD group as shown in Figure 2.5 a) and the tether complexation occurs to give c) in Figure 2.5 subsequently. The initial formation of the tether complex arising from passage of the AD group through the β-CD annulus shown in Figure 2.5 d) and subsequent complexation of the AD group in a second β-CD annulus (Figure 2.5 e) also provides a possible route to the complexation of an ADddn substituent by two β-CD substituents as indicated by the ITC data and also simultaneous complexation of the AD group and its dodecyl tether as indicated by ^{1}H NMR spectroscopy. The likelihood of the AD group passing through the β-CD annulus instead of remaining complexed therein is not readily assessed. Thus, an apportioning of probabilities of the two sequences a) to c) and d) to e) occurring is not readily made on the basis of the ITC and NMR data.

The 2D NOESY ^{1}H NMR spectrum of the PAAβ-CDen/PAAADddn system (Figure 2.7) shows cross-peaks arising from dipolar interactions between the β-CD group H3,5,6 protons and those of both the AD group and the methylene protons of its dodecyl tether, also consistent with the a) - e) complexation modes of Figure 2.5. While the ^{1}H NMR data indicate the complexation of the AD group and its dodecyl tether, and thereby the plausibility of simultaneous complexation by two β-CD groups, they neither facilitate distinctions between modes b) and d) nor between modes c) and e) in which a second β-CD group may complex the AD group.

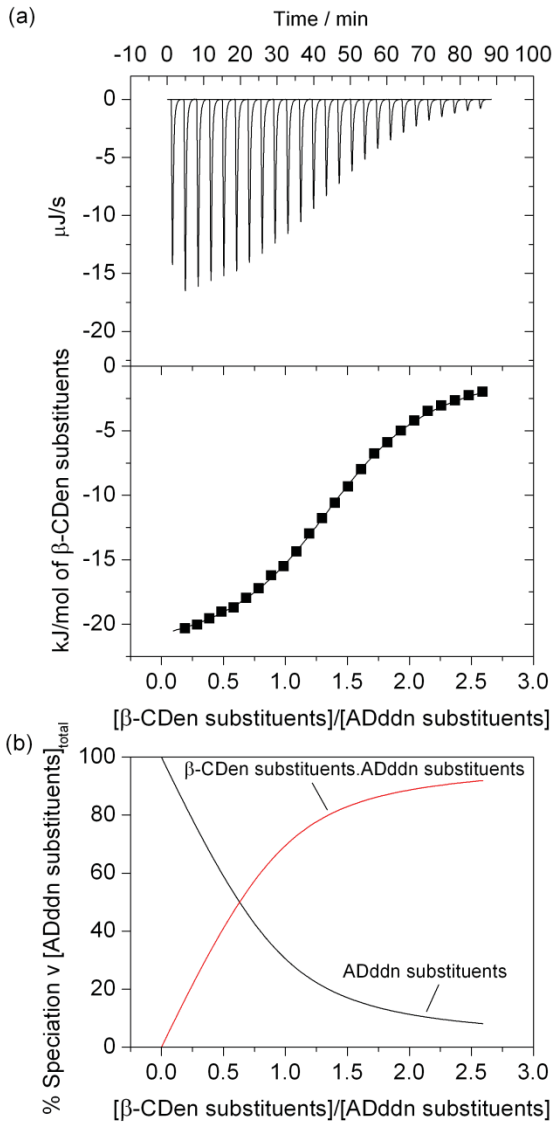

Figure 2.6. (a) (Top) ITC data for the titration of 10 mm^3 aliquots of a 0.62 wt% PAAβ-CDen solution ([β-CDen substituents] = 2.84 × 10^{-3} mol dm^{-3}) into 1.46 cm^3 of a 0.072 wt% PAAADddn ([ADddn substituents] = 2.03 × 10^{-4} mol dm^{-3}) solution at 298.2 K. Both solutions were prepared in aqueous Na_2HPO_4/KH_2PO_4 buffer solutions at pH = 7.0 and I = 0.10 mol dm^{-3}. (Bottom) The solid curve shows the best-fit of an algorithm for host-guest complexation between the β-CDen and ADddn substituents to the experimental data points. (b) Speciation plot with $[ADddn\ substituents]_{total}$ = 100%.

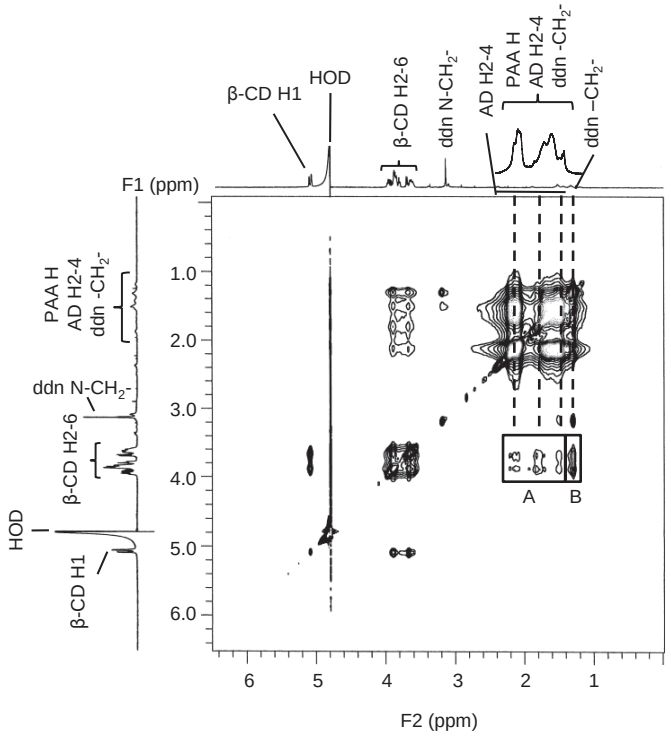

Figure 2.7. 2D NOESY ^{1}H NMR spectrum of 0.44 wt% PAAβ-CDen ([β-CDen substituents] = 2.0×10^{-3} mol dm^{-3}) and 0.70 wt% PAAADddn ([ADddn substituents] = 2.0×10^{-3} mol dm^{-3}) in D_2O Na_2HPO_4/KH_2PO_4 buffer solution at pD = 7.0 and I = 0.10 mol dm^{-3} at 298.2 K. Cross-peaks in box A arise from dipolar interactions between the annular H3,5,6 protons of the β-CD groups and the H2-4 protons of the AD groups. Cross-peaks in box B arise from dipolar interactions between the annular H3,5,6 protons of the β-CD groups and the tether dodecyl methylene protons (ddn-CH_2).

The large K_{ITC} for the PAAβ-CDen/PAAADen and PAAβ-CDen/PAAADhn systems are dominantly due to substantial ΔH contributions. The negative $T\Delta S$ are attributable to the entropy loss arising from the combination of the β-CD and AD groups into a single complex, and also the loss of mobility, outweighing the entropy gain[16,49] anticipated from the displacement of water from the β-CD annulus by the AD group. The K_{ITC} for the PAAβ-CDen/PAAADddn system is the largest observed and, despite showing a smaller ΔH than the other two systems, the positive $T\Delta S$ causes greater stabilization of the complexes in

this system. This entropy increase may arise from substantial aggregation between the long ADddn hydrophobic substituents in PAAADddn and the consequent decrease in entropy, being disrupted through complexation by PAAβ-CDen and the entropy decreases arising from the network formation not compensating for that lost through disruption of ADddn substituent aggregation. Because more than one complexation mode appears to operate, as discussed above in conjunction with Figure 2.5, it is not possible to further analyze these thermodynamic differences other than to attribute them to the greater length of the dodecyl tether and the correspondingly increased flexibility in the PAAβ-CDen/PAAADddn system.

A comparison with the complexation parameters for the β-CD/PAAADen, β-CD/PAAADhn and β-CD/PAAADddn systems (Table 2.1) shows these systems to be characterized by significantly smaller K_{ITC} and ΔH and more positive $T\Delta S$. (The N = 0.86 - 0.83 are also consistent with either steric hindrance by the poly(acrylate) backbone, or hydrophobic association of the AD substituents, or both hindering complexation). The greater stabilities of the PAAβ-CDen/PAAADen and PAAβ-CDen/PAAADhn systems by comparison with the analogous β-CD systems is attributable to a cooperative effect whereby the formation of inter-poly(acrylate) strand cross-links formed by β-CDen-substituent/ADen-substituent or β-CDen-substituent/ADhn-substituent complexation is mutually reinforcing whereas the independent complexation by β-CD of the ADen substituents in the β-CD/PAAADen system or ADhn substituents in the β-CD/PAAADhn system lacks this reinforcement. The cooperative effect of the PAAβ-CDen/PAAADen and PAAβ-CDen/PAAADhn systems is likely to decrease freedom of motion through network formation, thereby decreasing entropy by comparison with the analogous β-CD systems.

The N = 1.45 and 0.83 (Table 2.1) for the PAAβ-CDen/PAAADddn and β-CD/PAAADddn systems, respectively, indicate that the inter-strand cross-links formed in the first system

stabilize complexation of an ADddn substituent by up to two β-CDen substituents whereas such stabilization in the second system is absent. It is likely that this stabilization of the PAAβ-CDen/PAAADddn system is also the source of the greater overall K_{ITC} and ΔH and less positive $T\Delta S$ observed for the PAAβ-CDen/PAAADddn system although these cannot be apportioned between the possible complexation modes shown in Figure 2.5.

At the low substituted poly(acrylate) concentrations of the ITC studies, the solutions retain high fluidity consistent with localized cross-linked networks forming, but at higher substituted poly(acrylate) concentrations the solutions become viscous and are characterized by rheology as discussed below.

2.5. UV-Vis and 2D ROESY and NOESY ^{1}H NMR characterization of dye complexation

The complexation of MR, MO and EO by β-CD alone are first considered as a basis for assessing the effects of the substitution of β-CD onto the poly(acrylate) in PAAβ-CDen and the subsequent network formation with PAAADen, PAAADhn and PAAADddn on dye complexation. Thus, the variation of absorbance of all three dyes with added β-CD was consistent with the dominant formation of 1:1 β-CD.dye complexes (Equations 2.4 and 2.5), as exemplified for EO in Figure 2.8. (Analogous absorbance variations are seen for MR and MO in Figures 2.24 and 2.25 in Section 2.10 Appendix, respectively.) The wavelengths at which maximum absorbance occur for the free dyes and in their complexed states, λ_{max}, and the derived K for the three dyes are given in Table 2.2. The smallest and largest K characterize the β-CD.MR and β-CD.EO host-guest complexes, respectively, and reflect the more favorable stereochemistry of EO for complexation and its greater hydrophobicity.

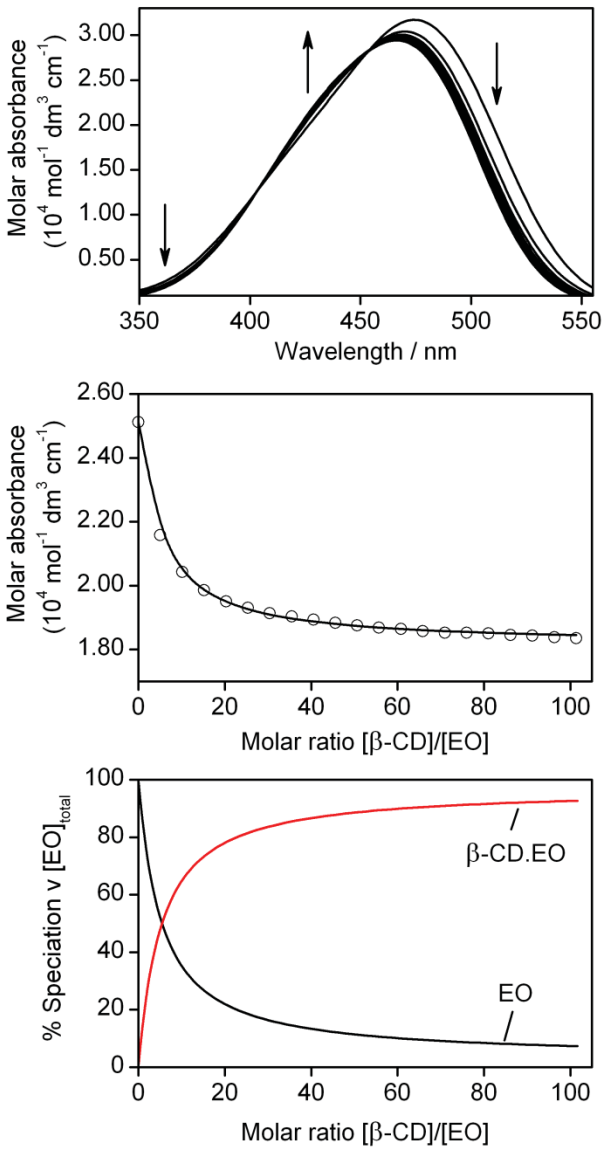

Figure 2.8. (Top) Molar absorbance variation of a EO solution ([EO] = 2.00×10^{-5} mol dm^{-3}) with 20 sequential additions of a β-CD solution (50 mm^3 each, [β-CD] = 3.04×10^{-3} mol dm^{-3}) at 298.2 K. Both solutions were prepared in aqueous Na_2HPO_4/KH_2PO_4 buffer at pH 7.0 and I = 0.10 mol dm^{-3}. The arrows indicate the direction of molar absorbance change upon each addition of the β-CD solution. (Middle) Molar absorbance variation at 500 nm and the line representing the best-fit of an algorithm for a 1:1 host-guest complexation of EO by β-CD over the wavelength range 475 - 525 nm. (Bottom) Speciation plot with $[EO]_{total}$ = 100%.

Table 2.2. UV-Vis spectroscopic titration data.[a]

Host	Guest	λ_{max} nm	K[b] $dm^3\ mol^{-1}$
None	MR	430	–
	MO	464	–
	EO	474	–
β-CD	MR	414	772 ± 10
	MO	455	3255 ± 35
	EO	466	10515 ± 110
β-CD substituents of PAAβ-CDen	MR	415	76 ± 1
	MO	458	1454 ± 20
	EO	463	2230 ± 30
β-CD substituents in PAAβ-CDen/PAAADen networks	MR	[c]	[c]
	MO	457	1001 ± 10
	EO	463	1475 ± 20
β-CD substituents in PAAβ-CDen/PAAADhn networks	MR	[c]	[c]
	MO	457	875 ± 10
	EO	463	1411 ± 20
β-CD substituents in PAAβ-CDen/PAAADddn networks	MR	[c]	[c]
	MO	457	713 ± 10
	EO	467	986 ± 20

[a]Obtained in aqueous Na_2HPO_4/KH_2PO_4 buffer at pH = 7.0 and I = 0.10 mol dm^3 at 298.2 K.

[b]The errors shown are fitting errors and the overall error is ± 5%.

[c]Data not determined.

A 2D ROESY ^{1}H NMR spectrum (Figure 2.9) of an equimolar solution of β-CD and EO shows cross-peaks arising from dipolar interactions between the β-CD annular H3,5,6 protons and the EO Ha-f protons which, on the basis of the EO length being greater than the depth of the β-CD annulus, is consistent with a to and fro movement of EO within the annulus facilitating all six EO proton dipolar interactions. (Cross-peaks arising from dipolar interactions between EO methylene (Hb) protons and adjacent aromatic (Hc) and methyl (Ha)

protons of EO, respectively, as observed for a solution of EO alone (Figure 2.26 in Section 2.10 Appendix) also contribute to the spectrum shown in Figure 2.9.) Analogous 2D ROESY ^{1}H NMR spectra are observed for the MR and MO complexes in Figures 2.27 and 2.28 in Section 2.10 Appendix, respectively.

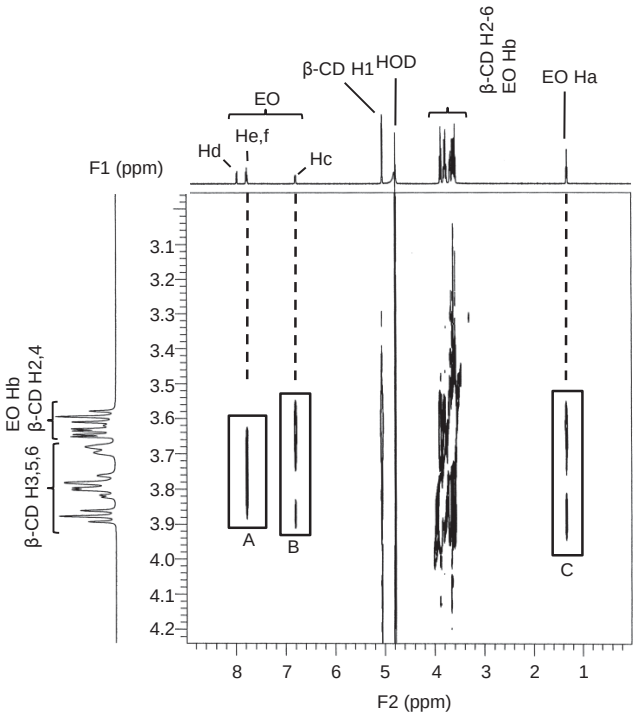

Figure 2.9. 2D ROESY ^{1}H NMR spectrum of EO ([EO] = 2.0×10^{-3} mol dm^{-3}) and β-CD ([β-CD] = 2.0×10^{-3} mol dm^{-3}) in D_2O Na_2HPO_4/KH_2PO_4 buffer solution at pD = 7.0 and I = 0.10 mol dm^{-3} at 298.2 K. Cross-peaks in boxes A, B, and C arise from dipolar interactions between the β-CD annular H3,5,6 protons and the EO aromatic (Hc, He and Hf) and methyl (Ha) protons, respectively. Dipolar interactions between EO methylene (Hb) protons and adjacent aromatic (Hc) and methyl (Ha) protons of EO, respectively, also contribute to the cross-peaks in boxes B and C, respectively.

Systematic UV-Vis absorbance changes were also observed for the dyes upon addition of PAAβ-CDen as seen for EO in Figure 2.10 and MR and MO in Figures 2.29 and 2.30 in Section 2.10 Appendix, respectively. The K derived through Equation 2.10 are substantially decreased

in magnitude particularly for MR (Table 2.2), and this is attributable to a combination of steric hindrance between the poly(acrylate) backbone and also repulsion between the PAAβ-CDen carboxylate groups and the negatively charged dyes. Despite the small *K* characterizing the complexation of MR by PAAβ-CDen, significant cross-peaks arising from dipolar interactions between the β-CD group annular H3,5,6 protons and the MR Ha-g protons were observed in the 2D NOESY ^{1}H NMR spectrum of a D_2O solution in which MR and the β-CDen substituents were equimolar (Figure 2.11). Analogous cross-peaks were observed for the corresponding MO and EO solutions (Figures 2.31 and 2.32 in Section 2.10 Appendix), respectively.

The UV-Vis absorbance changes accompanying complexation of EO in PAAβ-CDen/PAAADen solution are shown in Figure 2.12, and the accompanying changes in free β-CDen substituents, β-CDen substituents.ADen substituents complex and β-CDen substituents.EO complex are shown in Figure 2.13. The analogous data for EO in PAAβ-CDen/PAAADhn and PAAβ-CDen/PAAADddn solutions appear in Figures 2.33 - 2.36 in Section 2.10 Appendix. The analogous data for MO in PAAβ-CDen/PAAADen, PAAβ-CDen/PAAADhn and PAAβ-CDen/PAAADddn solutions appear in Figures 2.37 - 2.42, in Section 2.10 Appendix. Collectively, these data facilitate determination of *K* for all six systems. The derived *K* appear in Table 2.2 from which it is seen that in each case *K* is further decreased by comparison with that determined for complexation by β-CD and PAAβ-CDen, probably as a result of increased steric crowding within the network. The largest decreases in *K* occur for the PAAβ-CDen/PAAADddn/MO and PAAβ-CDen/PAAADddn/EO systems; decrease which may reflect the effect of the additional competition between the ADddn substituent tether and the dyes for complexation by the β-CDen substituents. The UV-Vis changes observed for MR in the three networks (Figures 2.43 - 2.45 in Section 2.10 Appendix) are too small for derivation of *K* which may indicate that the decrease in *K* observed for

complexation of MO and EO by β-CD and PAAβ-CDen occurs for MR also.

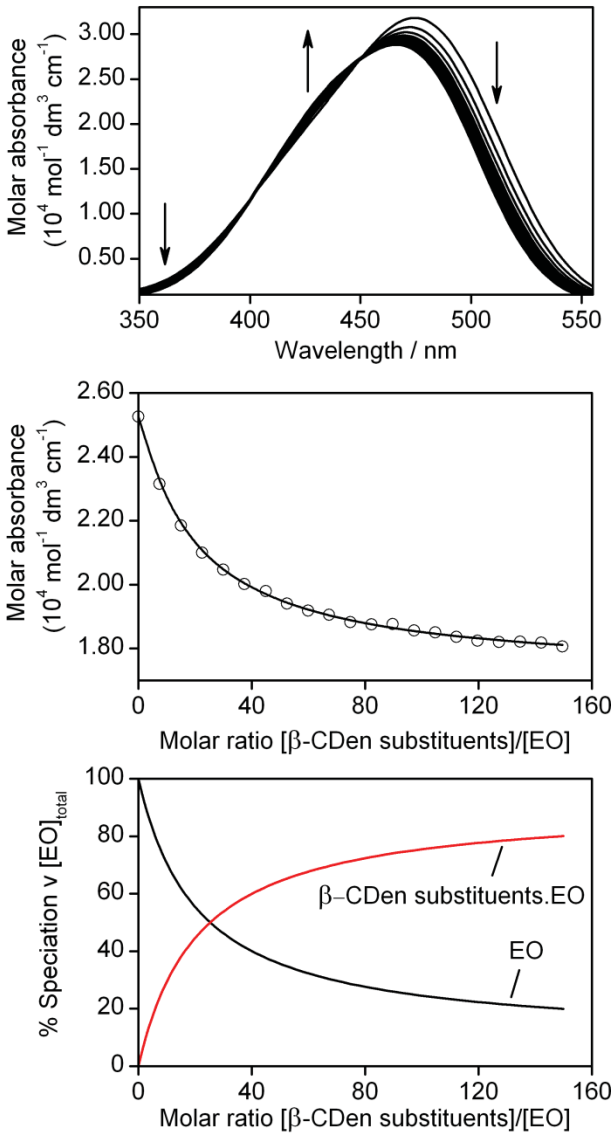

Figure 2.10. (Top) Molar absorbance variation of a EO solution ([EO] = 2.00 × 10^{-5} mol dm^{-3}) upon 20 sequential additions of a PAAβ-CDen solution (50 mm^3 each, 0.98 wt%, [β-CDen substituents] = 4.49 × 10^{-3} mol dm^{-3}) at 298.2 K. Both solutions were prepared in aqueous Na_2HPO_4/KH_2PO_4 buffer solutions at pH 7.0 and I = 0.10 mol dm^{-3}. The arrows indicate the direction of molar absorbance variation upon each addition of the PAAβ-CDen solution. (Middle) Molar absorbance variation at 500 nm and the line representing the best-fit of an algorithm for a 1:1 host-guest complexation of EO by β-CDen substituents of PAAβ-CDen over the wavelength range 475 - 525 nm. (Bottom) Speciation plot with $[EO]_{total}$ = 100%.

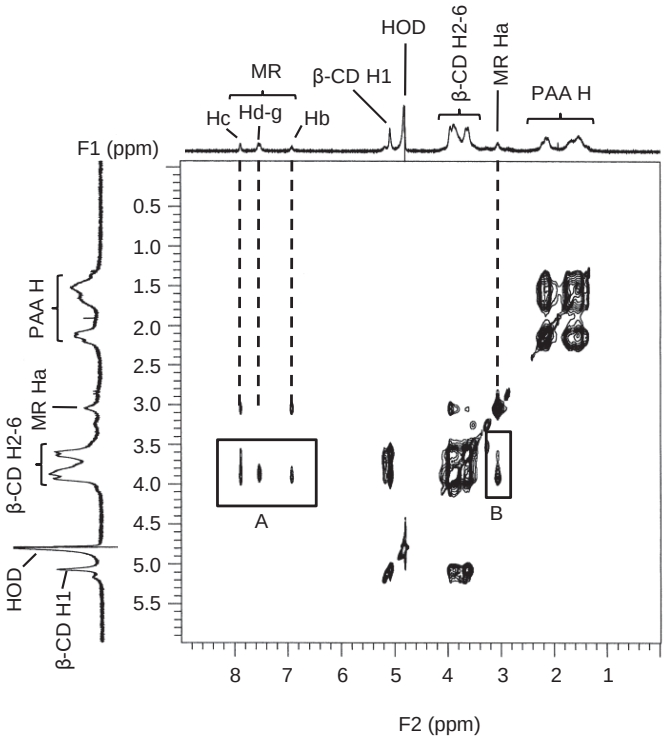

Figure 2.11. 2D NOESY ^{1}H NMR spectrum of MR ([MR] = 2.0 × 10^{-3} mol dm^{-3}) and PAAβ-CDen (0.44 wt%, [β-CDen substituents] = 2.0 × 10^{-3} mol dm^{-3}) in D_2O Na_2HPO_4/KH_2PO_4 buffer solution at pD = 7.0 and I = 0.10 mol dm^{-3} at 298.2 K. Cross-peaks in boxes A and B arise from dipolar interactions between the annular H3,5,6 protons of the β-CD groups and the aromatic (Hb-g) and methyl (Ha) protons of MR, respectively.

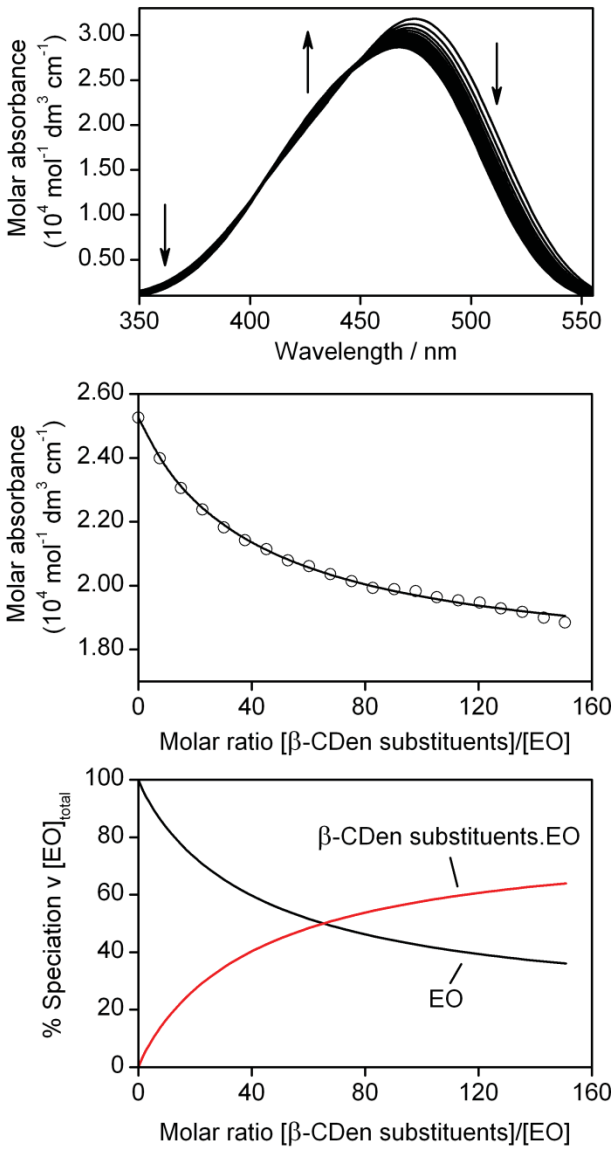

Figure 2.12. (Top) Molar absorbance variation of a EO solution ([EO] = 2.00 × 10^{-5} mol dm^{-3}) upon 20 sequential additions of a PAAβ-CDen solution (25 mm^3 each, 1.93 wt%, [β-CDen substituents] = 9.03 × 10^{-3} mol dm^{-3}) and a PAAADen solution (25 mm^3 each, 0.91 wt%, [ADen substituents] = 3.09 × 10^{-3} mol dm^{-3}) at 298.2 K. All solutions were prepared in aqueous Na_2HPO_4/KH_2PO_4 buffer solutions at pH 7.0 and I = 0.10 mol dm^{-3}. The arrows indicate the direction of molar absorbance variation upon each addition of the PAAβ-CDen and PAAADen solutions. (Middle) Molar absorbance variation at 500 nm and the line representing the best-fit of an algorithm for a 1:1 host-guest complexation of EO by β-CDen substituents in self-assembled PAAβ-CDen/PAAADen network over the wavelength range 475 - 525 nm. (Bottom) Speciation plot with $[EO]_{total}$ = 100%.

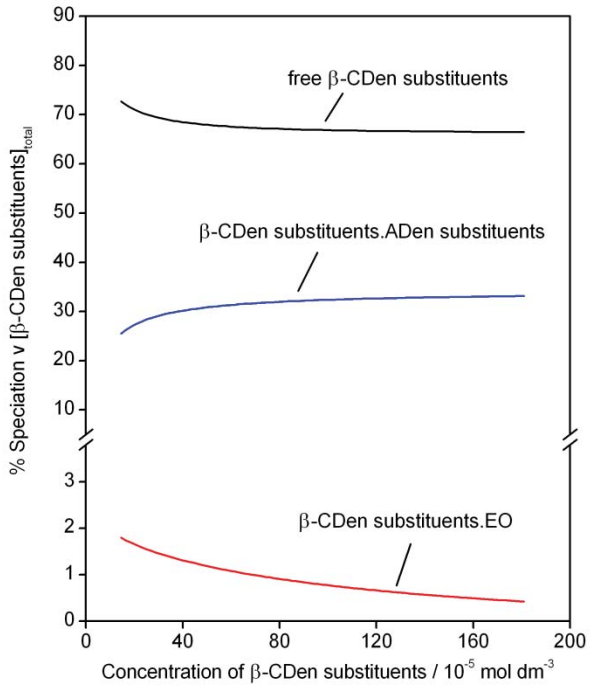

Figure 2.13. Speciation plot with $[\beta\text{-CDen substituents}]_{total}$ = 100% for the PAAβ-CDen/PAAADen/EO system.

Interestingly, cross-peaks arising from dipolar interactions between the β-CD group protons and the MR protons and the AD group protons are observed for solutions of MR and PAAβ-CDen/PAAADen (Figure 2.14), PAAβ-CDen/PAAADhn (Figure 2.46 in Section 2.10 Appendix) and PAAβ-CDen/PAAADddn (Figure 2.47 in Section 2.10 Appendix). This is consistent with MR being complexed in these systems to a greater extent in the more concentrated solutions (PAAβ-CDen/PAAADen 1.14 wt%, PAAβ-CDen/PAAADhn 1.18 wt%, PAAβ-CDen/PAAADddn 1.21 wt%) prepared for ^{1}H NMR studies than in the lower concentration solutions (PAAβ-CDen/PAAADen 0.77 wt%, PAAβ-CDen/PAAADhn 0.79 wt%, PAAβ-CDen/PAAADddn 0.81 wt%) prepared for UV-Vis studies. Analogous cross-peaks are observed for MO (Figures 2.48 - 2.50 in Section 2.10 Appendix) and EO (Figures 2.51 - 2.53 in Section 2.10 Appendix).

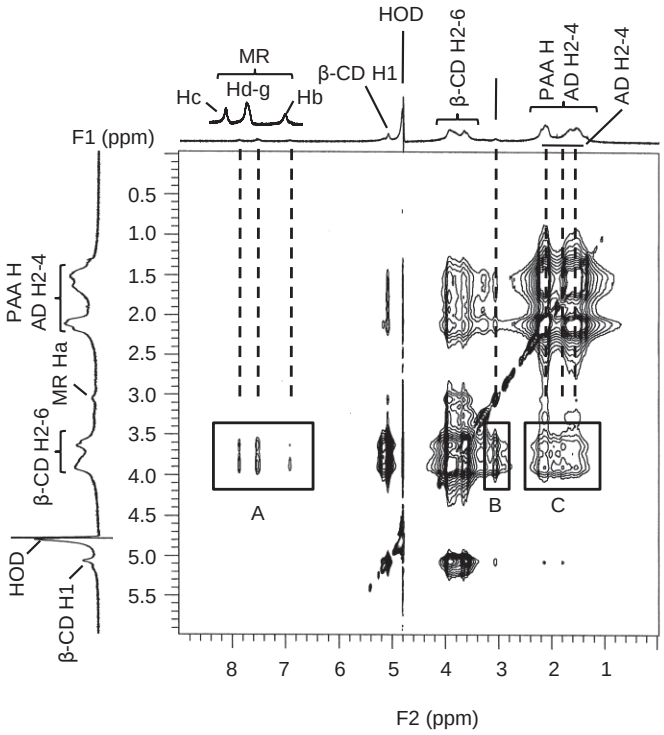

Figure 2.14. 2D NOESY ^{1}H NMR spectrum of MR ([MR] = 2.0×10^{-3} mol dm^{-3}) in mixture with PAAβ-CDen (0.78 wt%, [β-CDen substituents] = 3.6×10^{-3} mol dm^{-3}) and PAAADen (0.40 wt%, [ADen substituents] = 1.2×10^{-3} mol dm^{-3}) in D_2O Na_2HPO_4/KH_2PO_4 buffer solution at pD = 7.0 and I = 0.10 mol dm^{-3} at 298.2 K. Cross-peaks in boxes A and B arise from dipolar interactions between the annular H3,5,6 protons of the β-CD groups and the aromatic (Hb-g) and methyl (Ha) protons of MR, respectively. Cross-peaks in box C arise from dipolar interactions between the annular H3,5,6 protons of the β-CD groups and the H2-4 protons of the AD groups.

2.6. Rheological studies of aqueous substituted poly(acrylate) systems

At higher concentrations than those studied by UV-Vis spectroscopy in Section 2.5, the networks formed by the three combinations: PAAβ-CDen/PAAADen, PAAβ-CDen/PAAADhn and PAAβ-CDen/PAAADddn separately, and when complexing either MR, MO or EO form hydrogels, the viscosities of which were determined by rheology. (Because it was necessary to quantitatively determine the rates of dye release from the hydrogels, their fluidities had to be sufficient to allow their quantitative transfer into the dye release measurement apparatus, and this determined the maximum concentrations of their components.) In each hydrogel, the overall concentration of substituted poly(acrylate)s was approximately 1.20 wt% as indicated in the captions to Figure 2.15 and Figure 2.54 in Section 2.10 Appendix. Thus, in each hydrogel [β-CDen substituents] = 3.60 $\times 10^{-3}$ mol dm^{-3} and [ADen substituents], [ADhn substituents], or [ADddn substituents] = 1.20 $\times 10^{-3}$ mol dm^{-3} and the concentration of each dye was 2.00 $\times 10^{-3}$ mol dm^{-3}. (These hydrogel compositions are identical to those used in the dye release studies discussed in Section 2.7. However, the dye concentrations now approach those of the ADen, ADhn and ADddn substituents whereas they were much lower in the solutions studied by UV-Vis spectroscopy.) The viscosity variation of each system with shear rate was determined as shown for the binary systems PAAβ-CDen/PAAADen, PAAβ-CDen/PAAADhn and PAAβ-CDen/PAAADddn in Figure 2.15, and for the ternary systems in which each of the binary systems complexes the three dyes (Figure 2.54 in Section 2.10 Appendix). The viscosities show small variations with shear rate and those determined at 0.03 s^{-1} were selected for comparison purposes.

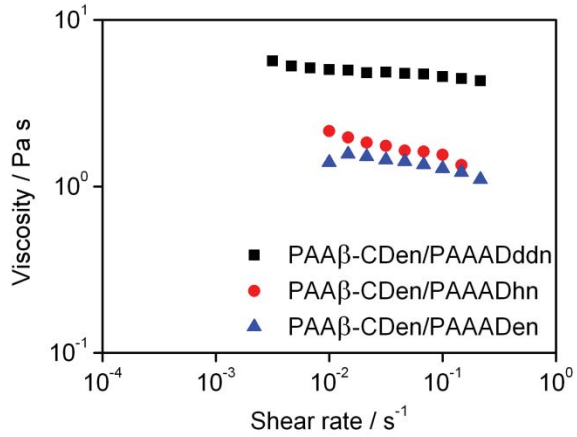

Figure 2.15. Variation of the viscosity with shear rate of either PAAADen (0.36 wt%, [ADen substituents] = 1.20×10^{-3} mol dm^{-3}), PAAADhn (0.40 wt%, [ADhn substituents] = 1.20×10^{-3} mol dm^{-3}), or PAAADddn (0.42 wt%, [ADddn substituents] = 1.20×10^{-3} mol dm^{-3}) in mixtures with PAAβ-CDen (0.78 wt%, [β-CDen substituents] = 3.60×10^{-3} mol dm^{-3}) in aqueous Na_2HPO_4/KH_2PO_4 buffer at pH 7.0 and I = 0.10 mol dm^{-3} at 298.2 K.

The viscosity variations at a 0.03 s^{-1} shear rate for all twelve hydrogels are shown in Figure 2.16 from which it is seen that, in the absence of dyes, the viscosities of the binary systems increase in the sequence: PAAβ-CDen/PAAADen (1.44 Pa s) < PAAβ-CDen/PAAADhn (1.75 Pa s) < PAAβ-CDen/PAAADddn (4.85 Pa s), which coincides with $10^{-3}K_{ITC}$ increasing in the sequence: PAAβ-CDen/PAAADen (28.2 dm^3 mol^{-1}) ≈ PAAβ-CDen/PAAADhn (28.4 dm^3 mol^{-1}) < PAAβ-CDen/PAAADddn (39.5 dm^3 mol^{-1}). This is consistent with the significantly larger K_{ITC} and double β-CDen substituent complexation of the ADddn substituent in the PAAβ-CDen/PAAADddn system found for the relatively dilute 0.15 wt% solutions studied by ITC also stabilizing network formation to the greatest extent in the three systems in the more concentrated 1.20 wt% solutions of the rheological studies.

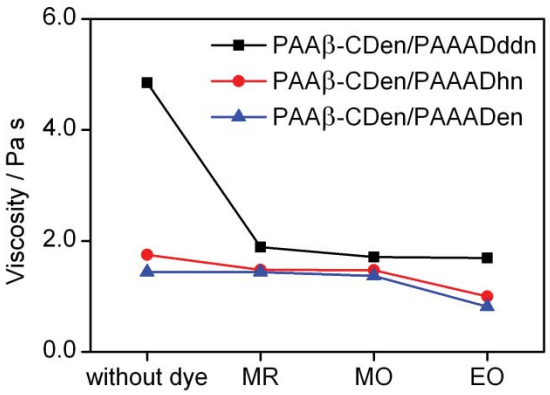

Figure 2.16. Viscosity variations at a 0.03 s^{-1} shear rate of aqueous Na_2HPO_4/KH_2PO_4 buffer at pH 7.0 and I = 0.10 mol dm^{-3} of either 1.14 wt% PAAβ-CDen/PAAADen, 1.18 wt% PAAβ-CDen/PAAADhn, or 1.20 wt% PAAβ-CDen/PAAADddn in the absence and presence of either MR, MO, or EO at 298.2 K. In each system, the concentration of β-CDen substituents and ADen, ADhn, or ADddn substituents is 3.60 × 10^{-3} mol dm^{-3} and 1.20 × 10^{-3} mol dm^{-3}, respectively, and the concentration of dye is 2.00 × 10^{-3} mol dm^{-3}.

Upon addition of either MR, MO or EO, a substantial decrease in the viscosity of the ternary PAAβ-CDen/PAAADddn solutions occurs (viscosities = 1.89, 1.71 and 1.59 Pa s in the presence of MR, MO and EO, respectively) whereas the changes in the 0.03 s^{-1} shear rate viscosities of the PAAβ-CDen/PAAADen (viscosities = 1.49, 1.37 and 0.87 Pa s in the presence of MR, MO and EO, respectively) and PAAβ-CDen/PAAADhn (viscosities = 1.48, 1.53 and 1.00 Pa s in the presence of MR, MO and EO, respectively) solutions are smaller. This is consistent with the dye complexation competing with ADddn substituent complexation by a second β-CDen substituent in the PAAβ-CDen/PAAADddn solutions, even with the β-CDen substituent concentration being 1.8 times greater than that of the dyes, whereas this option is not available in the PAAβ-CDen/PAAADen and PAAβ-CDen/PAAADhn solutions. Nevertheless, the 0.03 s^{-1} shear rate viscosities of the PAAβ-CDen/PAAADddn solutions in the presence of the three dyes are still greater than those for solutions of PAAβ-CDen/PAAADen

and PAAβ-CDen/PAAADhn and in the presence of the three dyes which may indicate some residual complexation of the ADddn substituents by two β-CDen substituents with a consequent viscosity enhancement. The viscosities of the PAAβ-CDen/PAAADen and PAAβ-CDen/PAAADhn solutions show little variation in the presence of MR and MO, but a small decrease occurred in the presence of EO consistent with it showing the largest *K* for both systems as determined in the UV-Vis spectroscopic titration studies.

2.7. Dye release studies

2.7.1. Qualitative investigation into dye release behavior

Dye release through a dialysis membrane with pores allowing passage of species with a molecular weight up to 3500 g mol^{-1} into an aqueous Na_2HPO_4/KH_2PO_4 buffer at pH 7.0, I = 0.10 mol dm^{-3} and 298.2 K was characterized for each system. Reference solutions of MR, MO and EO were prepared in Na_2HPO_4/KH_2PO_4 buffer at pH 7.0 and I = 0.10 mol dm^{-3}. All other dye solutions were prepared in the same buffer, and to render the dye environment as similar as possible with respect to poly(acrylate), PAA, concentration, each solution containing neither PAAβ-CDen/PAAADen, PAAβ-CDen/PAAADhn nor PAAβ-CDen/PAAADddn had an appropriate amount of PAA added. The composition of the thirty-three solutions studied appears in Table 2.4 in Section 2.10 Appendix.

The dye release profiles for EO, MR and MO are shown in Figures 2.17 and 2.18 and Figure 2.55 in Section 2.10 Appendix, respectively. The solutions of EO in Na_2HPO_4/KH_2PO_4 buffer alone, PAA, PAAADen, PAAADhn and PAAADddn all show very similar release profiles with 90% of EO released within 20 h consistent with little interaction between EO and the other solutes such that the major factors determining the appearance of EO in the receiving solution is its diffusion within the particular EO sample and its interaction with the dialysis membrane

as it passes through its pores. (Similar release profiles are observed for the release of MR and MO from PAA and AD substituted PAA as shown in Figure 2.18 and Figure 2.55 in Section 2.10 Appendix.) However, the release of EO from a solution of PAA and β-CD was slower reaching 87% after 48 h consistent with substantial formation of the β-CD.EO complex which although of lower molecular weight than the membrane 3500 g mol^{-1} limit is likely to pass through the membrane less readily than free EO and is also less mobile than free EO. An even slower release of EO from the PAAβ-CDen solution occurred reaching only 69% after 48 h consistent with substantial formation of the PAAβ-CDen.EO complex which is of much too high a molecular weight to pass through the membrane such that passage is limited to free EO alone. These data are consistent with complexation of EO by β-CD alone or a β-CDen substituent controlling the amount of free EO in solution and thereby the rate of dye release through the membrane.

The EO release profiles from the 1.14 wt% PAAβ-CDen/PAAADen, 1.18 wt% PAAβ-CDen/PAAADhn and 1.20 wt% PAAβ-CDen/PAAADddn networks fall between those for the 1.20 wt% PAA/β-CD and 1.18 wt% PAA/PAAβ-CDen solutions consistent with EO complexation by the β-CDen substituents being of major importance in controlling the rate of EO release. The release of EO is significantly more rapid from the 1.20 wt% PAAβ-CDen/PAAADddn solution than from 1.18 wt% PAAβ-CDen/PAAADhn and 1.14 wt% PAAβ-CDen/PAAADen solutions, but this variation is much less for MR and MO (Figure 2.18 and Figure 2.55 in Section 2.10 Appendix). This coincides with the EO containing PAAβ-CDen/PAAADddn solution being substantially more viscous than the EO containing PAAβ-CDen/PAAADhn and the EO containing PAAβ-CDen/PAAADen solutions whereas the viscosities of the corresponding MO solutions are more similar as is also the case for the MR solutions (Figure 2.16). This indicates that viscosity is a significant rate determining factor for

dye release, and as the fluid solutions under discussion probably contain dispersions of poly(acrylate) network aggregates of a range of sizes it is possible that these variations also influence the rate of dye release.

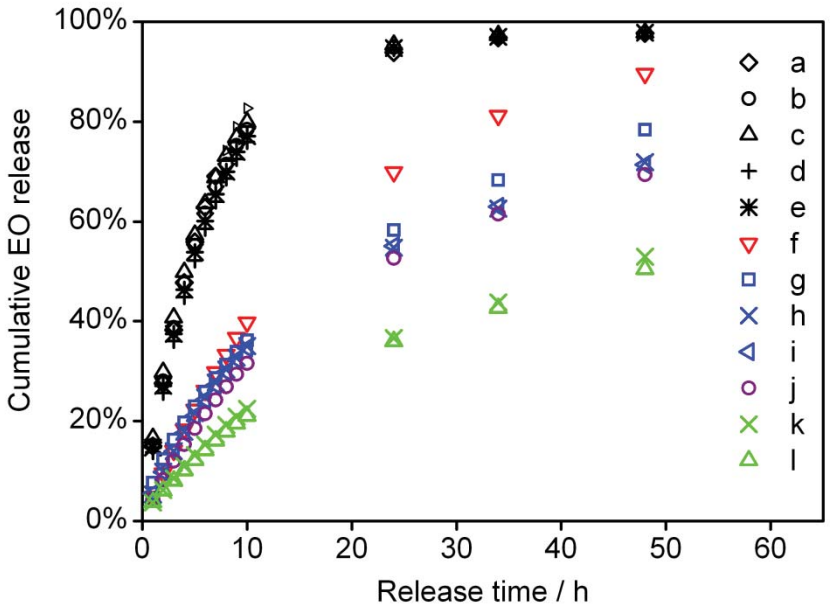

Figure 2.17. Release profiles for EO from (a) Na_2HPO_4/KH_2PO_4 buffer, (b) PAA, (c) PAA/PAAADddn, (d) PAA/PAAADhn, (e) PAA/PAAADen, (f) PAA/β-CD, (g) 1.20 wt% PAAβ-CDen/PAAADddn, (h) 1.18 wt% PAAβ-CDen/PAAADhn, (i) 1.14 wt% PAAβ-CDen/PAAADen, (j) 1.18 wt% PAA/PAAβ-CDen, (k) 1.96 wt% PAAβ-CDen/PAAADhn, and (l) 1.89 wt% PAAβ-CDen/PAAADen in aqueous Na_2HPO_4/KH_2PO_4 buffer at pH 7.0 and I = 0.10 mol dm^{-3} at 298.2 K. The EO concentration = 2.00×10^{-3} mol dm^{-3}.

The effect of increasing network extension and viscosity on the rate of EO release is illustrated by the profiles for the more viscous 1.89 wt% PAAβ-CDen/PAAADen and 1.96 wt% PAAβ-CDen/PAAADhn solutions from which 50% of EO is released in 48 h, and is attributed to an increase in β-CDen substituent concentration increasing the proportion of EO complexed and the more extensive network slowing free EO movement. (The 1.90 wt% PAAβ-CDen/PAAADddn was too viscous to transfer quantitatively to the release measurement

apparatus.)

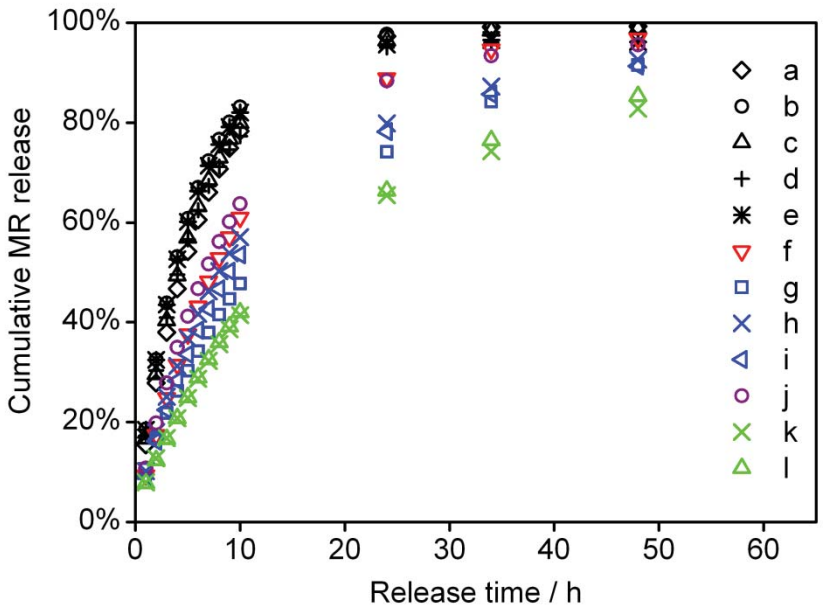

Figure 2.18. Release profiles for MR from (a) Na_2HPO_4/KH_2PO_4 buffer, (b) PAA, (c) PAA/PAAADddn, (d) PAA/PAAADhn, (e) PAA/PAAADen, (f) PAA/β-CD, (g) 1.20 wt% PAAβ-CDen/PAAADddn, (h) 1.18 wt% PAAβ-CDen/PAAADhn, (i) 1.14 wt% PAAβ-CDen/PAAADen, (j) 1.18 wt% PAA/PAAβ-CDen, (k) 1.96 wt% PAAβ-CDen/PAAADhn, and (l) 1.89 wt% PAAβ-CDen/PAAADen in aqueous Na_2HPO_4/KH_2PO_4 buffer at pH 7.0 and I = 0.10 mol dm^{-3} at 298.2 K. The MR concentration = 2.00×10^{-3} mol dm^{-3}.

The release of MR (Figure 2.18) in Na_2HPO_4/KH_2PO_4 buffer alone, PAA, PAA/PAAADen, PAA/PAAADhn and PAA/PAAADddn show profiles similar to those observed for EO (Figure 2.17). However, the profiles for MR release from the other seven solutions are compressed into a shorter time-frame of more rapid release than observed for the corresponding EO solutions consistent with the weaker complexing of MR and higher proportion of free MR facilitating more facile release. The release profiles for MO (Figure 2.55 in Section 2.10 Appendix) more closely resembling those of EO as anticipated from the strength of complexing of MO being between that of EO and MR (Table 2.2). It is notable that the release of both MR and MO from

their more concentrated 1.96 wt% PAAβ-CDen/PAAADhn and 1.89 wt% PAAβ-CDen/PAAADen solutions are also slower by comparison with their release from the 1.18 wt% PAAβ-CDen/PAAADhn and 1.14 wt% PAAβ-CDen/PAAADen solutions. This is also consistent with the higher β-CDen substituent in the more concentrated solutions increasing the proportion of MR and MO complexed and the more extensive network slowing free dye movement.

The release profiles of the three dyes from their PAAβ-CDen/PAAADen solutions show the release rate to decrease in the order MR > MO > EO (Figure 2.19) consistent with the decrease in *K* for dye complexation (Table 2.2) largely determining the release rate. Similar release profiles are observed for the 1.20 wt% PAA/β-CD and 1.18 wt% PAA/PAAβ-CDen, 1.20 wt% PAAβ-CDen/PAAADddn and 1.18 wt% PAAβ-CDen/PAAADhn solutions (Figures 2.56 - 2.59 in Section 2.10 Appendix).

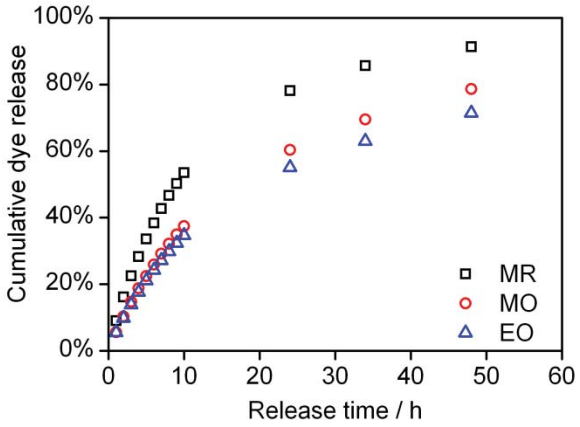

Figure 2.19. Release profiles of three dyes from a 1.14 wt% PAAβ-CDen/PAAADen aqueous Na_2HPO_4/KH_2PO_4 buffer solution at pH 7.0 and I = 0.10 mol dm^{-3} at 298.2 K. The dye concentration = 2.00×10^{-3} mol dm^{-3}.

2.7.2. Theoretical investigation into dye release behavior

A range of mathematical models have been proposed to describe the kinetics of drug release

from delivery systems.[50] These models depend to a greater or lesser extent on the nature of the delivery systems and the manner in which the drug release is measured. One model which has received substantial attention is that proposed by Peppas *et al.*[51-53] through which the release of guest species from polymer networks is described by Equation 2.20

$$M_t/M_\infty = kt^n \qquad (\mathbf{2.20})$$

where M_t and M_∞ are the amount of released drug (or dye) at time t and infinite time, respectively. k is a kinetic constant indicative of release rate, and n is a release exponent which is related to the release mechanism.[51-53] A $n = 0.5$ indicates that a Fickian diffusional release applies while $n = 1$ indicates that the mechanism of release from the network controls the release rate. Both the diffusion and network release mechanism can apply simultaneously such that n is between 0.5 and 1. Equation 2.19 only applies for up to 60% of the drug being released.

Although this model was originally developed to simulate the release of molecular entities, or cargo, from covalently cross-linked polymer networks,[51-54] it has also been applied to physically cross-linked polymer networks.[12] The n values derived in the present study are between 0.5 and 1 (Table 2.3), irrespective of the presence or otherwise of a physically cross-linked poly(acrylate) network. Thus, for the PAA (1.2 wt%) system n ranges from 0.71 to 0.77 probably as a consequence of diffusion in the dye solution and the process of dye passage through the membrane both contributing to the rate of dye release. For the PAA/β-CD (1.2 wt%) and PAA/PAAβ-CDen (0.40 wt%/0.78 wt%) systems, an additional factor, dye complexation, slows the dye release. For the less concentrated network systems, PAAβ-CDen/PAAADddn (0.78 wt%/ 0.42 wt%), PAAβ-CDen/PAAADhn (0.78 wt%/ 0.40 wt%) and PAAβ-CDen/PAAADen (0.78 wt%/ 0.36 wt%), it is likely that an additional slowed diffusion in the networks contributes to the slowed rate of dye release, and in the more concentrated networks, PAAβ-CDen/PAAADhn (1.30 wt%/ 0.66 wt%) and

PAAβ-CDen/PAAADen (1.30 wt%/ 0.59 wt%), more extensive dye complexation and further slowing of diffusion in the network further slows dye release. Thus, for the network systems studied, the dye release rate reflects variation of dye complexation by β-CDen substitutents and variation of dye diffusion rates upon which is superimposed the interactions between the dye and the membrane. Combinations of Fickian diffusion and guest release from complexation have been reported for hydrogel networks containing cyclodextrin groups.[28,54,55]

While the above model yields plausible *n* and *k* values through Equation 2.19, it is likely that the PAAβ-CDen/PAAADddn, PAAβ-CDen/PAAADhn and PAAβ-CDen/PAAADen systems are too complex to be analyzed through this model as they incorporate the dynamics of β-CDen substituent complexation of the dye, the dynamics of the poly(acrylate) network, the diffusion of the dye within the network, and finally the dynamics of the passage of the dye through the membrane. A similar view has been expressed for similar modelling of the controlled release of two drugs from β-CD cross-linked poly(acrylate)s.[28] Alternative models are available but do not appear to offer solutions to this complexity problem.[50]

Table 2.3. Analysis of the dye release mechanism according to Equation 2.20:

$$M_t/M_\infty = kt^n$$

System		n	10^2k h^{-n}	R^2
PAA (1.2 wt%)	EO	0.77	16.3	0.996
	MO	0.72	19.5	0.996
	MR	0.71	19.7	0.996
PAA/β-CD (1.2 wt%)	EO	0.87	5.45	0.999
	MO	0.93	4.29	0.999
	MR	0.76	10.8	0.997
PAA/PAAβ-CDen (0.40 wt%/0.78 wt%)	EO	0.68	6.30	0.989
	MO	0.68	7.02	0.989
	MR	0.71	12.8	0.995
PAAβ-CDen/PAAADddn (0.78 wt%/0.42 wt%)	EO	0.60	8.76	0.996
	MO	0.62	8.78	0.989
	MR	0.65	10.6	0.999
PAAβ-CDen/PAAADhn (0.78 wt%/0.40 wt%)	EO	0.63	7.68	0.986
	MO	0.65	7.23	0.986
	MR	0.73	10.2	0.998
PAAβ-CDen/PAAADen (0.78 wt%/0.36 wt%)	EO	0.62	7.94	0.982
	MO	0.64	7.16	0.986
	MR	0.70	11.6	0.996
PAAβ-CDen/PAAADhn (1.30 wt%/0.66 wt%)	EO	0.61	5.20	0.994
	MO	0.64	4.24	0.992
	MR	0.74	7.59	0.999
PAAβ-CDen/PAAADen (1.30 wt%/0.59 wt%)	EO	0.62	4.79	0.993
	MO	0.65	4.29	0.994
	MR	0.76	7.35	0.999

2.8. Conclusions

The self-assembled poly(acrylate) networks in aqueous solutions have been characterized as potential sustained drug delivery systems, in terms of dye complexation and release. The formation of associative poly(acrylate) networks in aqueous solutions is due to the host-guest complexation of ADen, ADhn, or ADddn substituents by β-CDen substituents, which has been thermodynamically characterized. The length of the tether grafting AD groups onto poly(acrylate) backbones has a significant influence on the complexation of AD substituents by β-CDen substituents. In comparison with PAAβ-CDen/PAAADen and

PAAβ-CDen/PAAADhn showing substantial Δ*H* contribution and small unfavorable negative *T*Δ*S*, PAAβ-CDen/PAAADddn shows a smaller Δ*H* and favorable positive *T*Δ*S*. In addition, the longest tether between the AD group and poly(acrylate) backbone in PAAADddn results in the least steric hindrance and greatest flexibility between the ADddn and β-CDen substituents of substituted poly(acrylate)s, which coincides with the largest K_{ITC} values observed for the three systems in 0.06-0.15 wt% solutions. (This also coincides with the largest viscosity in 1.20 wt% solution.) According to the stoichiometry determined by ITC and the cross-peaks in 2D NOESY ^{1}H NMR spectra, AD groups and their dodecyl tether in PAAADddn are complexed in the annuli of the β-CD groups of PAAβ-CDen, while ethyl and hexyl tether complexation is absent in PAAADen and PAAADhn. The dye complexation capability of the β-CDen substituents in the three networks characterized by the complexation constants, *K*, are less than those characterizing dye complexation by β-CD and the β-CDen substituents of PAAβ-CDen. This is attributable to the increased steric crowding within poly(acrylate) network of the binary PAAβ-CDen/PAAADen, PAAβ-CDhn/PAAADhn and PAAβ-CDen/PAAADddn systems. By comparison with the rate of release of the dyes from their aqueous solutions, the release of the dyes from aqueous solutions of the self-assembled PAAβ-CDen/PAAADen, PAAβ-CDen/PAAADhn and PAAβ-CDen/PAAADddn networks is slower. This is consistent with extent of complexation of the dyes by the β-CDen substituents of the PAAβ-CDen/PAAADen, PAAβ-CDen/PAAADhn and PAAβ-CDen/PAAADddn systems controlling the amount of dye in the free state and thereby the rate of dye release. In summary, the β-CDen substituents in the self-assembled PAAβ-CDen/PAAADen, PAAβ-CDen/PAAADhn and PAAβ-CDen/PAAADddn systems retain the complexation capability and thereby the advantages of cyclodextrins in pharmaceutical applications exemplified by drug solubility enhancement and prevention of drug degradation.[22,23,27,56] In

addition, the complexation of drugs by the β-CDen substituents in the PAAβ-CDen/PAAADen, PAAβ-CDen/PAAADhn and PAAβ-CDen/PAAADddn hydrogel networks has the potential to control the subsequent release of drugs to improve drug efficacy. It is envisaged that at higher concentrations than those studied herein the PAAβ-CDen/PAAADen, PAAβ-CDen/PAAADhn and PAAβ-CDen/PAAADddn hydrogels could be developed for topical application and also for insertion into wounds as drug delivery systems.

2.9. References

(1) Xing, B.; Yu, C.-W.; Chow, K.-H.; Ho, P.-L.; Fu, D.; Xu, B. Hydrophobic interaction and hydrogen bonding cooperatively confer a vancomycin hydrogel: A potential candidate for biomaterials. *J. Am. Chem. Soc.* **2002,** *124*, 14846-14847.

(2) Chujo, Y.; Sada, K.; Saegusa, T. Cobalt (III) bipyridyl-branched polyoxazoline complex as a thermally and redox reversible hydrogel. *Macromolecules* **1993,** *26*, 6320-6323.

(3) Appel, E. A.; del Barrio, J.; Loh, X. J.; Scherman, O. A. Supramolecular polymeric hydrogels. *Chem. Soc. Rev.* **2012,** *41*, 6195-6214.

(4) Kuo, C. K.; Ma, P. X. Ionically crosslinked alginate hydrogels as scaffolds for tissue engineering: Part 1. Structure, gelation rate and mechanical properties. *Biomaterials* **2001,** *22*, 511-521.

(5) Kisiday, J.; Jin, M.; Kurz, B.; Hung, H.; Semino, C.; Zhang, S.; Grodzinsky, A. Self-assembling peptide hydrogel fosters chondrocyte extracellular matrix production and cell division: Implications for cartilage tissue repair. *Proc. Natl. Acad. Sci. U.S.A.* **2002,** *99*, 9996-10001.

(6) Cheng, T.-Y.; Chen, M.-H.; Chang, W.-H.; Huang, M.-Y.; Wang, T.-W. Neural stem cells encapsulated in a functionalized self-assembling peptide hydrogel for brain tissue engineering. *Biomaterials* **2013,** *34*, 2005-2016.

(7) West, J. L.; Hubbell, J. A. Comparison of covalently and physically cross-linked polyethylene glycol-based hydrogels for the prevention of postoperative adhesions in a rat model. *Biomaterials* **1995,** *16*, 1153-1156.

(8) Kimura, M.; Takai, M.; Ishihara, K. Tissue-compatible and adhesive polyion complex hydrogels composed of amphiphilic phospholipid polymers. *J. Biomater. Sci. Polymer Edn.* **2007,** *18*, 623-640.

(9) Yang, Z.; Liang, G.; Ma, M.; Abbah, A. S.; Lu, W. W.; Xu, B. d-Glucosamine-based supramolecular hydrogels to improve wound healing. *Chem. Commun.* **2007**, 843-845.

(10) Appel, E. A.; Loh, X. J.; Jones, S. T.; Dreiss, C. A.; Scherman, O. A. Sustained release of proteins from high water content supramolecular polymer hydrogels. *Biomaterials* **2012,** *33*, 4646-4652.

(11) Zeng, F.; Shen, Y.; Chen, C.-F. Cross-linked supramolecular polymer networks with responsive and elastic gel properties via host-guest complexation: controlled release of squaraine dyes. *Soft Matter* **2013,** *9*, 4875-4882.

(12) Appel, E. A.; Forster, R. A.; Rowland, M. J.; Scherman, O. A. The control of cargo release from physically crosslinked hydrogels by crosslink dynamics. *Biomaterials* **2014,** *35*, 9897-9903.

(13) Harada, T.; Pham, D.-T.; Lincoln, S. F.; Kee, T. W. The Capture and stabilization of curcumin using hydrophobically modified polyacrylate aggregates and hydrogels. *J. Phys. Chem. B* **2014,** *118*, 9515-9523.

(14) Yu, J.; Ha, W.; Chen, J.; Shi, Y.-p. pH-Responsive supramolecular hydrogels for codelivery of hydrophobic and hydrophilic anticancer drugs. *RSC Adv.* **2014,** *4*, 58982-58989.

(15) Li, J.; Li, H.; Yang, X.; Luo, P.; Wu, Z.; Zhang, X. The supramolecular hydrogel based on hyperbranched polyglycerol and dextran as a scaffold for living cells and drug delivery. *RSC Adv.* **2015,** *5*, 86730-86739.

(16) Rekharsky, M. V.; Inoue, Y. Complexation thermodynamics of cyclodextrins. *Chem. Rev.* **1998,** *98*, 1875-1918.

(17) Easton, C.; Lincoln, S. *Modified Cyclodextrins: Scaffolds and Templates for Supramolecular Chemistry*; Imperial College Press: London1999.

(18) Wenz, G. Recognition of monomers and polymers by cyclodextrins. In *Inclusion Polymers*; Springer, 2009, pp 204-254.

(19) Lincoln, S. F.; Pham, D.-T. Cyclodextrins: From Nature to Nanotechnology. In *Supramolecular Chemistry*; John Wiley & Sons, Ltd, 2012, pp 955-982.

(20) Hirayama, F.; Uekama, K. Cyclodextrin-based controlled drug release system. *Adv. Drug Deliv. Rev.* **1999,** *36*, 125-141.

(21) Bibby, D. C.; Davies, N. M.; Tucker, I. G. Mechanisms by which cyclodextrins modify drug release from polymeric drug delivery systems. *Int. J. Pharm.* **2000,** *197*, 1-11.

(22) Davis, M. E.; Brewster, M. E. Cyclodextrin-based pharmaceutics: past, present and future. *Nat. Rev. Drug Discov.* **2004,** *3*, 1023-1035.

(23) Loftsson, T.; Duchêne, D. Cyclodextrins and their pharmaceutical applications. *Int. J. Pharm.* **2007,** *329*, 1-11.

(24) van de Manakker, F.; Vermonden, T.; van Nostrum, C. F.; Hennink, W. E. Cyclodextrin-based polymeric materials: synthesis, properties, and pharmaceutical/biomedical applications. *Biomacromolecules* **2009,** *10*, 3157-3175.

(25) Layre, A.-M.; Volet, G. l.; Wintgens, V. r.; Amiel, C. Associative network based on cyclodextrin polymer: a model system for drug delivery. *Biomacromolecules* **2009,** *10*, 3283-3289.

(26) Zhou, J.; Ritter, H. Cyclodextrin functionalized polymers as drug delivery systems.

Polym. Chem. **2010,** *1*, 1552-1559.

(27) Harada, T.; Pham, D.-T.; Leung, M. H. M.; Ngo, H. T.; Lincoln, S. F.; Easton, C. J.; Kee, T. W. Cooperative binding and stabilization of the medicinal pigment curcumin by diamide linked γ-cyclodextrin dimers: a spectroscopic characterization. *J. Phys. Chem. B* **2011,** *115*, 1268-1274.

(28) Kutyła, M. J.; Lambert, L. K.; Davies, N. M.; McGeary, R. P.; Shaw, P. N.; Ross, B. P. Cyclodextrin-crosslinked poly (acrylic acid): synthesis, physicochemical characterization and controlled release of diflunisal and fluconazole from hydrogels. *Int. J. Pharm.* **2013,** *444*, 175-184.

(29) Harada, T.; McTernan, H. L.; Pham, D.-T.; Lincoln, S. F.; Kee, T. W. Femtosecond transient absorption spectroscopy of the medicinal agent curcumin in diamide linked γ-cyclodextrin dimers. *J. Phys. Chem. B* **2015,** *119*, 2425-2433.

(30) Li, Y.; Guo, H.; Gan, J.; Zheng, J.; Zhang, Y.; Wu, K.; Lu, M. Novel fast thermal-responsive poly(N-isopropylacrylamide) hydrogels with functional cyclodextrin interpenetrating polymer networks for controlled drug release. *J. Polym. Res.* **2015,** *22*, 1-14.

(31) Eftink, M. R.; Andy, M. L.; Bystrom, K.; Perlmutter, H. D.; Kristol, D. S. Cyclodextrin inclusion complexes: studies of the variation in the size of alicyclic guests. *J. Am. Chem. Soc.* **1989,** *111*, 6765-6772.

(32) Nguyen, H.-T.; Pham, D.-T.; Lincoln, S. F.; Wang, J.; Guo, X.; Easton, C. J.; Prud'homme, R. K. Host-guest chemistry of linked β-cyclodextrin trimers and adamantyl substituted poly(acrylate)s in aqueous solution. *Polym. Chem.* **2013,** *4*, 820-829.

(33) Wang, J.; Xu, Y.; Wang, Y.; Liu, J.; Xu, J.; Li, L.; Nguyen, H.-T.; Pham, D.-T.; Lincoln, S. F.; Guo, X. Bridged-cyclodextrin supramolecular hydrogels: host-guest interaction between a cyclodextrin dimer and adamantyl substituted poly(acrylate)s. *RSC Adv.* **2015,** *5*, 46067-46073.

(34) Wang, J.; Pham, D.-T.; Guo, X.; Li, L.; Lincoln, S. F.; Luo, Z.; Ke, H.; Zheng, L.; Prud'homme, R. K. Polymeric networks assembled by adamantyl and β-cyclodextrin substituted poly(acrylate)s: host−guest interactions, and the effects of ionic strength and extent of substitution. *Ind. Eng. Chem. Res.* **2010,** *49*, 609-612.

(35) Maciollek, A.; Munteanu, M.; Ritter, H. New generation of polymeric drugs: copolymer from NIPAAM and cyclodextrin methacrylate containing supramolecular-attached antitumor derivative. *Macromol. Chem. Phys.* **2010,** *211*, 245-249.

(36) Stadermann, J.; Komber, H.; Erber, M.; Däbritz, F.; Ritter, H.; Voit, B. Diblock

copolymer formation via self-assembly of cyclodextrin and adamantyl end-functionalized polymers. *Macromolecules* **2011,** *44*, 3250-3259.

(37) Auzély-Velty, R.; Rinaudo, M. New Supramolecular assemblies of a cyclodextrin-grafted chitosan through specific complexation. *Macromolecules* **2002,** *35*, 7955-7962.

(38) Charlot, A.; Auzély-Velty, R. Synthesis of novel supramolecular assemblies based on hyaluronic acid derivatives bearing bivalent β-cyclodextrin and adamantane moieties. *Macromolecules* **2007,** *40*, 1147-1158.

(39) Li, L.; Guo, X.; Wang, J.; Liu, P.; Prud'homme, R. K.; May, B. L.; Lincoln, S. F. Polymer networks assembled by host−guest inclusion between adamantyl and β-cyclodextrin substituents on poly (acrylic acid) in aqueous solution. *Macromolecules* **2008,** *41*, 8677-8681.

(40) Guo, X.; Wang, J.; Li, L.; Pham, D.-T.; Clements, P.; Lincoln, S. F.; May, B. L.; Chen, Q.; Zheng, L.; Prud'homme, R. K. Steric effects and competitive intra- and intermolecular host-guest complexation between beta-cyclodextrin and adamantyl substituted poly(acrylate)s in water: A ^{1}H NMR, rheological and preparative study. *J. Polym. Sci., Part B: Polym. Phys.* **2010,** *48*, 1818-1825.

(41) Guo, X.; Wang, J.; Li, L.; Pham, D.-T.; Clements, P.; Lincoln, S. F.; May, B. L.; Chen, Q.; Zheng, L.; Prud'homme, R. K. Tailoring polymeric hydrogels through cyclodextrin host–guest complexation. *Macromol. Rapid Commun.* **2010,** *31*, 300-304.

(42) Wang, J.; Qiu, Z.; Wang, Y.; Li, L.; Guo, X.; Pham, D.-T.; Lincoln, S. F.; Prud'homme, R. K. Supramolecular polymer assembly in aqueous solution arising from cyclodextrin host–guest complexation. *Beilstein J. Org. Chem.* **2016,** *12*, 50-72.

(43) Wang, J.; Li, L.; Ke, H.; Liu, P.; Zheng, L.; Guo, X.; Lincoln, S. F. Rheology control by modulating hydrophobic and inclusive associations of side-groups in poly (acrylic acid). *Asia-pac. J. Chem. Eng.* **2009,** *4*, 537-543.

(44) Guo, X.; Abdala, A. A.; May, B. L.; Lincoln, S. F.; Khan, S. A.; Prud'homme, R. K. Rheology control by modulating hydrophobic and inclusion associations in modified poly(acrylic acid) solutions. *Polymer* **2006,** *47*, 2976-2983.

(45) Li, L.; Guo, X.; Fu, L.; Prud'homme, R. K.; Lincoln, S. F. Complexation behavior of α-, β-, and γ-Cyclodextrin in modulating and constructing polymer networks. *Langmuir* **2008,** *24*, 8290-8296.

(46) MicroCal, 22 Industrial Drive East, Northampton, MA01060, USA.

(47) Gans, P.; Sabatini, A.; Vacca, A. Investigation of equilibria in solution. Determination

of equilibrium constants with the HYPERQUAD suite of programs. *Talanta* **1996,** *43*, 1739-1753.

(48) HypSpec. Protonic Software: 2 Templegate Avenue, Leeds LS15 0HD, UK.

(49) Harries, D.; Rau, D. C.; Parsegian, V. A. Solutes probe hydration in specific association of cyclodextrin and adamantane. *J. Am. Chem. Soc.* **2005,** *127*, 2184-2190.

(50) Fu, Y.; Kao, W. J. Drug release kinetics and transport mechanisms of non-degradable and degradable polymeric delivery systems. *Expert Opin. Drug Deliv.* **2010,** *7*, 429-444.

(51) Ritger, P. L.; Peppas, N. A. A simple equation for description of solute release I. Fickian and non-Fickian release from non-swellable devices in the form of slabs, spheres, cylinders or discs. *J. Control. Release* **1987,** *5*, 23-36.

(52) Ritger, P. L.; Peppas, N. A. A simple equation for description of solute release II. Fickian and anomalous release from swellable devices. *J. Control. Release* **1987,** *5*, 37-42.

(53) Peppas, N. A.; Sahlin, J. J. A simple equation for the description of solute release. III. Coupling of diffusion and relaxation. *Int. J. Pharm.* **1989,** *57*, 169-172.

(54) Machín, R.; Isasi, J. R.; Vélaz, I. Hydrogel matrices containing single and mixed natural cyclodextrins. Mechanisms of drug release. *Eur. Polym. J.* **2013,** *49*, 3912-3920.

(55) Teixeira, R. S.; Veiga, F. J.; Oliveira, R. S.; Jones, S. A.; Silva, S.; Carvalho, R. A.; Valente, A. J. Effect of cyclodextrins and pH on the permeation of tetracaine: supramolecular assemblies and release behavior. *Int. J. Pharm.* **2014,** *466*, 349-358.

(56) Kurkov, S. V.; Loftsson, T. Cyclodextrins. *Int. J. Pharm.* **2013,** *453*, 167-180.

2.10. Appendix

2.10.1. Experimental setup and composition of solutions for dye release studies

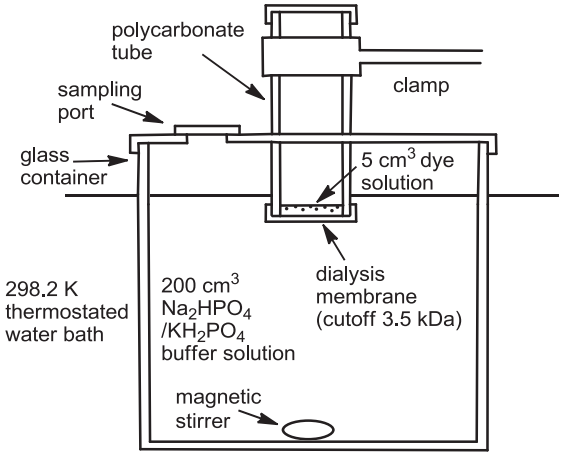

Figure 2.20. Schematic illustration of dye release measurement apparatus.

Table 2.4. Composition of solutions for dye release studies.[a]

Solution	Composition
Na_2HPO_4/KH_2PO_4buffer	pH =7.0, I = 0.10 mol dm^{-3}
PAA	PAA, 1.20 wt%
PAAADen	PAAADen, 0.36 wt%, [ADen substituents] = 1.20×10^{-3} mol dm^{-3} PAA, 0.78 wt%, total wt% = 1.14
PAAADhn	PAAADhn, 0.40 wt%, [ADhn substituents] = 1.20×10^{-3} mol dm^{-3} PAA, 0.78 wt%, total wt% = 1.18
PAAADddn	PAAADddn, 0.42 wt%, [ADddn substituents] = 1.20×10^{-3} mol dm^{-3} PAA, 0.78 wt%, total wt% = 1.20
PAA/β-CD	[β-CD] = 3.60×10^{-3} mol dm^{-3} PAA, 1.20 wt%, total wt% = 1.20
PAA/β-CDen	PAAβ-CDen, 0.78 wt%, [β-CDen substituents] = 3.60×10^{-3} mol dm^{-3} PAA, 0.40 wt%, total wt% = 1.18
PAAβ-CDen/PAAADen	PAAβ-CDen, 0.78 wt%, [β-CDen substituents] = 3.60×10^{-3} mol dm^{-3} PAAADen, 0.36 wt%, total wt% = 1.14 [ADen substituents] = 1.20×10^{-3} mol dm^{-3}
PAAβ-CDen/PAAADhn	PAAβ-CDen, 0.78 wt%, [β-CDen substituents] = 3.60×10^{-3} mol dm^{-3} PAAADhn, 0.40 wt%, total wt% = 1.18 [ADhn substituents] = 1.20×10^{-3} mol dm^{-3}
PAAβ-CDen/PAAADddn	PAAβ-CDen, 0.78 wt%, [β-CDen substituents] = 3.60×10^{-3} mol dm^{-3} PAAADddn, 0.42 wt%, total wt% = 1.20 [ADddn substituents] = 1.20×10^{-3} mol dm^{-3}
High concentration PAAβ-CDen/PAAADen	PAAβ-CDen, 1.30 wt%, [β-CDen substituents] = 6.00×10^{-3} mol dm^{-3} PAAADen, 0.59 wt%, total wt% =1.89 [ADen substituents] = 2.00×10^{-3} mol dm^{-3}
High concentration PAAβ-CDen/PAAADhn	PAAβ-CDen, 1.30 wt%, [β-CDen substituents] = 6.00×10^{-3} mol dm^{-3} PAAADhn, 0.66 wt%, total wt% = 1.96 [ADhn substituents] = 2.00×10^{-3} mol dm^{-3}

[a]All solutions were prepared in aqueous Na_2HPO_4/KH_2PO_4 buffer at pH 7.0 and I = 0.10 mol dm^{-3} at 298.2 K. Dye concentration was 2.00×10^{-3} mol dm^{-3} for all samples.

2.10.2. ITC data and 2D NOESY ^{1}H NMR spectra for substituted poly(acrylate) aqueous network formation characterization

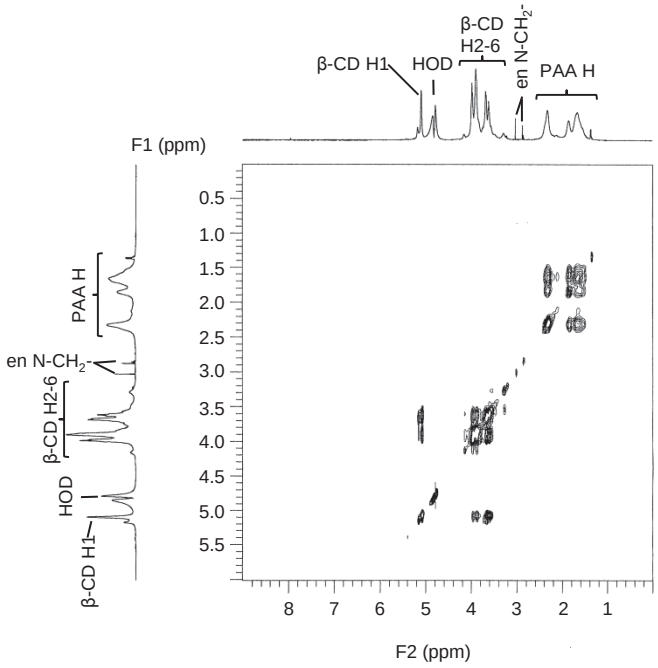

Figure 2.21. 2D NOESY ^{1}H NMR spectrum of 0.44 wt% PAAβ-CDen ([β-CDen substituents] = 2.0×10^{-3} mol dm^{-3}) in D_2O Na_2HPO_4/KH_2PO_4 buffer solution at pD = 7.0 and I = 0.10 mol dm^{-3} at 298.2 K.

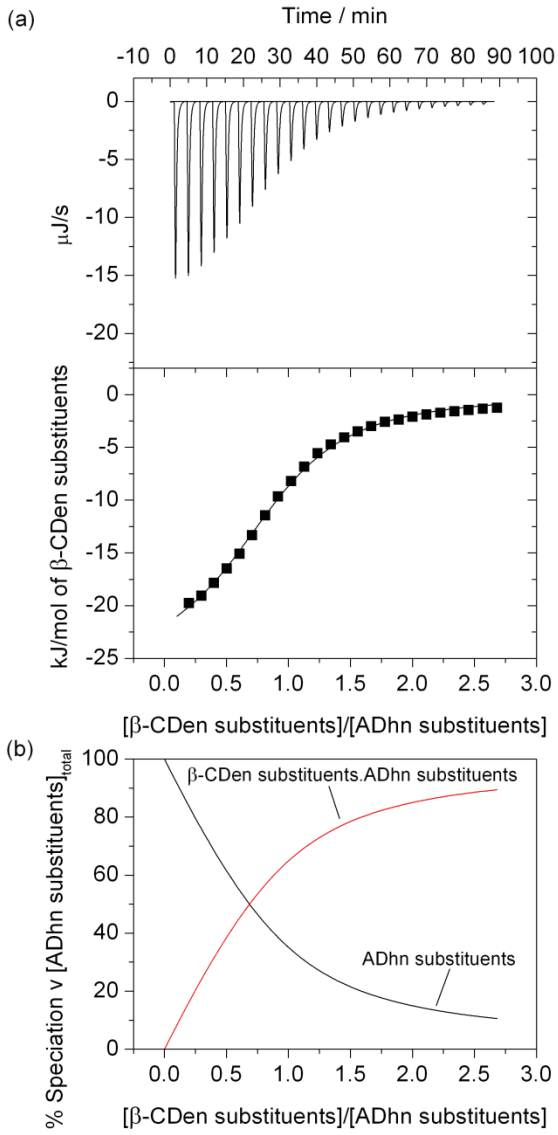

Figure 2.21. (a) (Top) ITC data for the titration of 10 mm^3 aliquots of a 0.62 wt% PAAβ-CDen solution ([β-CDen substituents] = 2.84 × 10^{-3} mol dm^{-3}) into 1.46 cm^3 of a 0.064 wt% PAAADhn ([ADhn substituents] = 1.91 × 10^{-4} mol dm^{-3}) solution at 298.2 K. Both solutions were buffered at pH 7.0 in aqueous Na_2HPO_4/KH_2PO_4 buffer at I = 0.10 mol dm^{-3}. (Bottom) The solid curve shows the best-fit to an algorithm for host-guest complexation between the β-CDen and ADhn substituents to the experimental data points. (b) Speciation plot with [ADhn substituents]$_{total}$ = 100%.

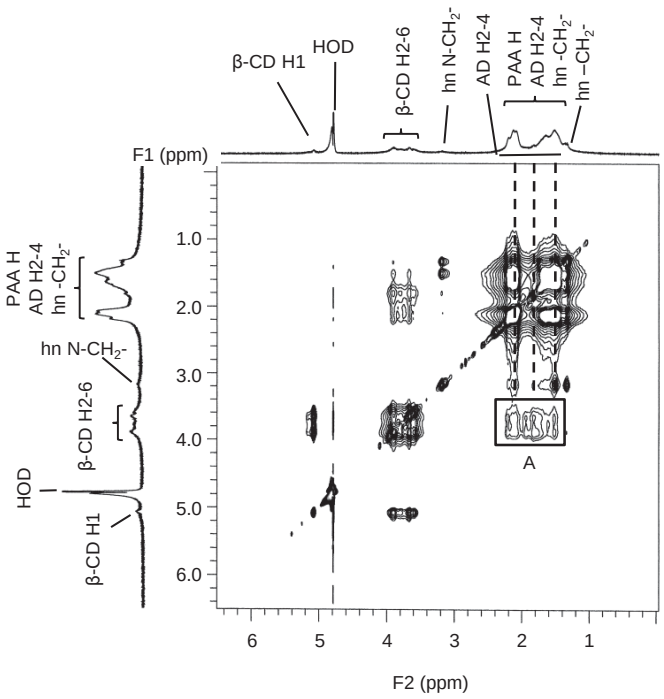

Figure 2.23. 2D ^{1}H NOESY NMR spectrum of 0.44 wt% PAAβ-CDen ([β-CDen substituents] = 2.0×10^{-3} mol dm^{-3}) and 0.67 wt% PAAADhn ([ADhn substituents] = 2.0×10^{-3} mol dm^{-3}) in D_2O Na_2HPO_4/KH_2PO_4 buffer solution at pD = 7.0 and I = 0.10 mol dm^{-3} at 298.2 K. Cross-peaks in box A arise from dipolar interactions between the annular H3,5,6 protons of the β-CD groups and the H2-4 protons of the AD groups.

2.10.3. UV-Vis spectroscopic titration data and 2D ROESY and NOESY ^{1}H NMR spectra for dye complexation

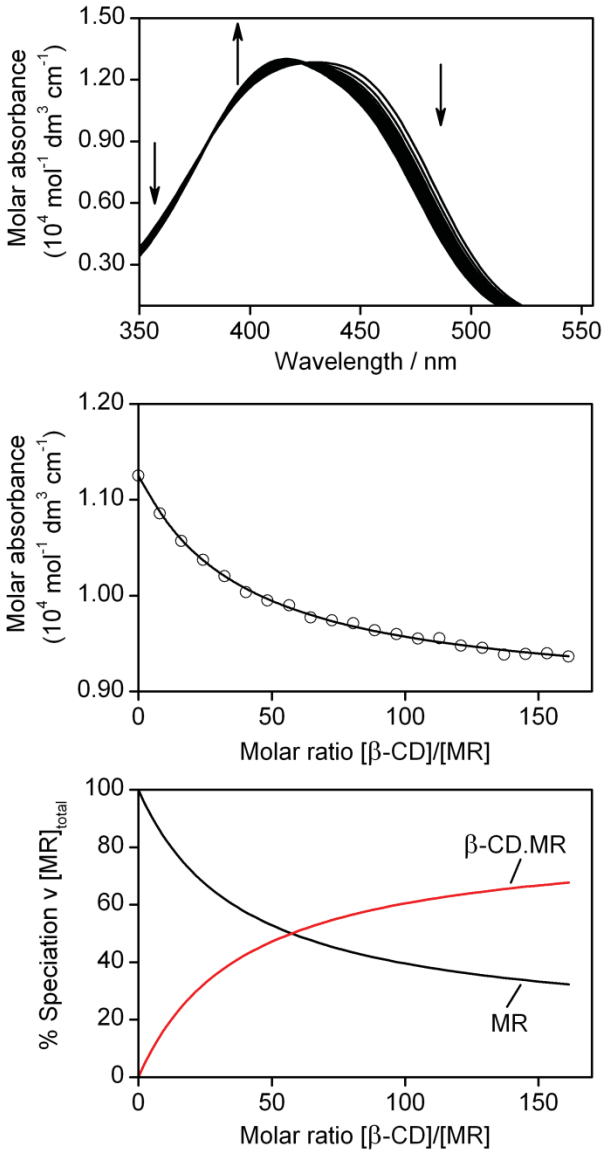

Figure 2.24. (Top) Molar absorbance variation of a MR solution ([MR] = 2.80 × 10^{-5} mol dm^{-3}) upon 20 sequential additions of a β-CD solution (50 mm^3 each, [β-CD] = 6.77 × 10^{-3} mol dm^{-3}) at 298.2 K. Both solutions were prepared in aqueous Na_2HPO_4/KH_2PO_4buffer at pH 7.0 and *I* = 0.10 mol dm^{-3}. The arrows indicate the direction of molar absorbance variation upon each addition of the β-CD solution. (Middle) Molar absorbance variation at 460 nm and the line representing the best-fit of an algorithm for a 1:1 host-guest complexation of MR by β-CD over the wavelength range 430 - 480 nm. (Bottom) Speciation plot with $[MR]_{total}$ =100%.

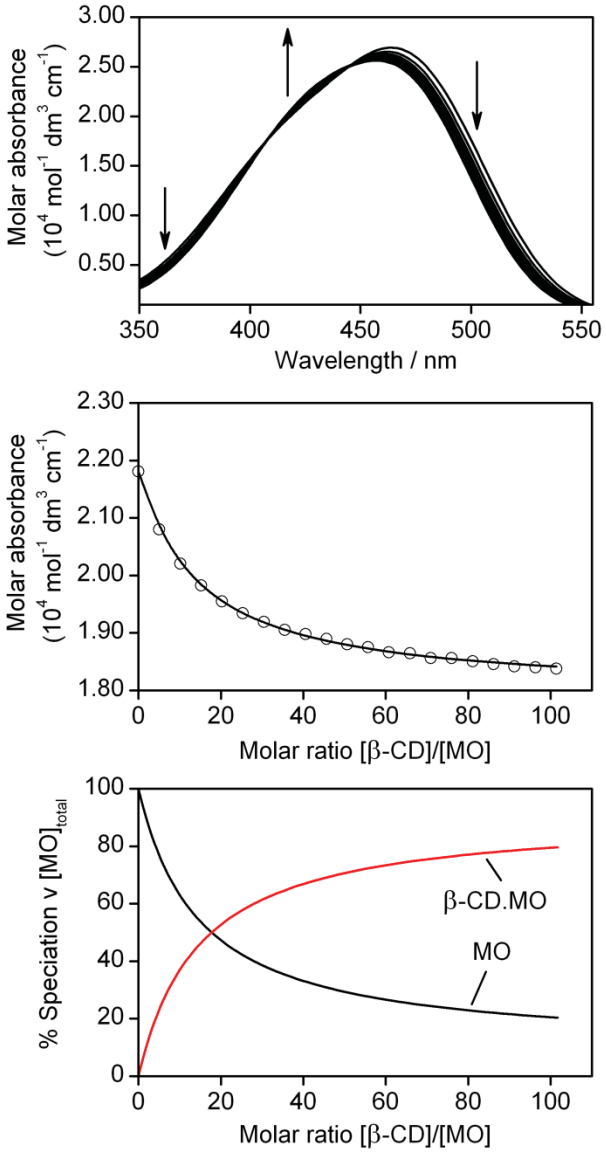

Figure 2.25. (Top) Molar absorbance variation of a MO solution ([MO] = 2.00×10^{-5} mol dm^{-3}) upon 20 sequential additions of a β-CD solution (50 mm^3 each, [β-CD] = 3.04×10^{-3} mol dm^{-3}) at 298.2 K. Both solutions were prepared in aqueous Na_2HPO_4/KH_2PO_4buffer at pH 7.0 and I = 0.10 mol dm^{-3}. The arrows indicate the direction of molar absorbance variation upon each addition of the β-CD solution. (Middle) Molar absorbance variation at 490 nm and the line representing the best-fit of an algorithm for a 1:1 host-guest complexation of MO by β-CD over the wavelength range 465 - 515 nm. (Bottom) Speciation plot with $[MO]_{total}$ = 100%.

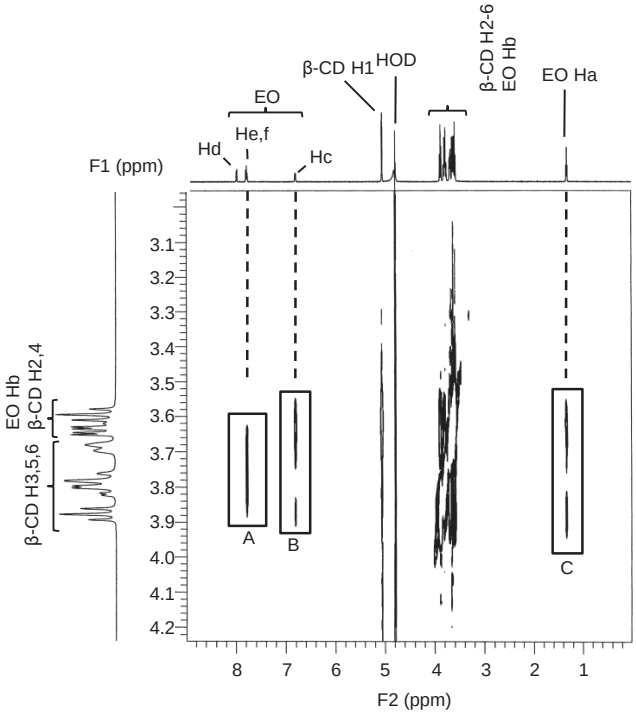

Figure 2.26. 2D ROESY ^{1}H NMR spectrum of EO ([EO] = 2.0 × 10^{-3} mol dm^{-3}) in D_2O Na_2HPO_4/KH_2PO_4 buffer solution at pD = 7.0 and I = 0.10 mol dm^{-3} at 298.2 K. Cross-peaks in boxes A and B arise from dipolar interactions between the EO methylene (Hb) protons and the adjacent aromatic (Hc) and methyl (Ha) protons of EO, respectively.

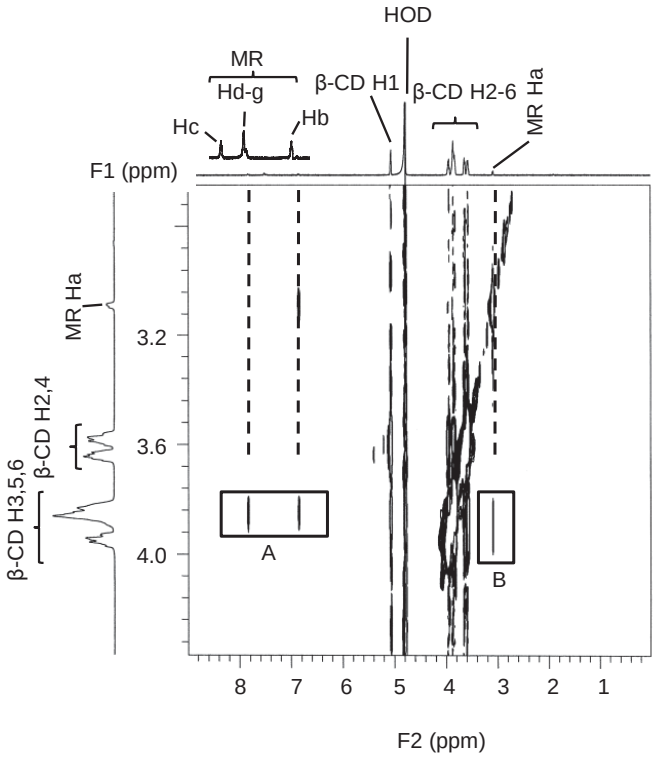

Figure 2.27. 2D ROESY ^{1}H NMR spectrum of MR ([MR] = 2.0×10^{-3} mol dm^{-3}) and β-CD ([β-CD] = 2.0×10^{-3} mol dm^{-3}) in D_2O Na_2HPO_4/KH_2PO_4 buffer solution at pD = 7.0 and I = 0.10 mol dm^{-3} at 298.2 K. Cross-peaks in boxes A and B arise from dipolar interactions between the β-CD annular H3,5,6 protons and the aromatic (Hb and Hc) and methyl (Ha) protons of MR, respectively.

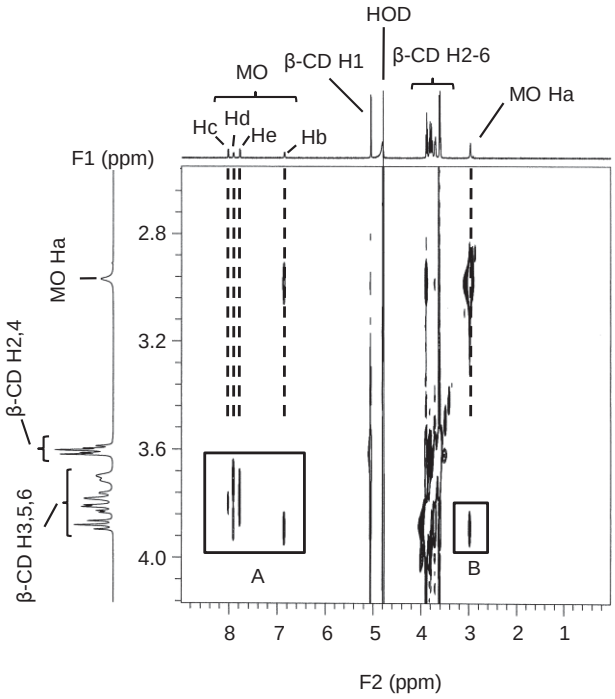

Figure 2.28. 2D ROESY ^{1}H NMR spectrum of MO ([MO] = 2.0×10^{-3} mol dm^{-3}) and β-CD ([β-CD] = 2.0×10^{-3} mol dm^{-3}) in D_2O Na_2HPO_4/KH_2PO_4 buffer solution at pD = 7.0 and I = 0.10 mol dm^{-3} at 298.2 K. Cross-peaks in boxes A and B arise from dipolar interactions between the β-CD annular H3,5,6 protons and the aromatic (Hb-e) and methyl (Ha) protons of MO, respectively.

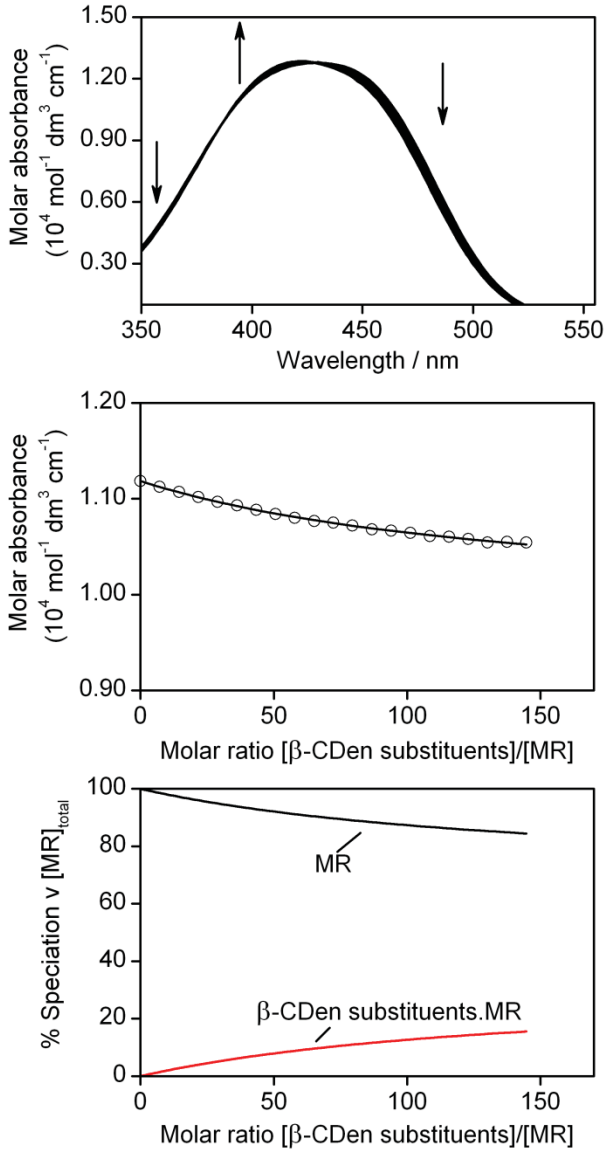

Figure 2.29. (Top) Molar absorbance variation of a MR solution ([MR] = 2.80 × 10^{-5} mol dm^{-3}) upon 20 sequential additions of a PAAβ-CDen solution (50 mm^3 each, 1.32 wt%, [β-CDen substituents] = 6.10 × 10^{-3} mol dm^{-3}) at 298.2 K. Both solutions were prepared in aqueous Na_2HPO_4/KH_2PO_4 buffer at pH 7.0 and I = 0.10 mol dm^{-3}. The arrows indicate the direction of molar absorbance variation upon each addition of the PAAβ-CDen solution. (Middle) Molar absorbance variation at 460 nm and the line representing the best-fit of an algorithm for a 1:1 host-guest complexation of MR by β-CDen substituents of PAAβ-CDen over the wavelength range 430 - 480 nm. (Bottom) Speciation plot with $[MR]_{total}$ = 100%.

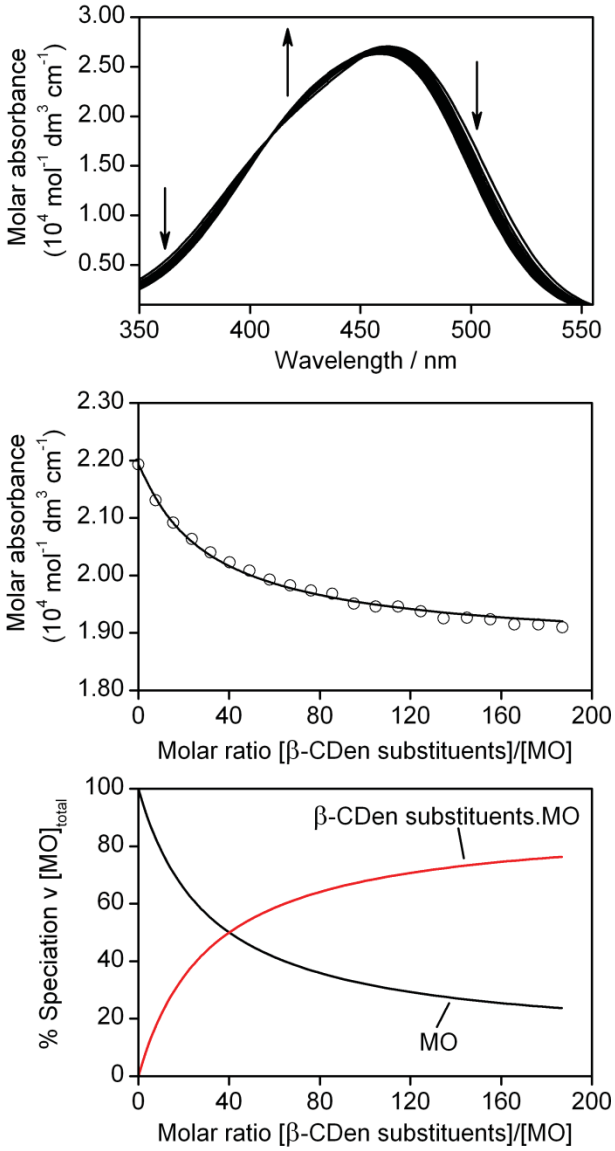

Figure 2.30. (Top) Molar absorbance variation of a MO solution ([MO] = 2.00 × 10^{-5} mol dm^{-3}) upon 20 sequential additions of a PAAβ-CDen solution (50 mm^3 each, 0.98 wt%, [β-CDen substituents] = 4.50 × 10^{-3} mol dm^{-3}) at 298.2 K. Both solutions were prepared in aqueous Na_2HPO_4/KH_2PO_4 buffer at pH 7.0 and I = 0.10 mol dm^{-3}. The arrows indicate the direction of molar absorbance variation upon each addition of the PAAβ-CDen solution. (Middle) Molar absorbance variation at 490 nm and the line representing the best-fit of an algorithm for a 1:1 host-guest complexation of MO by β-CDen substituents of PAAβ-CDen over the wavelength range 465 - 515 nm. (Bottom) Speciation plot with $[MO]_{total}$ = 100%.

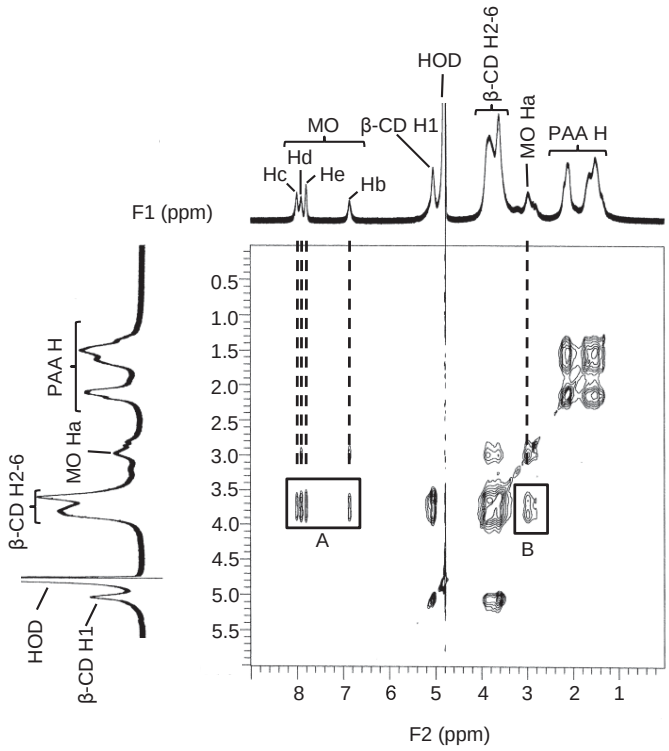

Figure 2.31. 2D NOESY ^{1}H NMR spectrum of MO ([MO] = 2.0 × 10^{-3} mol dm^{-3}) and PAAβ-CDen (0.44 wt%, [β-CDen substituents] = 2.0 × 10^{-3} mol dm^{-3}) in D_2O Na_2HPO_4/KH_2PO_4 buffer solution at pD = 7.0 and I = 0.10 mol dm^{-3} at 298.2 K. Cross-peaks in boxes A and B arise from dipolar interactions between the annular H3,5,6 protons of the β-CD groups and the aromatic (Hb-e) and methyl (Ha) protons of MO, respectively.

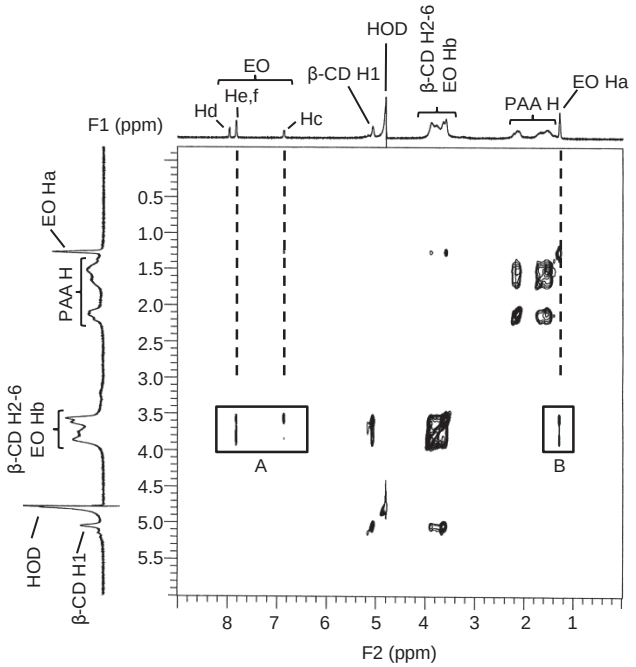

Figure 2.32. 2D NOESY ^{1}H NMR spectrum of EO ([EO] = 2.0 × 10^{-3} mol dm^{-3}) and PAAβ-CDen (0.44 wt%, [β-CDen substituents] = 2.0 × 10^{-3} mol dm^{-3}) in D_2O Na_2HPO_4/KH_2PO_4 buffer solution at pD = 7.0 and I = 0.10 mol dm^{-3} at 298.2 K. Cross-peaks in boxes A and B arise from dipolar interactions between the annular H3,5,6 protons of the β-CD groups and the aromatic (Hc, He and Hf) and methyl (Ha) protons of EO, respectively.

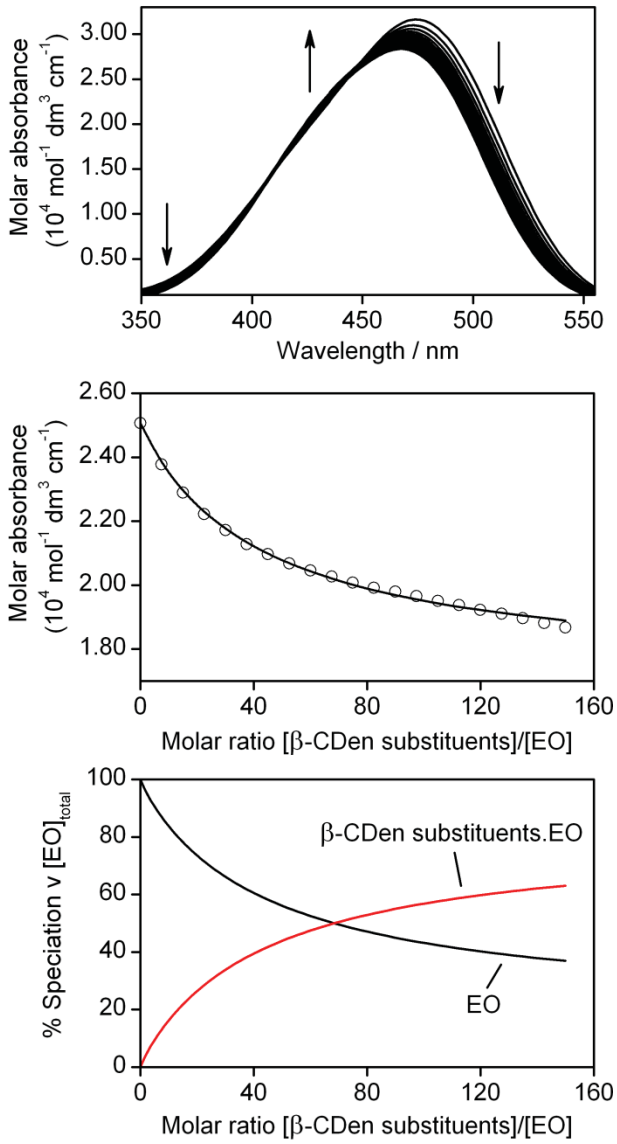

Figure 2.33. (Top) Molar absorbance variation of a EO solution ([EO] = 2.00 × 10^{-5} mol dm^{-3}) upon 20 sequential additions of a PAAβ-CDen solution (25 mm^3 each, 1.93 wt%, [β-CDen substituents] = 9.00 × 10^{-3} mol dm^{-3}) and a PAAADhn solution (25 mm^3 each, 0.98 wt%, [ADhn substituents] = 3.00 × 10^{-3} mol dm^{-3}) at 298.2 K. All solutions were prepared in aqueous Na_2HPO_4/KH_2PO_4 buffer at pH 7.0 and I = 0.10 mol dm^{-3}. The arrows indicate the direction of molar absorbance variation upon each addition of the PAAβ-CDen and PAAADhn solutions. (Middle) Molar absorbance variation at 500 nm and the line representing the best-fit of an algorithm for a 1:1 host-guest complexation of EO by β-CDen substituents in self-assembled PAAβ-CDen/PAAADhn network over the wavelength range 475 - 525 nm. (Bottom) Speciation plot with $[EO]_{total}$ = 100%.

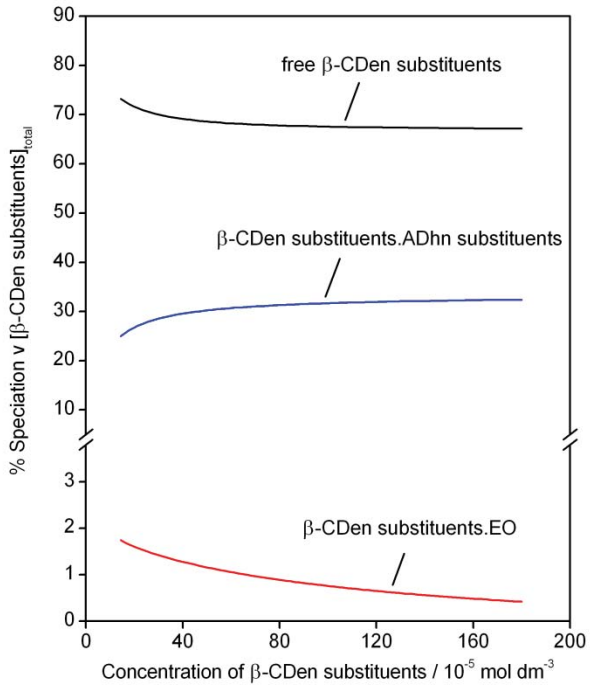

Figure 2.34. Speciation plot with $[\beta\text{-CDen substituents}]_{total}$ = 100% for the PAAβ-CDen/PAAADhn/EO system.

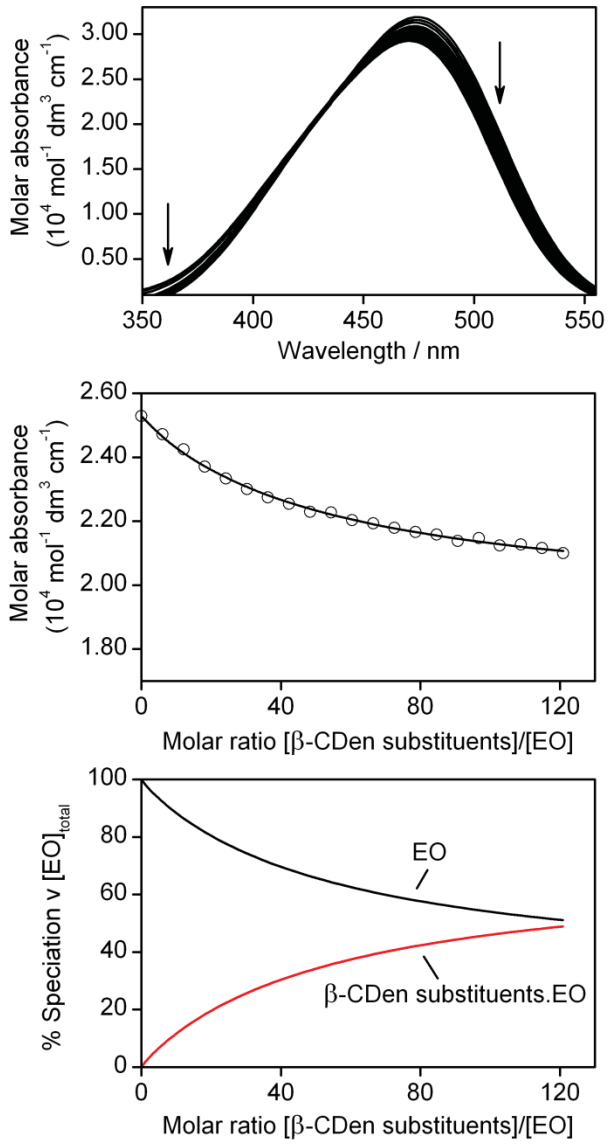

Figure 2.35. (Top) Molar absorbance variation of a EO solution ([EO] = 2.00 × 10^{-5} mol dm^{-3}) upon 20 sequential additions of a PAAβ-CDen solution (25 mm^3 each, 1.56 wt%, [β-CDen substituents] = 7.26 × 10^{-3} mol dm^{-3}) and a PAAADddn solution (25 mm^3 each, 0.85 wt%, [ADddn substituents] = 2.43 × 10^{-3} mol dm^{-3}) at 298.2 K. All solutions were prepared in aqueous Na_2HPO_4/KH_2PO_4 buffer at pH 7.0 and I = 0.10 mol dm^{-3}. The arrows indicate the direction of molar absorbance variation upon each addition of the PAAβ-CDen and PAAADddn solutions. (Middle) Molar absorbance variation at 500 nm and the line representing the best-fit of an algorithm for a 1:1 host-guest complexation of EO by β-CDen substituents in self-assembled PAAβ-CDen/PAAADddn network over the wavelength range 475 - 525 nm. (Bottom) Speciation plot with $[EO]_{total}$ = 100%.

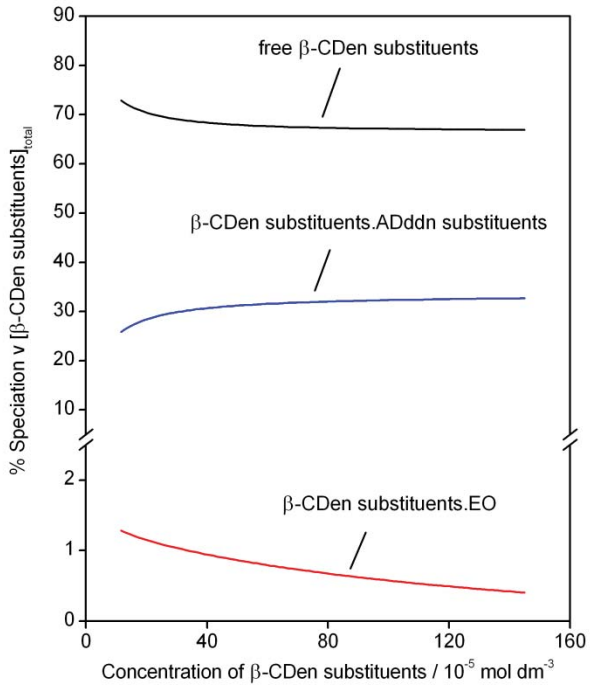

Figure 2.36. Speciation plot with $[\beta\text{-CDen substituents}]_{total}$ = 100% for the PAAβ-CDen/PAAADddn/EO system.

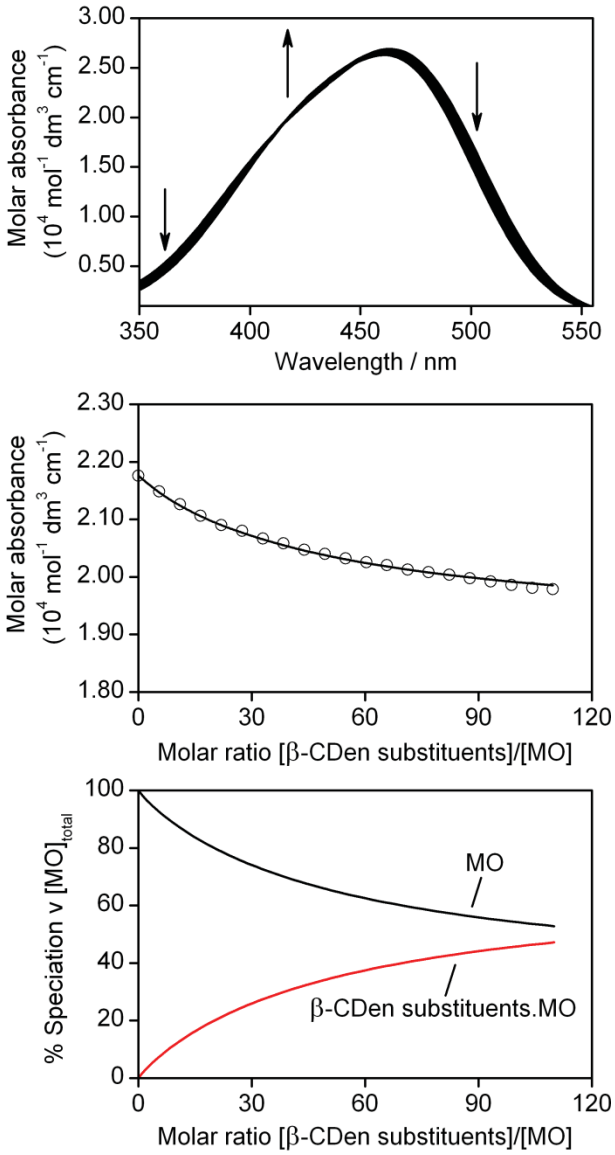

Figure 2.37. (Top) Molar absorbance variation of a MO solution ([MO] = 2.00×10^{-5} mol dm^{-3}) upon 20 sequential additions of a PAAβ-CDen solution (25 mm^3 each, 1.42 wt%, [β-CDen substituents] = 6.58×10^{-3} mol dm^{-3}) and a PAAADen solution (25 mm^3 each, 0.65 wt%, [ADen substituents] = 2.19×10^{-3} mol dm^{-3}) at 298.2 K. All solutions were prepared in aqueous Na_2HPO_4/KH_2PO_4 buffer solutions at pH 7.0 and I = 0.10 mol dm^{-3}. The arrows indicate the direction of molar absorbance variation upon each addition of the PAAβ-CDen and PAAADen solutions. (Middle) Molar absorbance variation at 490 nm and the line representing the best-fit of an algorithm for a 1:1 host-guest complexation of MO by β-CDen substituents in self-assembled PAAβ-CDen/PAAADen network over the wavelength range 465 - 515 nm. (Bottom) Speciation plot with $[MO]_{total}$ = 100%.

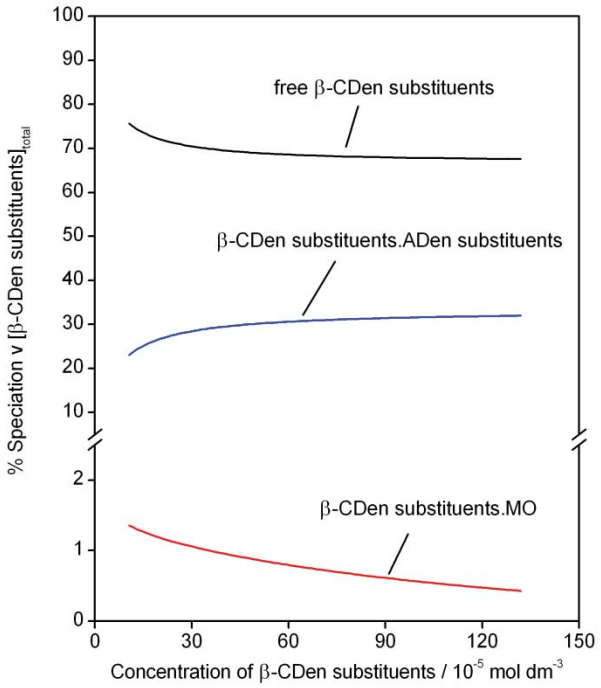

Figure 2.38. Speciation plot with $[\beta\text{-CDen substituents}]_{total}$ = 100% for the PAAβ-CDen/PAAADen/MO system.

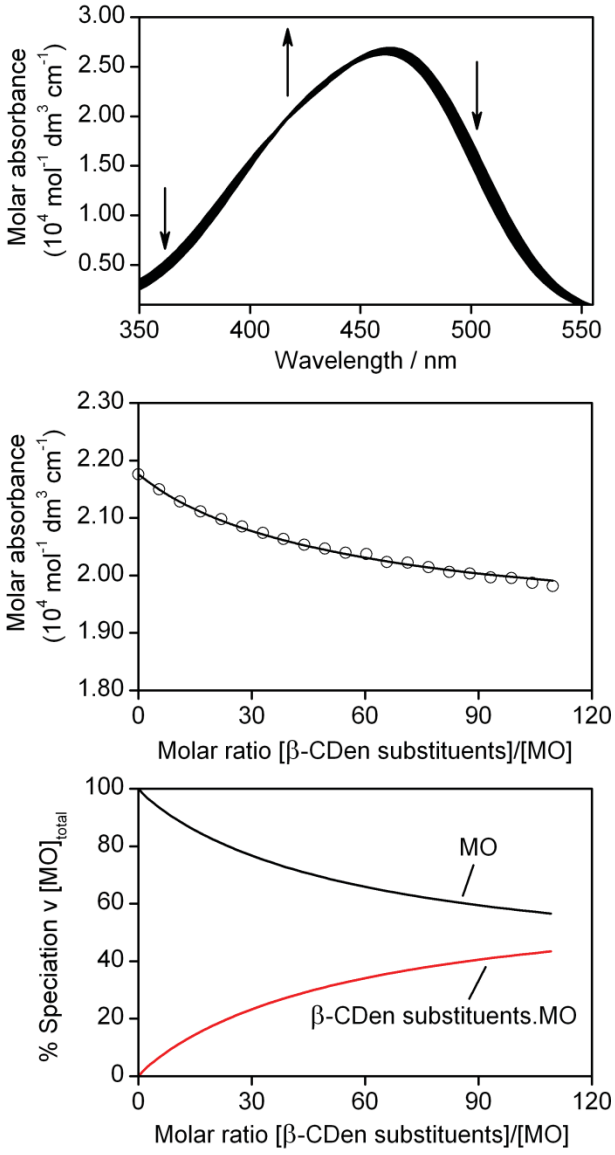

Figure 2.39. (Top) Molar absorbance variation of a MO solution ([MO] = 2.00 × 10^{-5} mol dm^{-3}) upon 20 sequential additions of a PAAβ-CDen solution (25 mm^3 each, 1.42 wt%, [β-CDen substituents] = 6.58 × 10^{-3} mol dm^{-3}) and a PAAADhn solution (25 mm^3 each, 0.74 wt%, [ADhn substituents] = 2.23 × 10^{-3} mol dm^{-3}) at 298.2 K. All solutions were prepared in aqueous Na_2HPO_4/KH_2PO_4 buffer at pH 7.0 and I = 0.10 mol dm^{-3}. The arrows indicate the direction of molar absorbance variation upon each addition of the PAAβ-CDen and PAAADhn solutions. (Middle) Molar absorbance variation at 490 nm and the line representing the best-fit of an algorithm for a 1:1 host-guest complexation of MO by β-CDen substituents in self-assembled PAAβ-CDen/PAAADhn network over the wavelength range 465 - 515 nm. (Bottom) Speciation plot with $[MO]_{total}$ = 100%.

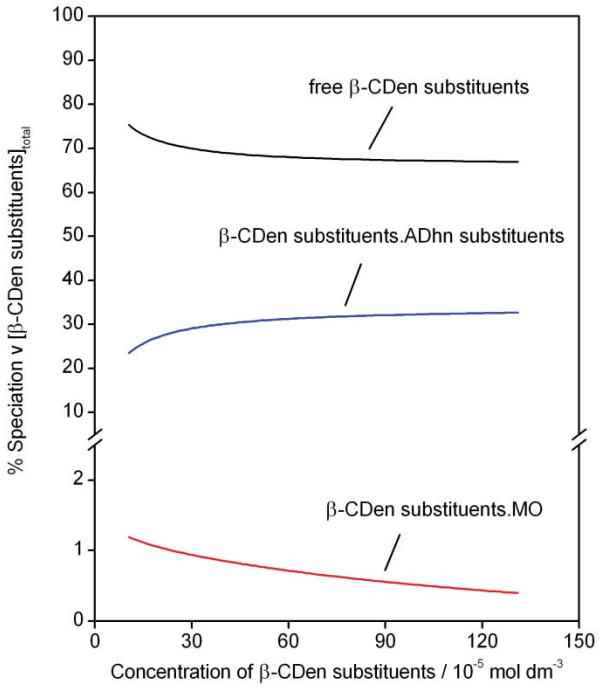

Figure 2.40. Speciation plot with $[\beta\text{-CDen substituents}]_{total}$ = 100% for the PAAβ-CDen/PAAADhn/MO system.

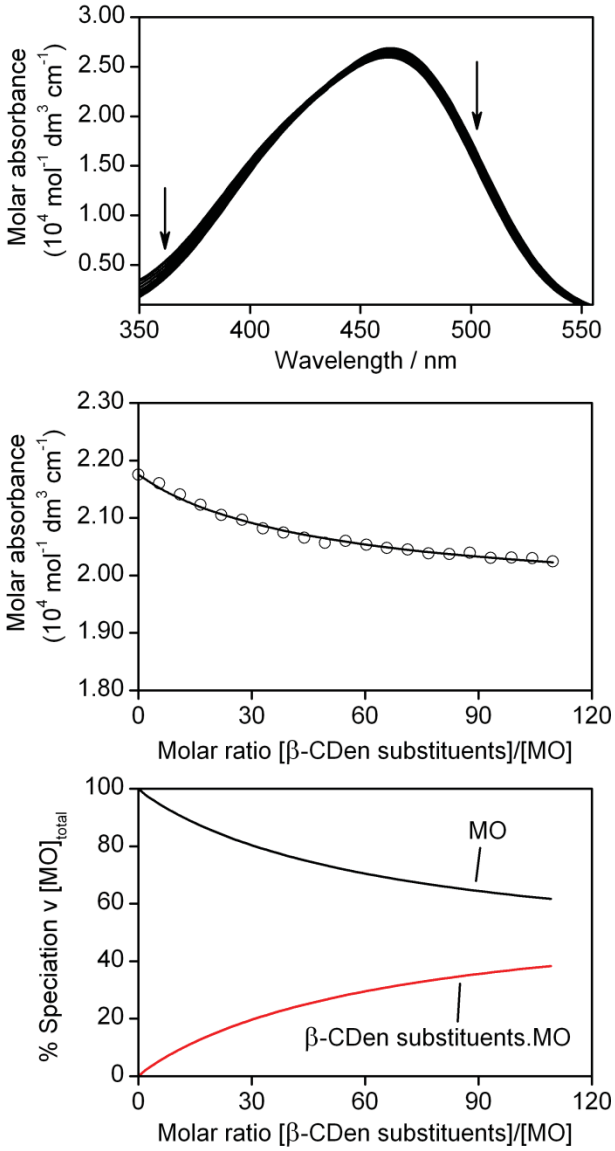

Figure 2.41. (Top) Molar absorbance variation of a MO solution ([MO] = 2.00 × 10^{-5} mol dm^{-3}) upon 20 sequential additions of a PAAβ-CDen solution (25 mm^3 each, 1.42 wt%, [β-CDen substituents] = 6.58 × 10^{-3} mol dm^{-3}) and a PAAADddn solution (25 mm^3 each, 0.78 wt%, [ADddn substituents] = 2.23 × 10^{-3} mol dm^{-3}) at 298.2 K. All solutions were prepared in aqueous Na_2HPO_4/KH_2PO_4 buffer at pH 7.0 and I = 0.10 mol dm^{-3}. The arrows indicate the direction of molar absorbance variation upon each addition of the PAAβ-CDen and PAAADddn solutions. (Middle) Molar absorbance variation at 490 nm and the line representing the best-fit of an algorithm for a 1:1 host-guest complexation of MO by β-CDen substituents in self-assembled PAAβ-CDen/PAAADddn network over the wavelength range 465 - 515 nm. (Bottom) Speciation plot with $[MO]_{total}$ = 100%.

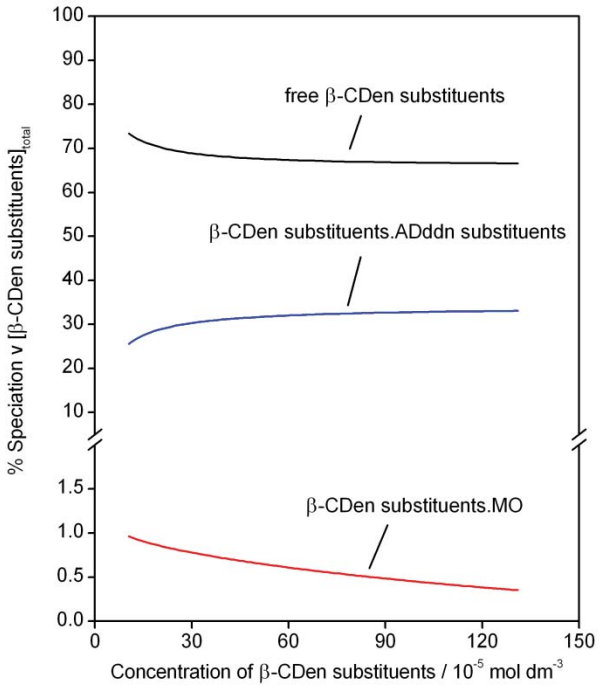

Figure 2.42. Speciation plot with $[\beta\text{-CDen substituents}]_{total}$ = 100% for the PAAβ-CDen/PAAADddn/MO system.

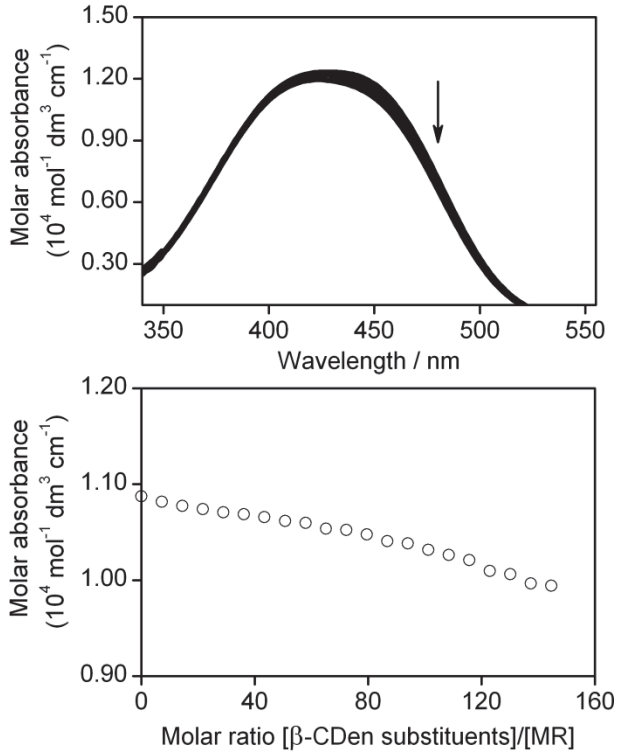

Figure 2.43. (Top) Molar absorbance variation of a MR solution ([MR] = 2.80×10^{-5} mol dm^{-3}) upon 20 sequential additions of a PAAβ-CDen solution (25 mm^3 each, 2.59 wt%, [β-CDen substituents] = 1.22×10^{-2} mol dm^{-3}) and a PAAADen solution (25 mm^3 each, 1.18 wt%, [ADen substituents] = 4.03×10^{-3} mol dm^{-3}) at 298.2 K. All solutions were prepared in aqueous Na_2HPO_4/KH_2PO_4 buffer at pH 7.0 and I = 0.10 mol dm^{-3}. The arrow indicates the direction of molar absorbance variation upon each addition of the PAAβ-CDen and PAAADen solutions. (Bottom) Molar absorbance variation at 460 nm is insufficient to fit to an algorithm for host-guest complexation of MR by β-CDen substituents in self-assembled PAAβ-CDen/PAAADen network.

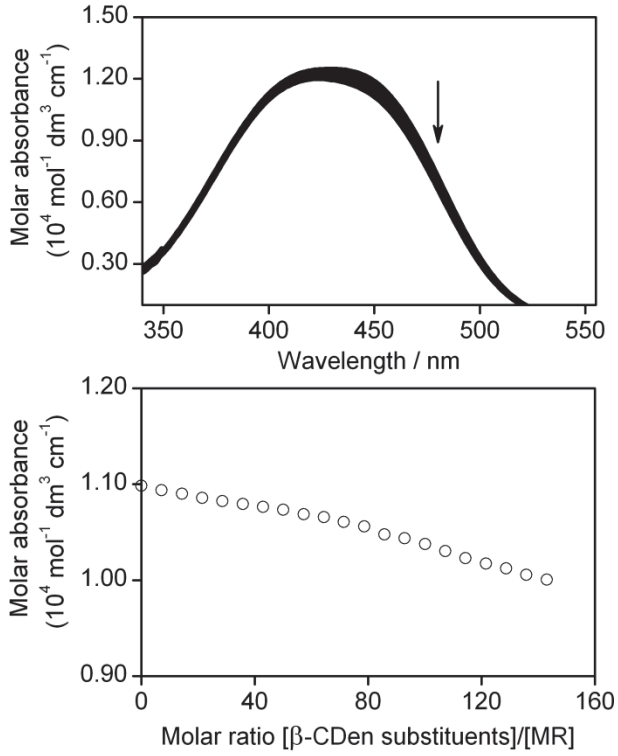

Figure 2.44. (Top) Molar absorbance variation of a MR solution ([MR] = 2.80×10^{-5} mol dm^{-3}) upon 20 sequential additions of a PAAβ-CDen solution (25 mm^3 each, 2.54 wt%, [β-CDen substituents] = 1.20×10^{-2} mol dm^{-3}) and a PAAADhn solution (25 mm^3 each, 1.30 wt%, [ADhn substituents] = 4.00×10^{-3} mol dm^{-3}) at 298.2 K. All solutions were prepared in aqueous Na_2HPO_4/KH_2PO_4 buffer at pH 7.0 and I = 0.10 mol dm^{-3}. The arrow indicates the direction of molar absorbance variation upon each addition of the PAAβ-CDen and PAAADhn solutions. (Bottom) Molar absorbance variation at 460 nm is insufficient to fit to an algorithm for host-guest complexation of MR by β-CDen substituents in self-assembled PAAβ-CDen/PAAADhn network.

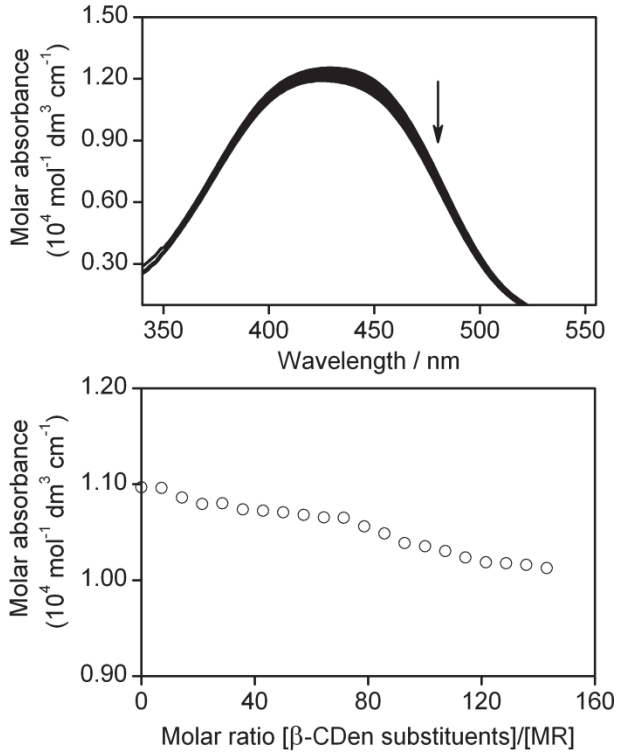

Figure 2.45. (Top) Molar absorbance variation of a MR solution ([MR] = 2.80×10^{-5} mol dm^{-3}) upon 20 sequential additions of a PAAβ-CDen solution (25 mm^3 each, 2.54 wt%, [β-CDen substituents] = 1.20×10^{-2} mol dm^{-3}) and a PAAADddn solution (25 mm^3 each, 1.37 wt%, [ADddn substituents] = 4.01×10^{-3} mol dm^{-3}) at 298.2 K. All solutions were prepared in aqueous Na_2HPO_4/KH_2PO_4 buffer at pH 7.0 and I = 0.10 mol dm^{-3}. The arrow indicates the direction of molar absorbance variation upon each addition of the PAAβ-CDen and PAAADddn solutions. (Bottom) Molar absorbance variation at 460 nm is insufficient to fit to an algorithm for host-guest complexation of MR by β-CDen substituents in self-assembled PAAβ-CDen/PAAADddn network.

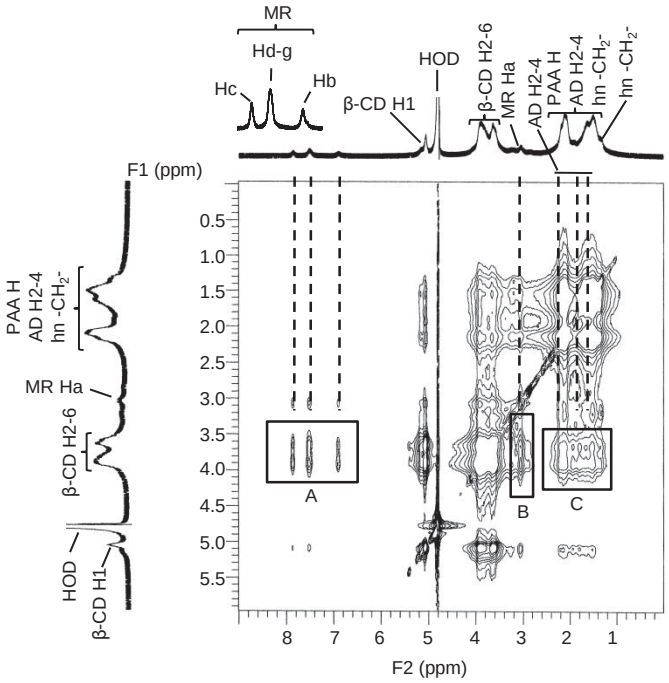

Figure 2.46. 2D NOESY ^{1}H NMR spectrum of MR ([MR] = 2.0×10^{-3} mol dm^{-3}) in mixture with PAAβ-CDen (0.78 wt%, [β-CDen substituents] = 3.6×10^{-3} mol dm^{-3}) and PAAADhn (0.40 wt%, [ADhn substituents] = 1.2×10^{-3} mol dm^{-3}) in D_2O Na_2HPO_4/KH_2PO_4 buffer solution at pD = 7.0 and I = 0.10 mol dm^{-3} at 298.2 K. Cross-peaks in boxes A and B arise from dipolar interactions between the annular H3,5,6 protons of the β-CD groups and the aromatic (Hb-g) and methyl (Ha) protons of MR, respectively. Cross-peaks in box C arise from dipolar interactions between the annular H3,5,6 protons of the β-CD groups and the H2-4 protons of the AD groups.

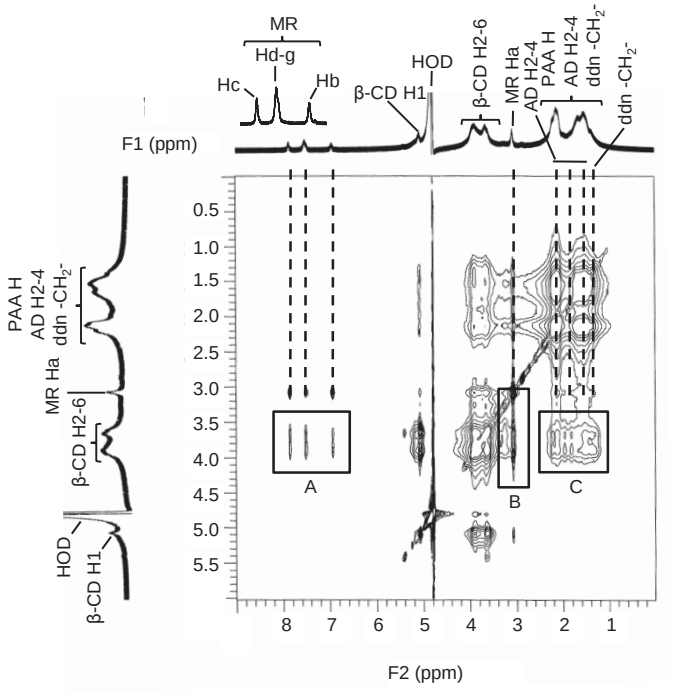

Figure 2.47. 2D NOESY ^{1}H NMR spectrum of MR ([MR] = 2.0×10^{-3} mol dm^{-3}) in mixture with PAAβ-CDen (0.78 wt%, [β-CDen substituents] = 3.6×10^{-3} mol dm^{-3}) and PAAADddn (0.42 wt%, [ADddn substituents] = 1.2×10^{-3} mol dm^{-3}) in D_2O Na_2HPO_4/KH_2PO_4 buffer solution at pD = 7.0 and I = 0.10 mol dm^{-3} at 298.2 K. Cross-peaks in boxes A and B arise from dipolar interactions between the annular H3,5,6 protons of the β-CD groups and the aromatic (Hb-g) and methyl (Ha) protons of MR, respectively. Cross-peaks in box C arise from dipolar interactions between the annular H3,5,6 protons of the β-CD groups and the H2-4 protons of the AD groups and the tether dodecyl methylene protons, respectively.

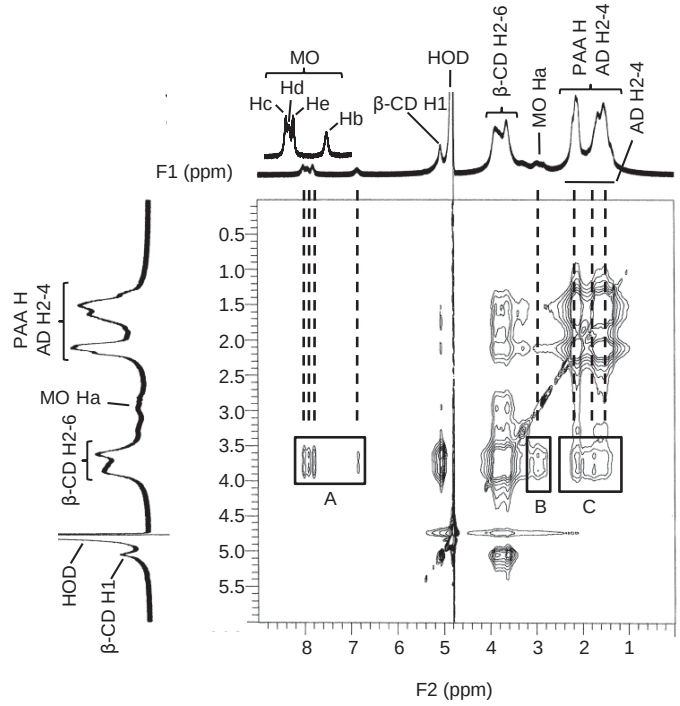

Figure 2.48. 2D NOESY ^{1}H NMR spectrum of MO ([MO] = 2.0×10^{-3} mol dm^{-3}) in mixture with PAAβ-CDen (0.78 wt%, [β-CDen substituents] = 3.6×10^{-3} mol dm^{-3}) and PAAADen (0.36 wt%, [ADen substituents] = 1.2×10^{-3} mol dm^{-3}) in D_2O Na_2HPO_4/KH_2PO_4 buffer solution at pD = 7.0 and I = 0.10 mol dm^{-3} at 298.2 K. Cross-peaks in boxes A and B arise from dipolar interactions between the annular H3,5,6 protons of the β-CD groups and the aromatic (Hb-e) and methyl (Ha) protons of MO, respectively. Cross-peaks in box C arise from dipolar interactions between the annular H3,5,6 protons of the β-CD groups and the H2-4 protons of the AD groups.

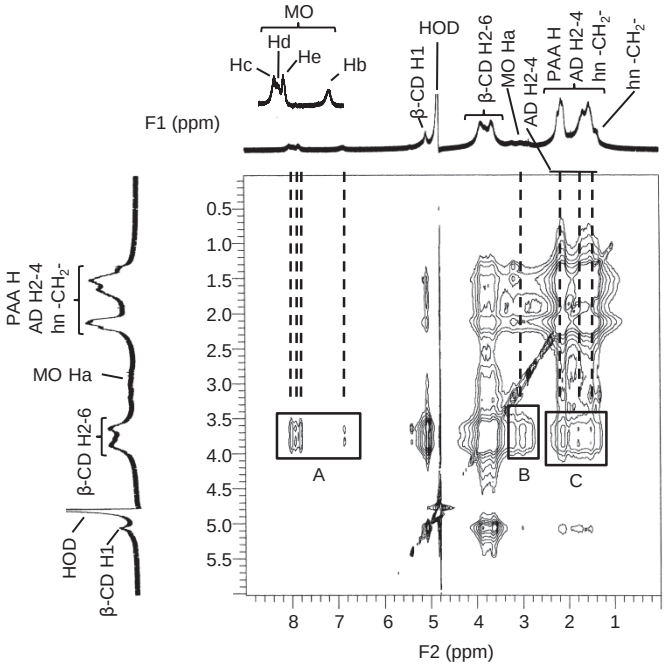

Figure 2.49. 2D NOESY ^{1}H NMR spectrum of MO ([MO] = 2.0×10^{-3} mol dm^{-3}) in mixture with PAAβ-CDen (0.78 wt%, [β-CDen substituents] = 3.6×10^{-3} mol dm^{-3}) and PAAADhn (0.40 wt%, [ADhn substituents] = 1.2×10^{-3} mol dm^{-3}) in D_2O Na_2HPO_4/KH_2PO_4 buffer solution at pD = 7.0 and I = 0.10 mol dm^{-3} at 298.2 K. Cross-peaks in boxes A and B arise from dipolar interactions between the annular H3,5,6 protons of the β-CD groups and the aromatic (Hb-e) and methyl (Ha) protons of MO, respectively. Cross-peaks in box C arise from dipolar interactions between the annular H3,5,6 protons of the β-CD groups and the H2-4 protons of the AD groups.

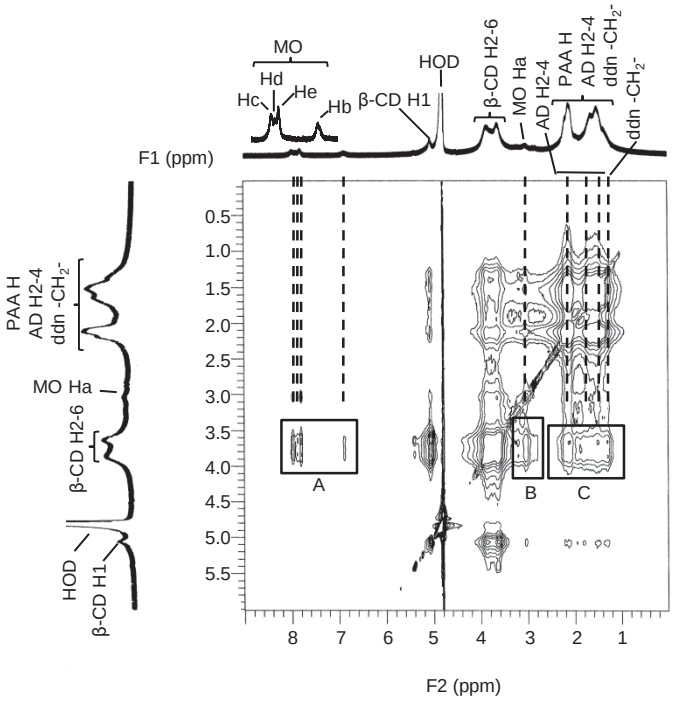

Figure 2.50. 2D NOESY ^{1}H NMR spectrum of MO ([MO] = 2.0×10^{-3} mol dm^{-3}) in mixture with PAAβ-CDen (0.78 wt%, [β-CDen substituents] = 3.6×10^{-3} mol dm^{-3}) and PAAADddn (0.42 wt%, [ADddn substituents] = 1.2×10^{-3} mol dm^{-3}) in D_2O Na_2HPO_4/KH_2PO_4 buffer solution at pD = 7.0 and I = 0.10 mol dm^{-3} at 298.2 K. Cross-peaks in boxes A and B arise from dipolar interactions between the annular H3,5,6 protons of the β-CD groups and the aromatic (Hb-e) and methyl (Ha) protons of MO, respectively. Cross-peaks in box C arise from dipolar interactions between the annular H3,5,6 protons of the β-CD groups and the H2-4 protons of the AD groups and the tether dodecyl methylene protons, respectively.

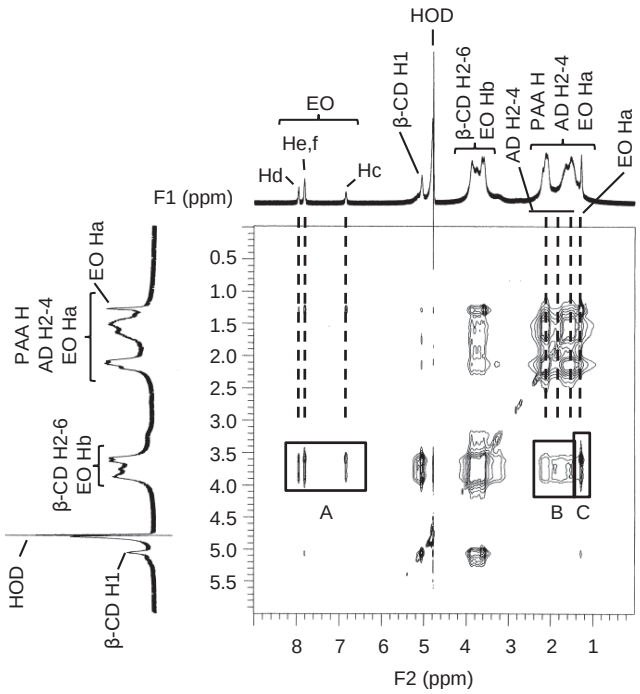

Figure 2.51. 2D NOESY ^{1}H NMR spectrum of EO ([EO] = 2.0×10^{-3} mol dm^{-3}) in mixture with PAAβ-CDen (0.78 wt%, [β-CDen substituents] = 3.6×10^{-3} mol dm^{-3}) and PAAADen (0.36 wt%, [ADen substituents] = 1.2×10^{-3} mol dm^{-3}) in D_2O Na_2HPO_4/KH_2PO_4 buffer solution at pD = 7.0 and I = 0.10 mol dm^{-3} at 298.2 K. Cross-peaks in boxes A and C arise from dipolar interactions between the annular H3,5,6 protons of the β-CD groups and the aromatic (Hc-f) and methyl (Ha) protons of EO, respectively. Cross-peaks in box B arise from dipolar interactions between the annular H3,5,6 protons of the β-CD groups and the H2-4 protons of the AD groups.

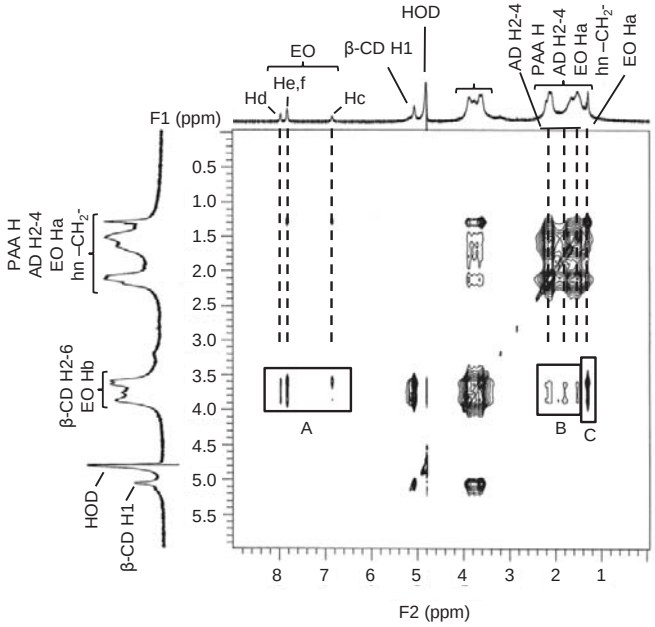

Figure 2.52. 2D NOESY ^{1}H NMR spectrum of EO ([EO] = 2.0 × 10^{-3} mol dm^{-3}) in mixture with PAAβ-CDen (0.78 wt%, [β-CDen substituents] = 3.6 × 10^{-3} mol dm^{-3}) and PAAADhn (0.40 wt%, [ADhn substituents] = 1.2 × 10^{-3} mol dm^{-3}) in D_2O Na_2HPO_4/KH_2PO_4 buffer solution at pD = 7.0 and I = 0.10 mol dm^{-3} at 298.2 K. Cross-peaks in boxes A and C arise from dipolar interactions between the annular H3,5,6 protons of the β-CD groups and the aromatic (Hc-f) and methyl (Ha) protons of EO, respectively. Cross-peaks in box B arise from dipolar interactions between the annular H3,5,6 protons of the β-CD groups and the H2-4 protons of the AD groups.

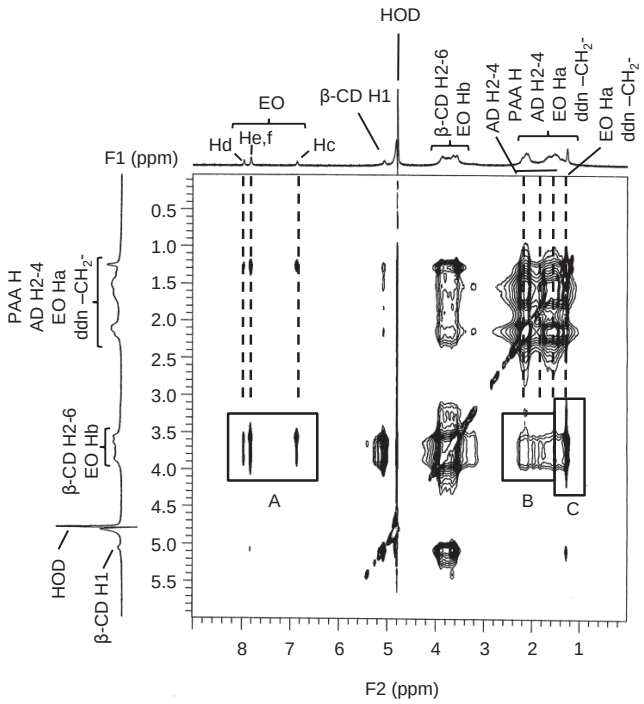

Figure 2.53. 2D NOESY ^{1}H NMR spectrum of EO ([EO] = 2.0×10^{-3} mol dm^{-3}) in mixture with PAAβ-CDen (0.78 wt%, [β-CDen substituents] = 3.6×10^{-3} mol dm^{-3}) and PAAADddn (0.42 wt%, [ADddn substituents] = 1.2×10^{-3} mol dm^{-3}) in D_2O Na_2HPO_4/KH_2PO_4 buffer solution at pD = 7.0 and I = 0.10 mol dm^{-3} at 298.2 K. Cross-peaks in box A arise from dipolar interactions between the annular H3,5,6 protons of the β-CD groups and the aromatic (Hc-f) protons of EO. Cross-peaks in box B arise from dipolar interactions between the annular H3,5,6 protons of the β-CD groups and the H2-4 protons of the AD groups. Cross-peaks in box C arise from dipolar interactions between the annular H3,5,6 protons of the β-CD groups and the tether dodecyl methylene protons of the ADddn substituents and the methyl (Ha) protons of EO, respectively.

2.10.4. Rheological data of aqueous substituted poly(acrylate)s

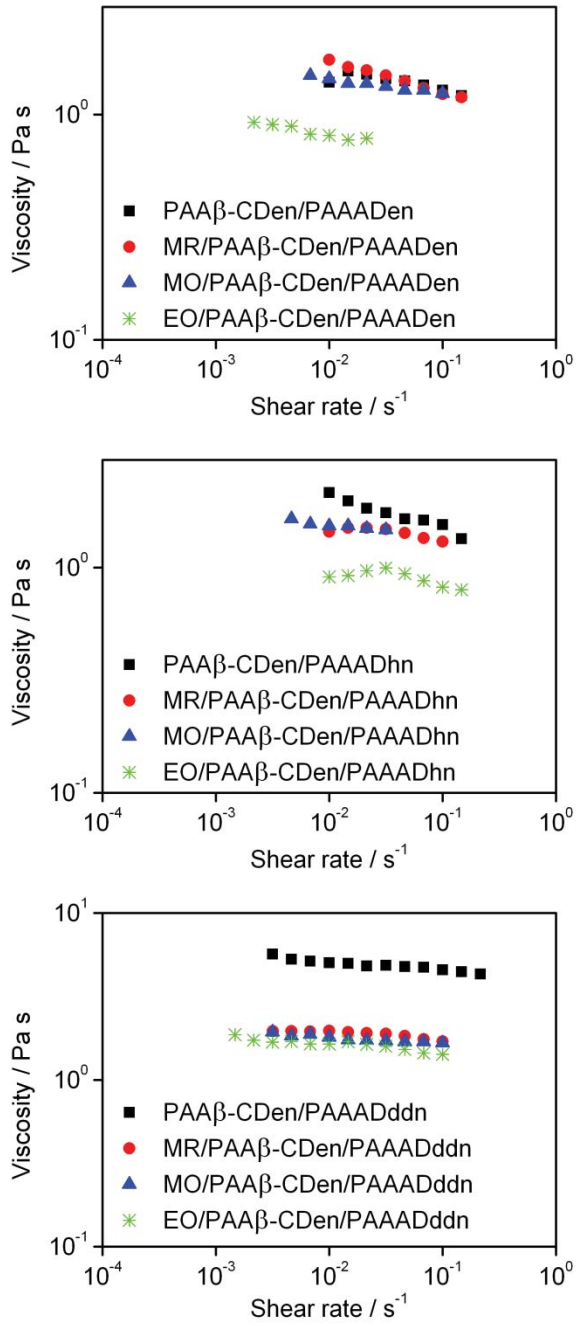

Figure 2.54. Viscosity variations of aqueous Na_2HPO_4/KH_2PO_4 buffer at pH 7.0 and I = 0.10 mol dm^{-3} of (Top) PAAβ-CDen (0.78 wt%, [β-CDen substituents] = 3.60 × 10^{-3} mol dm^{-3}) and PAAADen (0.36 wt%, [ADen substituents] = 1.20 × 10^{-3} mol dm^{-3}), (Middle) PAAβ-CDen (0.78 wt%, [β-CDen substituents] = 3.60 × 10^{-3} mol dm^{-3}) and PAAADhn (0.40 wt%, [ADhn substituents] = 1.20 × 10^{-3} mol dm^{-3}), (Bottom) PAAβ-CDen (0.78 wt%, [β-CDen substituents] = 3.60 × 10^{-3} mol dm^{-3}) and PAAADddn (0.42 wt%, [ADddn substituents] = 1.20 × 10^{-3} mol dm^{-3}), and their mixtures with 2.00 × 10^{-3} mol dm^{-3} either MR, MO, or EO at 298.2 K with shear rate.

2.10.5. Dye release data

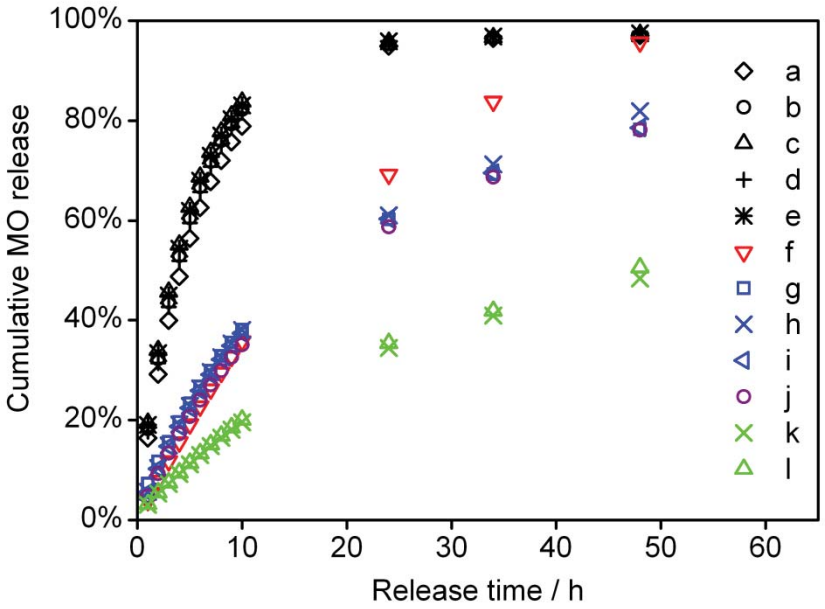

Figure 2.55. Release profiles for MO from (a) Na_2HPO_4/KH_2PO_4 buffer, (b) PAA, (c) PAA/PAAADddn, (d) PAA/PAAADhn, (e) PAA/PAAADen, (f) PAA/β-CD, (g) 1.20 wt% PAAβ-CDen/PAAADddn, (h) 1.18 wt% PAAβ-CDen/PAAADhn, (i) 1.14 wt% PAAβ-CDen/PAAADen, (j) 1.18 wt% PAA/PAAβ-CDen, (k) 1.96 wt% PAAβ-CDen/PAAADhn, and (l) 1.89 wt% PAAβ-CDen/PAAADen in aqueous Na_2HPO_4/KH_2PO_4 buffer at pH 7.0 and I = 0.10 mol dm^{-3} at 298.2 K. The MO concentration = 2.00×10^{-3} mol dm^{-3}.

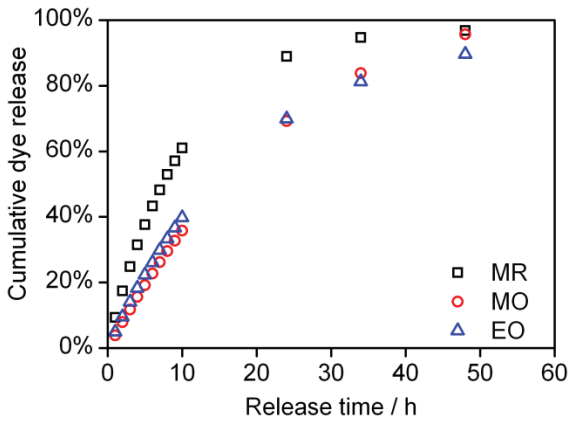

Figure 2.56. Release profiles of three dyes from a 1.20 wt% PAA/β-CD aqueous Na_2HPO_4/KH_2PO_4 buffer solution at pH 7.0 and I = 0.10 mol dm^{-3} at 298.2 K. The dye concentration = 2.00×10^{-3} mol dm^{-3}.

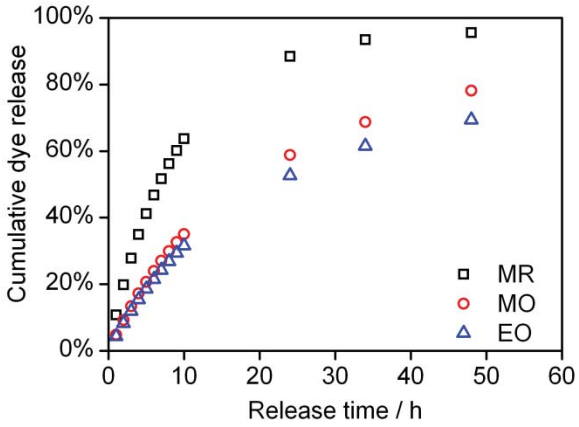

Figure 2.57. Release profiles of three dyes from a 1.18 wt% PAA/PAAβ-CDen aqueous Na_2HPO_4/KH_2PO_4 buffer solution at pH 7.0 and I = 0.10 mol dm^{-3} at 298.2 K. The dye concentration = 2.00×10^{-3} mol dm^{-3}.

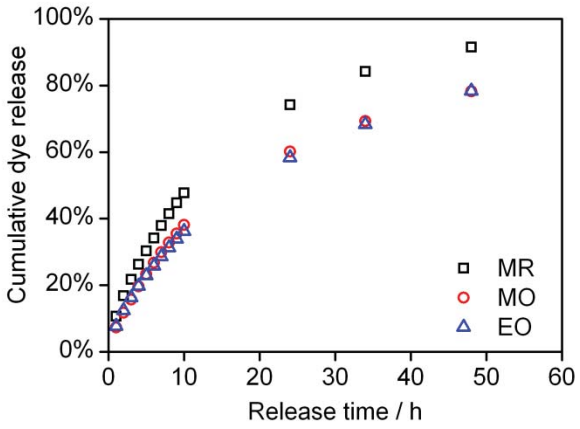

Figure 2.58. Release profiles of three dyes from a 1.20 wt% PAAβ-CDen/PAAADddn aqueous Na_2HPO_4/KH_2PO_4 buffer solution at pH 7.0 and I = 0.10 mol dm^{-3} at 298.2 K. The dye concentration = 2.00×10^{-3} mol dm^{-3}.

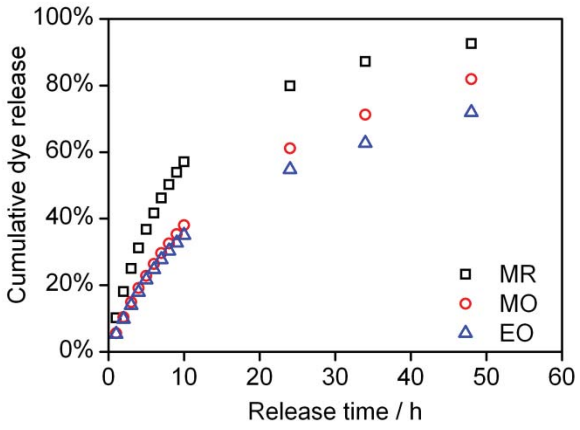

Figure 2.59. Release profiles of three dyes from a 1.18 wt% PAAβ-CDen/PAAADhn aqueous Na_2HPO_4/KH_2PO_4 buffer solution at pH 7.0 and I = 0.10 mol dm^{-3} at 298.2 K. The dye concentration = 2.00×10^{-3} mol dm^{-3}.

This page is intentionally left blank.

CHAPTER 3

DYE COMPLEXATION AND RELEASE IN β-CYCLODEXTRIN- AND OCTADECYL-SUBSTITUTED POLY(ACRYLATE) AQUEOUS NETWORK

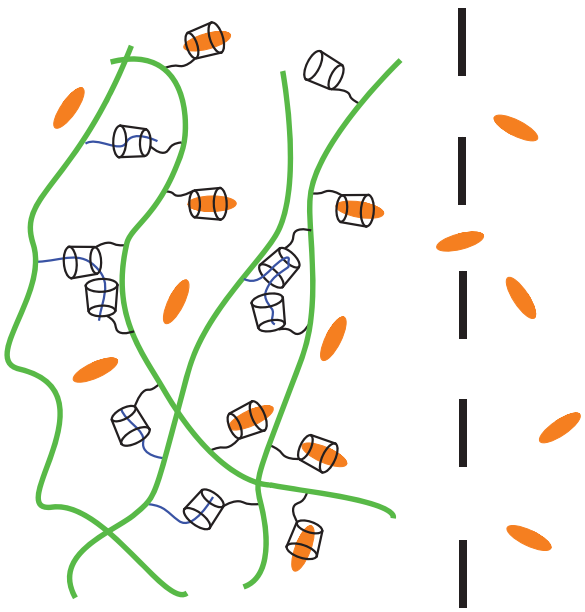

3.1. Introduction

Physical hydrogel networks cross-linked by cyclodextrin-guest complexation have attracted extensive research interests, on account of their scientific significance and wide ranges of biomedical applications. Consequently, it is important to advance the understanding of cyclodextrin-guest interactions at the molecular level in aqueous polymer systems, which in turn sheds light on the polymeric hydrogel network formation at the macroscopic level.[1-13] Practically, hydrogel networks containing cyclodextrins are highly promising biomaterials, particularly in drug delivery, as they combine the advantages of hydrogel networks and cyclodextrins in drug delivery.

Hydrogel networks are promising drug delivery candidates as a consequence of their high water content and biocompatibility,[14,15] and their porous structure allows ready drug loading and subsequent sustained release.[16] Sometimes they possess surface biorecognition sites which facilitate targeted drug delivery,[17] and sometimes they show an environmental responsiveness which triggers controlled drug release.[18-21]

Cyclodextrins have a capacity to complex a range of hydrophobic guest including drugs and as a consequence have been widely used in pharmaceutical research to enhance drug solubility, stability and bioavailability, to reduce odors and tastes, to alleviate local and systemic toxicity, and to control drug release profiles.[22-31] Thus, incorporation of cyclodextrins into hydrogel networks is a promising strategy for the development of sustained drug delivery systems.

In chapter 2 of this thesis, poly(acrylate) networks formed through complexation by a β-cyclodextrin-substituted poly(acrylate) of adamantyl-substituted poly(acrylate)s have been investigated as potential sustained drug delivery systems. We have characterized the complexation of adamantyl-substituted poly(acrylate)s by a β-cyclodextrin-substituted

poly(acrylate) and the complexation of dyes within these networks and the release therefrom in aqueous solution. As an extension research of Chapter 2, a poly(acrylate) network formed through the complexation of a octadecyl substituted-poly(acrylate) by a β-cyclodextrin-substituted poly(acrylate) has been chosen to advance the understanding of the complexation capability of β-cyclodextrin substituents in the formed poly(acrylate) network and its influence on the subsequent release of dyes. In this Chapter 3, β-cyclodextrin, β-CD, is attached to poly(acrylate) (average M_W = 250,000 g mol^{-1}) through a -(2-aminoethyl)amino-tether to give the 9.3% 6^A-(2-aminoethyl)amino-6^A-deoxy-6^A-β-CD, β-CDen, randomly substituted poly(acrylate), PAAβ-CDen, which acts as the host polymer in this study (Figure 3.1). The 3.5% octadecyl, C18, randomly substituted poly(acrylate), PAAC18, was chosen as the guest polymer (Figure 3.1).

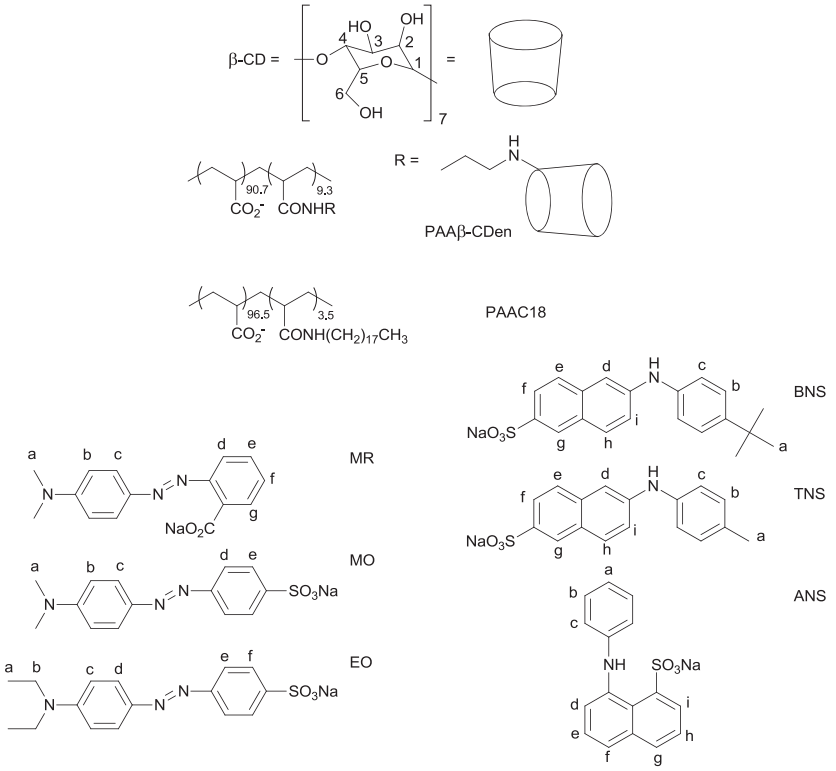

Figure 3.1. β-Cyclodextrin, and octadecyl substituted poly(acrylate)s, PAAβ-CDen and PAAC18, and the sodium salts of the dyes ethyl orange, EO, methyl orange, MO, methyl red, MR, 8-anilinonaphthalene-1-sulfonate, ANS, 6-(*p*-toluidino)naphthalene-2-sulfonate, TNS, and 6-(*p*-*t*-butylphenylamino)naphthalene-2-sulfonate, BNS

In aqueous mixtures of PAAβ-CDen and PAAC18, the concentration ratio of β-CDen substituents to C18 substituents is designed to be ~9:3 such that self-assembly of the substituted poly(acrylate) (PAA) network leaves a surplus of β-CDen substituents available to complex other guest species. The dyes, methyl red, MR, methyl orange, MO, ethyl orange, EO, 8-anilinonaphthalene-1-sulfonate, ANS, 6-(*p*-toluidino)naphthalene-2-sulfonate, TNS, and 6-(*p*-*t*-butylphenylamino)naphthalene-2-sulfonate, BNS, (Figure 3.1) are selected as the small molecule guest species complexed by the surplus β-CDen substituents of PAAβ-CDen as their environment sensitive-UV-Vis and fluorescence spectra facilitate quantification of their complexation and also because they are of similar structure and dimension to a variety of drugs.

Network formation by PAAβ-CDen and PAAC18 was characterized by isothermal titration calorimetry, 2D NOESY ^{1}H NMR spectroscopy and rheology. Complexation of MR, MO and EO by the β-CDen substituents in the PAAβ-CDen/PAAC18 network was characterized by UV-Vis and 2D NOESY ^{1}H NMR spectroscopy; Complexation of ANS, TNS and BNS by the β-CDen substituents in the PAAβ-CDen/PAAC18 network was characterized by fluorescence and 2D NOESY ^{1}H NMR spectroscopy; and release of the dyes from the PAAβ-CDen/PAAC18 network and their components was characterized by UV-Vis spectroscopy.

3.2. Experimental section

3.2.1. Materials

The sodium salts of methyl red (BDH), methyl orange (BDH), ethyl orange (Sigma-Aldrich), 8-anilinonaphthalene-1-sulfonate (Sigma-Aldrich), and 6-(*p*-toluidino)naphthalene-2-sulfonate (Sigma-Aldrich) were used as received.

6-(*p*-*t*-butylphenylamino)naphthalene-2-sulfonate sodium salt was prepared according to literature method.[32] Randomly 9.3 ± 0.2 % β-CD substituted poly(acrylate), PAAβ-CDen,[5] and randomly 3.5 ± 0.1% octadecyl substituted poly(acrylate), PAAC18,[1] were prepared according to reported methods.

3.2.2. Characterization

1D ^{1}H NMR spectra were run on a Varian Inova 600 spectrometer at an operating frequence of 599.96 MHz. 2D NOESY and ROESY ^{1}H NMR spectra were run on the same spectrometer using standard pulse sequences with a mixing time of 0.3 s. All sample solutions were prepared in D_2O Na_2HPO_4/KH_2PO_4 buffer solutions at pD = 7.0 and I = 0.10 mol dm^{-3} and were equilibrated at the thermostated probe temperature of 298.2 ± 0.1 K for 30 min in 5 mm NMR tubes prior to their spectra being recorded. Chemical shifts (δ, ppm) were internally referenced to residual HOD at δ = 4.79 ppm. The substitution percentage of the β-CDen substituents on the PAAβ-CDen backbones was determined from a comparison of the resonance area of the β-CD H1 protons with that of the poly(acrylate) protons. The substitution percentage of the C18 substituents on the PAAC18 backbones was determined through a comparison of the resonance area of the methyl protons of C18 substituents with the superimposed resonance areas of the poly(acrylate) and methylene protons of C18 substituents. The composition of sample solutions are detailed in the corresponding figure captions.

Rheological measurements were carried out with a Physica MCR 501 (Anton Parr GmbH) stress-controlled rheometer with a 25 mm cone and plate geometry. Temperature was controlled at 298.2 K by a Peltier plate. All solutions were prepared in aqueous Na_2HPO_4/KH_2PO_4 buffer solutions at pH = 7.0 and I = 0.10 mol dm^{-3}. The composition of sample solutions are detailed in the corresponding figure captions. The rheological

measurements were performed by Dr. Jie Wang in Professor Xuhong Guo's research group in East China University of Science and Technology.

3.2.3. Isothermal titration calorimetric studies

Isothermal titration calorimetric, ITC, measurements were made using a MicroCal VP isothermal titration calorimeter. In the titration, 10 mm^3 aliquots of a 1.19 wt% PAAβ-CDen solution ([β-CDen substituents] = 5.60×10^{-3} mol dm^{-3}) were titrated into 1.46 cm^3 of a 0.13 wt% PAAC18 ([C18 substituents] = 4.48×10^{-4} mol dm^{-3}) solution at 298.2 K using a computer-controlled micro-syringe at intervals of 210 s. Both solutions were prepared in aqueous Na_2HPO_4/KH_2PO_4 buffer solutions at pH = 7.0 and I = 0.10 mol dm^{-3}.

In aqueous solution, the β-CDen substituents of PAAβ-CDen complex the C18 substituents of PAAC18 to form self-assembled poly(acrylate) network according to Equation 3.1.

$$\text{PAAβ-CDen} + \text{PAAC18} \underset{}{\overset{K_{ITC}}{\rightleftharpoons}} \text{PAAβ-CDen.PAAC18} \qquad (\mathbf{3.1})$$

The complexation constant, K_{ITC}, for the host-guest complexation for this equilibrium is given by Equation 3.2,

$$K_{ITC} = [\text{PAAβ-CDen.PAAC18}]/([\text{PAAβ-CDen}][\text{PAAC18}]) \qquad (\mathbf{3.2})$$

where [PAAβ-CDen], [PAAC18] and [PAAβ-CDen.PAAC18] represent the concentration of the β-CDen substituents of PAAβ-CDen, the C18 substituents of PAAC18 and their complex at equilibrium, respectively, and,

$$N = [\text{β-CDen substituents complexed}]/[\text{C18 substituents complexed}] \qquad (\mathbf{3.3})$$

in the poly(acrylate) network. In case of simple 1:1 complexation, it is expected that N = 1. However, if two β-CDen substituents complex one C18 substituent, a single titration curve characterized by $N > 1$ will be observed. The N = 1.44 for the PAAβ-CDen/PAAC18 system infers that of the complexes formed approximately 55% have 1:1 β-CDen.C18 substituent

stoichiometry and approximately 45% have a 2:1 $(\beta\text{-CDen})_2$.C18 substituent stoichiometry as is discussed in more detail in Section 3.4.

The heats of dilution were determined by titrating aqueous Na_2HPO_4/KH_2PO_4 buffer (pH = 7.0 and I = 0.10 mol dm^{-3}) into similarly buffered PAAC18 solution, and by titrating similarly buffered PAAβ-CDen solution into the same buffer. These heats of dilution were subtracted from the total evolved to give the heats of host-guest complexation from which the thermodynamic parameters of the host-guest complexation were calculated. The Origin 7.0 MicroCal protocol was used to derive K_{ITC}, ΔH, $T\Delta S$, and N, based on a one-site complexation model.[33]

3.2.4. UV-Vis and Fluorescence spectroscopic titration studies

Complexation of either MR, MO, or EO by β-CDen substituents in the PAAβ-CDen/PAAC18 network was quantitatively characterized through UV-Vis spectroscopic titrations. The UV-Vis spectra were recorded on a Cary-Varian 5000 UV-Vis spectrophotometer using 1 cm path length matched quartz cells. All the UV-Vis titration studies were performed in aqueous Na_2HPO_4/KH_2PO_4 buffer solutions at pH = 7.0 and I = 0.10 mol dm^{-3} at 298.2 K. For the PAAβ-CDen/PAAC18/dye titration studies, 25 mm^3 aliquots of a PAAβ-CDen solution followed by 25 mm^3 aliquots of a PAAC18 solution were sequentially titrated into 1.5 cm^3 of each dye solution and 1.5 cm^3 of each reference solution. The UV-Vis absorbance spectra were recorded prior to and after each of 20 sequential additions of PAAβ-CDen and PAAC18 solutions. The concentrations of all the solutions used in the UV-Vis titration studies are detailed in the corresponding titration figure captions.

Complexation of either ANS, TNS, or BNS by β-CDen substituents in the PAAβ-CDen/PAAC18 network was quantitatively characterized through fluorescence

spectroscopic titrations. The fluorescence spectra were recorded on a Cary-Varian Eclipse fluorescence spectrophotometer using a 1 cm path length quartz cell. All the fluorescence titration studies were performed in aqueous Na_2HPO_4/KH_2PO_4 buffer solutions at pH = 7.0 and I = 0.10 mol dm^{-3} at 298.2 K. For the β-CD/ANS titration studies, 50 mm^3 aliquots of a β-CD solution were sequentially titrated into 2.0 cm^3 of an ANS solution. The fluorescence spectra were recorded prior to and after each of 20 sequential additions of β-CD solution. For the PAAβ-CDen/ANS titration studies, 50 mm^3 aliquots of a PAAβ-CDen solution were sequentially titrated into 2.0 cm^3 of an ANS solution. The fluorescence spectra were recorded prior to and after each of 20 sequential additions of PAAβ-CDen solution. For the PAAβ-CDen/PAAC18/dye titration studies, 25 mm^3 aliquots of a PAAβ-CDen solution followed by 25 mm^3 aliquots of a PAAC18 solution were sequentially titrated into 2.0 cm^3 of each dye solution. The fluorescence spectra were recorded prior to and after each of 20 sequential additions of PAAβ-CDen and PAAC18 solutions. The concentrations of all the solutions used in the fluorescence titration studies are detailed in the corresponding titration figure captions.

In the ternary mixtures of PAAβ-CDen and PAAC18 and a dye in aqueous solution, the β-CDen substituents of PAAβ-CDen complex both C18 substituents and dye molecules. Thus, the equilibria for the self-assembled PAAβ-CDen/PAAC18 network and for dye complexation by β-CDen substituents within the network shown in Equations 3.1 and 3.4, respectively, together control the extent of dye complexation.

$$\text{PAAβ-CDen} + \text{PAAC18} \overset{K_{ITC}}{\rightleftharpoons} \text{PAAβ-CDen.PAAC18} \qquad (\mathbf{3.1})$$

$$\text{PAAβ-CDen} + \text{dye} \overset{K}{\rightleftharpoons} \text{PAAβ-CDen.dye} \qquad (\mathbf{3.4})$$

The complexation constant, K_{ITC}, for the host-guest complexation between the β-CDen substituents and C18 substituents has been determined in ITC titration studies.

$$K_{ITC} = [PAA\beta\text{-}CDen.PAAC18]/([PAA\beta\text{-}CDen][PAAC18]) \quad (\mathbf{3.2})$$

The complexation constant, *K*, for the host-guest complexation between the β-CDen substituents in the PAAβ-CDen/PAAC18 network and dye molecules at equilibrium is defined by Equation 3.5,

$$K = [PAA\beta\text{-}CDen.dye]/([PAA\beta\text{-}CDen][dye]) \quad (\mathbf{3.5})$$

where [PAAβ-CDen], [dye] and [PAAβ-CDen.dye] represent the concentration of the β-CDen substituents in the self-assembled PAAβ-CDen/PAAC18 network, the dye, and their complex at equilibrium, respectively. Given that $[PAA\beta\text{-}CDen]_{total}$, $[dye]_{total}$ and $[PAAC18]_{total}$ are the initial concentrations, mass balances are given by Equations 3.6 - 3.8.

$$[PAA\beta\text{-}CDen]_{total} = [PAA\beta\text{-}CDen] + [PAA\beta\text{-}CDen.PAAC18] + [PAA\beta\text{-}CDen.dye] \quad (\mathbf{3.6})$$

$$[dye]_{total} = [dye] + [PAA\beta\text{-}CDen.dye] \quad (\mathbf{3.7})$$

$$[PAAC18]_{total} = [PAAC18] + [PAA\beta\text{-}CDen.PAAC18] \quad (\mathbf{3.8})$$

The absorbance or fluorescence at a particular wavelength is given by

$$A = \varepsilon_{dye}[dye] + \varepsilon_{PAA\beta\text{-}CD.dye}[PAA\beta\text{-}CDen.dye] \quad (\mathbf{3.9})$$

$$F = f_{dye}[dye] + f_{PAA\beta\text{-}CD.dye}[PAA\beta\text{-}CDen.dye] \quad (\mathbf{3.10})$$

where *A*, ε_{dye} and $\varepsilon_{PAA\beta\text{-}CDen.dye}$ represent the observed absorbance and molar absorbance of the dye and the host-guest complex, respectively, and *F*, f_{dye} and $f_{PAA\beta\text{-}CDen.dye}$ represent the observed fluorescence intensity and molar fluorescence intensity of the dye and the host-guest complex, respectively.

In the event that the concentrations of the β-CDen and C18 substituents and the dye were of similar concentrations in the UV-Vis absorbance or fluorescence titration studies of dye complexation, *N* = 1.44 for the PAAβ-CDen/PAAC18 would have to be taken into account in deriving *K* from the UV-Vis absorbance or fluorescence titration data. However, typically

$[\beta\text{-CDen substituents}]_{total}$ and $[\text{C18 substituents}]_{total}$ are approximately 8 times, or above, as the initial [dye] after the first substituent titres are added and increase with the addition of subsequent titres such that both $[\beta\text{-CDen substituents}]_{total}$ and $[\text{C18 substituents}]_{total}$ are in substantial excess of the [dye]. Thus, *N* does not have to be included in the derivation of *K* for dye complexation.

The value of ε_{dye} or f_{dye} measured from the corresponding dye solution and K_{ITC} measured from the ITC titration study were used as input to the calculation. The complexation constants, *K*, were derived through solving Equations 3.2 and 3.5-3.9 for UV-Vis spectroscopic titrations or Equations 3.2, 3.5 - 3.8 and 3.10 for fluorescence spectroscopic titrations which were also best-fitted to the data using a nonlinear least-squares program, *HypSpec*.[34,35]

3.2.5. Dye release studies

Dye release studies were performed using a membrane diffusion system (Figure 2.20 in Section 2.10 Appendix of Chapter 2) in which a 3500 g mol^{-1} molecular weight cut-off dialysis membrane (Spectr/Por 3) of surface area 7.0 cm^2 separated 5.0 cm^3 of the dye containing solution (made up in Na_2HPO_4/KH_2PO_4 buffer at pH = 7.0 and I = 0.10 mol dm^{-3} with initial concentrations of MR, MO and EO = 2.00×10^{-3} mol dm^{-3} and those of ANS, TNS and BNS = 7.80×10^{-4} mol dm^{-3}) from 200 cm^3 of aqueous Na_2HPO_4/KH_2PO_4 buffer at pH = 7.0 and I = 0.10 mol dm^{-3} which acted as the receiving solution. During the release experiment, the receiving solution was stirred at 298.2 K. At appropriate time intervals, a 2.0 cm^3 (For MR, MO and EO) or 10 cm^3 (For ANS, TNS and BNS) sample of the receptor solution was withdrawn, its UV-Vis spectrum was measured and the sample was then returned to the receiving solution. The dye concentration in the receiving solution was calculated by reference to its molar absorbance spectrum determined under the same conditions. Each dye solution composition is given in the corresponding figure caption. All solutions were stirred and

equilibrated for 16 h at 298.2 K before use.

3.3. Synthesis of β-cyclodextrin and octadecyl substituted poly(acrylate)s

The substituted poly(acrylate)s (Figure 3.1): PAAβ-CDen[5] and PAAC18[1] were synthesized according to the reported procedures, and the degree of random substitution of the β-CDen substituents and C18 substituents per mole of acrylate unit were determined from their ^{1}H NMR spectra to be 9.3 ± 0.2% and 3.5 ± 0.1%, respectively. The substituted poly(acrylate) network formation by PAAβ-CDen and PAAC18 arising from host-guest complexation between their β-CDen and C18 substituents is central to this study and has been characterized by isothermal titration calorimetry, ITC, 2D NOESY ^{1}H NMR spectroscopy and rheology. Complexation of the dyes MR, MO and EO by the β-CDen substituents in the PAAβ-CDen/PAAC18 network was characterized by UV-Vis and 2D NOESY ^{1}H NMR spectroscopy. Complexation of the dyes ANS, TNS and BNS by the β-CDen substituents in the PAAβ-CDen/PAAC18 network was characterized by fluorescence and 2D NOESY ^{1}H NMR spectroscopy. The general picture which emerges for dye complexation in the PAAβ-CDen/PAAC18 network is broadly shown in Figure 3.2. Subsequently, the release of the dyes from the PAAβ-CDen/PAAC18 network and their components through a dialysis membrane was characterized by UV-Vis spectroscopy.

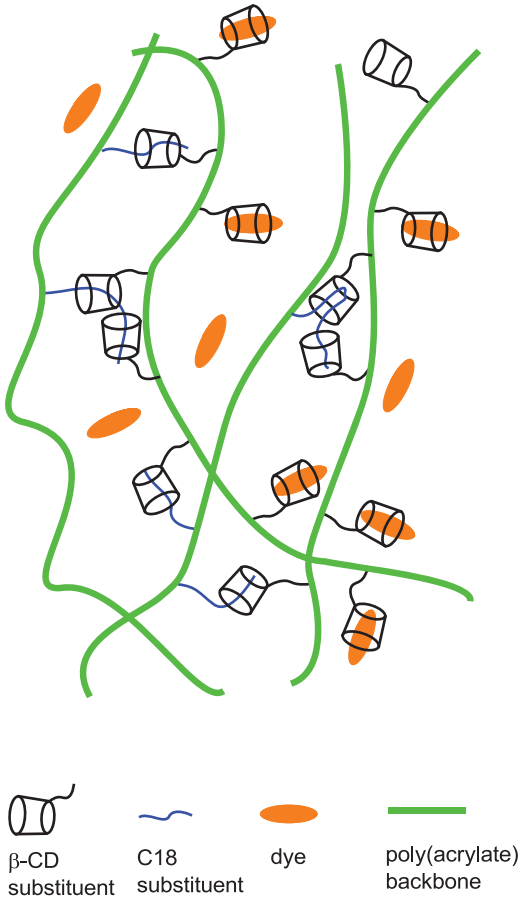

Figure 3.2. Representation of complexation of dye species in the PAAβ-CDen/PAAC18 network.

3.4. ITC and 2D NOESY ^{1}H NMR characterization of poly(acrylate) network formation

Isothermal titration calorimetry, ITC, was used to determine the complexation constant, K_{ITC}, and ΔH and $T\Delta S$ characterizing the host-guest complexes formed by the β-CDen and C18 substituents of the substituted poly(acrylate)s. The ITC data also yields the ratio of the number of β-CDen to C18 substituents in the complex formed, *N*, which is equal to the ratio corresponding to the inflexion point in the ITC titration curve for the titration of a PAAβ-CDen solution into a solution of PAAC18. The experimental data for the titration of a PAAβ-CDen

solution into a PAAC18 solution together with the best-fit of an algorithm for a single complexation (Equation 3.1) to these data are shown in Figure 3.3. The derived K_{ITC}, ΔH, $T\Delta S$ and N appear in Table 3.1.

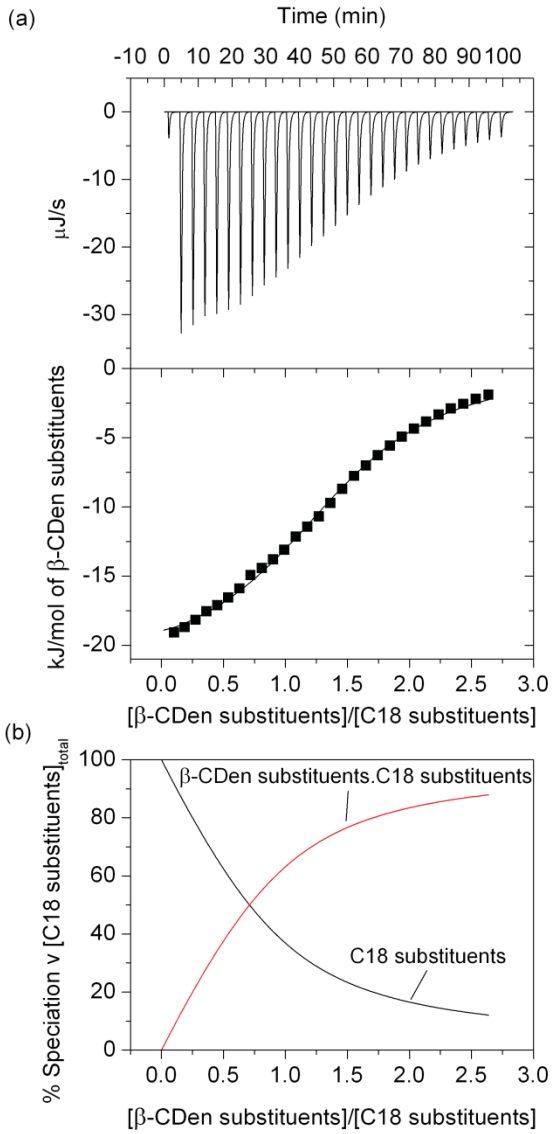

Figure 3.3. (a) (Top) ITC data for the titration of 10 mm^3 aliquots of a 1.19 wt% PAAβ-CDen solution ([β-CDen substituents] = 5.60×10^{-3} mol dm^{-3}) into 1.46 cm^3 of a 0.13 wt% PAAC18 ([C18 substituents] = 4.48×10^{-4} mol dm^{-3}) solution at 298.2 K. Both solutions were prepared in aqueous Na_2HPO_4/KH_2PO_4 buffer solutions at pH = 7.0 and at I = 0.10 mol dm^{-3}. (Bottom) The solid curve shows the best-fit of an algorithm for host-guest complexation between the β-CDen and C18 substituents to the experimental data points. (b) Speciation plot with [C18 substituents]$_{total}$ = 100%.

Table 3.1. Parameters determined for host-guest complexation between PAAβ-CDen and PAAC18 in aqueous Na_2HPO_4/KH_2PO_4 buffer at pH 7.0 and I = 0.10 mol dm^{-3}.[a]

Host	PAAβ-CDen
Guest	PAAC18
$10^{-4}K_{ITC}$ / dm^3 mol^{-1}	1.13 ± 0.05
ΔH / kJ mol^{-1}	-21.55 ± 0.24
$T\Delta S$ / kJ mol^{-1}	1.59 ± 0.36
N	1.44 ± 0.14

[a]The errors shown are the data fitting errors, and the experimental error is ≤ 5%.

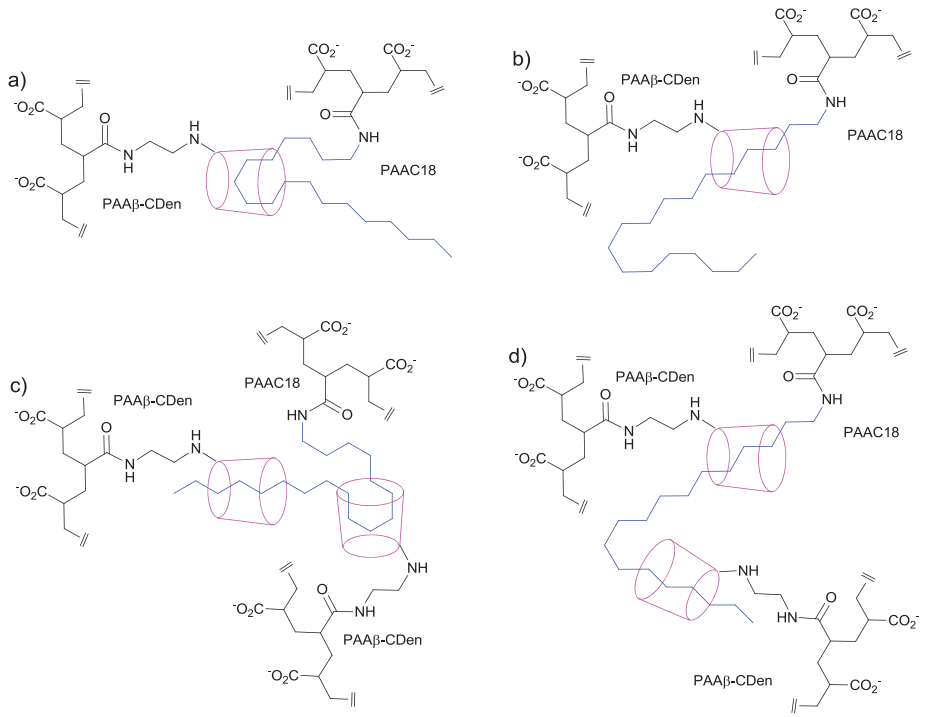

Figure 3.4. Modes of complexation between the β-CDen substituents of PAAβ-CDen and the C18 substituents of PAAC18. a) and b) Complexation of the C18 group in the β-CD annulus. c) As for a) and b) with complexation of the C18 group in a second β-CD annulus.

The observed N = 1.44 is larger than N = 1 anticipated for each β-CDen substituent complexing a single C18 substituent and is consistent with a single β-CDen substituent of PAAβ-CDen complexing a single C18 substituent of PAAC18 (Figure 3.4 a) and b)) and two β-CDen substituents complexing a single C18 substituent (Figure 3.4 c) and d)) in proportions

which average to N = 1.44 as a result of the great flexibility arising from the long C18 substituent. The individual contributions of these two complexations are not separately identifiable in the ITC titration curve, possibly consistent with the sequential complexations being characterized by similar ΔH and $T\Delta S$ such that the titration curve could not be resolved into two separate titration curves. (Both complexations involve β-CDen and octadecyl substituents.) The 2D NOESY ^{1}H NMR spectrum of a D_2O solution of PAAβ-CDen and PAAC18 in which the β-CDen and C18 substituents are equimolar (Figure 3.5) shows cross-peaks assigned to the anticipated dominant dipolar interactions between the annular H3,5,6 protons of the β-CD groups and the methylene protons of the C18 substituents, which is consistent with the a) - d) complexation modes of Figure 3.4. While the ^{1}H NMR data indicate the complexation of the C18 substituents and thereby the plausibility of simultaneous complexation by two β-CDen substituents (Figure 3.4 c) and d)), it is not possible to differentiate complexation modes between a) and b) or between c) and d).

The large K_{ITC} for the complexation of C18 substituents by β-CDen substituents is dominantly due to substantial ΔH contributions and small favorable $T\Delta S$ contributions. The positive $T\Delta S$ is attributable to the following factors. Firstly, substantial aggregation of the long C18 hydrophobic substituents both within a single poly(acrylate) strand and between strands exist in aqueous PAAC18 solution due to hydrophobic interactions, as observed in previous studies.[1,2,4,36] Upon addition of a PAAβ-CDen solution, the aggregation of C18 substituents is disrupted by the complexation of C18 substituents by β-CDen substituents of PAAβ-CDen. It is likely that the entropy decrease arising from the substantial aggregation of C18 substituents is larger than that for the complexation of C18 substituents by β-CDen substituents. (As discussed in Chapter 2, a positive $T\Delta S$ characterizes the PAAβ-CDen/PAAADddn system.) This probably contributes to the overall positive $T\Delta S$ for the PAAβ-CDen/PAAC18 network

formation. Secondly, the entropy increase is anticipated from the displacement of water from the β-CD annulus by the C18 substituent.[11,37,38]

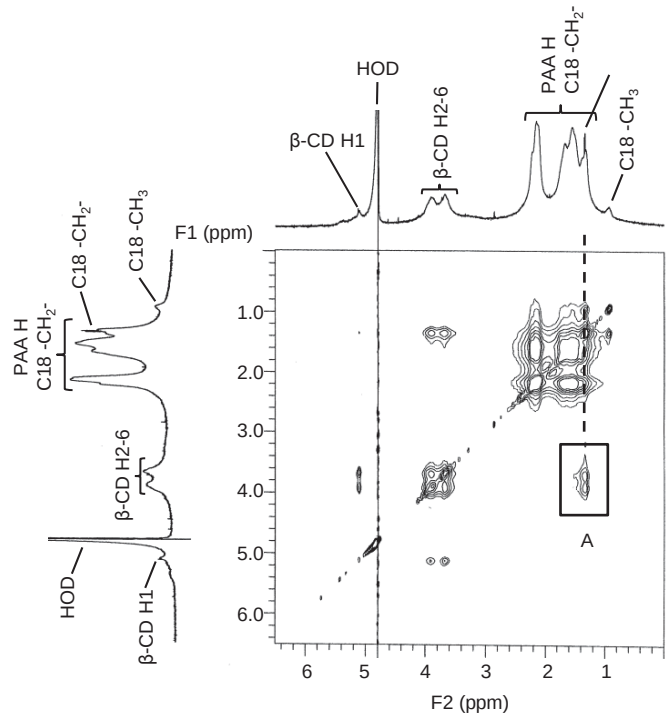

Figure 3.5. 2D NOESY ^{1}H NMR spectrum of 0.43 wt% PAAβ-CDen ([β-CDen substituents] = 2.0 × 10^{-3} mol dm^{-3}) and 0.58 wt% PAAC18 ([C18 substituents] = 2.0 × 10^{-3} mol dm^{-3}) in D_2O Na_2HPO_4/KH_2PO_4 buffer solution at pD = 7.0 and I = 0.10 mol dm^{-3} at 298.2 K. Cross-peaks in box A arise from dipolar interactions between the annular H3,5,6 protons of the β-CD groups and the methylene protons of the C18 substituents.

In the ITC studies, the concentrations of PAAβ-CDen and PAAC18 are low and therefore the solution retain high fluidity consistent with localized cross-linked PAAβ-CDen/PAAC18 network aggregates forming. However, at higher concentrations, the solution of PAAβ-CDen and PAAC18 becomes viscous, consistent with extensive PAAβ-CDen/PAAC18 network forming, and are characterized by rheology as discussed in Section 3.7.

3.5. UV-Vis and 2D NOESY ^{1}H NMR characterization of MR, MO and EO complexation

The UV-Vis absorbance changes of a EO solution upon sequential additions of PAAβ-CDen and PAAC18 solutions (Figure 3.6) are consistent with the dominant formation of 1:1 β-CD substituents.EO complexes (Equations 3.4 and 3.5), characterized by a complexation constant, K = 1675 dm^3 mol^{-1} with λ_{max} = 464 nm for β-CD substituents.EO complexes in the PAAβ-CDen/PAAC18 network. The accompanying changes in free β-CDen substituents, β-CDen substituents.C18 substituents complex and β-CDen substituents.EO complex are shown in Figure 3.7. The analogous data for MO in the PAAβ-CDen/PAAC18 network appear in Figures 3.18 and 3.19 in Section 3.11 Appendix. The decrease in λ_{max} of the complexed EO and MO by comparison with that of free EO and MO (Table 3.2) indicates a change from an aqueous environment to the hydrophobic environment of the annulus of the β-CD group, which is consistent with the complexation of either EO or MO by the β-CDen substituents in the PAAβ-CDen/PAAC18 network. By comparison with K for complexation by β-CD and PAAβ-CDen (Table 3.2), K for complexation by the β-CDen substituents in the PAAβ-CDen/PAAC18 network is further decreased probably because of increased steric crowding within the network. The UV-Vis absorbance variations observed for MR in the PAAβ-CDen/PAAC18 network (Figure 3.20 in Section 3.11 Appendix) are too small for a reliable derivation of K which may indicate that the decrease in K observed for complexation of MO and EO by β-CDen substituents in the PAAβ-CDen/PAAC18 network by comparison with K for complexation by β-CD and PAAβ-CDen also occurs for MR. The smallest and largest K characterize the β-CDen substituents.MR (too small to be determined) and β-CDen substituents.EO host-guest complexes, respectively, and reflect the more favorable

stereochemistry of EO for complexation and its greater hydrophobicity.

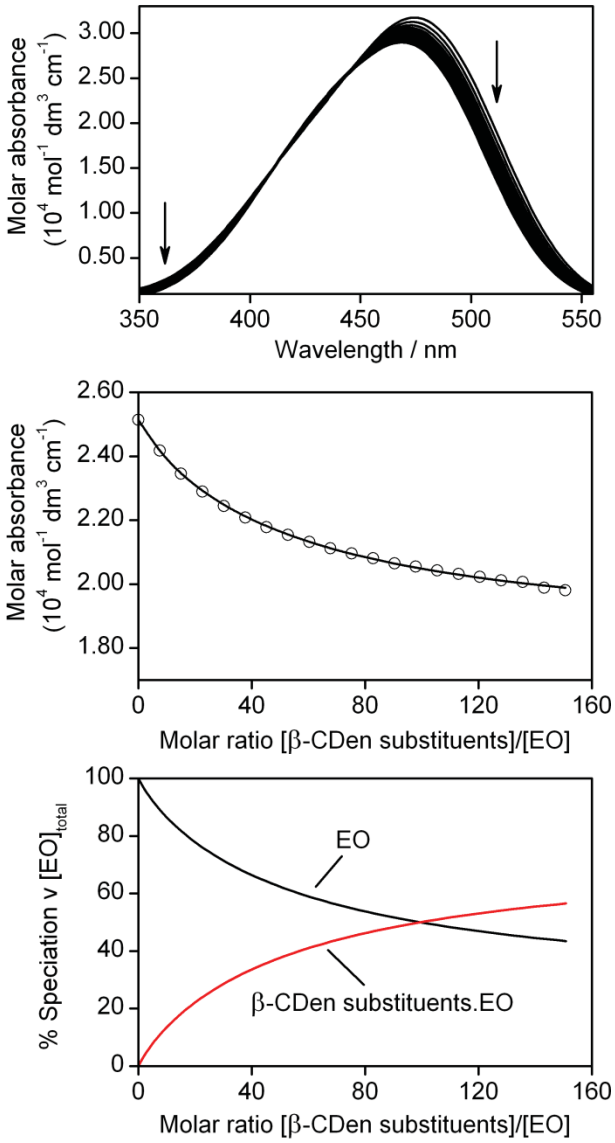

Figure 3.6. (Top) Molar absorbance variation of a EO solution ([EO] = 2.00 × 10^{-5} mol dm^{-3}) upon 20 sequential additions of a PAAβ-CDen solution (25 mm^3 each, 1.90 wt%, [β-CDen substituents] = 9.04 × 10^{-3} mol dm^{-3}) and a PAAC18 solution (25 mm^3 each, 0.87 wt%, [C18 substituents] = 3.02 × 10^{-3} mol dm^{-3}) at 298.2 K. All solutions were prepared in aqueous Na_2HPO_4/KH_2PO_4 buffer solutions at pH 7.0 and I = 0.10 mol dm^{-3}. The arrows indicate the direction of molar absorbance variation upon each addition of the PAAβ-CDen and PAAC18 solutions. (Middle) Molar absorbance variation at 500 nm and the line representing the best-fit of an algorithm for a 1:1 host-guest complexation of EO by β-CDen substituents in PAAβ-CDen/PAAC18 network over the wavelength range 475 - 525 nm. (Bottom) Speciation plot with $[EO]_{total}$ = 100%.

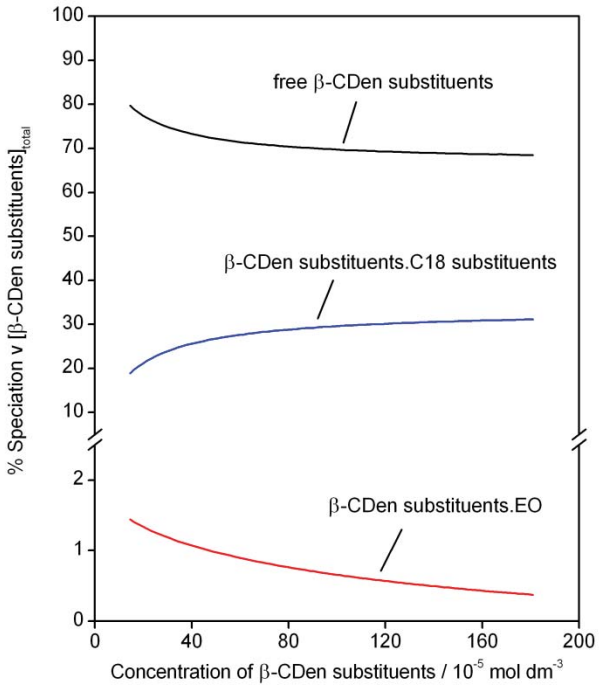

Figure 3.7. Speciation plot with $[\beta\text{-CDen substituents}]_{total}$ = 100% for the PAAβ-CDen/PAAC18/EO system.

Table 3.2. UV-vis spectroscopic titration data[a]

Host	Guest	λ_{max} nm	K[b] $dm^3\ mol^{-1}$
None[c]	MR	430	–
	MO	464	–
	EO	474	–
β-CD[c]	MR	414	772 ± 10
	MO	455	3255 ± 35
	EO	466	10515 ± 110
β-CD substituents of PAAβ-CDen[c]	MR	415	76 ± 1
	MO	458	1454 ± 20
	EO	463	2230 ± 30
β-CD substituents in PAAβ-CDen/PAAC18 network[d]	MR	[e]	[e]
	MO	449	356 ± 5
	EO	464	1049 ± 20

[a]Obtained in aqueous Na_2HPO_4/KH_2PO_4buffer at pH = 7.0 and I = 0.10 mol dm^3 at 298.2 K. [b]The errors shown are fitting errors and the overall error is ± 5%. [c]Data from Chapter 2. [d]This study. [e]Data not determined.

Interestingly, cross-peaks arising from dipolar interactions between the β-CD group protons and the MR protons and the C18 substituent protons are observed for solutions of MR and PAAβ-CDen/PAAC18 (Figure 3.8). This is consistent with MR being complexed in this system to a greater extent in the more concentrated solutions (1.42 wt%) prepared for ^{1}H NMR studies than in the lower concentration solutions prepared for UV-Vis studies (0.75 wt%). Analogous cross-peaks are observed for MO (Figure 3.21 in Section 3.11 Appendix) and EO (Figure 3.22 in Section 3.11 Appendix).

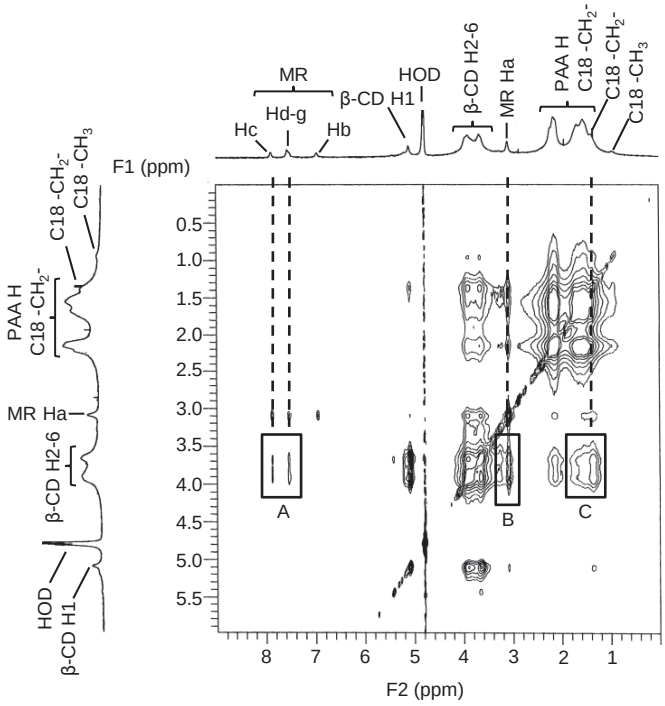

Figure 3.8. 2D NOESY ^{1}H NMR spectrum of MR ([MR] = 2.0×10^{-3} mol dm^{-3}) in mixture with PAAβ-CDen (0.85 wt%, [β-CDen substituents] = 4.0×10^{-3} mol dm^{-3}) and PAAC18 (0.57 wt%, [C18 substituents] = 2.0×10^{-3} mol dm^{-3}) in D_2O Na_2HPO_4/KH_2PO_4 buffer solution at pD = 7.0 and I = 0.10 mol dm^{-3} at 298.2 K. Cross-peaks in boxes A and B arise from dipolar interactions between the annular H3,5,6 protons of the β-CD groups and the aromatic (Hc-g) and methyl (Ha) protons of MR, respectively. Cross-peaks in box C arise from dipolar interactions between the annular H3,5,6 protons of the β-CD groups and the methylene protons of the C18 substituents.

3.6. Fluorescence and 2D NOESY ^{1}H NMR characterization of ANS, TNS and BNS complexation

For comparative purposes, the complexation of ANS, TNS and BNS by β-CD alone and PAAβ-CDen are first characterized. (The complexation of TNS and BNS by β-CD was characterized in previous studies.[39,40] The complexation of TNS by PAAβ-CDen was characterized by Mohammed Tajuddin Ghori and the complexation of BNS by PAAβ-CDen

was characterized by Mitchell B. Bacon. The derived K and λ_{max} are shown in Table 3.3.) The fluorescence variations of an ANS solution upon sequential additions of a β-CD solution (Figure 3.9) are consistent with the dominant formation of 1:1 β-CD.ANS complexes, characterized by a complexation constant, $K = 90\ dm^3\ mol^{-1}$ with $\lambda_{max} = 495$ nm for β-CD.ANS complexes. The decrease in λ_{max} of the complexed ANS by comparison with that of free ANS (Table 3.3) indicates a change from an aqueous environment to the hydrophobic environment of the β-CD annulus, which is consistent with the complexation of ANS by β-CD. A 2D ROESY ^{1}H NMR spectrum (Figure 3.10) for a solution of equimolar β-CD and ANS shows cross-peaks arising from dipolar interactions between the β-CD annular H3,5,6 protons and the ANS protons, which is consistent with the encapsulation of ANS into the β-CD annulus.

Table 3.3. Fluorescence spectroscopic titration data[a]

Host	Guest	λ_{max} nm	K[b] $dm^3\ mol^{-1}$
None	ANS[c]	524	–
	TNS[d]	487	–
	BNS[e]	481	–
β-CD	ANS[c]	495	90 ± 3
	TNS[d]	471	3300 ± 50
	BNS[e]	464	46700 ± 500
β-CD substituents of PAAβ-CDen	ANS[c]	[h]	[h]
	TNS[f]	433	231 ± 10
	BNS[g]	435	20184 ± 300
β-CD substituents in PAAβ-CDen/PAAC18 networks	ANS[c]	[h]	[h]
	TNS[c]	424	41 ± 1
	BNS[c]	437	6003 ± 500

[a]Obtained in aqueous Na_2HPO_4/KH_2PO_4 buffer at pH = 7.0 and I = 0.10 mol dm^3 at 298.2 K. [b]The errors shown are fitting errors and the overall error is ± 5%. [c]This study. [d]Data from Reference 38. [e]Data from Reference 39. [f]Data collected by Mohammed Tajuddin Ghori. [g]Data collected by Mitchell B. Bacon. [h]Data not determined.

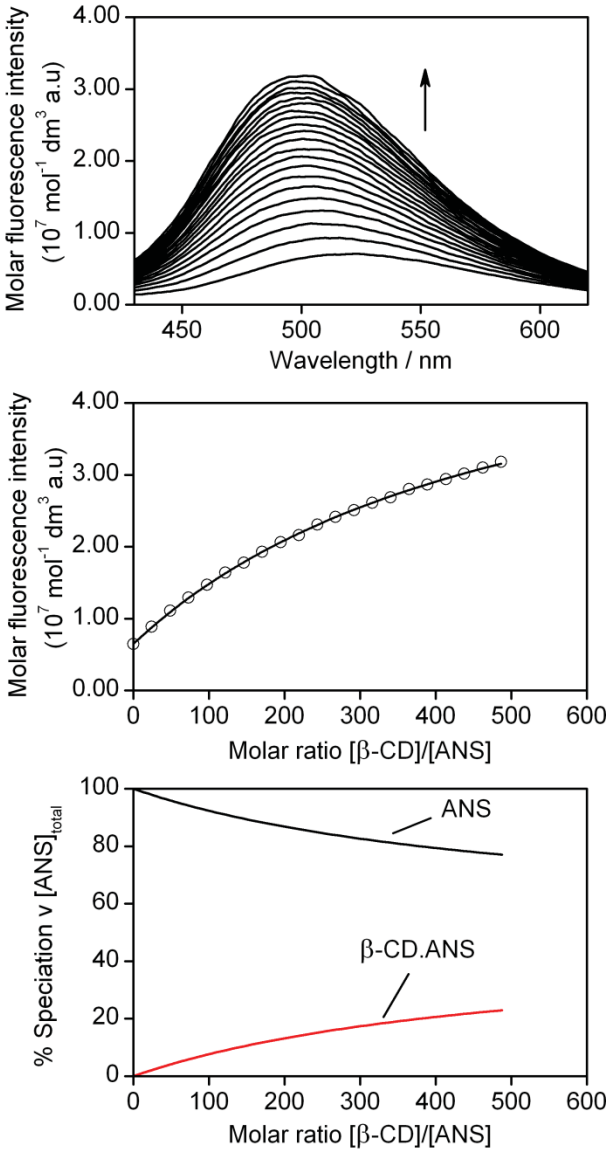

Figure 3.9. (Top) Molar fluorescence variation of a ANS solution ([ANS] = 1.03×10^{-5} mol dm^{-3}) with 20 sequential additions of a β-CD solution (50 mm^3 each, [β-CD] = 1.00×10^{-2} mol dm^{-3}) at 298.2 K. Both solutions were prepared in aqueous Na_2HPO_4/KH_2PO_4 buffer solutions at pH 7.0 and I = 0.10 mol dm^{-3}. The arrow indicates the direction of molar fluorescence change upon each addition of the β-CD solution. Excitation wavelength is 350 nm. (Middle) Molar fluorescence variation at 500 nm and the line representing the best-fit of an algorithm for a 1:1 host-guest complexation of ANS by β-CD over the wavelength range 450 - 550 nm. (Bottom) Speciation plot with $[ANS]_{total}$ = 100%.

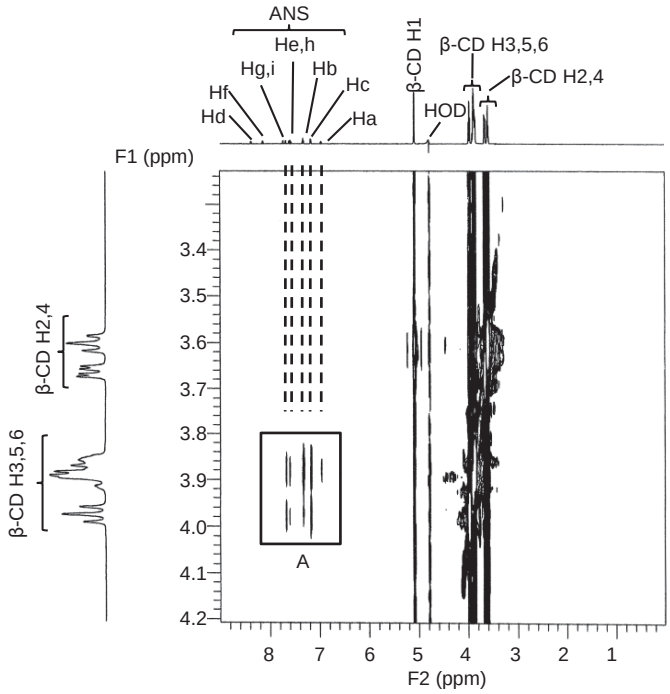

Figure 3.10. 2D ROESY ^{1}H NMR spectrum of ANS ([ANS] = 2.0×10^{-3} mol dm^{-3}) and β-CD ([β-CD] = 2.0×10^{-3} mol dm^{-3}) in D_2O Na_2HPO_4/KH_2PO_4 buffer solution at pD = 7.0 and I = 0.10 mol dm^{-3} at 298.2 K. Cross-peaks in boxes A arise from dipolar interactions between the β-CD annular H3,5,6 protons and the aromatic (Ha-c, He, and Hg-i) protons of ANS.

The fluorescence variations observed for either BNS or TNS with added PAAβ-CDen (Figures 3.23 and 3.24 in Section 3.11 Appendix) are consistent with the dominant formation of 1:1 β-CDen substituents.dye complexes, characterized by complexation constants, K = 20184 dm^3 mol^{-1} and 231 dm^3 mol^{-1}, respectively. However, the fluorescence variations observed for ANS with added PAAβ-CDen (Figure 3.25 in Section 3.11 Appendix) are too small for a reliable derivation of K. This is consistent with a weaker complexation by PAAβ-CDen than the complexation by β-CD, which is attributable to a combination of steric hindrance between the poly(acrylate) backbone and also repulsion between the PAAβ-CDen carboxylate groups and the negatively charged ANS. Similar weaker complexation by PAAβ-CDen, reflected by a decreased K as shown in Table 3.3, is also observed for BNS and

TNS.

The 2D NOESY ^{1}H NMR spectrum (Figure 3.26 in Section 3.11 Appendix) of a solution of PAAβ-CDen and BNS shows cross-peaks arising from dipolar interactions between the protons of β-CD groups and the BNS protons, which is consistent with the complexation of BNS by PAAβ-CDen. Analogous cross-peaks are observed for TNS (Figure 3.27 in Section 3.11 Appendix). However, no analogous cross-peaks occur in the 2D NOESY ^{1}H NMR spectrum (Figure 3.28 in Section 3.11 Appendix) of a solution of PAAβ-CDen and ANS in which the β-CDen substituents and ANS are equimolar. This is consistent with very weak complexation, or no complexation at all, of ANS by PAAβ-CDen.

The fluorescence changes of a BNS solution upon sequential additions of PAAβ-CDen and PAAC18 solutions (Figure 3.11) are consistent with the dominant formation of 1:1 β-CDen substituents.BNS complexes (Equations 3.4 and 3.5), characterized by a complexation constant, K = 17242 dm^3 mol^{-1} with λ_{max} = 437 nm for β-CDen substituents.BNS complexes in the PAAβ-CDen/PAAC18 network. The accompanying changes in free β-CDen substituents, β-CDen substituents.C18 substituents complex and β-CDen substituents.BNS complex are shown in Figure 3.12. The analogous data for TNS in the PAAβ-CDen/PAAC18 network appear in Figures 3.29 and 3.30 in Section 3.11 Appendix. The decrease in λ_{max} of the complexed BNS and TNS by comparison with that of free BNS and TNS (Table 3.3) indicates a change from an aqueous environment to the hydrophobic annulus of the β-CD group, which is consistent with the complexation of either BNS or TNS by β-CDen substituents in the PAAβ-CDen/PAAC18 network. By comparison with K determined for complexation by β-CD and PAAβ-CDen (Table 3.3), K for complexation by β-CDen substituents in the PAAβ-CDen/PAAC18 network is further decreased probably because of increased steric crowding within the network. The fluorescence variations observed for ANS in the

PAAβ-CDen/PAAC18 network (Figure 3.31 in Section 3.11 Appendix) are too small for a reliable derivation of *K*. The smallest and largest *K* characterize the β-CDen substituents.ANS (too small to be determined) and β-CDen substituents.BNS host-guest complexes, respectively, and reflect the more favorable stereochemistry of BNS for complexation and its greater hydrophobicity.

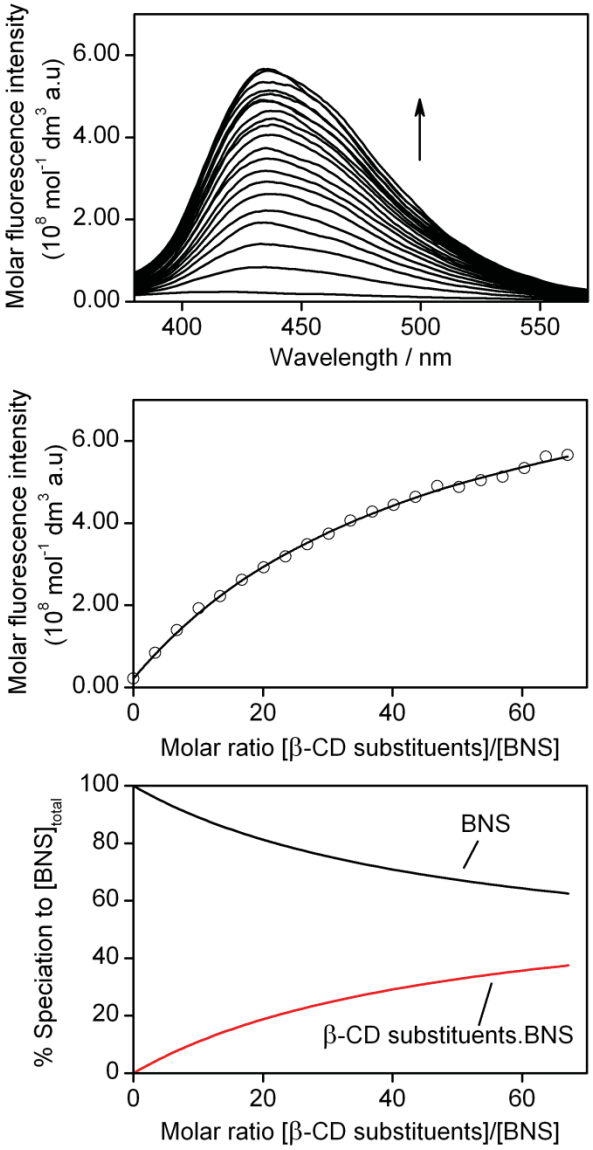

Figure 3.10. (Top) Molar fluorescence variation of a BNS solution ([BNS] = 7.67 × 10^{-7} mol dm^{-3}) upon 20 sequential additions of a PAAβ-CDen solution (25 mm^3 each, 0.10 wt%, [β-CD substituents] = 4.64 × 10^{-4} mol dm^{-3}) and a PAAADen solution (25 mm^3 each, 0.052 wt%, [C18 substituents] = 1.79 × 10^{-4} mol dm^{-3}) at 298.2 K. All solutions were prepared in aqueous Na_2HPO_4/KH_2PO_4 buffer solutions at pH 7.0 and I = 0.10 mol dm^{-3}. The arrow indicates the direction of molar fluorescence variation upon each addition of the PAAβ-CDen and PAAC18 solutions. Excitation wavelength is 320 nm. (Middle) Molar fluorescence variation at 435 nm and the line representing the best-fit of an algorithm for a 1:1 host-guest complexation of BNS by β-CD substituents in PAAβ-CDen/PAAC18 network over the wavelength range 410 - 480 nm. (Bottom) Speciation plot with $[BNS]_{total}$ = 100%.

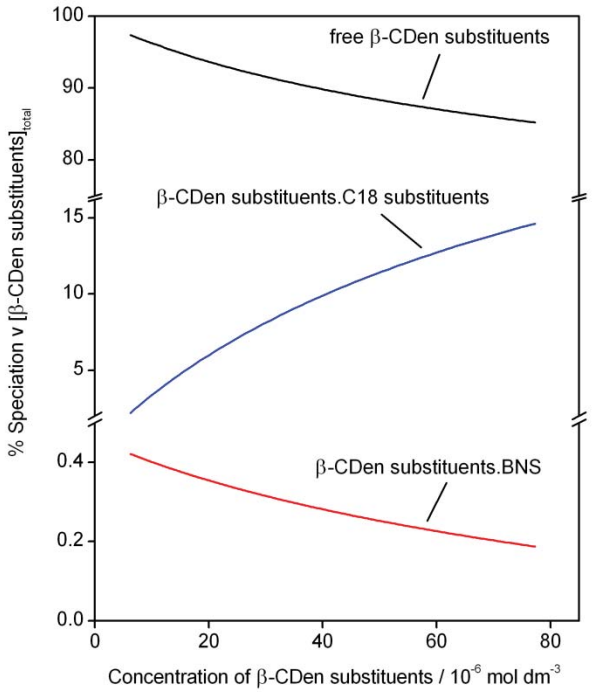

Figure 3.12. Speciation plot with $[\beta\text{-CDen substituents}]_{total}$ = 100% for the PAAβ-CDen/PAAC18/BNS system.

The 2D NOESY ^{1}H NMR spectrum of a solution of BNS and PAAβ-CDen/PAAC18 (Figure 3.13) shows cross-peaks arising from dipolar interactions between the β-CD group protons and the BNS protons and the C18 substituent protons. This is consistent with BNS being complexed in β-CDen substituents in the PAAβ-CDen/PAAC18 network, as indicated by fluorescence titration studies discussed above. Analogous cross-peaks are observed for TNS (Figure 3.32 in Section 3.11 Appendix). However, no analogous cross-peaks appear for ANS (Figure 3.33 in Section 3.11 Appendix), which is consistent with very weak complexation, or no complexation at all, of ANS by β-CDen substituents in the PAAβ-CDen/PAAC18 network.

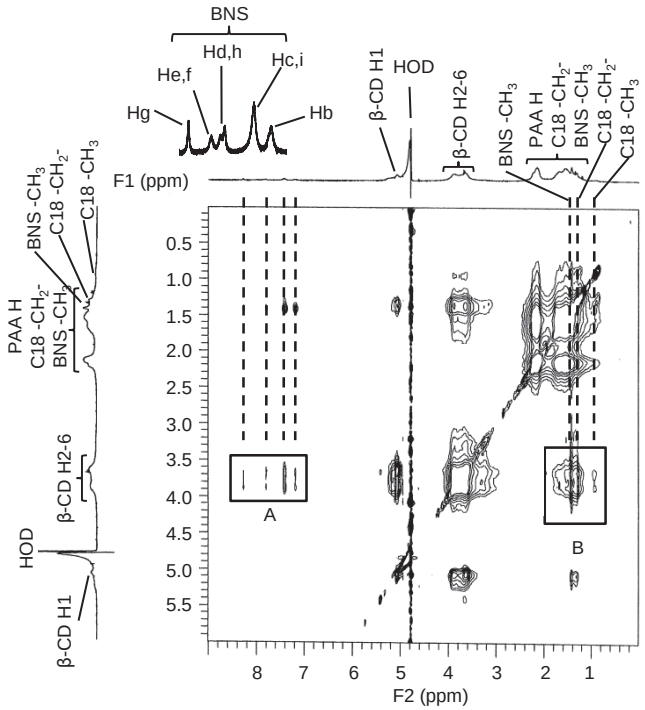

Figure 3.13. 2D NOESY ^{1}H NMR spectrum of BNS ([BNS] = 1.0×10^{-3} mol dm^{-3}) in mixture with PAAβ-CDen (0.85 wt%, [β-CDen substituents] = 4.0×10^{-3} mol dm^{-3}) and PAAC18 (0.57 wt%, [C18 substituents] = 2.0×10^{-3} mol dm^{-3}) in D_2O Na_2HPO_4/KH_2PO_4 buffer solution at pD = 7.0 and I = 0.10 mol dm^{-3} at 298.2 K. Cross-peaks in box A arise from dipolar interactions between the annular H3,5,6 protons of the β-CD groups and the aromatic (Hb-d and Hg-i) protons of BNS. Cross-peaks in box B arise from dipolar interactions between the annular H3,5,6 protons of the β-CD groups and the methyl (Ha) protons of BNS and the methylene and methyl protons of the C18 substituents, respectively.

3.7. Rheological studies of aqueous substituted poly(acrylate) systems

At higher concentrations than those used in the ITC and UV-Vis and fluorescence titration studies above, the viscosities of the PAAβ-CDen/PAAC18 network and when complexing dyes in aqueous solutions were determined by rheology. Because it was necessary to quantitatively determine the rates of dye release from the PAAβ-CDen/PAAC18 network, their solution fluidities had to be sufficient to allow their quantitative transfer into the measurement

apparatus, and this determined the maximum concentrations of their components. In the PAAβ-CDen/PAAC18 network, the concentration of PAAβ-CDen ([β-CDen substituents] = 6.00 ×10^{-3} mol dm^{-3}) and PAAC18 ([C18 substituents] = 2.00 ×10^{-3} mol dm^{-3}) were 1.27 wt% and 0.57 wt%, respectively. The concentration of either MR, MO or EO was 2.00 ×10^{-3} mol dm^{-3}, while the concentration of either ANS, TNS or BNS was 7.80 ×10^{-4} mol dm^{-3} because of the limitation of their aqueous solubility. These sample compositions are identical to those used in the dye release studies discussed below. The viscosity variations of PAAβ-CDen/PAAC18 and PAAβ-CDen/PAAC18/dye systems with shear rate were determined as shown in Figure 3.14. The viscosities show small variations with shear rate and those determined at 1 s^{-1} were selected for comparison purposes.

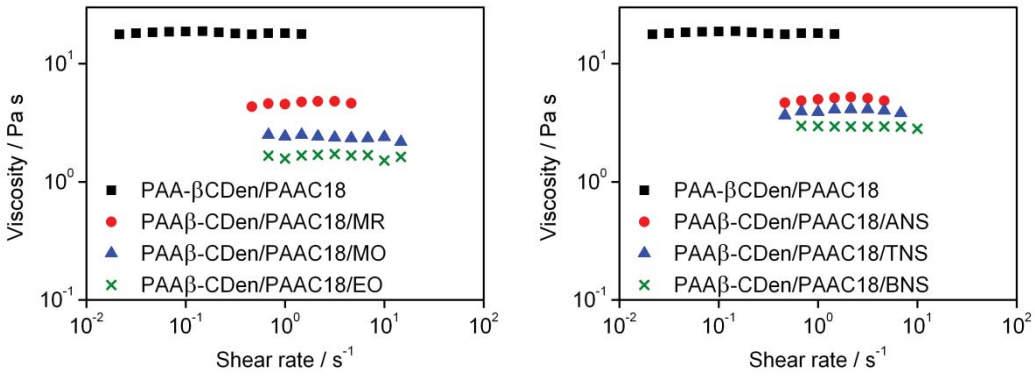

Figure 3.14. Viscosity variations with shear rate of aqueous Na_2HPO_4/KH_2PO_4 buffer solutions at pH 7.0 and I = 0.10 mol dm^{-3} of PAAβ-CDen/PAAC18 in the absence and presence of either MR, MO, EO (Left), ANS, TNS, or BNS (Right) at 298.2 K. The concentration of PAAβ-CDen and PAAC18 is 1.27 wt% ([β-CDen substituents] = 6.00 ×10^{-3} mol dm^{-3}) and 0.57 wt% ([C18 substituents] = 2.00 ×10^{-3} mol dm^{-3}), respectively. The concentration of MR, MO, and EO is 2.00 × 10^{-3} mol dm^{-3} and the concentration of ANS, TNS, and BNS is 7.80 × 10^{-4} mol dm^{-3}.

The viscosity variations at a 1 s^{-1} shear rate for all seven systems are shown in Figure 3.15. The viscosity of the binary PAAβ-CDen/PAAC18 solution is 18.1 Pa s. Upon addition of either MR, MO or EO, a substantial decrease in the viscosity of the ternary

PAAβ-CDen/PAAC18/dye solutions occurs (viscosities = 4.53, 2.41 and 1.57 Pa s in the presence of MR, MO and EO, respectively). This is consistent with the dye complexation competing with C18 substituent complexation by the β-CDen substituents, even with the β-CDen substituent concentration being 3 times greater than that of the dyes. In addition, the highest and lowest viscosity occurs for MR and EO consistent with them showing the smallest and largest *K* values as determined in the UV-Vis spectroscopic titration studies. This further indicates that dye complexation competes with C18 substitutent complextation by β-CDen substituent in the PAAβ-CDen/PAAC18 network. Similar viscosity variations occur for the PAAβ-CDen/PAAC18 solutions upon addition of either ANS, TNS, or BNS as shown in Figure 3.15 (Viscosities = 4.99, 3.89 and 2.96 Pa s in the presence of ANS, TNS and BNS, respectively).

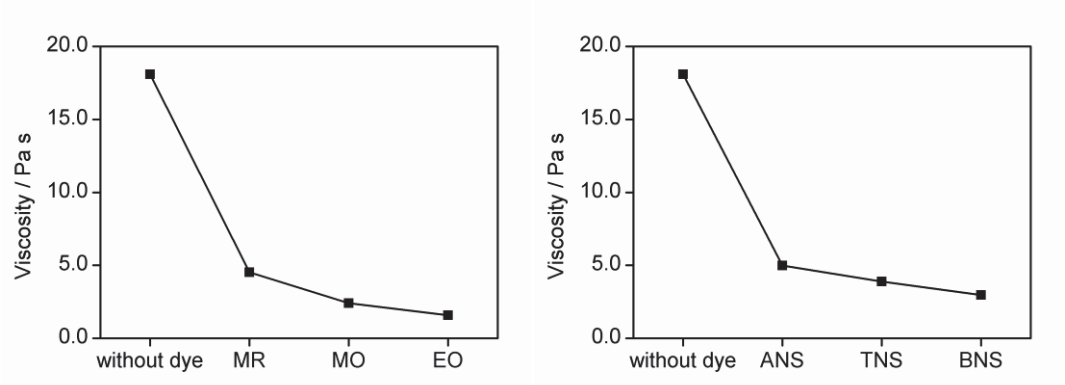

Figure 3.15. Viscosity variations at a 1 s^{-1} shear rate of aqueous Na_2HPO_4/KH_2PO_4 buffer at pH 7.0 and I = 0.10 mol dm^{-3} of PAAβ-CDen/PAAC18 in the absence and presence of either MR, MO, EO (Left), ANS, TNS, or BNS (Right) at 298.2 K. The concentration of PAAβ-CDen and PAAC18 is 1.27 wt% ([β-CDen substituents] = 6.00 ×10^{-3} mol dm^{-3}) and 0.57 wt% ([C18 substituents] = 2.00 ×10^{-3} mol dm^{-3}), respectively. The concentration of MR, MO, and EO is 2.00 × 10^{-3} mol dm^{-3} and the concentration of ANS, TNS, and BNS is 7.80 × 10^{-4} mol dm^{-3}.

3.8. Dye release studies

3.8.1. Qualitative investigation into dye release behavior

Dye release through a dialysis membrane with pores allowing passage of species with a molecular weight up to 3500 g mol^{-1} from each dye sample solution made up in aqueous Na_2HPO_4/KH_2PO_4 buffer at pH 7.0, I = 0.10 mol dm^{-3} into an aqueous Na_2HPO_4/KH_2PO_4 buffer at pH 7.0 and I = 0.10 mol dm^{-3} receiving solution at 298.2 K was characterized for each dye sample solution. As they are the more strongly complexed of the six dyes studied (Tables 3.2 and 3.3), EO and BNS were selected for a detailed study of the effect of the PAAC18, β-CD and PAAβ-CDen network components of the PAAβ-CDen/PAAC18 network and the network itself on the rate of dye release. These dye release profiles are shown in Figure 3.16. To eliminate any effects arising from variations of the concentration of the carboxylate goups of PAAC18 and PAAβ-CDen in the dye solutions studied, the total concentration of these groups was adjusted to be the same in each solution as shown in the caption to Figure 3.16. All solutions were made up in aqueous Na_2HPO_4/KH_2PO_4 buffer at pH 7.0 and I = 0.10 mol dm^{-3} and aqueous solutions of either EO or BNS in the same buffer were chosen as the reference solutions for dye release studies. The dye release profiles from these reference solutions to the receiving solutions are expected to reflect the dye diffusion in the reference solution and diffusion through the dialysis membrane such that any variation from this profile are attributable to the effects of the components of the PAAβ-CDen/PAAC18 network and the network itself.

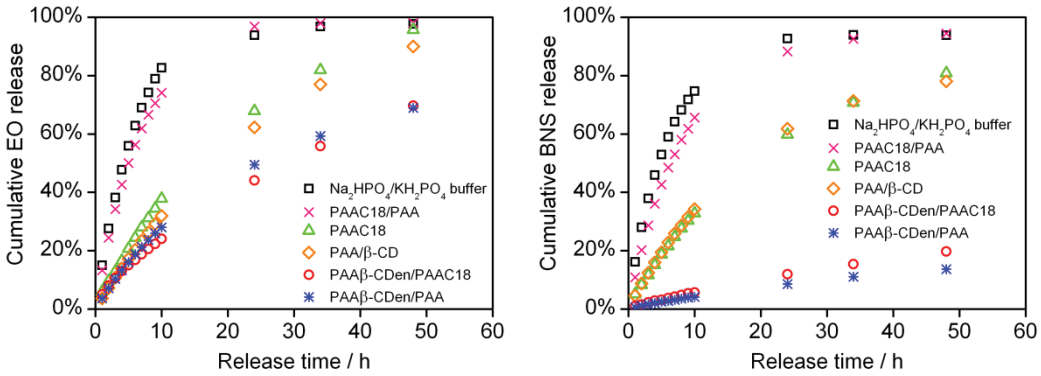

Figure 3.16. Release profiles for EO (Left) and BNS (Right) from Na_2HPO_4/KH_2PO_4 buffer, 1.84 wt% PAAC18/PAA (PAAC18, 0.57 wt%, [C18 substituents] = 2.00×10^{-3} mol dm^{-3}, PAA, 1.27 wt%), 1.84 wt% PAAC18 ([C18 substituents] = 6.43×10^{-3} mol dm^{-3}), 1.84 wt% PAA/β-CD ([β-CD] = 6.00×10^{-3} mol dm^{-3}, PAA, 1.84 wt%) 1.84 wt% PAAβ-CDen/PAAC18 (PAAβ-CDen, 1.27 wt%, [β-CDen substituents] = 6.00×10^{-3} mol dm^{-3}, PAAC18, 0.57 wt%, [C18 substituents] = 2.00×10^{-3} mol dm^{-3}), and 1.84 wt% PAAβ-CDen/PAA (PAAβ-CDen, 1.27 wt%, [β-CDen substituents] = 6.00×10^{-3} mol dm^{-3}, PAA, 0.57 wt%) in aqueous Na_2HPO_4/KH_2PO_4 buffer at pH 7.0 and I = 0.10 mol dm^{-3} at 298.2 K. The concentration of EO is 2.00×10^{-3} mol dm^{-3} and the concentration of BNS is 7.80×10^{-4} mol dm^{-3}.

By comparison with the release of EO from aqueous Na_2HPO_4/KH_2PO_4 buffer, the release of EO from a solution of PAAC18 (0.57 wt%) and PAA (1.27 wt%) is slower, especially within the first 10 hours. This is probably attributable to hydrophobic interactions between EO and hydrophobic domains arising from aggregation of hydrophobic C18 substituents in PAAC18 solution. This effect becomes substantially greater when the concentration of PAAC18 is increased to 1.84 wt% as shown in Figure 3.16 and is attributable to the increase in C18 substituents from 2.00×10^{-3} mol dm^{-3} to 6.43×10^{-3} mol dm^{-3} and a proportionate increase in hydrophobic aggregation.

The release of EO from a solution of PAA and β-CD is also slower, compared with the release of EO from aqueous Na_2HPO_4/KH_2PO_4 buffer. This is consistent with substantial formation of the β-CD.EO complex which although of lower molecular weight than the

membrane 3500 g mol^{-1} limit is likely to pass through the membrane less readily than EO alone and is also less mobile than free EO. An even slower release of EO from the PAAβ-CDen solution occurs. This is consistent with substantial formation of the PAAβ-CDen.EO complex which is of much too high a molecular weight to pass through the membrane such that passage is limited to free EO alone. Analogous trends occur for the BNS release, as shown in Figure 3.16. These data are consistent with complexation of dye by β-CD alone or a β-CD substituent controlling the amount of free dye and thereby the rate of dye release through the membrane.

The release rate of EO and BNS from the PAAβ-CDen/PAAC18 network is similar to that from PAAβ-CDen/PAA and much slower than that from aqueous Na_2HPO_4/KH_2PO_4 buffer. This suggests the complexation of dye by β-CDen substituents in the PAAβ-CDen/PAAC18 network is also of major importance in controlling the rate of dye release, besides the influence of increased viscosity due to the formation of the PAAβ-CDen/PAAC18 network. Due to the limitation of aqueous solubility of ANS, TNS and BNS, the concentration (7.80×10^{-4} mol dm^{-3}) of ANS, TNS and BNS in release samples are different from the concentration (2.00×10^{-3} mol dm^{-3}) of MR, MO and EO in release samples. For comparison purposes, the release rate of the six dyes will be discussed in two sets, ANS, TNS and BNS and MR, MO and EO. The release profiles of all six dyes from the PAAβ-CDen/PAAC18 network are shown in Figure 3.17, from which it is seen that the dye release rate decreases in sequences: MR > MO > EO and ANS > TNS > BNS. The sequence of dye release rate MR > MO > EO coincides with the increasing magnitude of the complexation constant, *K*, determined by UV-Vis spectroscopy in the sequence MR < MO < EO (Table 3.2). In addition, the sequence of dye release rate ANS > TNS > BNS also coincides with the increasing magnitude of the complexation constant, *K*, determined by fluorescence spectroscopy in the sequence ANS < TNS < BNS (Table 3.3). These results are consistent with the proportion of dye in the free state being a major determinant for the rate of release. Thus, the complexation of the dyes by

β-CDen substituents in the PAAβ-CDen/PAAC18 network predominantly controls the proportion of dye in the free state and thereby determines the rate of dye release.

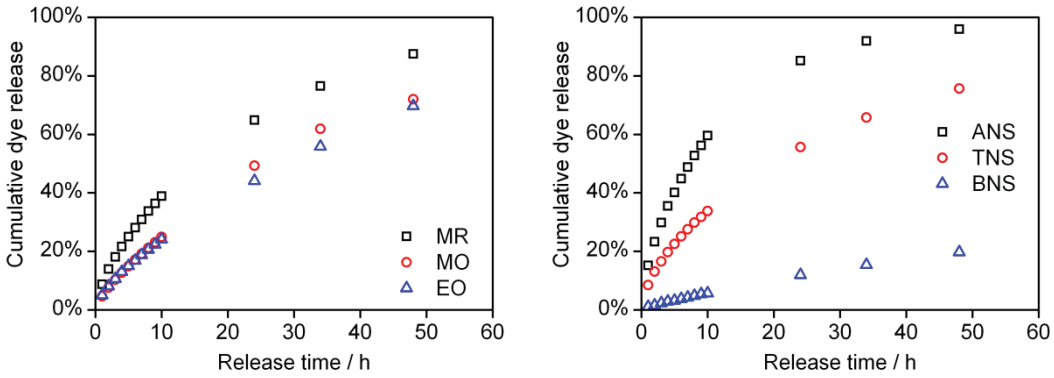

Figure 3.17. Release profiles of MR, MO, and EO (Left), and ANS, TNS, and BNS (Right) from a 1.84 wt% PAAβ-CDen/PAAC18 (PAAβ-CDen, 1.27 wt%, [β-CDen substituents] = 6.00×10^{-3} mol dm^{-3}, PAAC18, 0.57 wt%, [C18 substituents] = 2.00×10^{-3} mol dm^{-3}) aqueous Na_2HPO_4/KH_2PO_4 buffer at pH 7.0 and I = 0.10 mol dm^{-3} at 298.2 K. The concentration of MR, MO and EO is 2.00×10^{-3} mol dm^{-3} and the concentration of ANS, TNS and BNS is 7.80×10^{-4} mol dm^{-3}.

3.8.2. Theoretical investigation into dye release behavior

As previously discussed in Chapter 2, Peppas *et al.* have proposed Equation 3.11 to describe the release mechanism of guests from polymer networks.[41-43]

$$M_t/M_\infty = kt^n \qquad \textbf{(3.11)}$$

where M_t and M_∞ are the amount of released drug (or dye) at time t and infinite time, respectively. k is a kinetic constant indicative of release rate, and n is a release exponent which is related to the release mechanism. A n = 0.5 indicates that a diffusion-controlled release applies while n = 1 indicates the mechanism of release from the network controls the release rate. Both the diffusion and network release mechanism can apply simultaneously such that n is between 0.5 and 1. Equation 3.10 only applies for up to 60% of the drug being released.

Although this theoretical model was originally developed to simulate the cargo release from covalently cross-linked polymer networks, it has been widely used to elucidate the release mechanism and kinetics from a wide range of physically cross-linked polymer networks.[44] All derived *n* values are between 0.5 and 1 (Table 3.4), indicating that a combination of Fickian diffusion and release from complexation determines the overall rate of guest release. Similar combinations of Fickian diffusion and guest release from complexation have been observed for dye release from poly(acrylate) networks cross-linked through complexation of adamantyl substituents by β-CD substituents in Chapter 2, as well as being reported for cargo (guest) release from polymer networks containing cyclodextrin groups[45,46] and the release of cyclodextrin.guest complexes from polymer networks.[47]

As also found in Chapter 2, the above model yields plausible *n* and *k* values through Equation 3.10. However, it is possible that the PAAβ-CDen/PAAC18 network is too complex to be analyzed through this model as the release of a guest (in this case a dye) from it incorporates the dynamics of β-CDen substituent complexation of dye, the dynamics of the PAAβ-CDen/PAAC18 network, the diffusion of dye within the network, and the dynamics of the passage of the dye through the membrane. Alternative models are available but do not appear to offer solutions to this complexity problem.[48]

Table 3.4. Analysis of release mechanism according to Equation 3.11:

$$M_t/M_\infty = kt^n$$

		n	10^2k / h^{-n}	R^2
PAAβ-CDen/PAAC18 (1.27 wt%/0.57 wt%)	EO	0.69	4.95	0.999
	MO	0.74	4.53	0.999
	MR	0.61	9.39	0.999
	BNS	0.79	0.94	0.999
	TNS	0.56	9.14	0.999
	ANS	0.58	15.7	0.999

3.9. Conclusions

We have examined the feasibility of a self-assembled PAAβ-CDen/PAAC18 network as a potential sustained drug delivery system in this study. The formation of PAAβ-CDen/PAAC18 network in aqueous solution is due to the host-guest complexation of C18 substituents by β-CDen substituents, characterized by a high complexation constant, $K_{ITC} = 1.13 \times 10^4$ dm^3 mol^{-1}. This complexation process is driven by a substantial ΔH contribution and a small $T\Delta S$ contribution. The β-CDen substituents in the PAAβ-CDen/PAAC18 network retain a decreased complexation capability. This is reflected by the complexation constant, K for complexation of the dye by β-CDen substituents in the PAAβ-CDen/PAAC18 network being smaller than K for complexation of the dye by native β-CD and by PAAβ-CDen, which is probably a consequence of increased steric crowding within the network. In the subsequent release studies, the rate of dye release from the PAAβ-CDen/PAAC18 network follows the order: MR > MO > EO and ANS > TNS > BNS, which coincides with the reverse of the order of complexation strength reflected by the complexation constants increasing in the sequences: MR < MO < EO and ANS < TNS < BNS. These data highlight the major role of complexation of the dye by β-CDen substituents in the PAAβ-CDen/PAAC18 network in controlling the amount of dye in the free state and thereby the rate of dye release. In summary, β-CDen substituents in the self-assembled PAAβ-CDen/PAAC18 network retain the complexation capability and thereby the advantages of β-CD in pharmaceutical applications, such as enhancing drug solubility and preventing drug degradation.[22,23,26-29] On the other hand, the complexation of drugs by β-CD substituents has the potential to sustain the subsequent release of drugs to improve drug efficacy. Thus, it is envisaged that at higher concentrations than those studied herein the PAAβ-CDen/PAAC18 hydrogel could be developed for topical application and also for insertion into wounds as drug delivery systems.

3.10. References

(1) Guo, X.; Abdala, A. A.; May, B. L.; Lincoln, S. F.; Khan, S. A.; Prud'Homme, R. K. Novel associative polymer networks based on cyclodextrin inclusion compounds. *Macromolecules* **2005,** *38*, 3037.

(2) Guo, X.; Abdala, A. A.; May, B. L.; Lincoln, S. F.; Khan, S. A.; Prud'homme, R. K. Rheology control by modulating hydrophobic and inclusion associations in modified poly(acrylic acid) solutions. *Polymer* **2006,** *47*, 2976-2983.

(3) Li, L.; Guo, X.; Wang, J.; Liu, P.; Prud'homme, R. K.; May, B. L.; Lincoln, S. F. Polymer networks assembled by host-guest inclusion between adamantyl and β-cyclodextrin substituents on poly (acrylic acid) in aqueous solution. *Macromolecules* **2008,** *41*, 8677-8681.

(4) Li, L.; Guo, X.; Fu, L.; Prud'homme, R. K.; Lincoln, S. F. Complexation behavior of α-, β-, and γ-cyclodextrin in modulating and constructing polymer networks. *Langmuir* **2008,** *24*, 8290-8296.

(5) Wang, J.; Li, L.; Ke, H.; Liu, P.; Zheng, L.; Guo, X.; Lincoln, S. F. Rheology control by modulating hydrophobic and inclusive associations of side-groups in poly (acrylic acid). *Asia-pac. J. Chem. Eng.* **2009,** *4*, 537-543.

(6) Wang, J.; Pham, D.-T.; Guo, X.; Li, L.; Lincoln, S. F.; Luo, Z.; Ke, H.; Zheng, L.; Prud'homme, R. K. Polymeric networks assembled by adamantyl and β-cyclodextrin substituted poly(acrylate)s: host-guest interactions, and the effects of ionic strength and extent of substitution. *Ind. Eng. Chem. Res.* **2010,** *49*, 609-612.

(7) Guo, X.; Wang, J.; Li, L.; Pham, D.-T.; Clements, P.; Lincoln, S. F.; May, B. L.; Chen, Q.; Zheng, L.; Prud'homme, R. K. Steric effects and competitive intra- and inter-molecular host-guest complexation between β-cyclodextrin and adamantyl substituted poly(acrylate)s in water: A ^{1}H NMR, rheological and preparative study. *J. Polym. Sci., Part B: Polym. Phys.* **2010,** *48*, 1818-1825.

(8) Guo, X.; Wang, J.; Li, L.; Pham, D.-T.; Clements, P.; Lincoln, S. F.; May, B. L.; Chen, Q.; Zheng, L.; Prud'homme, R. K. Tailoring polymeric hydrogels through cyclodextrin host-guest complexation. *Macromol. Rapid Commun.* **2010,** *31*, 300-304.

(9) Wang, J.; Pham, D.-T.; Kee, T. W.; Clafton, S. N.; Guo, X.; Clements, P.; Lincoln, S. F.; Prud'homme, R. K.; Easton, C. J. Aggregation and host-guest interactions in dansyl-substituted poly(acrylate)s in the presence of β-cyclodextrin and a β-cyclodextrin dimer in aqueous solution: A UV-Vis, fluorescence, ^{1}H NMR, and rheological study. *Macromolecules* **2011,** *44*,

9782-9791.

(10) Nguyen, H.-T.; Pham, D.-T.; Lincoln, S. F.; Wang, J.; Guo, X.; Easton, C. J.; Prud'homme, R. K. Host-guest chemistry of linked β-cyclodextrin trimers and adamantyl substituted poly(acrylate)s in aqueous solution. *Polym. Chem.* **2013,** *4*, 820-829.

(11) Pham, D.-T.; Nguyen, H.-T.; Lincoln, S. F.; Wang, J.; Guo, X.; Easton, C. J.; Prud'homme, R. K. Complexation of dodecyl-substituted poly(acrylate) by linked β-cyclodextrin dimers and trimers in aqueous solution. *J. Polym. Sci., Part A: Polym. Chem.* **2015,** *53*, 1278-1286.

(12) Wang, J.; Xu, Y.; Wang, Y.; Liu, J.; Xu, J.; Li, L.; Nguyen, H.-T.; Pham, D.-T.; Lincoln, S. F.; Guo, X. Bridged-cyclodextrin supramolecular hydrogels: host-guest interaction between a cyclodextrin dimer and adamantyl substituted poly(acrylate)s. *RSC Adv.* **2015,** *5*, 46067-46073.

(13) Wang, J.; Qiu, Z.; Wang, Y.; Li, L.; Guo, X.; Pham, D.-T.; Lincoln, S. F.; Prud'homme, R. K. Supramolecular polymer assembly in aqueous solution arising from cyclodextrin host-guest complexation. *Beilstein J. Org. Chem.* **2016,** *12*, 50-72.

(14) Park, H.; Park, K. Biocompatibility issues of implantable drug delivery systems. *Pharm. Res.* **1996,** *13*, 1770-1776.

(15) Cadée, J. A.; van Luyn, M. J. A.; Brouwer, L. A.; Plantinga, J. A.; van Wachem, P. B.; de Groot, C. J.; den Otter, W.; Hennink, W. E. In vivo biocompatibility of dextran-based hydrogels. *J. Biomed. Mater. Res.* **2000,** *50*, 397-404.

(16) Hoffman, A. S. Hydrogels for biomedical applications. *Adv. Drug Deliv. Rev.* **2002,** *54*, 3-12.

(17) Peppas, N. A.; Hilt, J. Z.; Khademhosseini, A.; Langer, R. Hydrogels in biology and medicine: From molecular principles to bionanotechnology. *Adv. Mater.* **2006,** *18*, 1345-1360.

(18) Jeong, B.; Kim, S. W.; Bae, Y. H. Thermosensitive sol-gel reversible hydrogels. *Adv. Drug Deliv. Rev.* **2002,** *54*, 37-51.

(19) Morishita, M.; Lowman, A. M.; Takayama, K.; Nagai, T.; Peppas, N. A. Elucidation of the mechanism of incorporation of insulin in controlled release systems based on complexation polymers. *J. Control. Release* **2002,** *81*, 25-32.

(20) Torres-Lugo, M.; García, M.; Record, R.; Peppas, N. A. Physicochemical behavior and cytotoxic effects of p(methacrylic acid-g-ethylene glycol) nanospheres for oral delivery of proteins. *J. Control. Release* **2002,** *80*, 197-205.

(21) Peng, K.; Tomatsu, I.; Kros, A. Light controlled protein release from a supramolecular

hydrogel. *Chem. Commun.* **2010,** *46*, 4094-4096.

(22) Loftsson, T.; Brewster, M. E. Pharmaceutical applications of cyclodextrins. 1. Drug solubilization and stabilization. *J. Pharm. Sci.* **1996,** *85*, 1017-1025.

(23) Uekama, K.; Hirayama, F.; Irie, T. Cyclodextrin drug carrier systems. *Chem. Rev.* **1998,** *98*, 2045-2076.

(24) Hirayama, F.; Uekama, K. Cyclodextrin-based controlled drug release system. *Adv. Drug Deliv. Rev.* **1999,** *36*, 125-141.

(25) Stella, V. J.; Rao, V. M.; Zannou, E. A.; Zia, V. Mechanisms of drug release from cyclodextrin complexes. *Adv. Drug Deliv. Rev.* **1999,** *36*, 3-16.

(26) Davis, M. E.; Brewster, M. E. Cyclodextrin-based pharmaceutics: past, present and future. *Nat. Rev. Drug Discov.* **2004,** *3*, 1023-1035.

(27) Loftsson, T.; Jarho, P.; Másson, M.; Järvinen, T. Cyclodextrins in drug delivery. *Expert Opin. Drug Deliv.* **2005,** *2*, 335-351.

(28) Loftsson, T.; Duchêne, D. Cyclodextrins and their pharmaceutical applications. *Int. J. Pharm.* **2007,** *329*, 1-11.

(29) Kurkov, S. V.; Loftsson, T. Cyclodextrins. *Int. J. Pharm.* **2013,** *453*, 167-180.

(30) Concheiro, A.; Alvarez-Lorenzo, C. Chemically cross-linked and grafted cyclodextrin hydrogels: From nanostructures to drug-eluting medical devices. *Adv. Drug Deliv. Rev.* **2013,** *65*, 1188-1203.

(31) Simoes, S. M. N.; Rey-Rico, A.; Concheiro, A.; Alvarez-Lorenzo, C. Supramolecular cyclodextrin-based drug nanocarriers. *Chem. Commun.* **2015,** *51*, 6275-6289.

(32) Kosower, E. M.; Dodiuk, H.; Tanizawa, K.; Ottolenghi, M.; Orbach, N. Intramolecular donor-acceptor systems. Radiative and nonradiative processes for the excited states of 2-n-arylamino-6-naphthalenesulfonates. *J. Am. Chem. Soc.* **1975,** *97*, 2167-2178.

(33) MicroCal, 22 Industrial Drive East, Northampton, MA 01060, USA.

(34) Gans, P.; Sabatini, A.; Vacca, A. Investigation of equilibria in solution. Determination of equilibrium constants with the HYPERQUAD suite of programs. *Talanta* **1996,** *43*, 1739-1753.

(35) HypSpec. Protonic Software: 2 Templegate Avenue, Leeds LS15 0HD, UK.

(36) Harada, T.; Pham, D.-T.; Lincoln, S. F.; Kee, T. W. The capture and stabilization of curcumin using hydrophobically modified polyacrylate aggregates and hydrogels. *J. Phys. Chem. B* **2014,** *118*, 9515-9523.

(37) Rekharsky, M. V.; Inoue, Y. Complexation thermodynamics of cyclodextrins. *Chem. Rev.* **1998,** *98*, 1875-1918.

(38) Harries, D.; Rau, D. C.; Parsegian, V. A. Solutes probe hydration in specific association of cyclodextrin and adamantane. *J. Am. Chem. Soc.* **2005,** *127*, 2184-2190.

(39) Pham, D.-T.; Clements, P.; Easton, C. J.; Papageorgiou, J.; May, B. L.; Lincoln, S. F. Complexation of 6-(4′-(toluidinyl) naphthalene-2-sulfonate by β-cyclodextrin and linked β-cyclodextrin dimers. *New J. Chem.* **2008,** *32*, 712-718.

(40) Pham, D.-T.; Clements, P.; Easton, C. J.; Papageorgiou, J.; May, B. L.; Lincoln, S. F. Dimerisation and complexation of 6-(4′-t-butylphenylamino)naphthalene-2-sulphonate by β-cyclodextrin and linked β-cyclodextrin dimers. *Supramol. Chem.* **2009,** *21*, 510-519.

(41) Ritger, P. L.; Peppas, N. A. A simple equation for description of solute release I. Fickian and non-Fickian release from non-swellable devices in the form of slabs, spheres, cylinders or discs. *J. Control. Release* **1987,** *5*, 23-36.

(42) Ritger, P. L.; Peppas, N. A. A simple equation for description of solute release II. Fickian and anomalous release from swellable devices. *J. Control. Release* **1987,** *5*, 37-42.

(43) Peppas, N. A.; Sahlin, J. J. A simple equation for the description of solute release. III. Coupling of diffusion and relaxation. *Int. J. Pharm.* **1989,** *57*, 169-172.

(44) Appel, E. A.; Forster, R. A.; Rowland, M. J.; Scherman, O. A. The control of cargo release from physically crosslinked hydrogels by crosslink dynamics. *Biomaterials* **2014,** *35*, 9897-9903.

(45) Machín, R.; Isasi, J. R.; Vélaz, I. Hydrogel matrices containing single and mixed natural cyclodextrins. Mechanisms of drug release. *Eur. Polym. J.* **2013,** *49*, 3912-3920.

(46) Kutyła, M. J.; Lambert, L. K.; Davies, N. M.; McGeary, R. P.; Shaw, P. N.; Ross, B. P. Cyclodextrin-crosslinked poly (acrylic acid): synthesis, physicochemical characterization and controlled release of diflunisal and fluconazole from hydrogels. *Int. J. Pharm.* **2013,** *444*, 175-184.

(47) Teixeira, R. S.; Veiga, F. J.; Oliveira, R. S.; Jones, S. A.; Silva, S.; Carvalho, R. A.; Valente, A. J. Effect of Cyclodextrins and pH on the permeation of tetracaine: Supramolecular assemblies and release behavior. *Int. J. Pharm.* **2014,** *466*, 349-358.

(48) Fu, Y.; Kao, W. J. Drug release kinetics and transport mechanisms of non-degradable and degradable polymeric delivery systems. *Expert Opin. Drug Deliv.* **2010,** *7*, 429-444.

3.11. Appendix

3.11.1. UV-Vis spectroscopic titration data and 2D NOESY ^{1}H NMR spectra of MR, MO and EO complexation

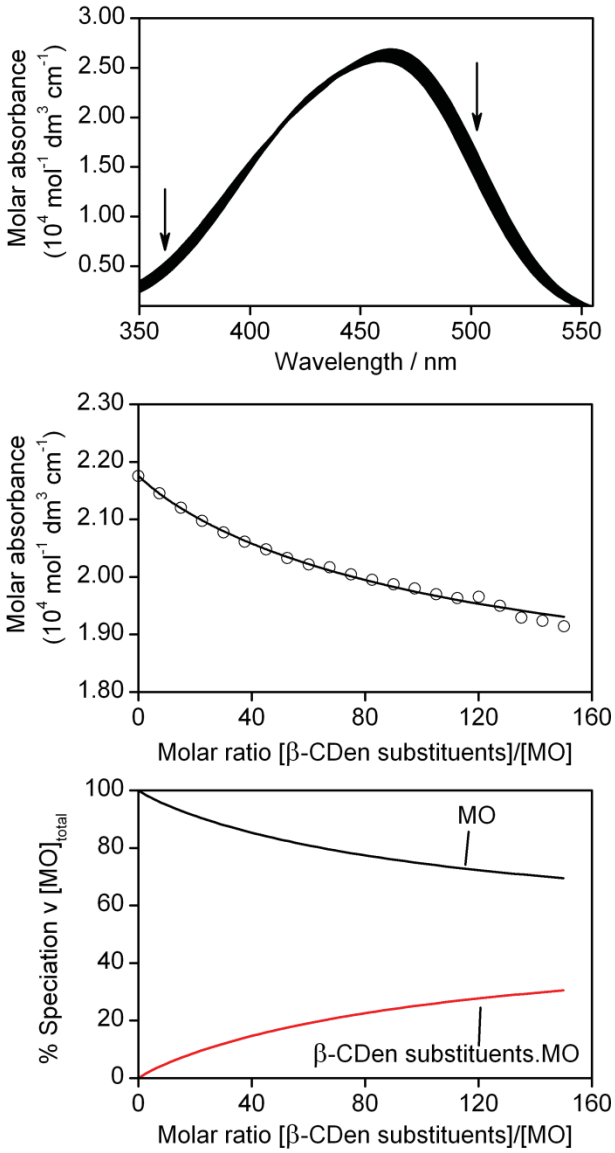

Figure 3.18. (Top) Molar absorbance variation of a MO solution ([MO] = 2.00 × 10^{-5} mol dm^{-3}) upon 20 sequential additions of a PAAβ-CDen solution (25 mm^3 each, 1.90 wt%, [β-CDen substituents] = 9.01 × 10^{-3} mol dm^{-3}) and a PAAC18 solution (25 mm^3 each, 0.87 wt%, [C18 substituents] = 3.02 × 10^{-3} mol dm^{-3}) at 298.2 K. All solutions were prepared in aqueous Na_2HPO_4/KH_2PO_4 buffer solutions at pH 7.0 and I = 0.10 mol dm^{-3}. The arrows indicate the direction of molar absorbance variation upon each addition of the PAAβ-CDen and PAAC18 solutions. (Middle) Molar absorbance variation at 490 nm and the line representing the best-fit of an algorithm for a 1:1 host-guest complexation of MO by β-CDen substituents in the PAAβ-CDen/PAAC18 network over the wavelength range 465 - 515 nm. (Bottom) Speciation plot with $[MO]_{total}$ = 100%.

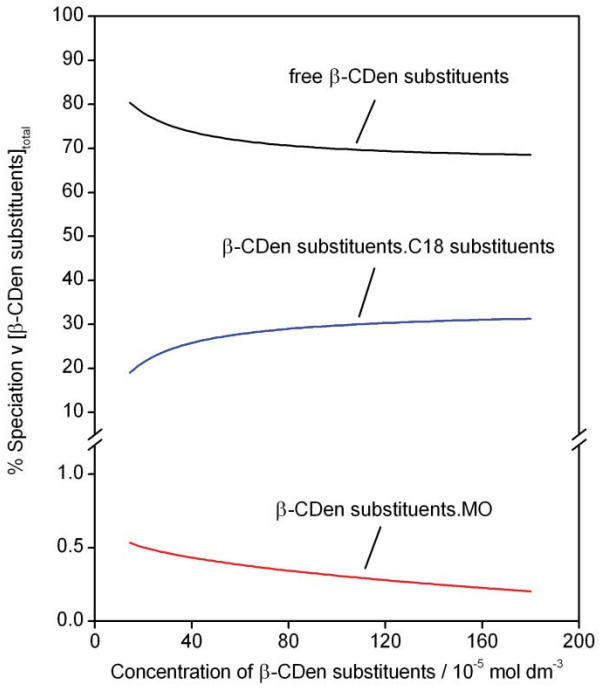

Figure 3.19. Speciation plot with $[\beta\text{-CDen substituents}]_{total}$ = 100% for the PAAβ-CDen/PAAC18/MO system.

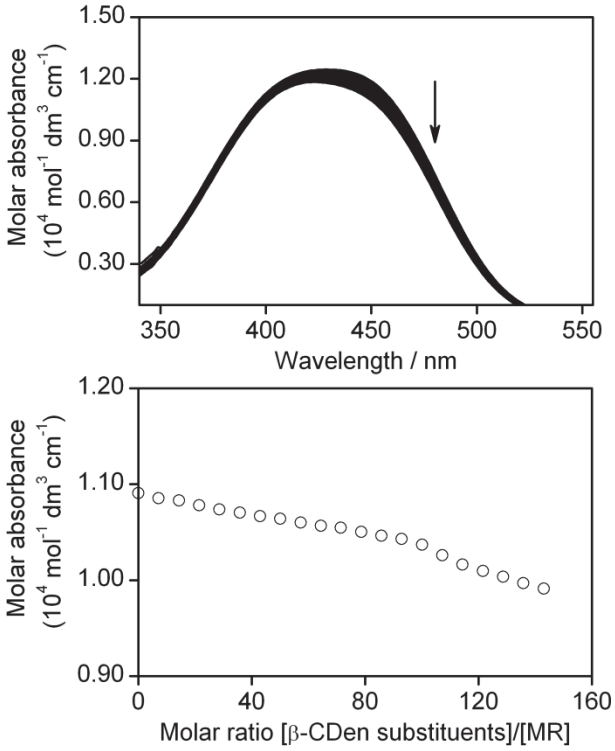

Figure 3.20. (Top) Molar absorbance variation of a MR solution ([MR] = 2.80×10^{-5} mol dm^{-3}) upon 20 sequential additions of a PAAβ-CDen solution (25 mm^3 each, 2.51 wt%, [β-CDen substituents] = 1.20×10^{-2} mol dm^{-3}) and a PAAC18 solution (25 mm^3 each, 1.16 wt%, [C18 substituents] = 4.03×10^{-3} mol dm^{-3}) at 298.2 K. All solutions were prepared in aqueous Na_2HPO_4/KH_2PO_4 buffer solutions at pH 7.0 and I = 0.10 mol dm^{-3}. The arrow indicates the direction of molar absorbance variation upon each addition of the PAAβ-CDen and PAAC18 solutions. (Bottom) Molar absorbance variation at 460 nm is insufficient to fit to an algorithm for host-guest complexation of MR by β-CDen substituents in the PAAβ-CDen/PAAC18 network.

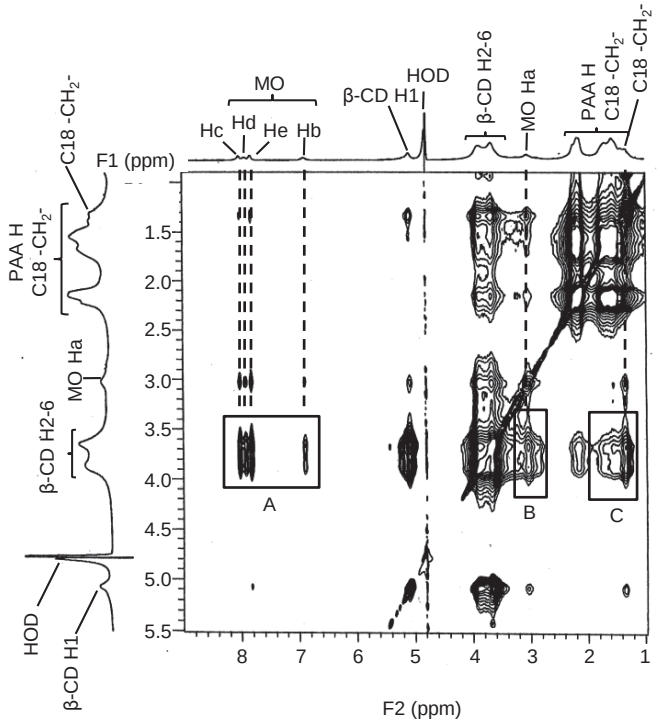

Figure 3.21. 2D NOESY ^{1}H NMR spectrum of MO ([MO] = 2.0×10^{-3} mol dm^{-3}) in mixture with PAAβ-CDen (0.85 wt%, [β-CDen substituents] = 4.0×10^{-3} mol dm^{-3}) and PAAC18 (0.57 wt%, [C18 substituents] = 2.0×10^{-3} mol dm^{-3}) in D_2O Na_2HPO_4/KH_2PO_4 buffer solution at pD = 7.0 and I = 0.10 mol dm^{-3} at 298.2 K. Cross-peaks in boxes A and B arise from dipolar interactions between the annular H3,5,6 protons of the β-CD groups and the aromatic (Hb-e) and methyl (Ha) protons of MO, respectively. Cross-peaks in box C arise from dipolar interactions between the annular H3,5,6 protons of the β-CD groups and the methylene protons of the C18 substituents.

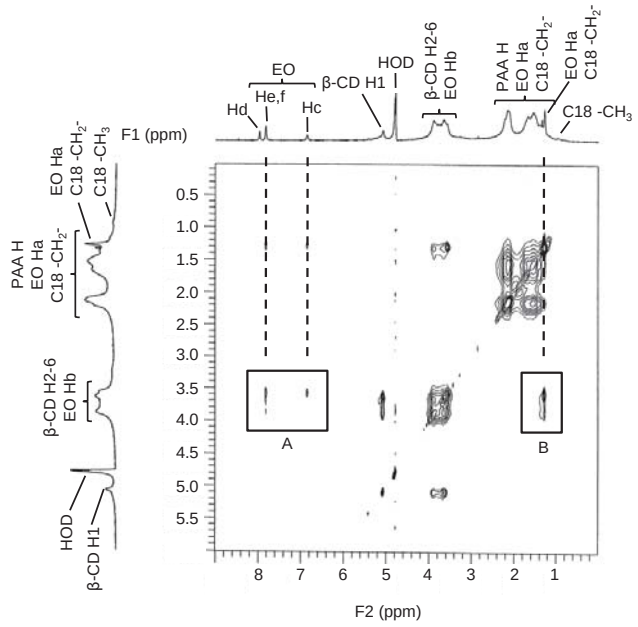

Figure 3.22. 2D NOESY ^{1}H NMR spectrum of EO ([EO] = 2.0×10^{-3} mol dm^{-3}) in mixture with PAAβ-CDen (0.85 wt%, [β-CDen substituents] = 4.0×10^{-3} mol dm^{-3}) and PAAC18 (0.57 wt%, [C18 substituents] = 2.0×10^{-3} mol dm^{-3}) in D_2O Na_2HPO_4/KH_2PO_4 buffer solution at pD = 7.0 and I = 0.10 mol dm^{-3} at 298.2 K. Cross-peaks in box A arise from dipolar interactions between the annular H3,5,6 protons of the β-CD groups and the aromatic (Hc,e,f) protons of EO. Cross-peaks in box B arise from dipolar interactions between the annular H3,5,6 protons of the β-CD groups and the methyl (Ha) protons of EO and the methylene protons of the C18 substituents, respectively.

3.11.2. Fluorescence spectroscopic titration data and 2D NOESY ^{1}H NMR spectra of ANS, TNS and BNS complexation

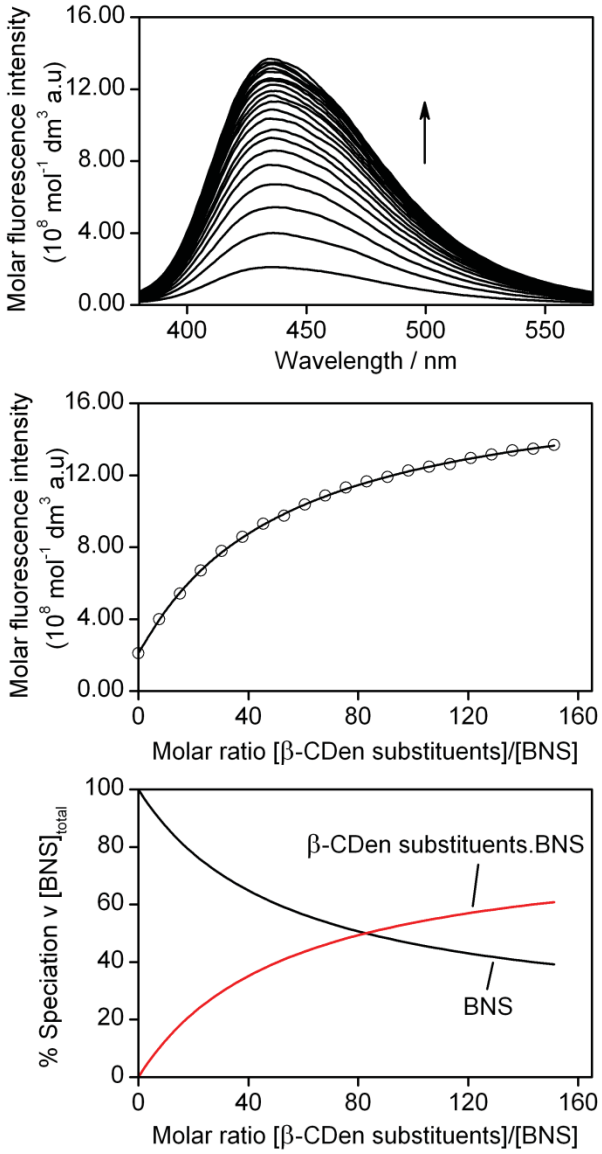

Figure 3.23. (Top) Molar fluorescence variation of a BNS solution ([BNS] = 7.67 × 10^{-7} mol dm^{-3}) upon 20 sequential additions of a PAAβ-CDen solution (50 mm^3 each, 0.050 wt%, [β-CDen substituents] = 2.32 × 10^{-4} mol dm^{-3}) at 298.2 K. Both solutions were prepared in aqueous Na_2HPO_4/KH_2PO_4 buffer solutions at pH 7.0 and I = 0.10 mol dm^{-3}. The arrow indicates the direction of molar fluorescence variation upon each addition of the PAAβ-CDen solution. Excitation wavelength is 320 nm. (Middle) Molar fluorescence variation at 435 nm and the line representing the best-fit of an algorithm for a 1:1 host-guest complexation of BNS by β-CDen substituents of PAAβ-CDen over the wavelength range 410 - 480 nm. (Bottom) Speciation plot with $[BNS]_{total}$ = 100%. Data collected by Mitchell B. Bacon.

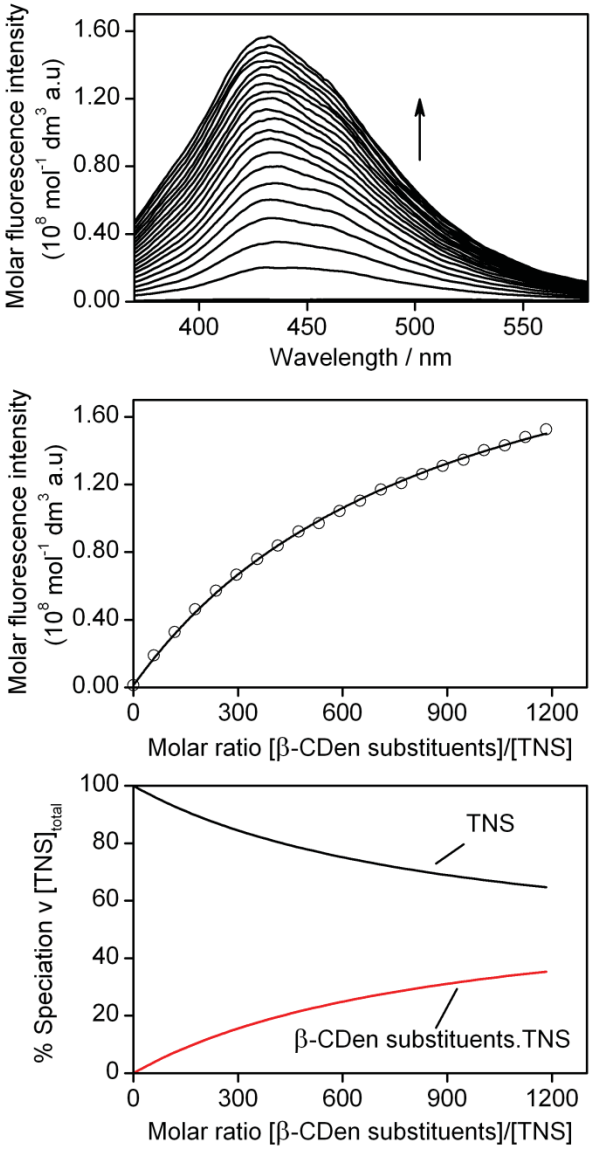

Figure 3.24. (Top) Molar fluorescence variation of a TNS solution ([TNS] = 3.00 × 10^{-6} mol dm^{-3}) upon 20 sequential additions of a PAAβ-CDen solution (50 mm^3 each, 1.50 wt%, [β-CDen substituents] = 7.10 × 10^{-3} mol dm^{-3}) at 298.2 K. Both solutions were prepared in aqueous Na_2HPO_4/KH_2PO_4 buffer solutions at pH 7.0 and I = 0.10 mol dm^{-3}. The arrow indicates the direction of molar fluorescence variation upon each addition of the PAAβ-CDen solution. Excitation wavelength is 320 nm. (Middle) Molar fluorescence variation at 424 nm and the line representing the best-fit of an algorithm for a 1:1 host-guest complexation of TNS by β-CDen substituents of PAAβ-CDen over the wavelength range 400 - 450 nm. (Bottom) Speciation plot with $[TNS]_{total}$ = 100%. Data collected by Mohammed Tajuddin Ghori.

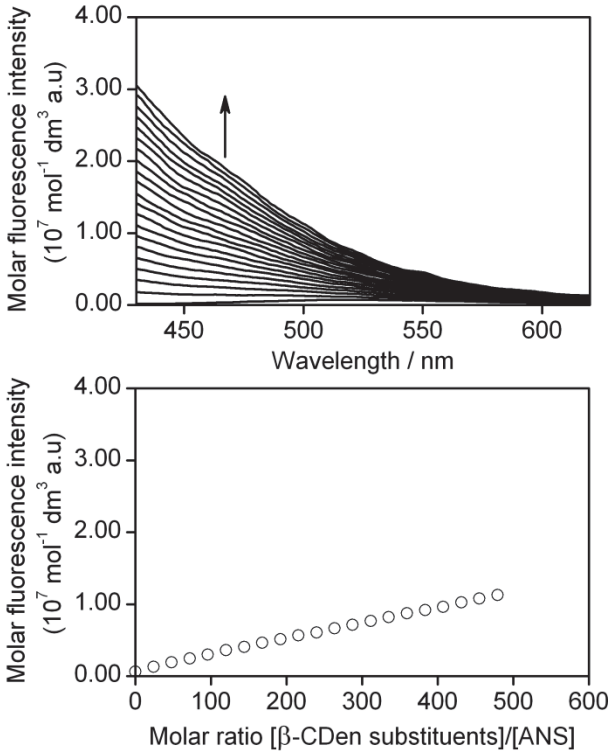

Figure 3.25. (Top) Molar fluorescence variation of an ANS solution ([ANS] = 1.03×10^{-5} mol dm^{-3}) upon 20 sequential additions of a PAAβ-CDen solution (50 mm^3 each, 4.06 wt%, [β-CDen substituents] = 1.97×10^{-2} mol dm^{-3}) at 298.2 K. Both solutions were prepared in aqueous Na_2HPO_4/KH_2PO_4 buffer solutions at pH 7.0 and I = 0.10 mol dm^{-3}.The arrow indicates the direction of molar fluorescence variation upon each addition of the PAAβ-CDen solution. (Middle) Molar fluorescence variation at 500 nm is insufficient to fit to an algorithm for host-guest complexation of ANS by β-CDen substituents of PAAβ-CDen.

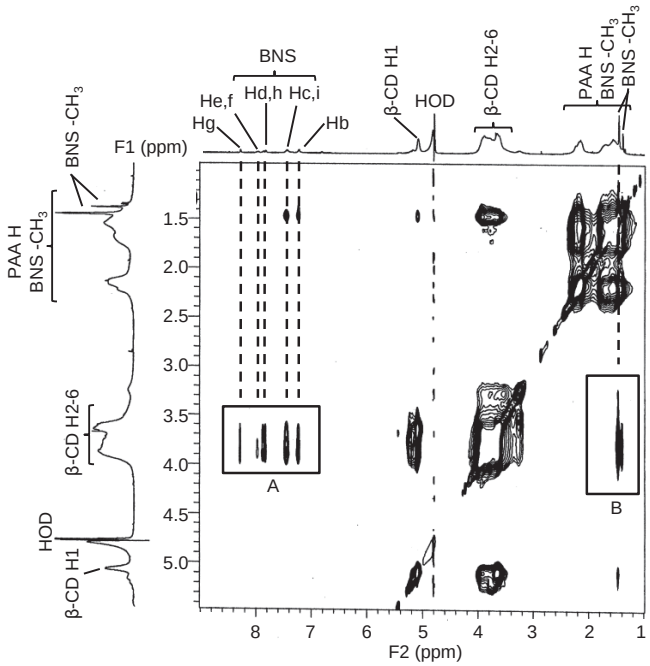

Figure 3.26. 2D NOESY ^{1}H NMR spectrum of BNS ([BNS] = 1.0 × 10^{-3} mol dm^{-3}) and PAAβ-CDen (0.43 wt%, [β-CDen substituents] = 2.0 × 10^{-3} mol dm^{-3}) in D_2O Na_2HPO_4/KH_2PO_4 buffer solution at pD = 7.0 and I = 0.10 mol dm^{-3} at 298.2 K. Cross-peaks in boxes A and B arise from dipolar interactions between the annular H3,5,6 protons of the β-CD groups and the aromatic (Hb-i) and methyl (Ha) protons of BNS, respectively. Data collected by Mitchell B. Bacon.

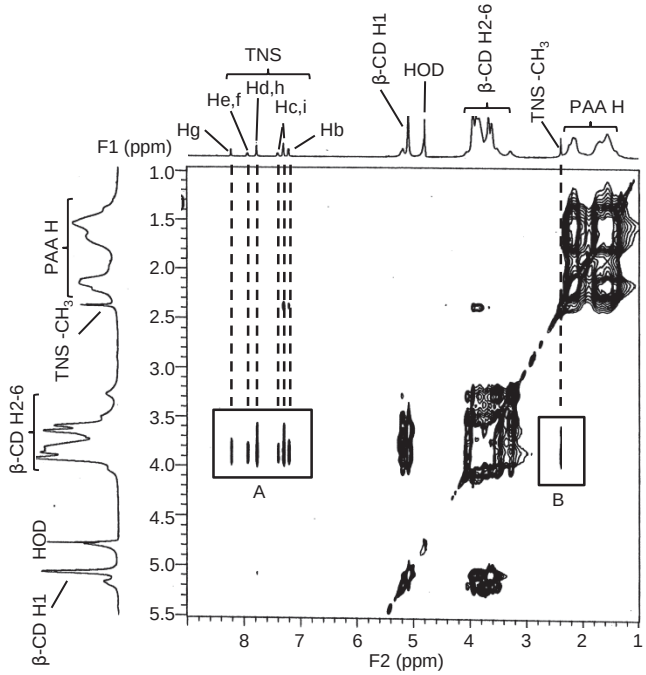

Figure 3.27. 2D NOESY ^{1}H NMR spectrum of TNS ([TNS] = 1.0 × 10^{-3} mol dm^{-3}) and PAAβ-CDen (0.43 wt%, [β-CDen substituents] = 2.0 × 10^{-3} mol dm^{-3}) in D_2O Na_2HPO_4/KH_2PO_4 buffer solution at pD = 7.0 and I = 0.10 mol dm^{-3} at 298.2 K. Cross-peaks in boxes A and B arise from dipolar interactions between the annular H3,5,6 protons of the β-CD groups and the aromatic (Hb-i) and methyl (Ha) protons of TNS, respectively. Data collected by Mohammed Tajuddin Ghori.

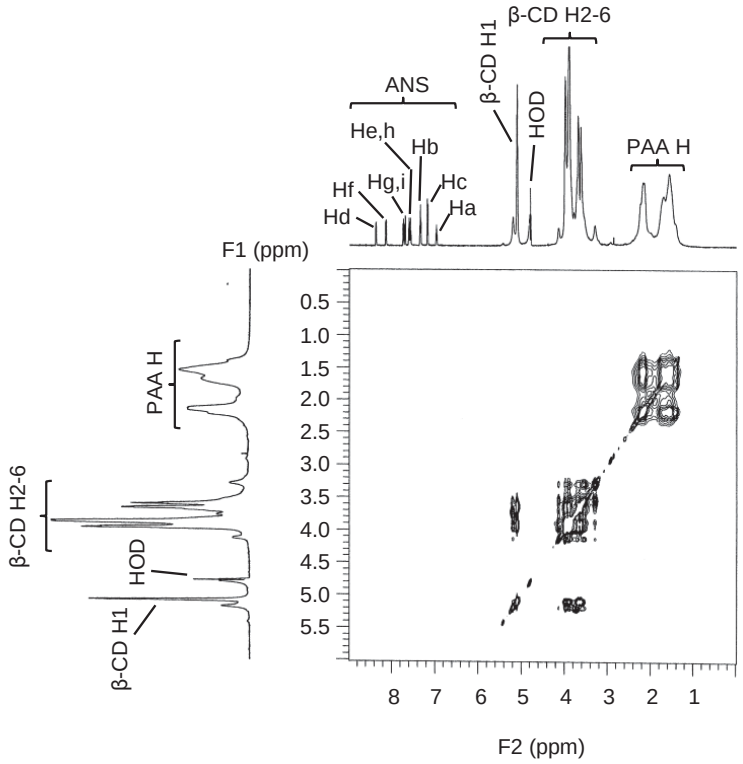

Figure 3.28. 2D NOESY ^{1}H NMR spectrum of ANS ([ANS] = 2.0 × 10^{-3} mol dm^{-3}) and PAAβ-CDen (0.43 wt%, [β-CDen substituents] = 2.0 × 10^{-3} mol dm^{-3}) in D_2O Na_2HPO_4/KH_2PO_4 buffer solution at pD = 7.0 and I = 0.10 mol dm^{-3} at 298.2 K.

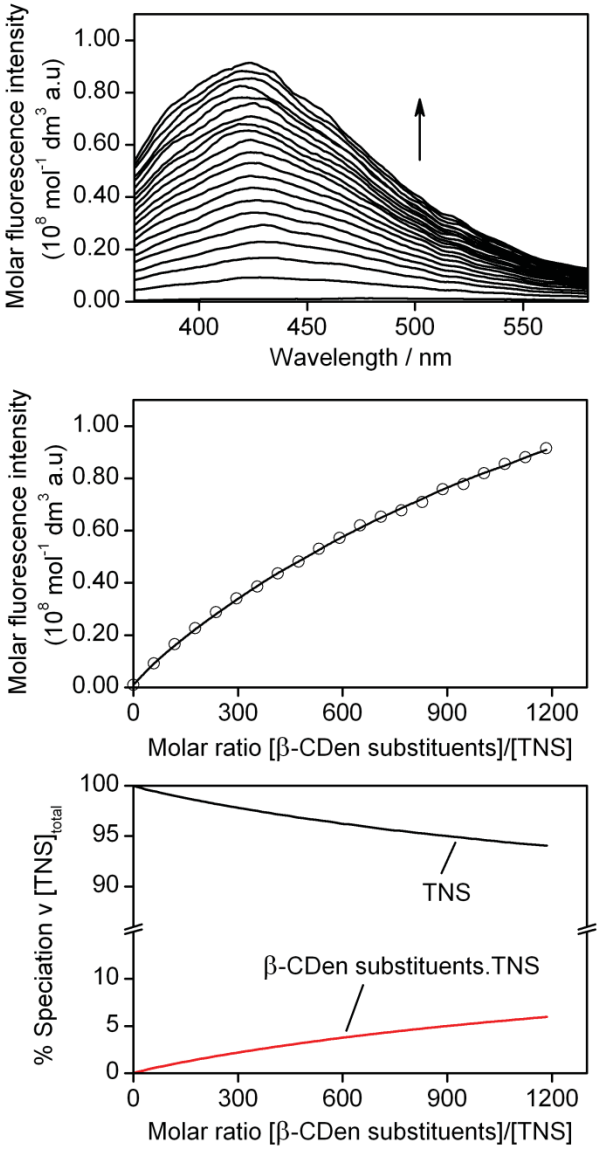

Figure 3.29. (Top) Molar fluorescence variation of a TNS solution ([TNS] = 3.00 × 10^{-6} mol dm^{-3}) upon 20 sequential additions of a PAAβ-CDen solution (25 mm^3 each, 2.96 wt%, [β-CDen substituents] = 1.42 × 10^{-2} mol dm^{-3}) and a PAAC18 solution (25 mm^3 each, 1.51 wt%, [C18 substituents] = 5.25 × 10^{-3} mol dm^{-3}) at 298.2 K. All solutions were prepared in aqueous Na_2HPO_4/KH_2PO_4 buffer solutions at pH 7.0 and I = 0.10 mol dm^{-3}. The arrow indicates the direction of molar fluorescence variation upon each addition of the PAAβ-CDen and PAAC18 solutions. Excitation wavelength is 320 nm. (Middle) Molar fluorescence variation at 424 nm and the line representing the best-fit of an algorithm for a 1:1 host-guest complexation of TNS by β-CDen substituents in the PAAβ-CDen/PAAC18 network over the wavelength range 400 - 450 nm. (Bottom) Speciation plot with $[TNS]_{total}$ = 100%.

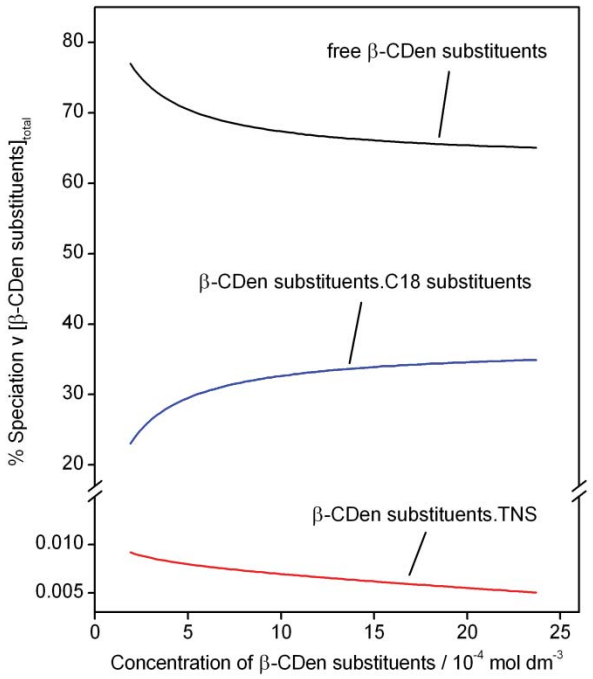

Figure 3.30. Speciation plot with $[\beta\text{-CDen substituents}]_{total}$ = 100% for the PAAβ-CDen/PAAC18/TNS system.

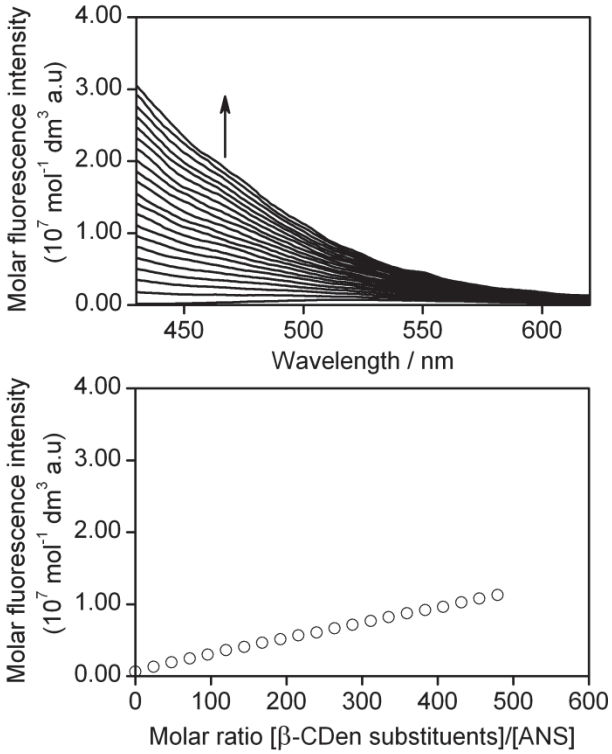

Figure 3.31. (Top) Molar fluorescence variation of an ANS solution ([ANS] = 1.03×10^{-5} mol dm^{-3}) upon 20 sequential additions of a PAAβ-CDen solution (25 mm^3 each, 4.06 wt%, [β-CDen substituents] = 1.97×10^{-2} mol dm^{-3}) and a PAAC18 solution (25 mm^3 each, 1.88 wt%, [C18 substituents] = 6.59×10^{-3} mol dm^{-3}) at 298.2 K. All solutions were prepared in aqueous Na_2HPO_4/KH_2PO_4 buffer solutions at pH 7.0 and I = 0.10 mol dm^{-3}. The arrow indicates the direction of molar fluorescence variation upon each addition of the PAAβ-CDen and PAAC18 solutions. Excitation wavelength is 350 nm. (Bottom) Molar fluorescence variation at 500 nm is insufficient to fit to an algorithm for host-guest complexation of ANS by β-CDen substituents in the PAAβ-CDen/PAAC18 network.

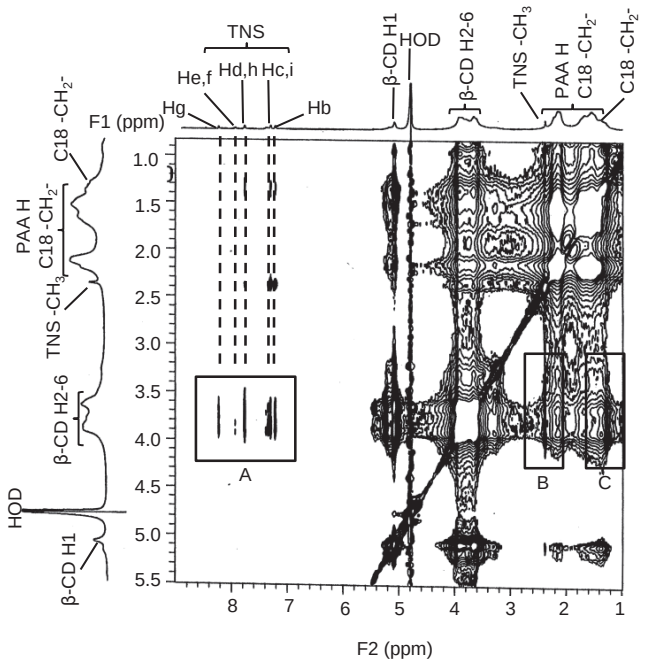

Figure 3.32. 2D NOESY ^{1}H NMR spectrum of TNS ([TNS] = 1.0×10^{-3} mol dm^{-3}) in mixture with PAAβ-CDen (0.85 wt%, [β-CDen substituents] = 4.0×10^{-3} mol dm^{-3}) and PAAC18 (0.57 wt%, [C18 substituents] = 2.0×10^{-3} mol dm^{-3}) in D_2O Na_2HPO_4/KH_2PO_4 buffer solution at pD = 7.0 and I = 0.10 mol dm^{-3} at 298.2 K. Cross-peaks in boxes A and B arise from dipolar interactions between the annular H3,5,6 protons of the β-CD groups and the aromatic (Hb-i) and methyl (Ha) protons of TNS, respectively. Cross-peaks in box C arise from dipolar interactions between the annular H3,5,6 protons of the β-CD groups and the methylene protons of the C18 substituents.

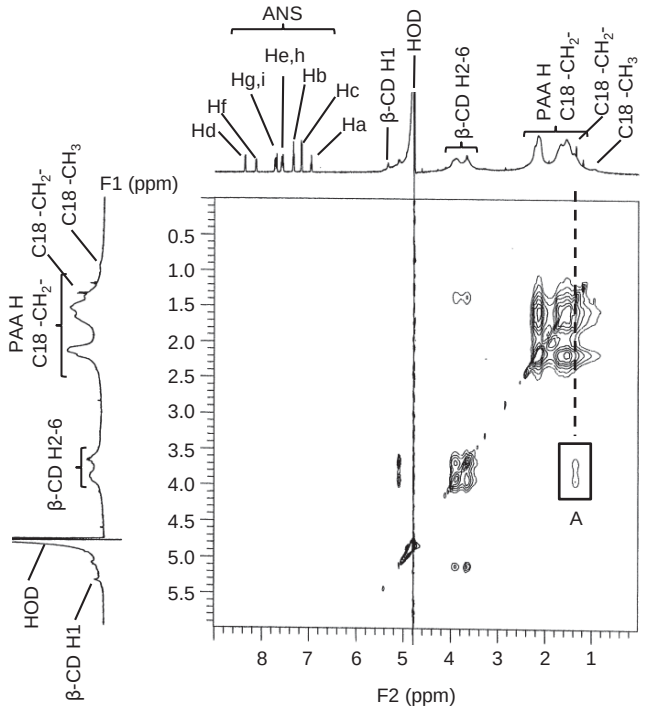

Figure 3.33. 2D NOESY ^{1}H NMR spectrum of ANS ([ANS] = 2.0×10^{-3} mol dm^{-3}) in mixture with PAAβ-CDen (0.85 wt%, [β-CDen substituents] = 4.0×10^{-3} mol dm^{-3}) and PAAC18 (0.57 wt%, [C18 substituents] = 2.0×10^{-3} mol dm^{-3}) in D_2O Na_2HPO_4/KH_2PO_4 buffer solution at pD = 7.0 and I = 0.10 mol dm^{-3} at 298.2 K. Cross-peaks in box A arise from dipolar interactions between the annular H3,5,6 protons of the β-CD groups and the methylene protons of the C18 substituents.

CHAPTER 4

STABILIZING FLUORESCENT CONJUGATED POLYMER NANOPARTICLES USING HYDROPHOBICALLY MODIFIED POLY(ACRYLATE)S FOR BIOLOGICAL IMAGING APPLICATIONS

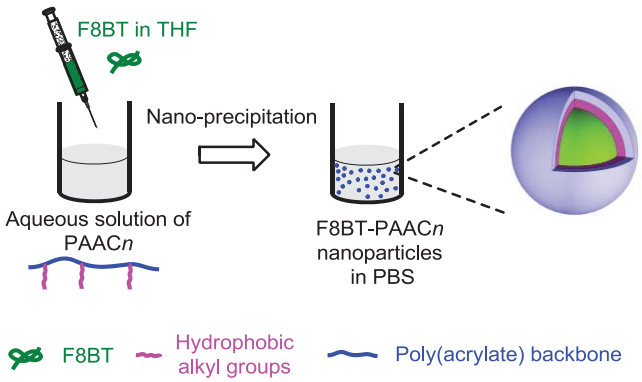

4.1. Introduction

The broad UV-Visible absorption cross-section and high fluorescence brightness and photostability of conjugated polymer nanoparticles have attracted substantial interests that has resulted in a wide range of applications.[1-18] An interesting application is to use conjugated polymer nanoparticles with emissions ranging from visible to near-infrared (NIR) spectral regions as fluorescent probes in cell imaging. Streptavidin modified conjugated polymer nanoparticles have been developed for labeling EpCAM, a cell-surface receptor and diagnostic marker for cancer cells, selectively.[2,3] Similarly, the integration of the NIR emitting chromophores dithienylbenzoselenadiazole and quinoxaline into conjugated polymer nanoparticles results in a high NIR fluorescence brightness and excellent photostability for deployment in cell imaging.[4,5] An alternative strategy for preparing brightly emitting NIR conjugated polymer nanoparticles involves the doping of these nanoparticles with either a NIR fluorescence dye[6] or quantum dot[7] which accepts energy from the conjugated polymer matrix through efficient Förster resonance energy transfer, FRET. In addition to their use in fluorescence imaging, conjugated polymer nanoparticles have also been used as ratiometric pH,[8,9] temperature,[10] oxygen,[11,12] fluoride[13] and mercury[14] sensors. These sensors are based on efficient FRET from conjugated polymer nanoparticles to either surface conjugated, doped or covalently attached functional groups. The change of environmental pH, temperature, oxygen level or concentration of fluoride or mercury ions triggers variation of emission properties of the corresponding functional group, thereby disrupting FRET to give rise to sensing function. In therapeutic applications, several conjugated polymer nanoparticle systems have been used as drug delivery vehicles[15,16] and as photothermal therapy[17] and photodynamic therapy[18] agents which provide concurrent fluorescence imaging.

Although conjugated polymer nanoparticles exhibit a wide range of biological applications,

their large-scale aggregation and precipitation under the high ionic strength conditions in physiological conditions are substantial challenges to advance their biological applications. Ionic surfactants and phospholipids including sodium dodecyl sulfate[19] and 1,2-dipalmitoyl-*sn*-glycero-3-phosphocholine[20,21] have been used to increase the surface charge and colloidal stability of conjugated polymer nanoparticles. However, the required high concentration of surfactants (up to 0.16 M) may result in either cytotoxicity or perturbations to cell membranes. To address this issue, Chiu *et al.* developed a co-precipitation strategy, in which amphiphilic polymers bearing functional groups and hydrophobic conjugated polymers were co-condensed into single nanoparticles.[2,22] In the resultant conjugated polymer nanoparticles, the hydrophobic segments of the amphiphilic polymers were most likely anchored inside the hydrophobic nanoparticles while the hydrophilic segments bearing functional groups are located on the surface to either enhance surface charge, or supply reactive sites for further bioconjugation, or both. A challenge of this approach is the limited number of amphiphilic polymers that are soluble in an organic solvent. More recently, conjugated polymer nanoparticles with both enhanced surface charge and bioconjugation sites were reported.[23] However, two polyelectrolytes were required; poly(styrene sulfonate) served as a stabilizer to improve colloidal stability and poly(sodium methacrylate) provided carboxylate groups as bioconjugation sites. Owing to the issues highlighted above, there is significant motivation to develop a single-component stabilizer that can provide conjugated polymer nanoparticles with colloidal stability in physiological conditions and bioconjugation sites.

A hydrophobic octadecyl substituted poly(acrylate) have been selected as a guest polymer in Chapter 3 to form self-assembled poly(acrylate) aqueous network through complexation by a β-cyclodextrin substituted poly(acrylate) as a host polymer. Inspired by the amphiphilic nature, poly(acrylate)s randomly substituted with hydrophobic linear alkyl groups, PAAC*n*, were used to stabilize conjugated polymer nanoparticles. The carboxylate groups of PAAC*n*

offer not only a negatively charged nanoparticle surface and an enhanced colloidal stability, but also supply potential reactive sites for biomolecule conjugation as described by Chiu *et al*.[23] A green-yellow emitting conjugated polymer, poly[(9,9-dioctylfluorenyl-2,7-diyl)-*alt*-*co*-(1,4-benzo-[2,1,3]-thiadiazole)], F8BT, was chosen to prepare nanoparticles stabilized with PAAC*n*. The F8BT-PAAC*n* nanoparticles have hydrodynamic diameters ranging from 49 ± 5 to 70 ± 3 nm and a high colloidal stability in phosphate buffered saline, PBS, at pH 7.4 over 4 weeks. In addition, the F8BT-PAAC*n* nanoparticles have a negatively charged surface arising from carboxylate groups of PAAC*n*, as reflected by a zeta potential value of approximately −58 ± 2 mV. The sub-100 nm size and negative surface charge hold the promise to facilitate the accumulation of F8BT-PAAC*n* nanoparticles in tumors through the enhanced permeability and retention effect, which is desired in tumor imaging or therapy.[24,25] The F8BT-PAAC*n* nanoparticles exhibit negligible cytotoxicity and can be internalized by cells. Confocal fluorescence images show high fluorescence brightness, indicating the potential use of F8BT-PAAC*n* nanoparticles as fluorescent probes for cell imaging.

4.2. Experimental section

4.2.1. Materials

Poly[(9,9-dioctylfluorenyl-2,7-diyl)-*alt*-*co*-(1,4-benzo-[2,1,3]-thiadiazole)] (F8BT, average molecular weight: 42,000 g mol^{-1}) was purchased from American Dye Source, Inc. Poly(acrylic acid) (35 wt% aqueous solution, average molecular weight: 250,000 g mol^{-1}), hexylamine, decylamine, dodecylamine, tetradecylamine, hexadecylamine, octadecylamine and fluorescein at 95% purity were purchased from Sigma-Aldrich. 1-Methyl-2-pyrrolidione and dicyclohexylcarbodiimide were purchased from Merck Schuchardt. Dulbecco's Modified

Eagle's Medium (DMEM), penicillin and fetal bovine serum were purchased from Gibco-BRL. 3-(4,5-Dimethylthiazol-2-yl)-2,5-Diphenyltetrazolium bromide (MTT) was purchased from Merck. All chemicals were used as received. Tetrahydrofuran was freshly distilled from sodium benzophenone ketyl before use. A stock phosphate buffered saline, PBS, solution was prepared at five times the standard concentration, 5 × PBS, by dissolving 40 g NaCl, 1 g KCl, 7.2 g Na_2HPO_4, and 1.2 g KH_2PO_4 in 800 cm^3 water. The pH of this solution was adjusted to 7.4 with 0.1 M NaOH and a final volume of 1 dm^3 was achieved by addition of water. Deionized water obtained using a Millipore NANO pure water system and filtered through a 0.22 μm nylon membrane (Merck Millipore) was used in all experiments.

4.2.2. Preparation of alkyl substituted poly(acrylate)s, PAAC*n*

Poly(acrylate)s randomly substituted with linear alkyl groups were synthesized according to a reported method.[26] Poly(acrylic acid) (1.50 g, 20.8 mmol repeating units) was added into 30 cm^3 1-methyl-2-pyrrolidione and the solution was stirred at 60 °C for 16 h, after which decylamine (0.33 g, 2.1 mmol) and dicyclohexylcarbodiimide (0.56 g, 2.7 mmol) were added and the solution was stirred for 120 h at 60 °C. The solution was then cooled to room temperature and was added 40 cm^3 40 % w/w aqueous sodium hydroxide solution. The formation of a precipitate was observed. The precipitate was collected by vacuum filtration and washed thoroughly with 30 cm^3 1-methyl-2-pyrrolidione at 60 °C twice and with 50 cm^3 methanol at room temperature twice. The collected precipitate was then dissolved in 15 cm^3 deionized water and reprecipitated through addition of 200 cm^3 methanol. The dissolution and precipitation process were repeated three times. The crude product was dissolved in 20 cm^3 deionized water and dialyzed (Spectr/Por 3, molecular weight cutoff: 3500 g/mol) against deionized water for 4 days with daily change of water. The final product was collected through lyophilization as a white solid. The substitution percentage of alkyl chain substituent was

determined using ^{1}H NMR spectroscopy according to Equation 4.1:

$$\text{Substitution percentage} = \frac{S_{\text{methyl group}}}{S_{\text{methine group}}} \times 100\% \qquad \textbf{(4.1)}$$

where $S_{\text{methyl group}}$ denotes the integrated area of the resonances of alkyl amine terminal CH_3 groups and $S_{\text{methine group}}$ denotes that of the resonances of poly(acrylate) backbone CH groups.

4.2.3. Preparation of F8BT-PAAC*n* nanoparticles

Dispersions of F8BT-PAAC*n* nanoparticles in PBS were prepared using a modified nano-precipitation method.[1] This involved the dissolution of 10 mg F8BT in 100 cm^3 of freshly distilled THF under sonication to obtain a ~100 ppm F8BT solution of which 1 cm^3 portions were rapidly injected into 10 cm^3 50 ppm aqueous solutions of 1% substituted PAAC18 under vigorous stirring. The THF was removed under vacuum using a rotary evaporator at ~40 °C to yield the F8BT-PAAC18 nanoparticles. This product was mixed with 2 cm^3 of 5 × PBS solution and deionized water to give a total volume of 10 cm^3 of a standard PBS (pH = 7.4) dispersion of F8BT-PAAC18 nanoparticles (10 ppm in F8BT). This solution was filtered through a 0.2 μm filter (Sartorius Stedim Biotech) to give the final PBS dispersion of F8BT-PAAC18 nanoparticles. An analogous method was used to prepare all other F8BT-PAAC*n* nanoparticle dispersions in PBS. The absorption spectra of the PBS dispersion of F8BT-PAAC*n* nanoparticles before and after filtration were recorded to measure the yield of nanoparticle preparation, which is defined in Equation 4.2 as:

$$\text{Yield} = \frac{A_{\text{after filtration}}}{A_{\text{before filtration}}} \times 100\% \qquad \textbf{(4.2)}$$

where $A_{\text{before filtration}}$ and $A_{\text{after filtration}}$ represent the absorbance at 455 nm of the PBS dispersion of F8BT-PAAC*n* nanoparticles before and after filtration through a 0.2 μm filter, respectively. Accordingly, the yield defined here describes the percentage of F8BT-PAAC*n* nanoparticles that passed through the 0.2 μm filter.

4.2.4. Characterization

^{1}H NMR spectra were recorded using a Varian Inova 500 spectrometer, operating at 500 MHz. Chemical shifts (δ) were recorded in parts per million (ppm) in D_2O with the resonances corresponding to the residual non-deuterated solvent, δ = 4.79 ppm, as the internal reference. UV-Vis absorption spectra were recorded on a Cary-Varian 5000 spectrophotometer using matched quartz cuvettes of 1 cm path length. Fluorescence spectra were recorded on a Cary-Varian Eclipse fluorescence spectrophotometer using a quartz cuvette of 1 cm path length.

4.2.5. Fluorescence quantum yield measurements

Fluorescein, with a reported quantum yield of 89%,[27] was used as the reference for fluorescence quantum yield measurements. Five samples of fluorescein in 0.1 M NaOH and F8BT-PAAC*n* nanoparticles in PBS over a range of five concentrations ($A < 0.1$) were prepared. The absorption (at 475 nm) and emission (excitation wavelength of 475 nm) spectra of each sample were recorded. For fluorescein and F8BT-PAAC*n* nanoparticles, the integrated fluorescence intensities were plotted against the corresponding absorbance to give a linear curve with a slope of *m* and an intercept of 0. The fluorescence quantum yield of F8BT-PAAC*n* nanoparticles with reference to fluorescein was calculated according to Equation 4.3:

$$\Phi_{\text{sample}} = \Phi_{\text{fluorescein}} \times \frac{m_{\text{sample}}}{m_{\text{fluorescein}}} \times \frac{\eta^2_{\text{sample}}}{\eta^2_{\text{fluorescein}}} \times 100\% \qquad \textbf{(4.3)}$$

where Φ represents the fluorescence quantum yield and η represents refractive index of the corresponding solvent. The quoted error of the fluorescence quantum yield in this study represents the linear fitting error of the calculation of the slope, *m*.

4.2.6. Morphology, size and zeta potential characterization

Transmission electron microscopy, TEM, was used to characterize the morphology of the F8BT-PAAC*n* nanoparticles. For sample preparation, a drop (~50 μL) of F8BT-PAAC*n* nanoparticle dispersion (10 ppm for F8BT) was placed onto a carbon-coated copper grid, and after 2 minutes the remaining solution was removed using a filter paper. This procedure was repeated 3 times. A drop (~50 μL) of 2% uranyl acetate solution was then applied onto the grid for staining, and after 2 minutes the remaining uranyl acetate solution was removed using a filter paper. Samples were observed on a FEI Tecnai G2 Spirit TEM at an operating voltage of 100 kV.

Dynamic light scattering, DLS, was used to measure the apparent hydrodynamic diameters and zeta potentials of the F8BT-PAAC*n* nanoparticles. Measurements were performed on a Malvern Zetasizer with a He-Ne laser (633 nm) and a back-scattering detector (173°). The hydrodynamic diameter and zeta potential were given as the mean value of three independent measurements. The error represents the standard deviation of the mean.

4.2.7. Cell culture

Human Embryonic Kidney 293 cells, HEK 293, were used for the cytotoxicity and cellular uptake studies. The HEK 293 cells were cultured in DMEM containing 10% FBS, and 100 units of penicillin per mL at 37 °C in a humidified atmosphere of 95% air and 5% CO_2.

4.2.8. In vitro cytotoxicity studies

The cytotoxicity of F8BT-PAAC*n* nanoparticles was evaluated using the MTT assay. The HEK 293 cells were seeded in a 96-well plate at a density of 5.0×10^4 cells cm^{-3} and allowed to adhere for 24 h. After removal of the culture medium, 150 mm^3 fresh culture medium

containing F8BT-PAAC*n* nanoparticles was added and allowed to incubate at 37 °C for 24 h. The five concentrations of F8BT-PAAC*n* nanoparticles tested in the culture medium were 5, 10, 15 and 20 ppm in F8BT. After 24 h incubation, 10 mm^3 of MTT (5.0 mg cm^{-3} in PBS) were added and incubated for 4 h. The medium was then replaced by 150 mm^3 of DMSO to completely dissolve the formazan crystals. The absorbance at 490 nm was measured using an ELX808 Absorbance Microplate Reader. The cell viability was calculated as a percentage of the culture medium only control.

4.2.9. Cellular uptake of F8BT-PAAC*n* nanoparticles

The cellular uptake of F8BT-PAAC*n* nanoparticles was characterized using confocal fluorescence microscopy. The HEK 293 cells were seeded in a 6-well plate loaded with cover-glass slides of 25 mm diameter at a density of 5.0×10^4 cells cm^{-3} and allowed to adhere for 24 h. After removal of the culture medium, the HEK 293 cells were incubated in 150 mm^{-3} of fresh culture medium containing F8BT-PAAC*n* nanoparticles (5 ppm in F8BT) at 37 °C for 24 h. The culture medium containing the F8BT-PAAC*n* nanoparticles was removed and cells were washed with PBS three times, and then fixed with 4% formaldehyde. The cell membrane was stained using 100 mm^{-3} of Alexa Fluor 594 (5.0 μg cm^{-3}) for 10 min at 25 °C. After thorough washing with PBS, the cells were incubated with 200 mm^{-3} of PBS. The cell culture, cell viability and cell samples for fluorescence images were performed by Xiaolin Cui in the School of Chemical Engineering at the University of Adelaide.

The fluorescence images were collected using a Leica TCS SP5 confocal laser scanning microscope. Fluorescent emission spectra were collected for Alexa Fluor 594 (λ_{ex} = 561 nm) and F8BT-PAAC*n* nanoparticles (λ_{ex} = 458 nm) over the wavelength ranges of 600 - 700 nm and 500 - 600 nm, respectively.

4.3. Synthesis of alkyl substituted poly(acrylate)s, PAAC*n*

Several poly(acrylate)s randomly substituted with linear alkyl groups were synthesized by reacting the appropriate alkyl amine with poly(acrylic acid) in the presence of a coupling agent, dicyclohexylcarbodiimide.[26] The molecular structures of the linear alkyl group substituted poly(acrylate)s are shown in Figure 4.1 and Figure 4.11 in Section 4.9 Appendix. In this study, the substituted poly(acrylate)s are abbreviated as PAAC*n*, where C*n* represents the alkyl substituent and *n* denotes the number of carbon atoms in that substituent. The 1H NMR spectra of synthesized PAACn and the corresponding substitution percentage are shown in Figures 4.12 - 4.14 in Section 4.9 Appendix.

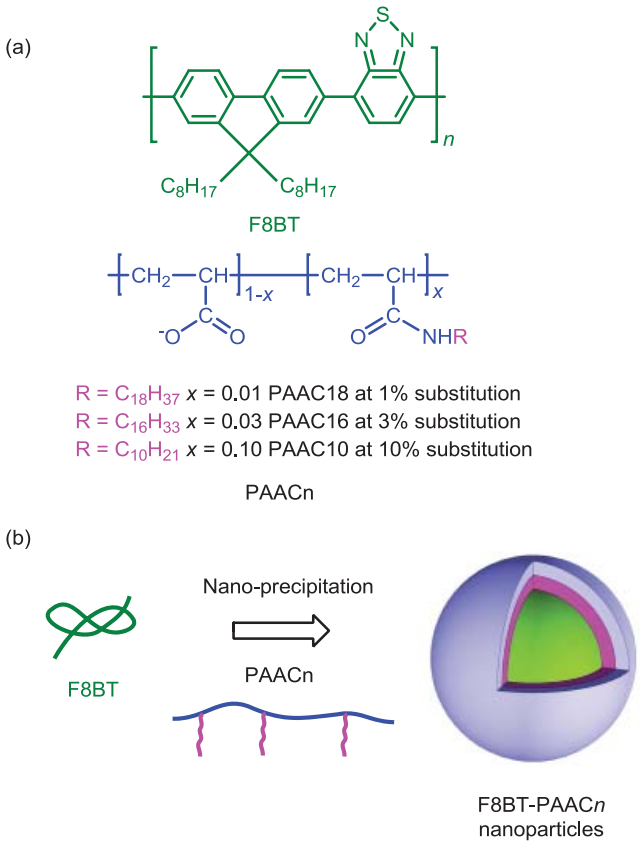

Figure 4.1. (a) Structures of F8BT and PAAC*n*. (b) Schematic illustration of the preparation of the F8BT-PAAC*n* nanoparticles.

4.4. Preparation of F8BT-PAAC*n* nanoparticles

A wide range of conjugated polymer nanoparticles have been prepared using the nano-precipitation method.[1,4,12,28,29] While such nanoparticles are highly stable in deionized water, they exhibit large-scale aggregation in salt solutions of high ionic strength,[23] which are often encountered in biological systems. Consequently, PAAC*n* is used to stabilize F8BT nanoparticles in PBS, a commonly used buffer with salt concentration similar to physiological conditions. In this study, a modified nano-precipitation method is employed to prepare stable PBS dispersions of F8BT-PAAC*n* nanoparticles. A THF solution of F8BT is injected by syringe into an aqueous solution of PAAC*n* under vigorous stirring. After removal of THF, a small quantity of 5 × PBS is added to the aqueous solution to yield a standard PBS dispersion of F8BT-PAAC*n* nanoparticles. When the solution of F8BT in THF is mixed with an aqueous solution of PAAC*n*, a decrease in F8BT solubility together with hydrophobic interactions within and between F8BT polymer chains causes F8BT aggregation and the formation of hydrophobic F8BT nanoparticles.[30] The hydrophobic alkyl substituents of PAAC*n* subsequently adsorb onto the surface of F8BT nanoparticles, yielding a negatively charged surface. Previously reported strong adsorption of alkyl chain segments of pluronic F-127 and Tween 80 at surface hydrophobic sites of polymer nanoparticles supports that the alkyl substituents of PAACn are adsorbed onto surface hydrophobic sites of F8BT nanoparticles.[31] As a consequence of the presence of the negatively charged carboxylate groups (Figure 4.1) on the surface, F8BT-PAAC*n* nanoparticles are stabilized in PBS.

4.4.1. Optimization of length and substitution percentage of the alkyl substituents of PAAC*n*

The length and substitution percentage of the alkyl substituents of PAAC*n* are expected to

influence their hydrophobic interactions with F8BT nanoparticles and thereby influence the adsorption of PAAC*n* onto the F8BT nanoparticle surface. Thus, the length and substitution percentage of the alkyl substituents were optimized according to the yield of F8BT-PAAC*n* nanoparticles in PBS (Equation 4.2), which represents the proportion of F8BT-PAAC*n* nanoparticles with a diameter less than 200 nm. The length of the linear alkyl substituents in PAAC*n* used in the preparation of the F8BT-PAAC*n* nanoparticles was varied from n = 6, 10, 12, 14, 16, to 18, and the extent of substitution was varied from 1% to 3% to 10%. Bare F8BT nanoparticles aggregate immediately upon being transferred to PBS forming aggregates that are larger than 200 nm. The aggregates give a yield of 0, as is also observed by another research group,[23] Similar aggregation of F8BT nanoparticles is also observed in the presence of sodium poly(acrylate), as shown in Figure 4.2. However, in the presence of 10% substituted PAAC10, 3% substituted PAAC16 or 1% substituted PAAC18, yields of F8BT-PAAC*n* nanoparticles in PBS approach 90%, which highlights the importance of the hydrophobic linear alkyl substituents of PAAC*n* in stabilizing F8BT-PAAC*n* nanoparticles in PBS.

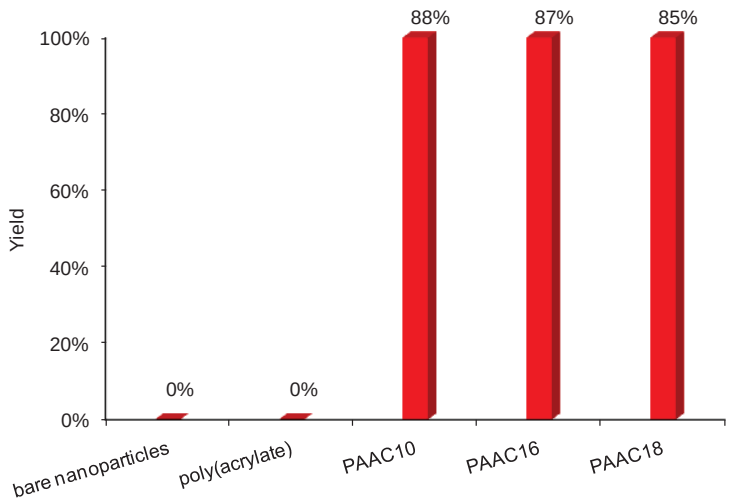

Figure 4.2. Yields of bare F8BT nanoparticles (< 200 nm) and F8BT nanoparticles (< 200 nm) stabilized with poly(acrylate), PAAC10 at 10% substitution, PAAC16 at 3% substitution and PAAC18 at 1% substitution in PBS.

The effect of the length of the linear alkyl substituent at a constant 3% substitution for PAAC*n* on the yield of F8BT-PAAC*n* nanoparticles of < 200 nm diameter is shown in Table 4.1. The zero yield obtained for PAAC6 indicates that the extent of hydrophobic interaction of the hexyl group with the F8BT nanoparticle surface is insufficient to stabilize the F8BT-PAAC6 nanoparticles. Substitution of the decyl group in PAAC10 results in a 74 ± 1% yield of F8BT-PAAC10 nanoparticles, and further lengthening of the alkyl substituent results in yields of 86 ± 1% and 87 ± 1% for F8BT-PAAC14 and F8BT-PAAC16 nanoparticles, respectively. Further lengthening of the alkyl substituent results in a decrease in yield to 83 ± 1% for F8BT-PAAC18 nanoparticles, consistent with hydrophobic interactions between the octadecyl groups within PAAC18 competing with hydrophobic interactions between PAAC18 and the F8BT nanoparticle surface. It has been reported that micelle-like aggregates formed in an aqueous solution of 3% substituted PAAC18 at or below a low concentration of 0.3 wt %, or 3000 ppm, through intra-PAAC18 hydrophobic octadecyl substituent interactions.[32] However, a viscous gel-like solution is observed at or above a high concentration of 2 wt % of 3% substituted PAAC18 due to inter-PAAC18 hydrophobic interactions between octadecyl substituents.[33] In the present study, because of the relatively low 50 ppm concentration of PAAC18, it is expected that only intra-PAAC18 chain hydrophobic octadecyl substituent interactions are involved.

Table 4.1. Yields of F8BT-PAAC*n* nanoparticles with diameters < 200 nm in PBS.[a]

Substitution percentage	Substituent					
	C6	C10	C12	C14	C16	C18
1%	[b]	[b]	55 ± 1%	[b]	[b]	85 ± 1%
3%	0	74 ± 1%	83 ± 1%	86 ± 1%	87 ± 1%	83 ± 1%
10%	80 ± 1%	88 ± 1%	81 ± 1%	[b]	[b]	[b]

[a]The yields are the mean of three independent deteminations. Quoted errors represent the standard deviations. A zero yield was obtained in the absence of PAAC*n*. [b]Yield not determined.

The substitution percentage onto the backbone of PAAC*n* also has an important role in stabilizing F8BT-PAAC*n* nanoparticles as is seen from Table 4.1. Thus, as substitution increases from 3% to 10% in PAAC6 the yield of F8BT-PAAC6 nanoparticles increases from 0% to 80 ± 1%. The increased substitution strengthens the hydrophobic interactions between the hexyl groups and F8BT nanoparticles as a result of the higher hexyl substituent density compensating for the lower hexyl homophobicity by comparison with those of longer alkyl groups. Similarly, for PAAC10 the yield increases from 74 ± 1% at 3% substitution to 88 ± 1% at 10% substitution. However, for PAAC12 an increase in substitution from 1% to 3% to 10% coincides with a change in yield from 55 ± 1% to 83 ± 1% to 81 ± 1%, respectively. The similarity between the yields at 3% and 10% substitution implies a weakening of the hydrophobic interactions between the dodecyl substituents and F8BT nanoparticles as a consequence of the increased dodecyl substituent density increasing competitive inter-substituent interactions. A similar effect is seen when the octadecyl substituent substitution increases from 1% to 3% in PAAC18 and the yield changes from 85 ± 1% to 83 ± 1%, respectively. Thus, the overall effect of the length and substitution percentage of the alkyl substituent determines the effectiveness of the PAAC*n* stabilizing F8BT nanoparticles in PBS.

4.4.2. Dependence of yields of preparing F8BT-PAAC*n* nanoparticles on the concentration of PAAC*n*

As the potential applications of PAAC*n* in stabilizing F8BT-PAAC*n* nanoparticles are an important consideration, the dependence of the yield of preparing F8BT-PAAC*n* nanoparticles in PBS on the concentration of aqueous solution of either PAAC18 at 1% substitution, PAAC16 at 3% substitution, and PAAC10 at 10% substitution was examined. As shown in Figure 4.3, these three PAAC*n* are able to adsorb effectively onto the surface of F8BT nanoparticles and stabilize them in PBS, as reflected by the observed high yields, at a low PAAC*n* concentration

of 50 ppm. This concentration is significantly lower than the SDS concentration (46,000 ppm) used in a recent study to stabilize F8BT nanoparticles.[19] When the concentration of either PAAC18 at 1% substitution or PAAC16 at 3% substitution is increased to 100 ppm, no significant increases in the yields occur. In contrast, a decreased yield is observed for PAAC10 at 10% substitution upon increase in concentration. The latter result may be attributable to competitive intra-chain hydrophobic interactions between decyl substituents, which weakens the hydrophobic interactions between decyl substituent and F8BT nanoparticles, given that a significantly higher number of decyl substituents are present at a concentration of 100 ppm.

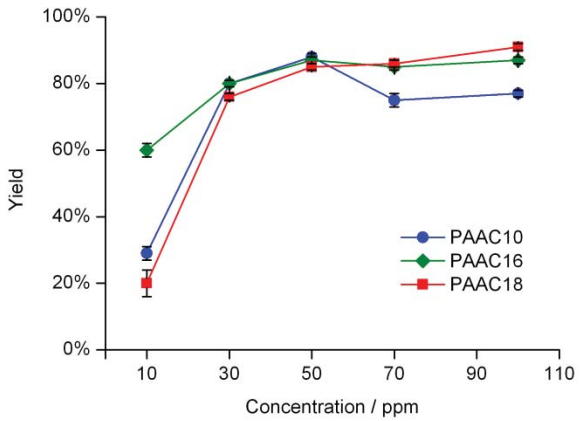

Figure 4.3. PAAC*n* concentration dependence of yields of F8BT nanoparticles (< 200 nm) stabilized with PAAC10 at 10% substitution, PAAC16 at 3% substitution, and PAAC18 at 1% substitution in PBS.

In summary, PAAC10 at 10% substitution, PAAC16 at 3% substitution, and PAAC18 at 1% substitution show similarly high yields (Figure 4.2) of 88 ± 1%, 87 ± 1%, and 85 ± 1%, at a low concentration of 50 ppm, and accordingly this concentration is used to prepare F8BT-PAAC*n* nanoparticles for further characterizations. In addition to their stabilizing effect, the PAAC*n* contain a high number of carboxylate groups, which are potential reactive sites for conjugation to functional biomolecules through well-established amide formation reaction. Chiu *et al.*

reported the preparation of conjugated polymer nanoparticles adsorbed with polyelectrolytes, which involved employment of two polyelectrolytes, poly(styrene sulfonate) as a stabilizer and poly(sodium methacrylate) to provide carboxylate groups as reactive sites for further bioconjugation.[23] In contrast, PAAC*n* surface functionalization offers the dual functions of offering stabilization and providing bioconjugation sites. Moreover, as the adsorption of PAAC*n* onto F8BT nanoparticles involves only hydrophobic interactions, PAAC*n* are expected to be useful stabilizers for other polymer nanoparticles or aggregates of organic materials.

4.5. Surface charge, size and colloidal stability of F8BT-PAAC*n* nanoparticles

4.5.1 Surface charge of F8BT-PAAC*n* nanoparticles

The negative surface charge of F8BT nanoparticles are evident from their zeta potentials of −26 ± 2, −57 ± 2, −58 ± 2 and −57 ± 4 mV for bare F8BT nanoparticles, F8BT-PAAC10, F8BT-PAAC16, and F8BT-PAAC18 nanoparticles, respectively, in deionized water, where PAAC10, PAAC16 and PAAC18 were 10%, 3% and 1% substituted, respectively. For bare conjugated polymer nanoparticles, the negatively charged surface has been attributed to surface chemical defects as a consequence of oxidation of the conjugated polymer in the formation of conjugated polymer nanoparticles.[34] By comparison with bare F8BT nanoparticles, F8BT-PAAC10, F8BT-PAAC16, and F8BT-PAAC18 nanoparticles have more negatively charged surfaces (Figure 4.4), as indicated by their more negative zeta potentials which are consistent with a high number of negatively charged carboxylate groups on the surface of the F8BT-PAAC*n* nanoparticles due to the presence of PAAC*n*.

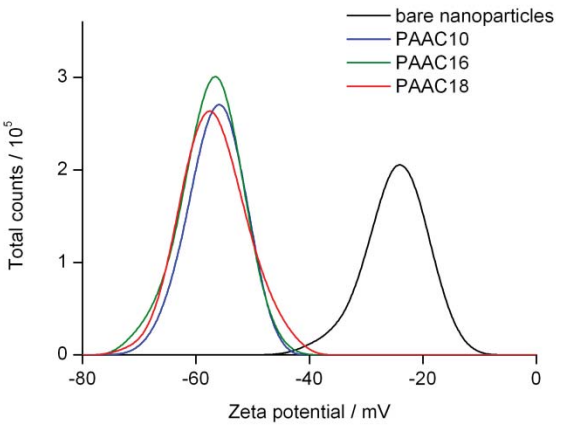

Figure 4.4. The zeta potentials of bare F8BT nanoparticles and F8BT nanoparticles stabilized with either PAAC10 at 10% substitution, PAAC16 at 3% substitution or PAAC18 at 1% substitution in deionized water.

4.5.2. Size of F8BT-PAAC*n* nanoparticles

The hydrodynamic diameters of bare F8BT nanoparticles and F8BT-PAAC*n* nanoparticles were measured using dynamic light scattering. Bare F8BT nanoparticles in deionized water have a hydrodynamic diameter of 39 ± 3 nm, while F8BT-PAAC10, F8BT-PAAC16, and F8BT-PAAC18 nanoparticles in PBS have hydrodynamic diameters of 49 ± 5, 57 ± 3 and 70 ± 3 nm, respectively (Figure 4.5). The larger hydrodynamic diameters of the F8BT-PAAC*n* nanoparticles in PBS than that of bare F8BT nanoparticles in deionized water are presumably due to a combination of salt-induced aggregation in PBS and the presence of the PAAC*n* on the surface. Figure 4.6 shows the transmission electron microscopy (TEM) images of the nanoparticles by using the negative stain, uranyl acetate. The spherical bare F8BT nanoparticles, F8BT-PAAC10, F8BT-PAAC16, and F8BT-PAAC18 nanoparticles appear as bright features surrounded by dark rings as a result of negative staining. The size of the F8BT-PAAC*n* nanoparticles in PBS increases slightly in the order: F8BT-PAAC10 < F8BT-PAAC16 < F8BT-PAAC18 consistent with a stronger binding between F8BT

nanoparticles and PAAC10 (at 10% substitution) and a weaker binding between F8BT nanoparticles and PAAC18 (at 1% substitution). This trend indicates that the higher alkyl substitution (10%) in PAAC10 enhances hydrophobic interactions with the F8BT nanoparticles and compensates for the weaker interaction between the decyl substituent and the F8BT nanoparticles by comparison with the stronger interaction of the octadecyl substituent of PAAC18 (at 1% substitution).

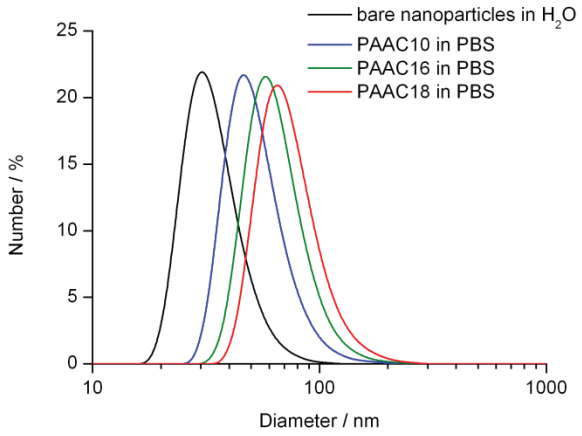

Figure 4.5. The apparent hydrodynamic diameters of bare F8BT nanoparticles in deionized water and F8BT nanoparticles stabilized with either PAAC10 at 10% substitution, PAAC16 at 3% substitution or PAAC18 at 1% substitution in PBS.

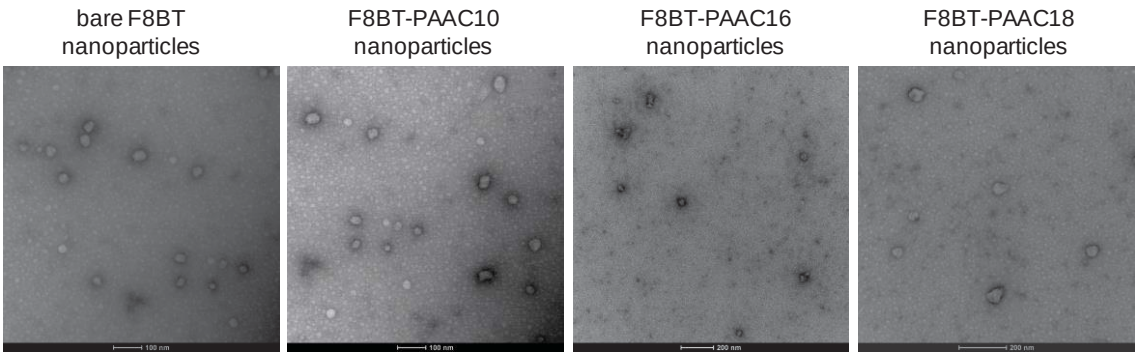

Figure 4.6. TEM images of bare F8BT nanoparticles and F8BT nanoparticles stabilized with either PAAC10 at 10% substitution, PAAC16 at 3% substitution or PAAC18 at 1% substitution.

4.5.3. Long-term colloidal stability of F8BT-PAAC*n* nanoparticles

The small size and long-term dispersion and colloidal stability of F8BT nanoparticles are critical characteristics for their biological imaging application. Figure 4.7 shows the F8BT nanoparticle size variation over a 4-week period. Bare F8BT nanoparticles in deionized water remain stable over four weeks without detectable size variations owing to a substantial zeta potential of −26 ± 2 mV. Similar colloidal stability has been reported for other conjugated polymer nanoparticles in deionized water.[1] In contrast, bare F8BT nanoparticles exhibit significant aggregation in PBS yielding aggregates larger than 200 nm, which is attributable to the ions in PBS providing a strong shielding effect of the negative surface charge of F8BT nanoparticles. However, when stabilized with PAAC*n* the resultant F8BT-PAAC*n* nanoparticles exhibit remarkable colloidal stability in PBS. As shown in Figure 4.7, the F8BT-PAAC10, F8BT-PAAC16 and F8BT-PAAC18 nanoparticles are very stable over 4 weeks without any aggregation. This phenomenon is attributed to the adsorption of either PAAC10, PAAC16 or PAAC18 on the F8BT nanoparticle surface, producing a negatively charged surface that greatly enhances their dispersion and colloidal stability. The small size, high

colloidal stability and negative surface charge pave the way for the deployment of F8BT-PAAC*n* nanoparticles in biological imaging applications.

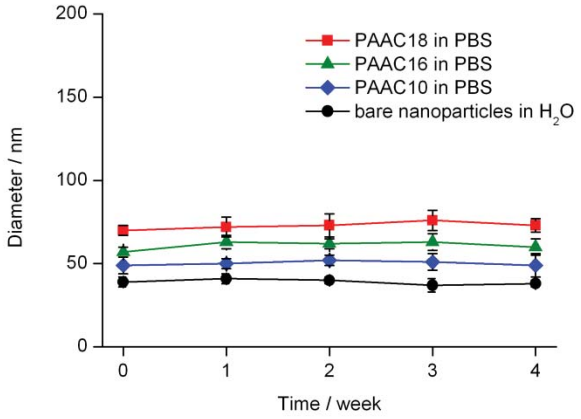

Figure 4.7. The size variation of bare F8BT nanoparticles in deionized water and F8BT nanoparticles stabilized with PAAC10 at 10% substitution, PAAC16 at 3% substitution, and PAAC18 at 1% substitution in PBS over a period of 4 weeks.

4.6. Fluorescence and cell imaging applications

4.6.1. UV-Vis absorption and fluorescence spectra of F8BT-PAAC*n* nanoparticles

The normalized UV-Vis absorption and fluorescence spectra of bare F8BT nanoparticles in deionized water and F8BT-PAAC16 nanoparticles in PBS are shown in Figure 4.8. The absorption and fluorescence spectra of F8BT-PAAC16 nanoparticles in PBS are similar to those of bare F8BT nanoparticles in deionized water. Similar absorption and fluorescence spectra are also observed for F8BT-PAAC18 and F8BT-PAAC10 nanoparticles in PBS (Figures 4.15 and 4.16 in Section 4.9 Appendix). In several studies the optical properties of conjugated polymer nanoparticles have been investigated and related to the polymer conformation in the nanoparticle, conjugation length of chromophores, intra- and

inter-polymer strand aggregation.[35-37] The similar absorption and fluorescence spectra of F8BT nanoparticles with and without PAAC*n* suggest that the F8BT nanoparticles have similar polymer chain conformation, packing and folding under both conditions. Thus, the presence of PAAC*n* does not interfere the formation of F8BT nanoparticles, indicating that the alkyl substituents are predominantly adsorbed onto the hydrophobic sites on the surface of the F8BT nanoparticles and do not penetrate deeply into the nanoparticle. This phenomenon has implications on the fluorescence quantum yields of bare F8BT NPs in deionized water and F8BT-PAAC*n* NPs in PBS. The fluorescence quantum yields of bare F8BT nanoparticles in deionized water, F8BT-PAAC18, F8BT-PAAC16, and F8BT-PAAC10 nanoparticles in PBS are 24 ± 1%, 25 ± 1%, 26 ± 1% and 27 ± 1%, respectively. The fluorescence quantum yield values from this study are comparable with literature values of 28%[22] and 30%.[2,19] The similar fluorescence quantum yields of bare F8BT nanoparticles in deionized water and F8BT-PAAC*n* nanoparticles in PBS indicate that the emitting chromophores of F8BT-PAAC*n* nanoparticles are located near the core of the nanoparticles such that the influence exerted by the alkyl substituents on the surface of the F8BT-PAAC*n* nanoparticles is negligible. This interpretation is consistent with a recent study which shows that the emitting chromophores of a conjugated polymer aggregate are located near the core and away from the surface of the aggregate.[38]

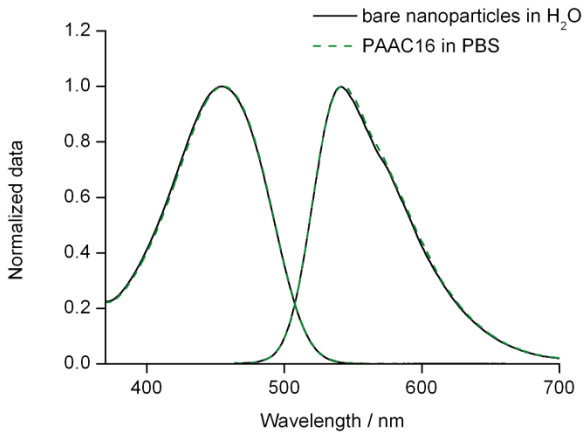

Figure 4.8. Normalized absorption and fluorescence spectra of bare F8BT nanoparticles (solid) and F8BT nanoparticles stabilized with PAAC16 at 3% substitution (dashed).

4.6.2. Cytotoxicity of F8BT-PAAC*n* nanoparticles

The biocompatibility of F8BT-PAAC*n* nanoparticles is critical for future biological imaging applications, and accordingly their cytotoxicities toward HEK 293 cells were examined using the MTT assay. The viability of HEK 293 cells incubated with F8BT-PAAC18, F8BT-PAAC16 and F8BT-PAAC10 nanoparticles at concentrations ranging from 0 to 20 ppm for 24 h is shown in Figure 4.9. No significant cytotoxicities toward HEK 293 cells are observed for these nanoparticles, although there is a minor decrease in cell viability as a function of concentration. With a concentration of 20 ppm and an incubation period of 24h, HEK 293 cells exhibit a cell viability value of approximately 70% for F8BT-PAAC16 and F8BT-PAAC10 nanoparticles and approximately 80% for F8BT-PAAC18 nanoparticles. The cell viability results reported herein are consistent with those reported in other studies.[19,39] For instance, Christensen *et al.* showed that bare F8BT nanoparticles (with a molecular weight of 10000 g mol^{-1}) had no discernible impact on the viability and growth of J774A.1 cells after 18 h incubation at a concentration ranging from 1 to 25 ppm.[39] In their study, a cell viability of approximately 75% was observed for bare F8BT nanoparticles at 25 ppm. In addition, Dailey *et al.* found that F8BT

nanoparticles stabilized with sodium dodecyl sulfate (F8BT-SDS nanoparticles) were highly biocompatible towards J774A.1 cells over the concentration range of 0 to 100 ppm.[22] A cell viability of 80% was observed when J774A.1 cells were incubated with 100 ppm of F8BT-SDS nanoparticles for 24 h. Overall, the results of the present study show that the F8BT-PAAC*n* nanoparticles are biocompatible and suitable for biological applications.

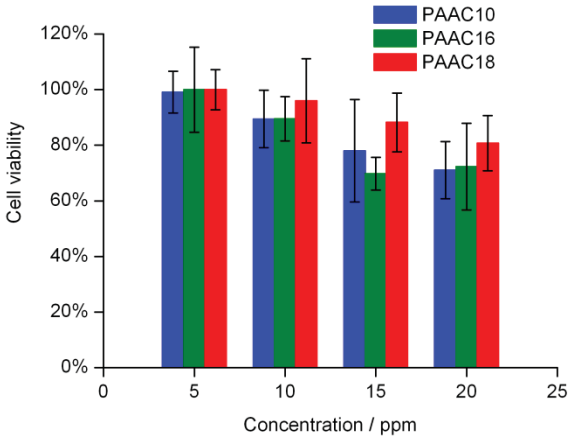

Figure 4.9. Viability of HEK 293 cells incubated with F8BT nanoparticles stabilized with PAAC18 at 1% substitution, PAAC16 at 3% substitution, and PAAC10 at 10% substitution at various concentrations ranging from 0 to 25 ppm, as determined using the MTT assay.

4.6.3. F8BT-PAAC*n* nanoparticles in a cell imaging application

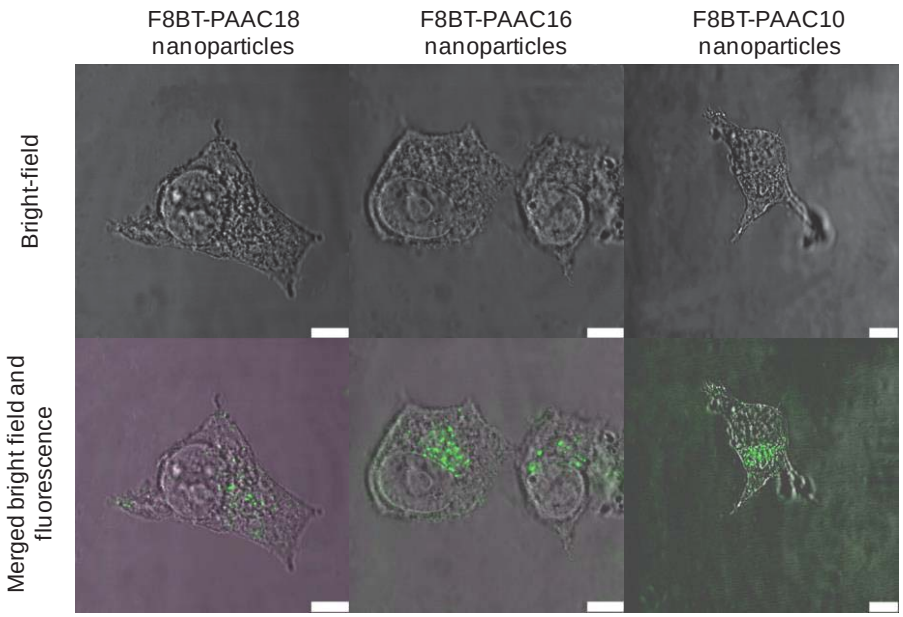

Figure 4.10. Bright-field images and confocal fluorescence images of HEK 293 cells treated with F8BT nanoparticles stabilized with PAAC18 at 1% substitution, PAAC16 at 3% substitution, and PAAC10 at 10% substitution, respectively. In the merged bright field and fluorescence images, the green emission is derived from F8BT-PAAC*n* nanoparticles. Scale bar: 7.5 μm.

As F8BT-PAAC*n* nanoparticles are of potential use in intracellular imaging[1] and drug delivery,[15,16] we examined their uptake by HEK 293 cells. Confocal fluorescence microscopy images of HEK 293 cells treated with F8BT-PAAC18, F8BT-PAAC16 and F8BT-PAAC10 nanoparticles, respectively, show a strong green fluorescence over the range 500 - 600 nm in the cell cytoplasm (Figure 4.10). In a separate study, the cell membranes of HEK 293 cells were stained with Alexa Fluor 594 and the images are shown in Figure 4.17 in Section 4.9 Appendix. These images show that the F8BT-PAAC*n* nanoparticles are located on the same focal plane as the membrane, which further support the internalization of F8BT-PAAC*n* nanoparticles by HEK 293 cells. These results strongly suggest the feasibility of using F8BT-PAAC*n* F8BT-PAAC*n* nanoparticles as fluorescence labels for cell imaging.

The mechanism of cellular uptake of bare F8BT nanoparticles (with a molecular weight of 10000 g mol^{-1}) by J774 A.1 cells has been investigated by Christensen *et al*.[39] These authors showed that F8BT nanoparticles previously treated with a number of pharmacological reagents exhibit inhibition of specific cellular process. They reported a significant inhibition of F8BT nanoparticle uptake for nanoparticles treated with wortmannin, LY294002, and methyl-β-cyclodextrin. This result is consistent with F8BT nanoparticle uptake occurring through a constitutive macropinocytosis mechanism. It is likely that a similar mechanism is involved in the uptake of F8BT-PAAC*n* nanoparticles. It is anticipated that loading of multifunctional materials or therapeutic agents into the F8BT-PAAC*n* nanoparticles may enable its further applications in diagnosis or therapeutics.

4.7. Conclusions

We report the preparation of highly fluorescent and stable F8BT-PAAC*n* nanoparticles with hydrodynamic diameters ranging from 49 ± 5 to 70 ± 3 nm. The successful functionalization of PAAC*n* onto the surface of F8BT nanoparticles is based on the association of the alkyl substituents, C*n*, with the hydrophobic sites on the F8BT nanoparticle surface. In contrast to the rapid, large-scale aggregation of bare F8BT nanoparticles in PBS, a high colloidal stability of F8BT-PAAC*n* nanoparticles in PBS is observed, as indicated by a negligible size variation over a 4-week period. This high colloidal stability under the condition of high ionic strength is ascribed to a high surface charge density as a consequence of the PAAC*n* adsorption bearing a large number of carboxylate groups. In addition, F8BT-PAAC*n* nanoparticles show very low toxicity to HEK 293 cells and are easily internalized by these cells. Consequently, F8BT-PAAC*n* nanoparticles hold considerable promise for use in cell imaging application given their high colloidal stability in PBS and high fluorescence quantum yield.

4.8. References

(1) Wu, C.; Bull, B.; Szymanski, C.; Christensen, K.; McNeill, J. Multicolor conjugated polymer dots for biological fluorescence imaging. *ACS Nano* **2008**, *2*, 2415-2423.

(2) Wu, C.; Schneider, T.; Zeigler, M.; Yu, J.; Schiro, P. G.; Burnham, D. R.; McNeill, J. D.; Chiu, D. T. Bioconjugation of ultrabright semiconducting polymer dots for specific cellular targeting. *J. Am. Chem. Soc*. **2010**, *132*, 15410-15417.

(3) Yu, J.; Wu, C.; Zhang, X.; Ye, F.; Gallina, M. E.; Rong, Y.; Wu, I. C.; Sun, W.; Chan, Y.-H.; Chiu, D. T. Stable functionalization of small semiconducting polymer dots via covalent cross-linking and their application for specific cellular imaging. *Adv. Mater*. **2012**, *24*, 3498-3504.

(4) Liu, H.-Y.; Wu, P.-J.; Kuo, S.-Y.; Chen, C.-P.; Chang, E.-H.; Wu, C.-Y.; Chan, Y.-H. Quinoxaline-based polymer dots with ultrabright red to near-infrared fluorescence for in vivo biological imaging. *J. Am. Chem. Soc*. **2015**, *137*, 10420-10429.

(5) Chen, C.-P.; Huang, Y.-C.; Liou, S.-Y.; Wu, P.-J.; Kuo, S.-Y.; Chan, Y.-H. Near-infrared fluorescent semiconducting polymer dots with high brightness and pronounced effect of positioning alkyl chains on the comonomers. *ACS Appl. Mater. Interfaces* **2014**, *6*, 21585-21595.

(6) Jin, Y.; Ye, F.; Zeigler, M.; Wu, C.; Chiu, D. T. Near-infrared fluorescent dye-doped semiconducting polymer dots. *ACS Nano* **2011**, *5*, 1468-1475.

(7) Chan, Y.-H.; Ye, F.; Gallina, M. E.; Zhang, X.; Jin, Y.; Wu, I. C.; Chiu, D. T. Hybrid semiconducting polymer dot-quantum dot with narrow-band emission, near-infrared fluorescence, and high brightness. *J. Am. Chem. Soc.* **2012**, *134*, 7309-7312.

(8) Chan, Y.-H.; Wu, C.; Ye, F.; Jin, Y.; Smith, P. B.; Chiu, D. T. Development of ultrabright semiconducting polymer dots for ratiometric pH sensing. *Anal. Chem*. **2011**, *83*, 1448-1455.

(9) Czaplyski, W. L.; Purnell, G. E.; Roberts, C. A.; Allred, R. M.; Harbron, E. J. Substituent effects on the turn-on kinetics of rhodamine-based fluorescent pH probes. *Org. Biomol. Chem.* **2014**, *12*, 526-533.

(10) Ye, F.; Wu, C.; Jin, Y.; Chan, Y.-H.; Zhang, X.; Chiu, D. T. Ratiometric temperature sensing with semiconducting polymer dots. *J. Am. Chem. Soc.* **2011**, *133*, 8146-8149.

(11) Wu, C.; Bull, B.; Christensen, K.; McNeill, J. Ratiometric single-nanoparticle oxygen sensors for biological imaging. *Angew. Chem. Int. Ed*. **2009**, *48*, 2741-2745.

(12) Dmitriev, R. I.; Borisov, S. M.; Düssmann, H.; Sun, S.; Müller, B. J.; Prehn, J.; Baklaushev, V. P.; Klimant, I.; Papkovsky, D. B. Versatile conjugated polymer nanoparticles for high-resolution O_2 imaging in cells and 3D tissue models. *ACS Nano* **2015**, *9*, 5275-5288.

(13) Huang, Y.-C.; Chen, C.-P.; Wu, P.-J.; Kuo, S.-Y.; Chan, Y.-H. Coumarin dye-embedded semiconducting polymer dots for ratiometric sensing of fluoride ions in aqueous solution and bio-imaging in cells. *J. Mater. Chem. B* **2014**, *2*, 6188-6191.

(14) Childress, E. S.; Roberts, C. A.; Sherwood, D. Y.; LeGuyader, C. L. M.; Harbron, E. J. Ratiometric fluorescence detection of mercury ions in water by conjugated polymer nanoparticles. *Anal. Chem.* **2012**, *84*, 1235-1239.

(15) Feng, X.; Lv, F.; Liu, L.; Tang, H.; Xing, C.; Yang, Q.; Wang, S. Conjugated polymer nanoparticles for drug delivery and imaging. *ACS Appl. Mater. Interfaces* **2010**, *2*, 2429-2435.

(16) Yuan, Y.; Wang, Z.; Cai, P.; Liu, J.; Liao, L.-D.; Hong, M.; Chen, X.; Thakor, N.; Liu, B. Conjugated polymer and drug co-encapsulated nanoparticles for chemo- and photo-thermal combination therapy with two-photon regulated fast drug release. *Nanoscale* **2015**, *7*, 3067-3076.

(17) Geng, J.; Sun, C.; Liu, J.; Liao, L.-D.; Yuan, Y.; Thakor, N.; Wang, J.; Liu, B. Biocompatible conjugated polymer nanoparticles for efficient photothermal tumor therapy. *Small* **2015**, *11*, 1603-1610.

(18) Shen, X.; Li, L.; Wu, H.; Yao, S. Q.; Xu, Q.-H. Photosensitizer-doped conjugated polymer nanoparticles for simultaneous two-photon imaging and two-photon photodynamic therapy in Living Cells. *Nanoscale* **2011**, *3*, 5140-5146.

(19) Ahmad Khanbeigi, R.; Abelha, T. F.; Woods, A.; Rastoin, O.; Harvey, R. D.; Jones, M.-C.; Forbes, B.; Green, M. A.; Collins, H.; Dailey, L. A. Surface chemistry of photoluminescent F8BT conjugated polymer nanoparticles determines protein corona formation and internalization by phagocytic cells. *Biomacromolecules* **2015**, *16*, 733-742.

(20) Pu, K.; Shuhendler, A. J.; Valta, M. P.; Cui, L.; Saar, M.; Peehl, D. M.; Rao, J. Phosphorylcholine-coated semiconducting polymer nanoparticles as rapid and efficient labeling agents for in vivo cell tracking. *Adv. Healthcare Mater*. **2014**, *3*, 1292-1298.

(21) Pu, K.; Shuhendler, A. J.; Jokerst, J. V.; Mei, J.; Gambhir, S. S.; Bao, Z.; Rao, J. Semiconducting polymer nanoparticles as photoacoustic molecular imaging probes in living mice. *Nature Nanotechnol*. **2014**, *9*, 233-239.

(22) Wu, C.; Jin, Y.; Schneider, T.; Burnham, D. R.; Smith, P. B.; Chiu, D. T. Ultrabright and bioorthogonal labeling of cellular targets using semiconducting polymer dots and click

chemistry. *Angew. Chem. Int. Ed*. **2010**, *49*, 9436-9440.

(23) Jin, Y.; Ye, F.; Wu, C.; Chan, Y.-H.; Chiu, D. T. Generation of functionalized and robust semiconducting polymer dots with polyelectrolytes. *Chem. Commun*. **2012**, *48*, 3161-3163.

(24) Davis, M. E.; Chem, Z.; Shin, D. M. Nanoparticle therapeutics: An emerging treatment modality for cancer. *Nat. Rev. Drug Discov.* **2008,** *7*, 771-782.

(25) Wang, S.; Huang, P.; Chen, X. Stimuli-responsive programmed specific targeting in nanomedicine. *ACS Nano* **2016**. [Online early access]. DOI: 10.1021/acsnano.6b00870. Published Online: February *16*, 2016. http://pubs.acs.org/doi/abs/10.1021/acsnano.6b00870 (accessed February *22*, 2016)

(26) Guo, X.; Abdala, A. A.; May, B. L.; Lincoln, S. F.; Khan, S. A.; Prud'Homme, R. K. Novel associative polymer networks based on cyclodextrin inclusion compounds. *Macromolecules* **2005**, *38*, 3037-3040.

(27) Würth, C.; Grabolle, M.; Pauli, J.; Spieles, M.; Resch-Genger, U. Relative and absolute determination of fluorescence quantum yields of transparent samples. *Nat. Protocols* **2013**, *8*, 1535-1550.

(28) Wu, C.; Szymanski, C.; McNeill, J. Preparation and encapsulation of highly fluorescent conjugated polymer nanoparticles. *Langmuir* **2006**, *22*, 2956-2960.

(29) Wu, C.; Szymanski, C.; Cain, Z.; McNeill, J. Conjugated polymer dots for multiphoton fluorescence imaging. *J. Am. Chem. Soc*. **2007**, *129*, 12904-12905.

(30) Wu, C.; Chiu, D. T. Highly fluorescent semiconducting polymer dots for biology and medicine. *Angew. Chem. Int. Ed*. **2013**, *52*, 3086-3109.

(31) Reisch, A.; Runser, A.; Arntz, Y.; Mély, Y.; Klymchenko, A. S. Charge-controlled nanoprecipitation as a modular approach to ultra small polymer nanocarriers: Making bright and stable nanoparticles. *ACS Nano* **2015**, *9*, 5104-5116.

(32) Harada, T.; Pham, D.-T.; Lincoln, S. F.; Kee, T. W. The capture and stabilization of curcumin using hydrophobically modified polyacrylate aggregates and hydrogels. *J. Phys. Chem. B* **2014**, *118*, 9515-9523.

(33) Li, L.; Guo, X.; Fu, L.; Prud'homme, R. K.; Lincoln, S. F. Complexation behavior of α-, β-, and γ-cyclodextrin in modulating and constructing polymer networks. *Langmuir* **2008**, *24*, 8290-8296.

(34) Clafton, S. N.; Beattie, D. A.; Mierczynska-Vasilev, A.; Acres, R. G.; Morgan, A. C.; Kee, T. W. Chemical defects in the highly fluorescent conjugated polymer dots. *Langmuir*

2010, *26*, 17785-17789.

(35) Sun, K.; Chen, H.; Wang, L.; Yin, S.; Wang, H.; Xu, G.; Chen, D.; Zhang, X.; Wu, C.; Qin, W. Size-dependent property and cell labeling of semiconducting polymer dots. *ACS Appl. Mater. Interfaces* **2014**, *6*, 10802-10812.

(36) Nguyen, T.-Q.; Doan, V.; Schwartz, B. J. Conjugated polymer aggregates in solution: Control of interchain interactions. *J. Chem. Phys*. **1999**, *110*, 4068-4078.

(37) Nguyen, T.-Q.; Martini, I. B.; Liu, J.; Schwartz, B. J. Controlling interchain interactions in conjugated polymers: The effects of chain morphology on exciton-exciton annihilation and aggregation in MEH-PPV Films. *J. Phys. Chem. B* **2000**, *104*, 237-255.

(38) Tapping, P. C.; Clafton, S. N.; Schwarz, K. N.; Kee, T. W.; Huang, D. M. Molecular-level details of morphology-dependent exciton migration in poly(3-hexylthiophene) nanostructures. *J. Phys. Chem. C* **2015**, *119*, 7047-7059.

(39) Fernando, L. P.; Kandel, P. K.; Yu, J.; McNeill, J.; Ackroyd, P. C.; Christensen, K. A. Mechanism of cellular uptake of highly fluorescent conjugated polymer nanoparticles. *Biomacromolecules* **2010**, *11*, 2675-2682.

4.9. Appendix

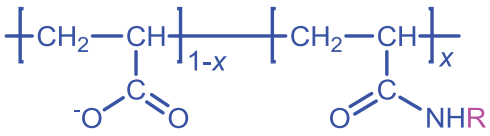

R = C_6H_{13} *x* = 0.03 PAAC6 at 3% substitution
R = C_6H_{13} *x* = 0.10 PAAC6 at 10% substitution
R = $C_{10}H_{21}$ *x* = 0.03 PAAC10 at 3% substitution
R = $C_{12}H_{25}$ *x* = 0.01 PAAC12 at 1% substitution
R = $C_{12}H_{25}$ *x* = 0.03 PAAC12 at 3% substitution
R = $C_{12}H_{25}$ *x* = 0.10 PAAC12 at 10% substitution
R = $C_{14}H_{29}$ *x* = 0.03 PAAC14 at 3% substitution
R = $C_{18}H_{37}$ *x* = 0.03 PAAC18 at 3% substitution

Figure 4.11. Chemical structures of PAAC*n*.

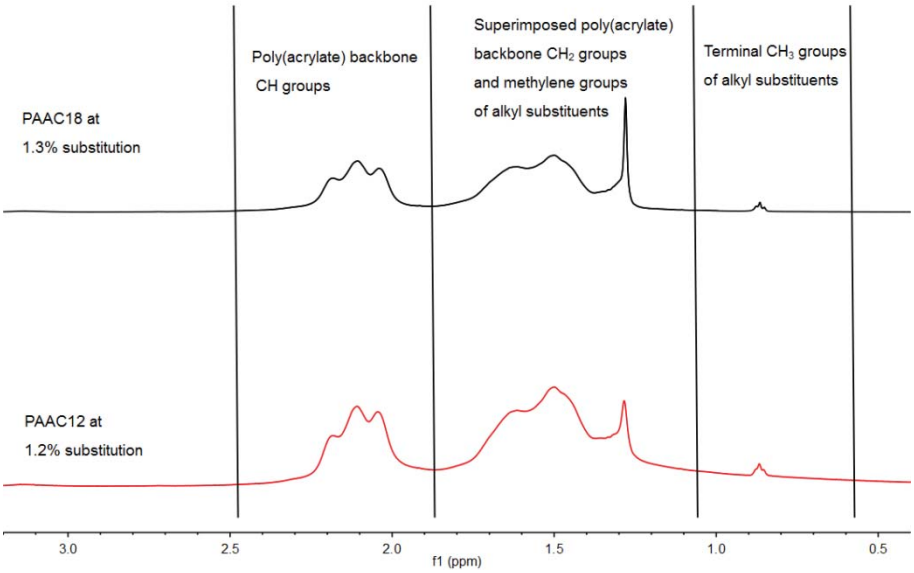

Figure 4.12. ^{1}H NMR spectra of PAAC18 and PAAC12 at 1% substitution.

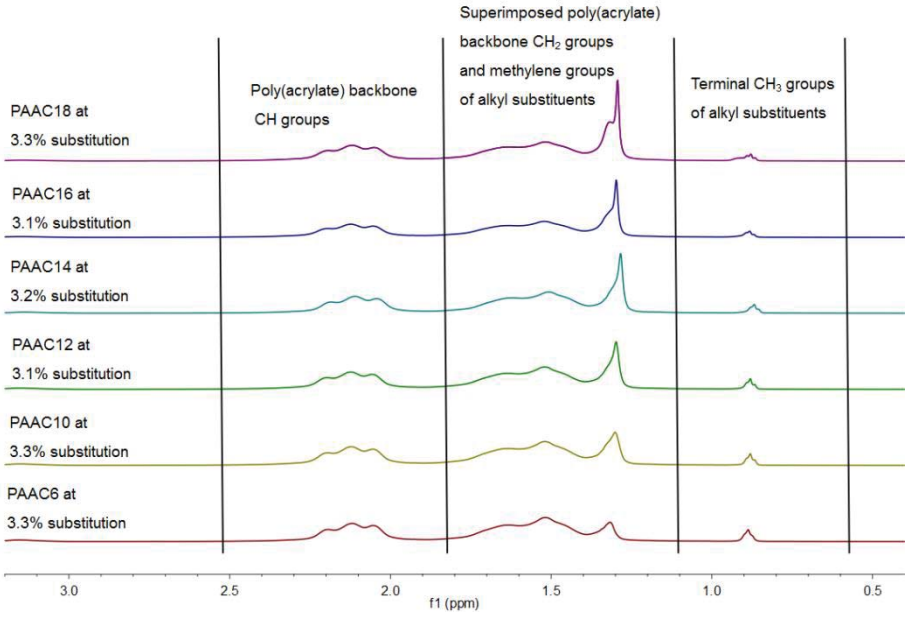

Figure 4.13. ^{1}H NMR spectra of PAAC18, PAAC16, PAAC14, PAAC12, PAAC10 and PAAC6 at 3% substitution.

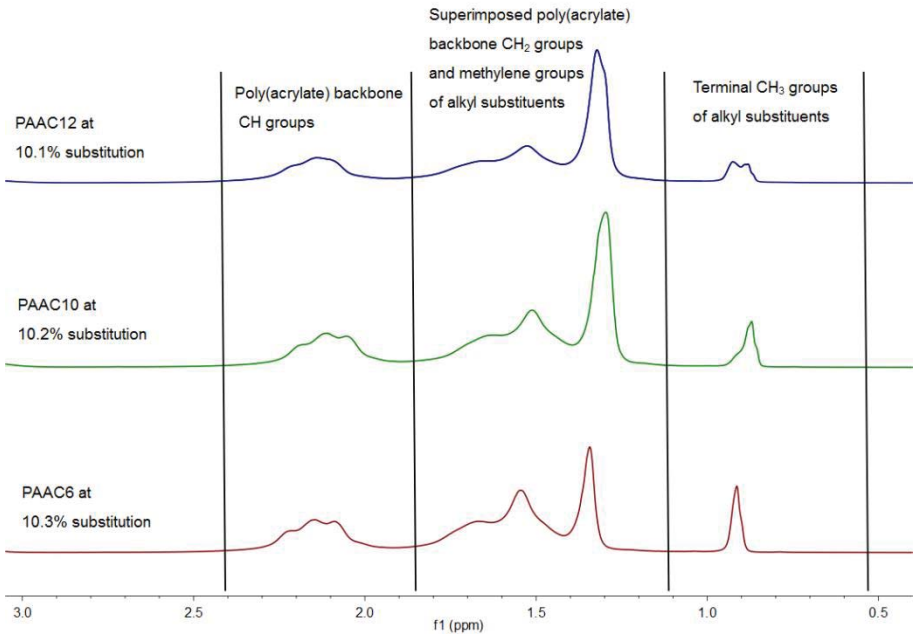

Figure 4.14. ^{1}H NMR spectra of PAAC12, PAAC10 and PAAC6 at 10% substitution.

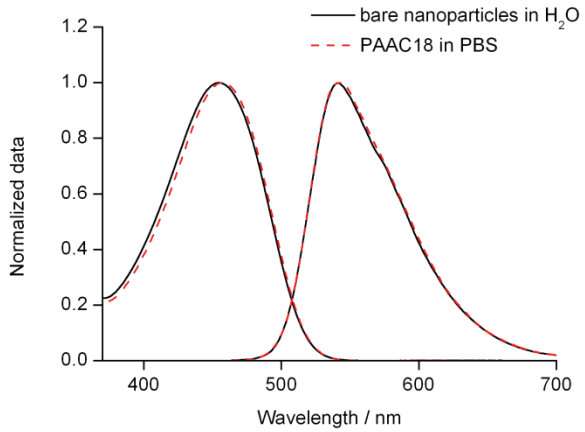

Figure 4.15. Normalized absorption and fluorescence spectra of bare F8BT nanoparticles in deionized water (solid) and F8BT nanoparticles stabilized with PAAC18 at 1% substitution in PBS (dashed).

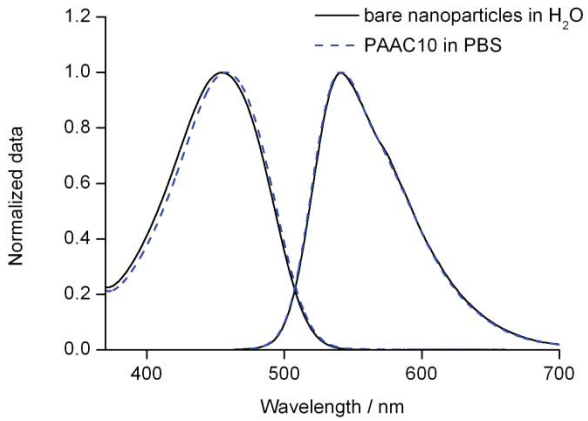

Figure 4.16. Normalized absorption and fluorescence spectra of bare F8BT nanoparticles in deionized water (solid) and F8BT nanoparticles stabilized with PAAC10 at 10% substitution in PBS (dashed).

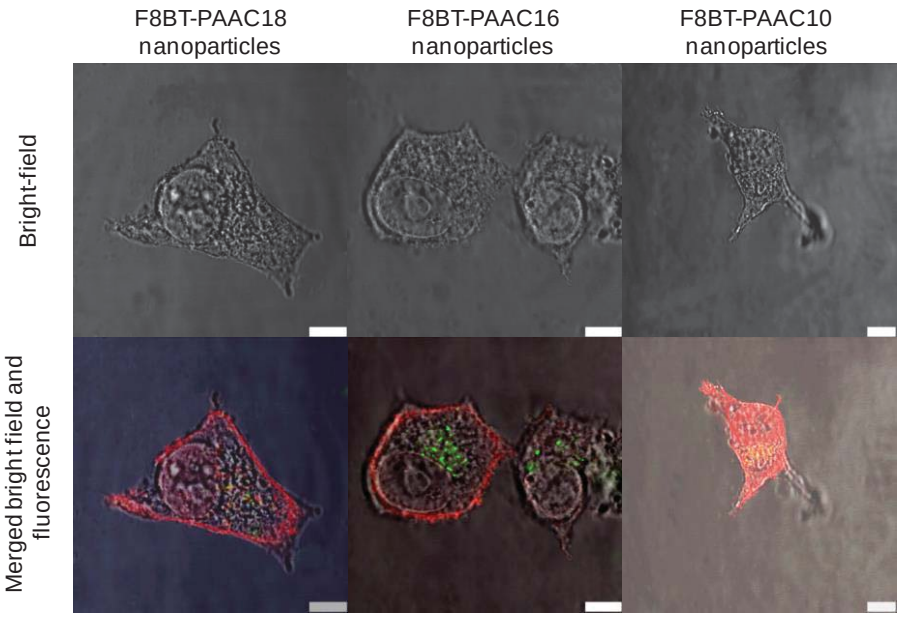

Figure 4.17. Bright-field images and confocal fluorescence images of HEK 293 cells treated with F8BT nanoparticles stabilized with PAAC18 at 1% substitution, PAAC16 at 3% substitution, PAAC10 at 10% substitution, respectively. In the merged bright field and fluorescence images, the red emission is derived from the membrane stain, Alexa Fluor 594, and the green emission is derived from F8BT-PAAC*n* nanoparticles. Scale bar: 7.5 μm.

CHAPTER 5

STABILIZING FLUORESCENTCONJUGATED POLYMER NANOPARTICLES USING BOVINE SERUM ALBUMIN

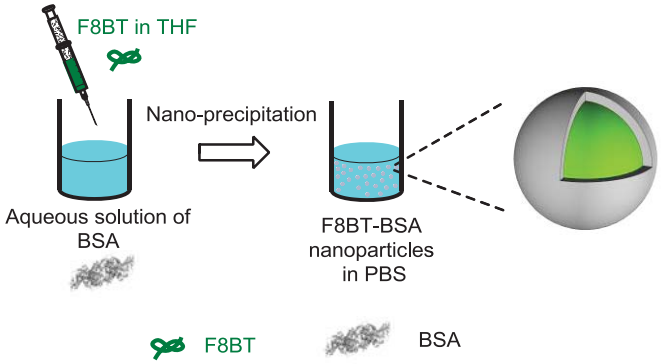

5.1. Introduction

Bovine serum albumin (BSA) is a major bovine blood plasma protein with well-defined structure and properties.[1] It is a complex amphiphilic biopolymer, comprising hydrophobic and hydrophilic domains. This feature facilitates the adhesion of BSA onto suitable solid interfaces, particularly surfaces of nanoparticles.[2-5] Taking its biocompatibility, non-cytotoxicity, and immunogenicity properties into account, BSA is an appealing coating material for nanoparticles in biological applications to provide stabilization effects[6,7] and binding sites[8] for biomolecules. Therefore, BSA has been widely used in the preparation of functional nanoparticles, ranging from metal and metal oxide,[8-13] semiconductors,[14,15] small organic molecules[16,17] to protein-polymer conjugate nanoparticles.[18-20] For instance, Ying *et al.* reported a BSA-directed preparation of fluorescent gold nanoclusters.[12] Upon addition of Au ions to the aqueous BSA solution, Au ions were sequestered and entrapped. After adjusting the reaction pH, the reduction ability of BSA was activated and the entrapped Au ions were reduced to form Au clusters. These Au-BSA nanoclusters were highly stable for at least two months and have a fluorescence quantum yield of 6%. In addition to metal nanoparticles, Tang *et al.* used BSA as the polymer matrix to prepare organic luminogen loaded BSA nanoparticles for in vitro and in vivo imaging applications.[17] This work led to a novel class of organic luminogen nanoparticles in which emission was greatly enhanced through aggregation. These organic luminogen-BSA nanoparticles showed uniform size, spherical morphology, and low cytotoxicity. They also showed an improved cancer-cell uptake and tumor-targeting capability arising from their enhanced permeability and retention effect with respect to these cells, and thus are promising fluorescent probes for cancer imaging and diagnostics.

Conjugated polymer nanoparticles have recently emerged as attractive fluorescent probes

in biological applications, due to their high brightness, excellent photostability and low cytotoxicity.[21] As a consequence of these features, conjugated polymer nanoparticles have a wide range of applications, exemplified by cellular imaging,[22-25] drug delivery,[26,27] photothermal[26,28] and photodynamic therapy,[29] and sensing of biological agents.[30-33] However, conjugated polymer nanoparticles exhibit large-scale aggregation and precipitation at high ionic strength found in physiological condition, which is a major obstacle to their biological application. Thus, it is desirable to develop conjugated polymer nanoparticles with a high colloidal stability under high ionic strength conditions. In addition, it is also desirable to functionalize conjugated polymer nanoparticles with surface reactive sites for conjugation to biomolecules. In chapter 4, we have developed alkyl chain substituted poly(acrylate)s as stabilizing materials, which can be adsorbed onto the surface of conjugated polymer naoparticles through hydrophobic interactions. The alkyl chain substituted poly(acrylate)s cover the surface of conjugated polymer nanoparticles with a large number of carboxylate groups, which simultaneously provide a high surface charge which stabilizes the nanoparticles and offer reactive surface sites for bioconjugation. As an extension to the research work described in Chapter 4, we selected BSA as a stabilizing material for conjugated polymer nanoparticles, not only because of its biocompatibility, commercial-availability and low cytotoxicity, but also because of its preferential accumulation in tumors through the enhanced permeability and retention effect.[34]

In this study, conjugated polymer nanoparticles stabilized with BSA, CP-BSA nanoparticles, were prepared using a modified nano-precipitation method.[35] The conjugated polymers, poly[(9,9-dioctylfluorenyl-2,7-diyl)-alt-co-(1,4-benzo-[2,1,3]-thiadiazole)], F8BT, poly(9,9-dioctylfluorenyl-2,7-diyl), PDOF, and poly[2-methoxy-5-(2-ethylhexyloxy) -1-4-phenylenevinylene], MEHPPV, were used to prepare F8BT-BSA, PDOF-BSA and MEHPPV-BSA nanoparticles. The hydrodynamic diameters of F8BT-BSA, PDOF-BSA and

MEHPPV-BSA nanoparticles are 59 ± 6, 37 ± 3 and 19 ± 1 nm, respectively. A high colloidal stability in phosphate buffered saline (PBS) at pH 7.4 over 4 weeks are observed for F8BT-BSA and PDOF-BSA nanoparticles, while MEHPPV-BSA nanoparticles exhibit partial aggregation after 3 weeks. In contrast to individual bare conjugated polymer nanoparticles which show large-scale aggregation in PBS, this high colloidal stability is ascribed to a combination of negative surface charge reflected by negative zeta potential values and steric stabilization as a consequence of the bulk 3D structure of BSA.[12] The optical properties of these CP-BSA nanoparticles in PBS are similar to those of the corresponding bare conjugated polymer nanoparticles in deionized water. Thus, they retain their high luminescence at high ionic strength conditions which paves the way for their use in biological applications.

5.2. Experimental section

5.2.1. Materials

Poly[(9,9-dioctylfluorenyl-2,7-diyl)-alt-co-(1,4-benzo-[2,1,3]-thiadiazole)] (F8BT, average molecular weight: 42,000 g mol^{-1}), poly(9,9-dioctylfluorenyl-2,7-diyl)-end-capped with DMP (PDOF, average molecular weight: 48,800 g mol^{-1}), and poly[2-methoxy-5-(2-ethylhexyloxy)-1-4-phenylenevinylene]-end-capped with DMP (MEHPPV, average molecular weight: 68,000 g mol^{-1}) were purchased from American Dye Source, Inc. (Quebec, Canada). Bovine serum albumin, fluorescein, rhodamine 6G, and quinine hemisulfate monohydrate were purchased from Sigma-Aldrich. Dulbecco's Modified Eagle's Medium (DMEM), penicillin and fetal bovine serum (FBS) were purchased from Gibco-BRL (Grand Island, NY). 3-(4,5-Dimethylthiazol-2-yl)-2,5-diphenyltetrazolium bromide (MTT) was purchased from Merck (Germany). All chemicals were used as received. Tetrahydrofuran was freshly distilled from sodium benzophenone ketyl before use. A stock

PBS solution at five times the standard concentration (5 × PBS) was prepared by dissolving 40 g NaCl, 1 g KCl, 7.2 g Na_2HPO_4, and 1.2 g KH_2PO_4 in 800 cm^3 H_2O and then adjusting the pH to 7.4 with 0.1 M NaOH and making up to 1 dm^3 with deionized water. Deionized water obtained from a Millipore NANO pure water system filtered through a 0.22 μm nylon membrane (Merck Millipore) was used in all experiments.

5.2.2. Preparation of CP-BSA nanoparticles

Dispersions of conjugated polymer nanoparticles stabilized with BSA, CP-BSA nanoparticles, in PBS were prepared using a modified nano-precipitation method.[35] The conjugation polymer (2 mg) was dissolved in 100 cm^3 freshly distilled THF under sonication to obtain a ~20 ppm solution. (The THF solution of MEHPPV was filtered through a 1.45 μm glass fiber filter (Whatman).) The 20-ppm conjugated polymer THF solution (5 cm^3) was quickly injected into 10 cm^3 of aqueous solutions of BSA (40 ppm) under vigorous stirring. The THF was removed using a rotary evaporator under vacuum in a water bath at approximately 40 °C. To this aqueous dispersion of CP-BSA nanoparticles, 2 cm^3 of 5 × PBS was added and the total volume was made up to 10 cm^3 with deionized water. This dilution produced a 10 ppm dispersion of CP-BSA nanoparticles in standard PBS (pH = 7.4), which was filtered through a 0.2 μm filter (Sartorius Stedim Biotech) to give the final PBS dispersion of CP-BSA nanoparticles. The absorption spectra of the PBS dispersion of CP-BSA nanoparticles before and after filtration were determined to measure the yield of nanoparticle preparation, as defined in Equation 5.1:

$$\text{Yield} = \frac{A_{\text{after filtration}}}{A_{\text{before filtration}}} \times 100\% \qquad \textbf{(5.1)}$$

where $A_{\text{before filtration}}$ and $A_{\text{after filtration}}$ represent the absorbance at 460 nm for F8BT-BSA nanoparticles, 380 nm for PDOF-BSA nanoparticles, and 490 nm for MEHPPV-BSA nanoparticles in PBS before and after filtration through a 0.2 μm filter, respectively. Thus, the

yield defined here describes the percentage of CP-BSA nanoparticles that passed through a 0.2 μm filter. UV-Vis absorption spectra were recorded on a Cary-Varian 5000 spectrophotometer using matched quartz cuvettes of 1 cm path length.

5.2.3. Size and zeta potential characterization

Dynamic light scattering (DLS) was used to measure the hydrodynamic diameters and zeta potentials of CP-BSA nanoparticles. Measurements were performed on a Malvern Zetasizer (Malvern Inst. Ltd. UK) with a He-Ne laser (633 nm) and a back-scattering detector (173°). The hydrodynamic diameter and zeta potential were reported as the mean value of three independent measurements. The reported error represents the standard deviation from the mean.

5.2.4. Fluorescence quantum yield measurements

Fluorescence spectra were recorded on a Cary-Varian Eclipse fluorescence spectrophotometer using a quartz cuvette of 1 cm path length. Quinine hemisulfate monohydrate, fluorescein and rhodamine 6G were used as references to measure fluorescence quantum yields of PDOF-BSA, F8BT-BSA and MEHPPV-BSA nanoparticles in PBS. The fluorescence quantum yields of the references are 59% for quinine hemisulfate monohydrate in 0.105 M $HClO_4$, 89% for fluorescein in 0.1 M NaOH and 91% for rhodamine 6G in ethanol.[36] The specific procedure is as follows. Five samples of varied concentrations ($A < 0.1$) of CP-BSA nanoparticles in PBS and the corresponding reference solutions were prepared. The absorption at 370 nm for PDOF-BSA nanoparticles and quinine hemisulfate monohydrate, at 475 nm for F8BT-BSA nanoparticles and fluorescein and at 535 nm for MEHPPV-BSA nanoparticles and rhodamine 6G, and the emission spectra (excitation wavelength of 370 nm) for PDOF-BSA nanoparticles and quinine hemisulfate monohydrate, (excitation wavelength

of 475 nm) for F8BT-BSA naoparticles and fluorescein and (excitation wavelength of 535 nm) for MEHPPV-BSA nanoparticles and rhodamine 6G of each sample were recorded. For each of the CP-BSA nanoparticles and the corresponding reference, integrated fluorescence intensities were plotted against the corresponding absorbance values to give a linear curve with a slope of m and an intercept of 0. The fluorescence quantum yields of the CP-BSA nanoparticles were then calculated according to Equation 5.2,

$$\Phi_{\text{sample}} = \Phi_{\text{reference}} \times \frac{m_{\text{sample}}}{m_{\text{reference}}} \times \frac{\eta^2_{\text{sample}}}{\eta^2_{\text{reference}}} \times 100\% \qquad \textbf{(5.2)}$$

where Φ represents the fluorescence quantum yield and η represents refractive index of the corresponding solvent. The error of the fluorescence quantum yield in this study represents the linear fitting error of the calculated slope, m.

5.3. Preparation of CP-BSA nanoparticles

The molecular structures of conjugated polymers used in this study are shown in Figure 5.1a. A modified nano-precipitation method is employed to prepare the CP-BSA nanoparticles. Upon injection of a THF solution of conjugated polymer into an aqueous solution of BSA under vigorous stirring, the sudden decrease in solubility of the conjugated polymer and hydrophobic interactions between intra and/or inter conjugated polymer chains cause the collapse and aggregation of conjugated polymer chains, leading to the formation of conjugated polymer nanoparticles.[21] Driven by hydrophobic interactions, the hydrophobic domains of BSA associate with the hydrophobic conjugated polymers to form a BSA coating (Figure 5.1b).

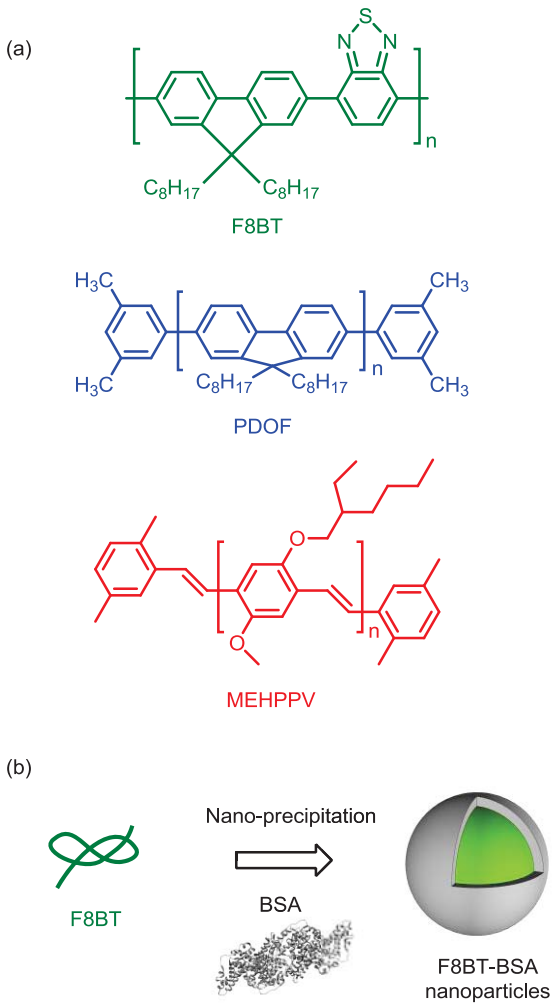

Figure 5.1. (a) Chemical structures of F8BT, PDOF, and MEHPPV. (b) Schematic illustration of the preparation of the CP-BSA nanoparticles, exemplified by F8BT-BSA nanoparticles.

While bare conjugated polymer nanoparticles are stable in deionized water, they exhibit large-scale aggregation and precipitation at high ionic strengths which occur under physiological conditions. Thus, to evaluate the effectiveness of BSA in stabilizing conjugated polymer nanoparticles, a quantity of high concentration PBS solution (5 × PBS) is added to an aqueous dispersion of CP-BSA nanoparticles to give a standard PBS (pH 7.4) dispersion of CP-BSA nanoparticles. The PBS dispersion of CP-BSA nanoparticles is then filtered through a 200 nm filter to remove large aggregates. The proportion of CP-BSA nanoparticles with diameters smaller than 200 nm, i.e. the yield defined in this study as shown in Equation 5.1, is then used as the parameter to evaluate the stabilization effect of BSA.

In order to understand the role of BSA in stabilizing conjugated polymer nanoparticles, F8BT serves as a model conjugated polymer to explore the dependence of yield on the concentration of BSA, as shown in Figure 5.2. A yield of 0 indicates that bare F8BT nanoparticles aggregate immediately upon being transferred to a PBS solution and that all of the aggregates are larger than 200 nm, which is consistent with bare conjugated polymer nanoparticles showing large-scale aggregation at high ionic strengths as reported by others.[29,37] Figure 5.2 shows that the yield increases from 56 ± 5% to 97 ± 2 % as the concentration of BSA increases from 10 to 20 ppm. When the concentration of BSA further increases to 40 ppm and 80 ppm, the yield remains constant at 99 ± 1%. Therefore, in terms of yield, a BSA concentration of 20 ppm is sufficient to stabilize F8BT nanoparticles in PBS. However, the size distribution of the obtained F8BT-BSA nanoparticles is broad, and a BSA concentration of 40 ppm was chosen in this study to prepare CP-BSA nanoparticles for further studies. In contrast to bare conjugated polymer nanoparticles exhibiting strong aggregation in PBS as reflected by negligible yields, high yields of 98 ± 2%, 99 ± 1%, and 98 ± 1% are observed for PDOF-BSA, F8BT-BSA, and MEHPPV-BSA nanoparticles (Figure 5.3), respectively. This highlights the ability of BSA to stabilize conjugated polymer nanoparticles in PBS at high ionic strength.

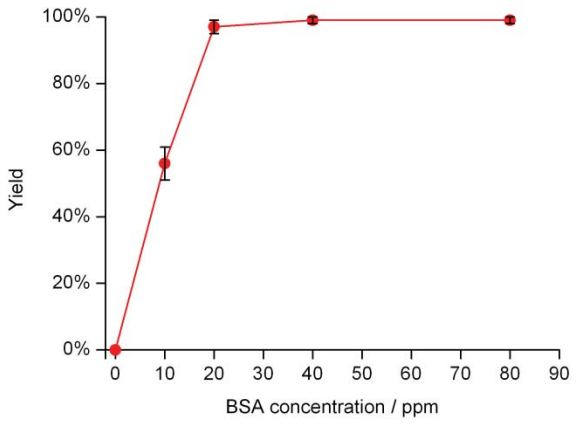

Figure 5.2. The dependence of the yield for preparation of F8BT-BSA nanoparticles in PBS on the concentration of BSA.

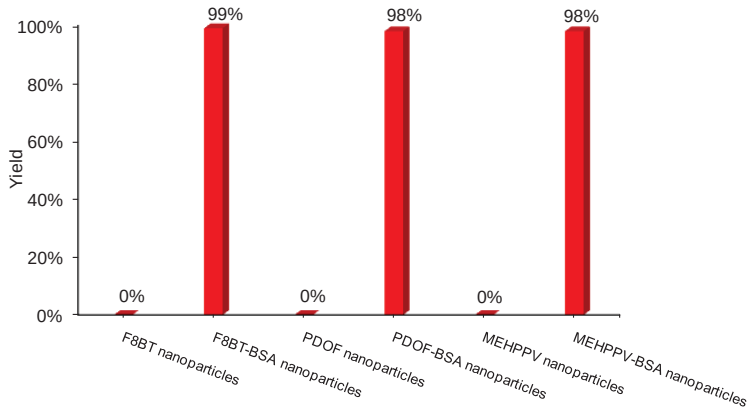

Figure 5.3. Yields of bare conjugated polymer nanoparticles (< 200 nm) and CP-BSA nanoparticles (< 200 nm) in PBS.

5.4. Surface charge, size and colloidal stability of CP-BSA nanoparticles

5.4.1. Surface charge of CP-BSA nanoparticles

The levels of surface charge of bare conjugated polymer nanoparticles and CP-BSA nanoparticles are characterized by their zeta potential values. Figure 5.4 shows that the zeta potentials of bare PDOF, F8BT, and MEHPPV nanoparticles in deionized water are −36 ± 3, −33 ± 3, and −34 ± 2 mV, respectively. These negative zeta potential values are indicative of the negatively charged surfaces of these nanoparticles, which has been attributed to surface chemical defects as a consequence of oxidation of the conjugated polymer in the formation of nanoparticles.[38] The zeta potentials of PDOF-BSA, F8BT-BSA, and MEHPPV-BSA nanoparticles in deionized water are −30 ± 3, −24 ± 3, and −30 ± 2 mV (Figure 5.4), respectively. Compared with bare conjugated polymer nanoparticles, CP-BSA nanoparticles have slightly less negative zeta potential values. The negatively charged surface of CP-BSA nanoparticles is attributable to the carboxylate groups of BSA forming an outer layer which screens the intrinsic negative charge of bare conjugated polymer nanoparticles. This

conclusion is in accord with a recent study in which a zeta potential value of −29 mV was reported for small organic molecules loaded BSA nanoparticles, and in which the negatively charged nanoparticle surface was attributed to the carboxylate groups of BSA.[17]

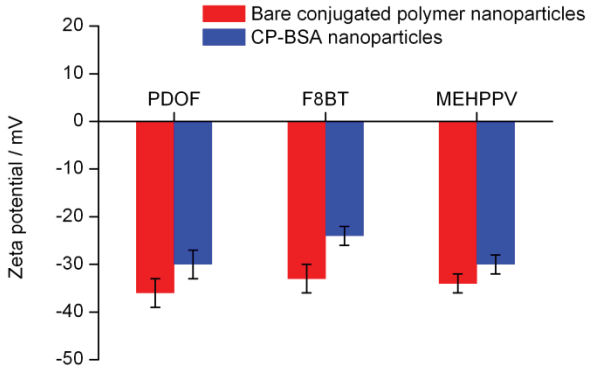

Figure 5.4. The zeta potentials bare conjugated polymer nanoparticles and CP-BSA nanoparticles in deinoized water.

5.4.2. Size of CP-BSA nanoparticles

The hydrodynamic diameters of bare conjugated polymer nanoparticles in deionized water and CP-BSA nanoparticles in PBS were measured using dynamic light scattering (DLS) technique. The hydrodynamic diameters of bare PDOF, F8BT, and MEHPPV nanoparticles in deionized water are 36 ± 3, 43 ± 4, and 18 ± 1 nm (Figure 5.5), respectively. Taking into account that these nanoparticles were prepared under identical condition and procedure, this result indicates that the particle size depends on the properties of the conjugated polymer, such as its molecular weight, polydispersity, and intra and/or inter chain interactions.[35] The hydrodynamic diameters of PDOF-BSA, F8BT-BSA, and MEHPPV-BSA nanoparticles in PBS are 37 ± 3, 59 ± 6, and 19 ± 1 nm (Figure 5.5), respectively. By comparison with bare F8BT nanoparticles in deionized water, F8BT-BSA nanoparticles in PBS have a larger hydrodynamic diameter, which is due to a combination of salt-induced aggregation in PBS

and the presence of BSA. However, a different pattern is observed for PDOF and MEHPPV. PDOF-BSA and MEHPPV-BSA nanoparticles in PBS have similar hydrodynamic diameters with those of bare PDOF and MEHPPV nanoparticles in deionized water.

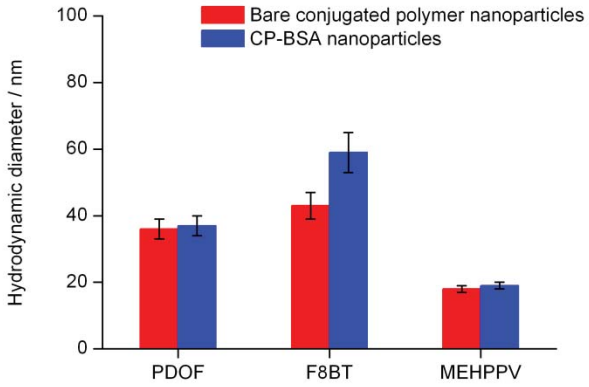

Figure 5.5. The hydrodynamic diameters of bare conjugated polymer nanoparticles in deionized water and CP-BSA nanoparticles in PBS.

5.4.3 Colloidal stability of CP-BSA nanoparticles

The long-term colloidal stability of CP-BSA nanoparticles, in addition to their small size, is a critical characteristic for their biological imaging applications. We have monitored their size variation over a 4-week period and the results are shown in Figure 5.6 and Tables 5.1 - 5.3 in Section 5.8 Appendix. Bare PDOF and F8BT nanoparticles in deionized water remain stable over 4 weeks without detectable size variations. However, bare MEHPPV nanoparticles are stable in deionized water over 2 weeks, but thereafter exhibit a partial aggregation as reflected by a substantially increased polydispersity index value (Table 5.3 in Section 5.8 Appendix) and the appearance of a new peak in the size distribution per intensity (Figure 5.9 in Section 5.8 Appendix). The high colloidal stability of the bare conjugated polymer nanoparticles in deionized water are the result of their negatively charged surfaces exerting electrostatic repulsion between individual nanoparticles, as reflected by the negative zeta potential values. In contrast, bare conjugated polymer nanoparticles are unstable in PBS and

show significant aggregation in PBS to produce aggregates larger than 200 nm, as reported in Chapter 4 of this thesis. This is attributed to the ions in PBS providing a strong shielding effect for the surface charge of bare conjugated polymer nanoparticles and thereby allowing aggregation.[39] In contrast, CP-BSA nanoparticles exhibit remarkable colloidal stability in PBS. Thus, as shown in Figure 5.6, PDOF-BSA and F8BT-BSA nanoparticles are stable in PBS over 4 weeks without any sign of aggregation. The MEHPPV-BSA nanoparticles are stable over 3 weeks and show a partial aggregation thereafter, as reflected by the increased polydispersity index value (Table 5.3 in Section 5.8 Appendix) and the appearance of a new peak in the size distribution per intensity (Figure 5.10 in Section 5.8 Appendix). These high colloidal stabilities of the CP-BSA nanoparticles are due to the combined effects of their negatively charged surfaces and the steric effect of the bulk 3D structure of BSA.[12,19] In addition to these effects, the hydrophilic domains of BSA also facilitate the dispersion of CP-BSA nanoparticles in PBS. As bare conjugated polymer nanoparticles exhibiting similar zeta potentials to those of the CP-BSA nanoparticles aggregate strongly in PBS, it is likely that the steric effect of the bulk 3D structure of BSA makes the larger contribution to the colloidal stability of CP-BSA nanoparticles in PBS.

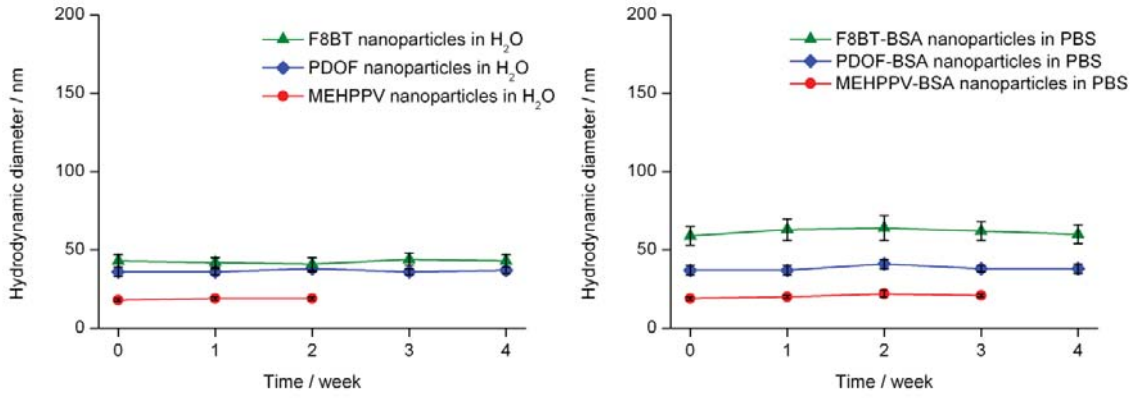

Figure 5.6. Size variation of (Left) bare conjugated polymer nanoparticles in deionized water and (Right) CP-BSA nanoparticles in PBS over 4 weeks.

5.5. UV-Vis absorption and fluorescence properties of CP-BSA nanoparticles

The normalized UV-Vis absorbance and fluorescence spectra of CP-BSA nanoparticles in PBS are shown in Figure 5.7 from which it is seen that their absorption occurs over a broad range from 350 to 550 nm which overlaps with a number of excitation wavelengths for fluorescence microscopy. The UV-Vis absorption and fluorescence properties of conjugated polymer nanoparticles are dependent on the conjugated polymer conformation and intra and/or inter polymer chain interactions inside individual nanoparticle, which are largely determined by the intrinsic properties of the specific conjugated polymer.[40-42] The UV-Vis absorbance and fluorescence spectra of bare conjugated polymer nanoparticles in deionized water are similar to those of CP-BSA nanoparticles in PBS, as shown in Figure 5.8, consistent with the conjugated polymer possessing similar chain conformation, packing and folding inside nanoparticles in the absence and presence of BSA. Thus, BSA appears not to penetrate deeply into the nanoparticles to influence conjugated polymer conformation. This has implications on the fluorescence quantum yields of CP-BSA nanoparticles in PBS. The fluorescence quantum yields of PDOF-BSA, F8BT-BSA, and MEHPPV-BSA nanoparticles in PBS, 42 ± 1%, 24 ± 1%, and 8 ± 1%, are similar to those of bare PDOF, F8BT, and MEHPPV nanoparticles in deionized water, 36 ± 1%, 25 ± 1%, and 6 ± 1%, respectively. The similar fluorescence quantum yields of CP-BSA nanoparticles in PBS and their analogous bare conjugated polymer nanoparticles in deionized water indicate that the emitting chromophores of CP-BSA nanoparticles are located near the nanoparticles core such that the influence on quantum yield exerted by BSA on the surface of the CP-BSA nanoparticles is negligible. This interpretation is consistent with a recent study which shows that the emitting chromophores of a conjugated polymer aggregate are located near the core, away from the surface of the

aggregate.[43]

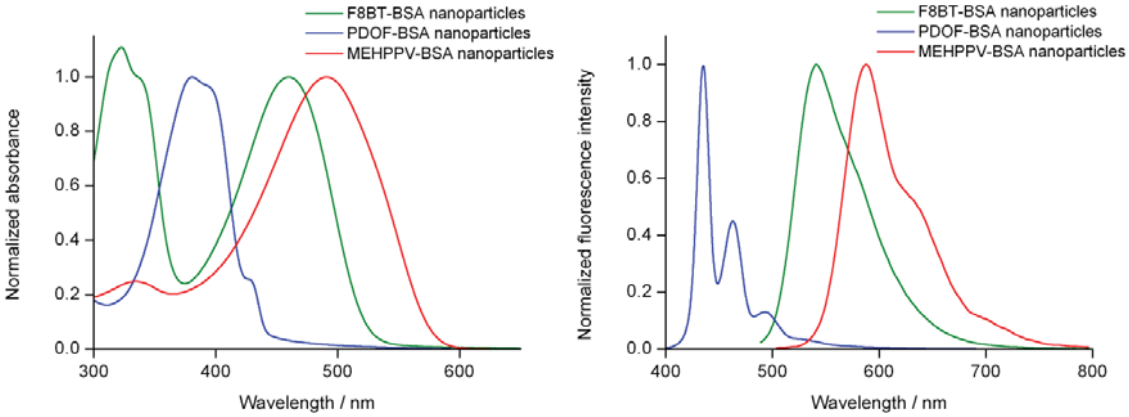

Figure 5.7. Normalized (Left) UV-Vis absorbance and (Right) fluorescence spectra of CP-BSA nanoparticles in PBS.

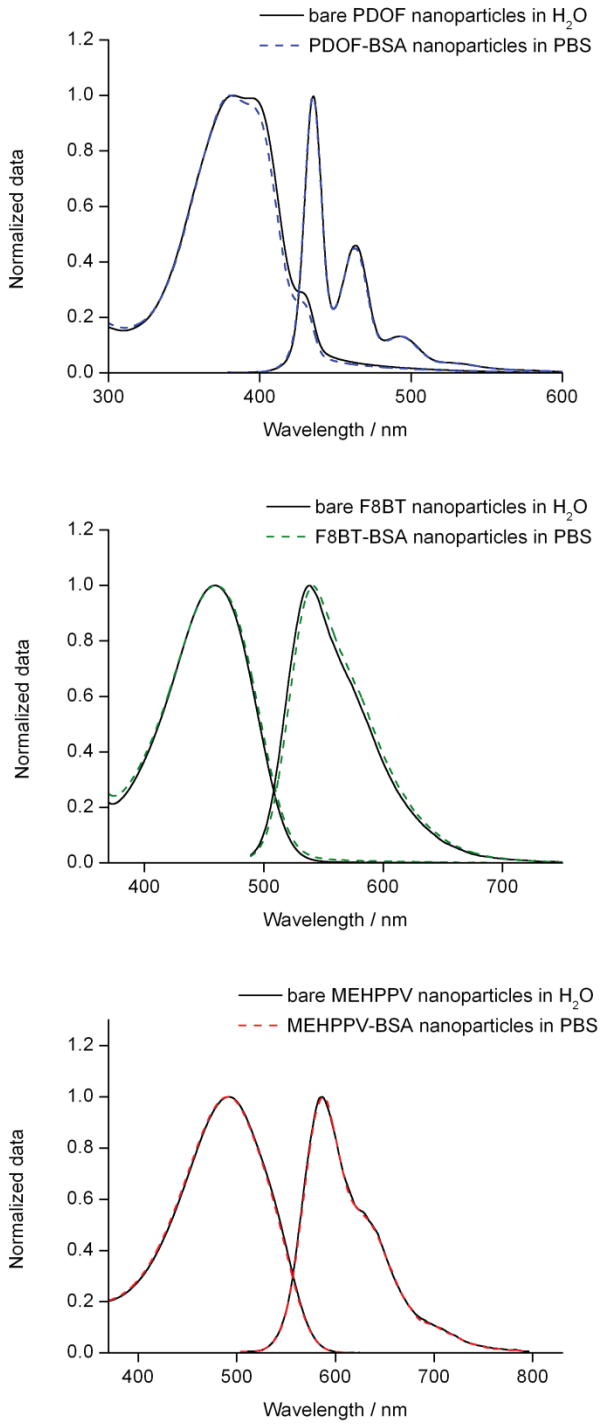

Figure 5.8. Normalized absorption and fluorescence spectra of bare conjugated polymer nanoparticles in deionized water (solid) and CP-BSA nanoparticles in PBS (dashed).

5.6. Conclusions

We have prepared highly fluorescent and stable CP-BSA nanoparticles for potential cell imaging applications. These CP-BSA nanoparticles in PBS have hydrodynamic diameters ranging from 19 ± 1 to 59 ± 6 nm. By comparison with the rapid, large-scale aggregation of bare conjugated polymer nanoparticles in PBS, a high colloidal stability of CP-BSA nanoparticles in PBS is observed, as reflected by a negligible size variation over a 4-week period. This remarkably high colloidal stability at high ionic strength is ascribed to a combination of a negative surface charge arising from the carboxylate groups of BSA and steric stabilization as a consequence of the bulk 3D structure of BSA, of which the steric stabilization makes the larger contribution. In addition to their high colloidal stability at high ionic strength conditions, the fluorescence brightness of CP-BSA nanoparticles in PBS is similar to that of the corresponding bare conjugated polymer nanoparticles in deionized water, reflected by similar fluorescence quantum yields. In summary, CP-BSA nanoparticles are promising fluorescent probes for cell imaging application, as they are of small size and high colloidal stability in PBS and exhibit high fluorescence quantum yields. Further studies are planned to explore the feasibility of using CP-BSA nanoparticles as fluorescent probes for cell imaging. Thus, their cytotoxicity, amenability towards surface bioconjugation and cellular uptake and mechanism will be examined..

5.7. References

(1) Peters Jr, T. Serum albumin. In *Advances in protein chemistry*, C.B. Anfinsen, J. T. E.; Frederic, M. R., Eds.; Academic Press, 1985; Vol. 37, pp 161-245.

(2) Cedervall, T.; Lynch, I.; Foy, M.; Berggård, T.; Donnelly, S. C.; Cagney, G.; Linse, S.; Dawson, K. A. Detailed identification of plasma proteins adsorbed on copolymer nanoparticles. *Angew. Chem. Int. Ed.* **2007,** *46*, 5754-5756.

(3) Lynch, I.; Dawson, K. A. Protein-nanoparticle interactions. *Nano Today* **2008,** *3*, 40-47.

(4) Mahmoudi, M.; Lynch, I.; Ejtehadi, M. R.; Monopoli, M. P.; Bombelli, F. B.; Laurent, S. Protein-nanoparticle interactions: Opportunities and challenges. *Chem. Rev.* **2011,** *111*, 5610-5637.

(5) Hlady, V.; Buijs, J. Protein adsorption on solid surfaces. *Curr. Opin. Biotechnol.* **1996,** *7*, 72-77.

(6) Wu, C.; Schneider, T.; Zeigler, M.; Yu, J.; Schiro, P. G.; Burnham, D. R.; McNeill, J. D.; Chiu, D. T. Bioconjugation of ultrabright semiconducting polymer dots for specific cellular targeting. *J. Am. Chem. Soc.* **2010,** *132*, 15410-15417.

(7) Liu, J.; Fu, S.; Yuan, B.; Li, Y.; Deng, Z. Toward a universal "adhesive nanosheet" for the assembly of multiple nanoparticles based on a protein-induced reduction/decoration of graphene oxide. *J. Am. Chem. Soc.* **2010,** *132*, 7279-7281.

(8) Yu, C. H.; Al-Saadi, A.; Shih, S.-J.; Qiu, L.; Tam, K. Y.; Tsang, S. C. Immobilization of bsa on silica-coated magnetic iron oxide nanoparticle. *J. Phys. Chem. C* **2009,** *113*, 537-543.

(9) Le Guével, X.; Hötzer, B.; Jung, G.; Hollemeyer, K.; Trouillet, V.; Schneider, M. Formation of fluorescent metal (Au, Ag) nanoclusters capped in bovine serum albumin followed by fluorescence and spectroscopy. *J. Phys. Chem. C* **2011,** *115*, 10955-10963.

(10) Singh, A. V.; Bandgar, B. M.; Kasture, M.; Prasad, B. L. V.; Sastry, M. Synthesis of gold, silver and their alloy nanoparticles using bovine serum albumin as foaming and stabilizing agent. *J. Mater. Chem.* **2005,** *15*, 5115-5121.

(11) Brewer, S. H.; Glomm, W. R.; Johnson, M. C.; Knag, M. K.; Franzen, S. Probing BSA binding to citrate-coated gold nanoparticles and surfaces. *Langmuir* **2005,** *21*, 9303-9307.

(12) Xie, J.; Zheng, Y.; Ying, J. Y. Protein-directed synthesis of highly fluorescent gold nanoclusters. *J. Am. Chem. Soc.* **2009,** *131*, 888-889.

(13) Yang, Q.; Liang, J.; Han, H. Probing the interaction of magnetic iron oxide

nanoparticles with bovine serum albumin by spectroscopic techniques. *J. Phys. Chem. B* **2009,** *113*, 10454-10458.

(14) Mamedova, N. N.; Kotov, N. A.; Rogach, A. L.; Studer, J. Albumin-CdTe nanoparticle bioconjugates: Preparation, structure, and interunit energy transfer with antenna effect. *Nano Lett.* **2001,** *1*, 281-286.

(15) Wang, Y.; Yang, T.; Ke, H.; Zhu, A.; Wang, Y.; Wang, J.; Shen, J.; Liu, G.; Chen, C.; Zhao, Y.; Chen, H. Smart albumin-biomineralized nanocomposites for multimodal imaging and photothermal tumor ablation. *Adv. Mater.* **2015,** *27*, 3874-3882.

(16) Yang, L.; Cui, F.; Cun, D.; Tao, A.; Shi, K.; Lin, W. Preparation, characterization and biodistribution of the lactone form of 10-hydroxycamptothecin (HCPT)-loaded bovine serum albumin (BSA) nanoparticles. *Int. J. Pharm.* **2007,** *340*, 163-172.

(17) Qin, W.; Ding, D.; Liu, J.; Yuan, W. Z.; Hu, Y.; Liu, B.; Tang, B. Z. Biocompatible nanoparticles with aggregation-induced emission characteristics as far-red/near-infrared fluorescent bioprobes for in vitro and in vivo imaging applications. *Adv. Funct. Mater.* **2012,** *22*, 771-779.

(18) Zhang, L.; Lu, Z.; Li, X.; Deng, Y.; Zhang, F.; Ma, C.; He, N. Methoxy poly(ethylene glycol) conjugated denatured bovine serum albumin micelles for effective delivery of camptothecin. *Polym. Chem.* **2012,** *3*, 1958-1961.

(19) Ge, J.; Lei, J.; Zare, R. N. Bovine serum albumin-poly(methyl methacrylate) nanoparticles: An example of frustrated phase separation. *Nano Lett.* **2011,** *11*, 2551-2554.

(20) Ge, J.; Neofytou, E.; Lei, J.; Beygui, R. E.; Zare, R. N. Protein-polymer hybrid nanoparticles for drug delivery. *Small* **2012,** *8*, 3573-3578.

(21) Wu, C.; Chiu, D. T. Highly fluorescent semiconducting polymer dots for biology and medicine. *Angew. Chem. Int. Ed.* **2013,** *52*, 3086-3109.

(22) Wu, I. C.; Yu, J.; Ye, F.; Rong, Y.; Gallina, M. E.; Fujimoto, B. S.; Zhang, Y.; Chan, Y.-H.; Sun, W.; Zhou, X.-H.; Wu, C.; Chiu, D. T. Squaraine-based polymer dots with narrow, bright near-infrared fluorescence for biological applications. *J. Am. Chem. Soc.* **2015,** *137*, 173-178.

(23) Liu, H.-Y.; Wu, P.-J.; Kuo, S.-Y.; Chen, C.-P.; Chang, E.-H.; Wu, C.-Y.; Chan, Y.-H. Quinoxaline-based polymer dots with ultrabright red to near-infrared fluorescence for in vivo biological imaging. *J. Am. Chem. Soc.* **2015,** *137*, 10420-10429.

(24) Pu, K.; Shuhendler, A. J.; Jokerst, J. V.; Mei, J.; Gambhir, S. S.; Bao, Z.; Rao, J. Semiconducting polymer nanoparticles as photoacoustic molecular imaging probes in living mice. *Nat. Nanotechnol.* **2014,** *9*, 233-239.

(25) Pu, K.; Shuhendler, A. J.; Valta, M. P.; Cui, L.; Saar, M.; Peehl, D. M.; Rao, J. Phosphorylcholine-coated semiconducting polymer nanoparticles as rapid and efficient labeling agents for in vivo cell tracking. *Adv. Healthcare Mater.* **2014,** *3*, 1292-1298.

(26) Yuan, Y.; Wang, Z.; Cai, P.; Liu, J.; Liao, L.-D.; Hong, M.; Chen, X.; Thakor, N.; Liu, B. Conjugated polymer and drug co-encapsulated nanoparticles for chemo- and photo-thermal combination therapy with two-photon regulated fast drug release. *Nanoscale* **2015,** *7*, 3067-3076.

(27) Feng, X.; Lv, F.; Liu, L.; Tang, H.; Xing, C.; Yang, Q.; Wang, S. Conjugated polymer nanoparticles for drug delivery and imaging. *ACS Appl. Mater. Interfaces* **2010,** *2*, 2429-2435.

(28) Geng, J.; Sun, C.; Liu, J.; Liao, L.-D.; Yuan, Y.; Thakor, N.; Wang, J.; Liu, B. Biocompatible conjugated polymer nanoparticles for efficient photothermal tumor therapy. *Small* **2015,** *11*, 1603-1610.

(29) Shen, X.; Li, L.; Wu, H.; Yao, S. Q.; Xu, Q.-H. Photosensitizer-doped conjugated polymer nanoparticles for simultaneous two-photon imaging and two-photon photodynamic therapy in living cells. *Nanoscale* **2011,** *3*, 5140-5146.

(30) Dmitriev, R. I.; Borisov, S. M.; Düssmann, H.; Sun, S.; Müller, B. J.; Prehn, J.; Baklaushev, V. P.; Klimant, I.; Papkovsky, D. B. Versatile conjugated polymer nanoparticles for high-resolution O_2 imaging in cells and 3D tissue models. *ACS Nano* **2015,** *9*, 5275-5288.

(31) Wu, C.; Bull, B.; Christensen, K.; McNeill, J. Ratiometric single-nanoparticle oxygen sensors for biological imaging. *Angew. Chem. Int. Ed.* **2009,** *48*, 2741-2745.

(32) Childress, E. S.; Roberts, C. A.; Sherwood, D. Y.; LeGuyader, C. L. M.; Harbron, E. J. Ratiometric fluorescence detection of mercury ions in water by conjugated polymer nanoparticles. *Anal. Chem.* **2012,** *84*, 1235-1239.

(33) Huang, Y.-C.; Chen, C.-P.; Wu, P.-J.; Kuo, S.-Y.; Chan, Y.-H. Coumarin dye-embedded semiconducting polymer dots for ratiometric sensing of fluoride ions in aqueous solution and bio-imaging in cells. *J. Mater. Chem. B* **2014,** *2*, 6188-6191.

(34) Tanaka, T.; Shiramoto, S.; Miyashita, M.; Fujishima, Y.; Kaneo, Y. Tumor targeting based on the effect of enhanced permeability and retention (EPR) and the mechanism of receptor-mediated endocytosis (RME). *Int. J. Pharm.* **2004,** *277*, 39-61.

(35) Wu, C.; Bull, B.; Szymanski, C.; Christensen, K.; McNeill, J. Multicolor conjugated polymer dots for biological fluorescence imaging. *ACS Nano* **2008,** *2*, 2415-2423.

(36) Würth, C.; Grabolle, M.; Pauli, J.; Spieles, M.; Resch-Genger, U. Relative and absolute determination of fluorescence quantum yields of transparent samples. *Nat. Protocols* **2013,** *8*, 1535-1550.

(37) Jin, Y.; Ye, F.; Wu, C.; Chan, Y.-H.; Chiu, D. T. Generation of functionalized and robust semiconducting polymer dots with polyelectrolytes. *Chem. Commun.* **2012,** *48*, 3161-3163.

(38) Clafton, S. N.; Beattie, D. A.; Mierczynska-Vasilev, A.; Acres, R. G.; Morgan, A. C.; Kee, T. W. Chemical defects in the highly fluorescent conjugated polymer dots. *Langmuir* **2010,** *26*, 17785-17789.

(39) Reisch, A.; Runser, A.; Arntz, Y.; Mély, Y.; Klymchenko, A. S. Charge-controlled nanoprecipitation as a modular approach to ultrasmall polymer nanocarriers: Making bright and stable nanoparticles. *ACS Nano* **2015,** *9*, 5104-5116.

(40) Sun, K.; Chen, H.; Wang, L.; Yin, S.; Wang, H.; Xu, G.; Chen, D.; Zhang, X.; Wu, C.; Qin, W. Size-dependent property and cell labeling of semiconducting polymer dots. *ACS Appl. Mater. Interfaces* **2014,** *6*, 10802-10812.

(41) Nguyen, T.-Q.; Doan, V.; Schwartz, B. J. Conjugated polymer aggregates in solution: Control of interchain interactions. *J. Chem. Phys.* **1999,** *110*, 4068-4078.

(42) Nguyen, T.-Q.; Martini, I. B.; Liu, J.; Schwartz, B. J. Controlling interchain interactions in conjugated polymers: The effects of chain morphology on exciton-exciton annihilation and aggregation in MEH-PPV films. *J. Phys. Chem. B* **2000,** *104*, 237-255.

(43) Tapping, P. C.; Clafton, S. N.; Schwarz, K. N.; Kee, T. W.; Huang, D. M. Molecular-level details of morphology-dependent exciton migration in poly(3-hexylthiophene) nanostructures. *J. Phys. Chem. C* **2015,** *119*, 7047-7059.

5.8. Appendix

Table 5.1. Size variation of bare PDOF nanoparticles in deionized water and PDOF-BSA nanoparticles in PBS over a period of 4 weeks.[a]

	PDOF nanoparticles in H_2O		PDOF-BSA nanoparticles in PBS	
	Hydrodynamic diameter / nm	Polydispersity index	Hydrodynamic diameter / nm	Polydispersity index
Original	36 ± 3	0.17 ± 0.01	37 ± 3	0.19 ± 0.03
1 week	36 ±2	0.18 ± 0.01	37 ± 3	0.17 ± 0.01
2 weeks	38 ±2	0.19 ± 0.02	41 ± 3	0.15 ± 0.01
3 weeks	36 ±2	0.19 ± 0.02	38 ±2	0.17 ± 0.02
4 weeks	37 ±2	0.19 ± 0.02	38 ± 3	0.18 ± 0.03

[a]The hydrodynamic diameters are given as the mean value of three independent measurements and the errors represent the standard deviation from the mean.

Table 5.2. Size variation of bare F8BT nanoparticles in deionized water and F8BT-BSA nanoparticles in PBS over a period of 4 weeks.[a]

	F8BT nanoparticles in H_2O		F8BT-BSA nanoparticles in PBS	
	Hydrodynamic diameter / nm	Polydispersity index	Hydrodynamic diameter / nm	Polydispersity index
Original	43 ±4	0.09 ± 0.02	59 ±6	0.12 ± 0.05
1 week	42 ±3	0.11 ± 0.01	63 ±7	0.09 ± 0.01
2 weeks	41 ±4	0.12 ± 0.02	64 ±8	0.09 ± 0.03
3 weeks	44 ±4	0.09 ± 0.02	62 ±6	0.10 ± 0.02
4 weeks	43 ±4	0.11 ± 0.02	60 ±6	0.10 ± 0.02

[a]The hydrodynamic diameters are given as the mean value of three independent measurements and the errors represent the standard deviation from the mean.

Table 5.3. Size variation of bare MEHPPV nanoparticles in deionized water and MEHPPV-BSA nanoparticles in PBS over a period of 4 weeks.[a]

	MEHPPV nanoparticles in H_2O		MEHPPV-BSA nanoparticles in PBS	
	Hydrodynamic diameter / nm	Polydispersity index	Hydrodynamic diameter / nm	Polydispersity index
Original	18 ±1	0.17 ± 0.01	19 ±1	0.18 ± 0.02
1 week	19 ±1	0.16 ± 0.01	20 ±1	0.18 ± 0.01
2 weeks	19 ±1	0.19 ± 0.02	19 ±1	0.19 ± 0.03
3 weeks	[b]	0.29 ± 0.04	20 ±2	0.19 ± 0.02
4 weeks	[b]	[b]	[b]	0.28 ± 0.05

[a]The hydrodynamic diameters are given as the mean value of three independent measurements and the errors represent the standard deviation from the mean.

[b]Values not determined due to partial aggregation resulting in a too broad size distribution as reflected by larger polydispersity index values.

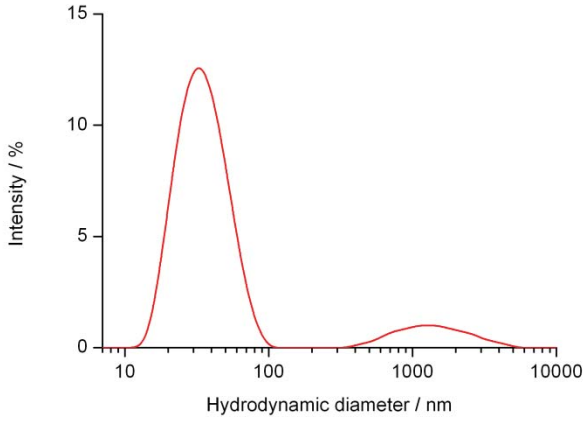

Figure 5.9. The hydrodynamic diameter distribution per intensity of bare MEHPPV nanoparticles in deionized water (Kept in dark at room temperature for 2 weeks). The appearance of the peak over the ranges 0.3-5 μm indicates partial aggregation of MEHPPV nanoparticles occurs.

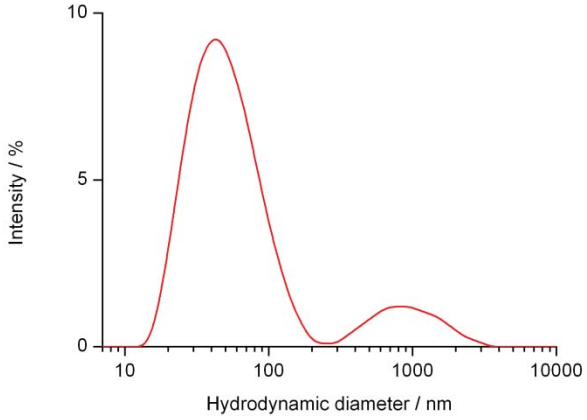

Figure 5.10. The hydrodynamic diameter distribution per intensity of MEHPPV-BSA nanoparticles in PBS (Kept in dark at room temperature for 3 weeks). The appearance of the peak over the ranges 0.2-3 μm indicates partial aggregation of MEHPPV-BSA nanoparticles occurs.